Scientific Excellence • Resource Protection & Conservation • Benefits for Canadians
Excellence scientifique • Protection et conservation des ressources • Bénéfices aux Canadiens

COUPLED WIND-SEA MODELS AND THEIR IMPACT ON FLUXES OF MOMENTUM, SENSIBLE HEAT AND LATENT HEAT

Liangming Wang and William Perrie

Physical and Chemical Sciences Branch
Scotia-Fundy Region
Department of Fisheries and Oceans

Bedford Institute of Oceanography
P.O. Box 1006
Dartmouth, Nova Scotia
Canada B2Y 4A2

1993

Canadian Technical Report of Hydrography and Ocean Sciences 149

Fisheries and Oceans Pêches et Océans

Canada

Canadian Technical Report of Hydrography and Ocean Sciences

Technical reports contain scientific and technical information that contributes to existing knowledge but which is not normally appropriate for primary literature. The subject matter is related generally to programs and interests of the Ocean Science and Surveys (OSS) sector of the Department of Fisheries and Oceans.

Technical reports may be cited as full publications. The correct citation appears above the abstract of each report. Each report is abstracted in *Aquatic Sciences and Fisheries Abstracts* and indexed in the Department's annual index to scientific and technical publications.

Technical reports are produced regionally but are numbered nationally. Requests for individual reports will be filled by the issuing establishment listed on the front cover and title page. Out of stock reports will be supplied for a fee by commercial agents.

Regional and headquarters establishments of Ocean Science and Surveys ceased publication of their various report series as of December 1981. A complete listing of these publications is published in the *Canadian Journal of Fisheries and Aquatic Sciences*, Volume 39: Index to Publications 1982. The current series, which begins with report number 1, was initiated in January 1982.

Rapport technique canadien sur l'hydrographie et les sciences océaniques

Les rapports techniques contiennent des renseignements scientifiques et techniques qui constituent une contribution aux connaissances actuelles, mais qui ne sont pas normalement appropriés pour la publication dans un journal scientifique. Le sujet est généralement lié aux programmes et intérêts du service des Sciences et levés océaniques (SLO) du ministère des Pêches et des Océans.

Les rapports techniques peuvent être cités comme des publications complètes. Le titre exact paraît au-dessus du résumé de chaque rapport. Les rapports techniques sont résumés dans la revue *Résumés des sciences aquatiques et halieutiques*, et ils sont classés dans l'index annuel des publications scientifiques et techniques du Ministère.

Les rapports techniques sont produits à l'échelon régional, mais numérotés à l'échelon national. Les demandes de rapports seront satisfaites par l'établissement auteur dont le nom figure sur la couverture et la page du titre. Les rapports épuisés seront fournis contre rétribution par des agents commerciaux.

Les établissements des Sciences et levés océaniques dans les régions et à l'administration centrale ont cessé de publier leurs diverses séries de rapports en décembre 1981. Une liste complète de ces publications figure dans le volume 39, Index des publications 1982 du *Journal canadien des sciences halieutiques et aquatiques*. La série actuelle a commencé avec la publication du rapport numéro 1 en janvier 1982.

Canadian Technical Report

Hydrography and Ocean Sciences 149

1993

COUPLED WIND-SEA MODELS AND THEIR IMPACT ON FLUXES OF MOMENTUM, SENSIBLE HEAT AND LATENT HEAT

by

Liangming Wang[1]
and
W. Perrie

Physical and Chemical Sciences Branch
Scotia-Fundy Region
Department of Fisheries and Oceans
Bedford Institute of Oceanography
P.O. Box 1006
Dartmouth, N.S.
Canada B2Y 4A2

---

[1]NO. 8, Da Hui Si, Hai Dian Division, National Research Center for Marine Environment Forecasts, Beijing, P.R. of China, 100081. (Presently visiting at Bedford Institute of Oceanography).

Cat. No. Fs 97-18/149E ISSN 0711-6764

Correct citation for this publication:

Wang, L. and W. Perrie. 1993. Coupled wind-sea models and their impact on fluxes of momentum, sensible heat and latent heat. Can. Tech. Rep. Hydrogr. Ocean Sci. 149: viii + 131 pp.

TABLE OF CONTENTS

List of Figures

List of tables

ABSTRACT

Wang, L. and W. Perrie. 1993. Coupled wind-sea models and their impact on fluxes of momentum, sensible heat and latent heat. Can. Tech. Rep. Hydrogr. Ocean Sci. 149: viii + 131 pp.

In this report, we discuss coupled models for the atmospheric boundary layer and wind-sea in one-dimension and in two-dimensions. A coupling mechanism for the interactions between boundary layer and sea surface layer is proposed. Various characteristics of this mechanism are discussed.

The coupled wind-sea model is used to estimate, study and discuss the fluxes of momentum, sensible heat and latent heat. A new mechanism for calculating these fluxes is proposed, after considering the impacts of the sea state on calculated fluxes.

Results show that the influence of sea states on sea surface roughness Z_o is very important for younger waves. The forecasted significant wave heights are clearly improved and the fluxes are increased in the coupled model, as compared to the uncoupled WAM model, particularly under stronger wind speeds.

RESUME

Wang, L. and W. Perrie. 1993. Coupled wind-sea models and their impact on fluxes of momentum, sensible heat and latent heat. Can. Tech. Rep. Hydrogr. Ocean Sci. 149: viii + 131 pp.

Le présent rapport traite de modèles unidimensionnels et bidimensionnels de couplage de la couche limite atmosphérique et de l'interface vent-mer. On y propose un mécanisme de couplage pour les interactions entre la couche limite et la couche de la surface de la mer. Diverses caractéristiques de ce mécanisme sont abordés.

Le modèle de couplage du vent et de la mer sert à estimer, à étudier et à analyser les flux de quantité de mouvement, de chaleur sensible et de chaleur latente. Un nouveau mécanisme est proposé pour calculer ces flux en tenant compte des effets de l'état de la mer sur ces calculs.

Les résultats montrent que l'effet des états de la mer sur la rugosité de la surface de la mer Z_o est très important dans le cas des jeunes vagues. Les prévisions de la hauteur significative des vagues sont nettement meilleures et les flux sont plus grands dans le modèle de couplage que dans le modèle WAM sans couplage, surtout lorsque la vitesse du vent est élevée.

1. INTRODUCTION

Experience shows that the forecasting of significant wave height using the WAM third generation model is usually lower by about 25-40 percent from the observations, especially in these cases where the wind speed is very strong or wind direction is suddenly changed (this will be presented also here). Although the wind speed and direction predicted in meteorological models may need some improvements, the WAM model should also have some improvements physically.

There are three inconsistencies the WAM model has. First of all, the WAM model uses the wind speed at 10 m height V_{10}, to produce a friction velocity U^* which is then used to predict the significant wave height. However, this V_{10} is produced by a meteorological boundary layer model using the friction velocity U^*, sea surface roughness Z_0 and some thermal conditions. The friction velocity U^* in the wave model is produced by empirical formulae which are obtained at specific locations, specific times and for specific cases and this U^* is not the same as the U^* in the atmospheric model. Secondly, the roughness Z_0, is dependent on the wind profile with height rather than the wind itself at 10 meters above the sea level. The WAM model uses the Charnock formula which states that Z_0 depends only on the wind speed at 10 m height. If we have two different wind profiles with height but they have the same wind speed at 10 meters above the sea level, the forecasting of significant wave height is the same in the WAM model, although it is under different conditions physically. This is unreasonable. Thirdly, the reaction of sea states on the wind profile with height is not taken into account in the WAM third generation model.

On the other hand, the geostrophic wind, in meteorology, is used to express the balance relationship between the gravitational potential field and the wind field. The thermal wind is used to express the balance relationship between the change of wind with height and the mean temperature field. The question remains as to the relationship between the wind profile with height and the sea states. The solution is to couple the wave model with the boundary layer model.

The calculated wind over the sea surface in meteorological models will be shown to be revised when the roughness of the sea surface is considered as a function of sea state. We assume that the revised wind is in such a balance state; that the roughness, friction velocity and wave age are in a balance state, that these variables have the same values in the boundary layer model as in the wind-sea model. We use such a roughness, friction velocity and revised thermal variables to calculate the revised wind. The revised wind is therefore shown to be a consequence of the sea state dependence of the sea surface roughness Z_0.

2. A MECHANISM ON COUPLING WIND AND SEA WAVE

The dynamic coupling between the atmosphere and the ocean has been the subject of much research. Although the effects of some characteristic properties are becoming more clear, the extremely complex processes of air-sea interaction are still not fully understood. The best-known expression for the roughness of the sea surface Z_o is the one proposed by *Charnock* (1955), which indicated that the roughness of the sea surface depends only on friction velocity: all characteristics of the wave field are missing. Several field data sets show different constants for *Charnock* formula. *Wu* (1980) proposed a value of 0.0185 as shown in Eq.(2.1) after averaging different constants from a wide range of circumstances.

$$Z_o = 0.0185 \times \left\{ \frac{U_*^2}{G} \right\} \qquad (2.1)$$

Several studies from laboratories and from the field (Toba and Koga, 1986; Toba et al. 1990; Geernaert et al. 1987 show that the wave age C_p/U_* (in which C_p is the phase velocity of the wave at the peak of the spectrum and U_* is the friction velocity in the air) is an important parameter for the description of roughness Z_o. They claim that the roughness actually decreases with decreasing wave age as expressed in Eq.(2.2),

$$Z_o = 0.025 \times \left\{ \frac{C_p}{U_*} \right\} \times \left\{ \frac{U_*^2}{G} \right\} \qquad (2.2)$$

which shows the roughness is in direct proportion to wave age.

Nordeng (1991) proposed that the roughness depends strongly on wave age with a maximum value for C_p/U_* around 5, for a young sea, and it is a function of wave age as shown in Eq. (2.3).

$$Z_o = 0.11 \times \left\{ \frac{C_p}{U_*} \right\}^{-3/4} \times \left[1 - e^{-W} \left(1 + \frac{W^2}{2} + \frac{W^3}{6} \right) \right]^{1/2} \left\{ \frac{U_*^2}{G} \right\} \qquad (2.3)$$

where $W = 2 \times \kappa \left\{ \frac{C_p}{U_*} \right\}$, and κ is the Von Kármán constant.

From the HEXMAX 1986 field data set, Maat et al., (1991) proposed that the roughness is assumed to depend mainly on the wave age in a relationship of the form:

1. INTRODUCTION

Experience shows that the forecasting of significant wave height using the WAM third generation model is usually lower by about 25-40 percent from the observations, especially in these cases where the wind speed is very strong or wind direction is suddenly changed (this will be presented also here). Although the wind speed and direction predicted in meteorological models may need some improvements, the WAM model should also have some improvements physically.

There are three inconsistencies the WAM model has. First of all, the WAM model uses the wind speed at 10 m height V_{10}, to produce a friction velocity U^* which is then used to predict the significant wave height. However, this V_{10} is produced by a meteorological boundary layer model using the friction velocity U^*, sea surface roughness Z_0 and some thermal conditions. The friction velocity U^* in the wave model is produced by empirical formulae which are obtained at specific locations, specific times and for specific cases and this U^* is not the same as the U^* in the atmospheric model. Secondly, the roughness Z_0, is dependent on the wind profile with height rather than the wind itself at 10 meters above the sea level. The WAM model uses the Charnock formula which states that Z_0 depends only on the wind speed at 10 m height. If we have two different wind profiles with height but they have the same wind speed at 10 meters above the sea level, the forecasting of significant wave height is the same in the WAM model, although it is under different conditions physically. This is unreasonable. Thirdly, the reaction of sea states on the wind profile with height is not taken into account in the WAM third generation model.

On the other hand, the geostrophic wind, in meteorology, is used to express the balance relationship between the gravitational potential field and the wind field. The thermal wind is used to express the balance relationship between the change of wind with height and the mean temperature field. The question remains as to the relationship between the wind profile with height and the sea states. The solution is to couple the wave model with the boundary layer model.

The calculated wind over the sea surface in meteorological models will be shown to be revised when the roughness of the sea surface is considered as a function of sea state. We assume that the revised wind is in such a balance state; that the roughness, friction velocity and wave age are in a balance state, that these variables have the same values in the boundary layer model as in the wind-sea model. We use such a roughness, friction velocity and revised thermal variables to calculate the revised wind. The revised wind is therefore shown to be a consequence of the sea state dependence of the sea surface roughness Z_0.

$$Z_o = \mu \times \left(\frac{U_*^2}{G} \right) \times \left(\frac{C_p}{U_*} \right)^n \qquad (2.4)$$

Several results may be summarized as follows:

(1). Charnock (1958)
$n = 0, \quad \mu = 0.012$

(2). Wu (1980)
$n = 0, \quad \mu = 0.0185$

(3). Toba and Koga (1986)
$n = 1, \quad \mu = 0.025$

(4). Hsu (1974, 1986)
$n = -1/2, \quad \mu = 0.90$

(5). Maat et al.,(1991) proposed a relationship from HEXMAX data, which shows :
$n = -1, \quad \mu = 0.80$

(6). Donelan (1990) reviewed several earlier published data and calculated the ratio Z_o/H_s as a function of wave age C_p/U_*, which also implies : $n \cong -1$.

(7). Theoretical studies with numerical models based on resonant wave-mean flow interaction and the quasilinear theory of wind-wave generation, Janssen (1989) calculated the effect of both gravity waves and air turbulence on the wind profile, which provides an exponent $n = -1.2$.

Recently, Smith et al., (1992) applied corrections to the HEXOS data for flow distortion and revised the Maat et al. formula and set $\mu = 0.48$ instead of 0.80. Therefore, roughness decreases with increasing wave age.

Fig.1a-c show the changes of surface roughness with wave age using different relationships as mentioned above. In these figures, "Wu" is calculated by Eq.(2.1), "RPN" is calculated using 0.032 instead of 0.0185 in Eq.(2.1). The operational model at RPN uses 0.032. Toba's result in Fig.1a shows that the older waves are rougher than younger waves. Donelan et al., (1993) pointed out that the conclusion is inappropriate and misleading. Scaling with U_* is unreliable because significant variations in U_* will produce a spurious correlation, masking the sought-after relation between roughness and sea state.

Hsu's result in Fig.1b seems also inappropriate. Although the roughness is decreasing with increasing wave age, the roughness is always greater than those calculated by "RPN" and "Charnock" which had support from field data. Nordeng's result is always less than Charnock's except when the wave age is less than 10.

Smith's result (see Fig.1c) seems reasonable. Wu's formula is the same as Smith's with the wave age around 26. RPN's parameterization is the same as Smith's with the wave age nearly 15. This indicates that the Charnock "CONSTANT" as selected as constant at any time or any location is unreasonable. The Charnock "CONSTANT" should be controlled by a sea state equation, such as the sea wave equation.

In this paper, we use Wu's formula Eq.(2.1) to calculate the roughness in our UNCOUPLED MODEL, and Smith's formula, which is expressed as follows :

$$Z_o = 0.48 \times \left\{\frac{C_p}{U_*}\right\}^{-1} \times \left\{\frac{U_*^2}{G}\right\} \qquad (2.5)$$

in our COUPLED MODEL.

3. WAVE AND BOUNDARY LAYER MODELS

3.1 Third generation wave (WAM) model

We integrate the spectral energy balance equation for wind-generated waves in time. We use the formulations of the **WAM** model (Hasselmann et al., 1989) for non-linear transfer, energy input due to the wind, and energy removed due to dissipative breaking.

The spectral energy density for surface gravity waves in deep water $E(f,\theta)$ evolves in space and time according to the relation

$$\frac{\partial E(f,\theta)}{\partial t} + \underline{c}_g \cdot \nabla E(f,\theta) = \varphi_{in} + \varphi_{nl} + \varphi_{ds} \qquad (3.1)$$

where φ_{in} is the spectral energy input by the wind, φ_{ds} is the dissipation due to wave breaking and white-cap formation and φ_{nl} is the change in spectral energy due to non-linear transfer resulting from wave-wave interactions.

Parameterizations for wind input energy φ_{in} are heavily motivated by the observations of Snyder et al (1981). The form is

$$\varphi_{in} \cong \beta\ E(f,\theta) \tag{3.2}$$

where β, as specified by Hasselmann et al (1989), is given by

$$\beta = \max\left\{0,\ 0.25\ \frac{\rho_a}{\rho_w}\ \left(\ 28\ \frac{U^*}{\zeta}\ \cos\ \theta\ -\ 1\ \right)\ \right\}\ \omega \tag{3.3}$$

where ρ_a and ρ_w are air and water density respectively, the friction velocity in the wave direction is $U^*\cos\theta$ with θ the direction of the wind relative to the wave propagation direction, phase velocity is $\zeta = \omega/k$ and angular frequency ω is related to wavenumber k through the deep water dispersion relation.

Dissipation due to wave breaking φ_{ds} is assumed to have a simple form, motivated by Hasselmann (1974), as well as numerical experiments completed in Hasselmann et al (1989), and may be written as follows:

$$\varphi_{ds} \cong g\ k^{-4}\ \mathcal{F}(k^4 F(\underline{k})) \tag{3.4}$$

where $k=|\underline{k}|$, $F(\underline{k})$ is the energy spectrum in vector wavenumber space $\underline{k}$ and $\mathcal{F}$ is an appropriate functional. It is usually taken as

$$\mathcal{F}_{ds} = -2.33 \times 10^{-5}\ \hat{\omega}\ \left(\frac{\omega}{\hat{\omega}}\right)^2\ \left(\frac{\hat{\alpha}}{\hat{\alpha}_{pm}}\right)^2\ \ E(f,\theta) \tag{3.5}$$

where

$$\hat{\omega} = \left(\ E_0^{-1}\ \iint\ E(f,\theta)\ \omega^{-1}\ df\ d\theta\ \right)^{-1} \tag{3.6}$$

$$\hat{\alpha} = E_0 \hat{\omega}^4 g^{-2}\ , \qquad E_0 = \iint\ E(f,\theta)\ df\ d\theta \tag{3.7}$$

and

$$\hat{\alpha}_{pm} = \frac{2}{3}\ E_0\ g^{-2}\ \left(\ E_0^{-1}\ \iint\ E(f,\theta)\ \omega df d\theta\ \right)^4\Big|_{\text{Pierson-Moskowitz}} \tag{3.8}$$

$$\cong 0.003$$

The complete representation for non-linear transfer due to wave-wave interactions φ_{nl} can be represented in term of a 6-fold Boltzmann integral in wavenumber space by Hasselmann (1961),

$$\mathcal{F}_{nl}(\underline{k}_1) = \iiint \zeta^2(\underline{k}_1,\underline{k}_2,\underline{k}_3,\underline{k}_4)\mathcal{D}(\underline{k}_1,\underline{k}_2,\underline{k}_3,\underline{k}_4)$$

$$\delta(\underline{k}_1+\underline{k}_2-\underline{k}_3-\underline{k}_4)\,\delta(\omega_1+\omega_2-\omega_3-\omega_4)\,d\underline{k}_2 d\underline{k}_3 d\underline{k}_4 \qquad (3.9)$$

The **WAM** approximation to equation (3.9) is described in Hasselmann et al (1989) and is based on the so-called discreted interaction approximation.

The two-dimensional wave spectrum $E(f,\theta)$ at every grid point is represented by 54 frequencies and 12 directions for a total of 648 spectral elements. The 54 frequencies range from 0.0417725 Hz to 0.65268 Hz increasing in geometric progression with a constant ratio of 1.1. The 12 directional bands have a bandwidth of 30 degrees everywhere.

The significant wave height is given by the total wave energy Eo as expressed

$$H_s = 4.0\sqrt{E_o} \qquad (3.10)$$

The total energy Eo can be obtained by summing $E(f,\theta)$ values over all frequency and directional bands.

3.2 Wave spectrum with frequency

We use an experimental spectrum (3.11) to compare with the Pierson-Moskowitz spectrum (3.12), JONSWAP -3/2 law (3.13) and JONSWAP -2/3 law (3.14). They are expressed as follows respectively :

(1). NEW SPECTRUM

$$F(f) = 0.48\left(\frac{C_p}{U^*}\right)^{-1} g^2 (2\pi)^{-4} f^{-5} \exp\left\{-\frac{5}{4}\left(\frac{f_p}{f}\right)^4\right\} \qquad (3.11)$$

(2). Pierson-Moskowitz SPECTRUM

$$F(f) = 0.0081\, g^2 (2\pi)^{-4} f^{-5} \exp\left\{-\frac{5}{4}\left(\frac{f_p}{f}\right)^4\right\} \times$$

$$\gamma \exp\left(-\frac{(f-f_p)^2}{2\sigma^2 f^2}\right) \qquad (3.12)$$

(3). JONSWAP -3/2 law

$$F(f) = 0.57 \left(\frac{C_p}{U^*}\right)^{3/2} g^2 (2\pi)^{-4} f^{-5} \exp\left\{-\frac{5}{4}\left(\frac{f_p}{f}\right)^4\right\} \times$$

$$\gamma \exp\left(-\frac{(f-f_p)^2}{2\sigma^2 f^2}\right) \qquad (3.13)$$

(4). JONSWAP -2/3 law

$$F(f) = 0.054 \left(\frac{C_p}{U^*}\right)^{-2/3} g^2 (2\pi)^{-4} f^{-5} \exp\left\{-\frac{5}{4}\left(\frac{f_p}{f}\right)^4\right\} \times$$

$$\gamma \exp\left(-\frac{(f-f_p)^2}{2\sigma^2 f^2}\right) \qquad (3.14)$$

Equations (3.13) and (3.14) are employed by Janssen (1989), using different interpretations of the JONSWAP results of Hasselmann et al (1973). Fig. 2a-b show the wave spectrum with frequency at different wind speeds (10 m/s, Fig.2a; and 20 m/s, Fig.2b). It is shown that the energy is higher in (3.11) than the other spectra in the higher frequency region. The peak frequency will move toward lower frequency when the wind speed increases.

3.3 Boundary-layer model

The boundary layer model used here is quite similar to the operational boundary layer model at RPN, as documented by Delage (1988a, 1988b).

The vertical surface fluxes of momentum, sensible heat and latent heat are computed from surface (i.e., subscript s), which can be written as follows respectively,

$$\overline{|w'V'|}_s = (C_m|V_a|)^2 \qquad (3.15)$$

$$\overline{(w'T')}_s = C_p C_m C_T |V_a| (T_s - T_a) \qquad (3.16)$$

$$\overline{(w'q')}_s = L\, C_m C_T |V_a| (q_s - q_a) \qquad (3.17)$$

Here C_m, C_T are transfer coefficients for momentum and heat and are functions of the Richardson number Ri_b, anemometer level Z_a and roughness Z_0. The L is latent heat and C_p is specific heat at constant pressure.

In the stable case, the transfer coefficients can be written as

$$C_m = \frac{\kappa}{\zeta_a} F_m \tag{3.18}$$

$$C_T = \frac{\kappa}{\zeta_a} F_T \tag{3.19}$$

Here κ=0.035 is Von Kármán constant and $\zeta_a = \ln\left(\frac{Z_a + Z_0}{Z_0}\right)$, Z_a is the reference level and F_M and F_T are transfer functions given below. Empirical expressions for F_m and F_T were selected for their ability to simulate the Wangara data (Delage, 1988a, 1988b).

$$F_m = 1 - \frac{Ri_b}{M}\left(\frac{2}{1+(1+\frac{2x}{M})^{1/2}}\right) \tag{3.20}$$

$$F_T = 1 - \frac{Ri_b}{M}\left(\frac{2}{1+(1+\frac{2x'}{M})^{1/2}}\right) \tag{3.21}$$

where $M = \mathrm{Max}(Ri_c, Ri_b + 1/a)$, $Ri_c = 0.2$ and $a = 10.0$; $x = \zeta_a z_* d/H$, $x' = \zeta_a z_* d'/H$, $z_* = \mathrm{Max}(Z_a - 10m, 0)$, d and d′ are parameters, H is the height of boundary layer.

In the unstable case, the functions for momentum and heat exchange at the surface are calculated as follows:

$$C_m = 1/FQ \tag{3.22}$$

$$C_T = 1/FH \tag{3.23}$$

where

$$FQ = \ln\left(\frac{Z_a+Z_0}{Z_0}\right) + \ln\left\{\frac{(X_0+1)^2\,(X_0^2-X_0+1)^{1/2}\,(X_0^2+X_0+1)^{3/2}}{(X+1)^2\,(X^2-X+1)^{1/2}\,(X^2+X+1)^{3/2}}\right\} + \sqrt{3}\left\{\tan^{-1}\left(\sqrt{3}\,\frac{(X^2-1)\,X_0-(X_0^2-1)\,X}{(X_0^2-1)(X^2-1)+3XX_0}\right)\right\} \tag{3.24}$$

$$FH = \ln\left(\frac{Z_a+Z_{OT}}{Z_{OT}}\right) + \frac{3}{2}\ln\left\{\frac{Y_0^2+Y_0+1}{Y^2+Y+1}\right\} + \sqrt{3}\tan^{-1}\left(\sqrt{3}\,\frac{2(Y-Y_0)}{(2Y_0+1)(2Y+1)+3}\right) \quad (3.25)$$

where

$$X = \left\{1-40.0 \times \left(Z_a+Z_0\right) \times \frac{\kappa \times C_T \times Rib}{C_m^2 \times Z_a}\right\}^{1/6} \quad (3.26)$$

$$X_0 = \left\{1-40.0 \times Z_0 \times \frac{\kappa \times C_T \times Rib}{C_m^2 \times Z_a}\right\}^{1/6} \quad (3.27)$$

$$Y = \left\{1-40.0 \times \left(Z_a+Z_{OT}\right) \times \frac{\kappa \times C_T \times Rib}{C_m^2 \times Z_a}\right\}^{1/3} \quad (3.28)$$

$$Y_0 = \left\{1-40.0 \times Z_{OT} \times \frac{\kappa \times C_T \times Rib}{C_m^2 \times Z_a}\right\}^{1/3} \quad (3.29)$$

The boundary layer model implies the drag coefficient C_d depends mainly on the roughness Z_0 rather than the wind speed at a desired anemometer level Z_a under neutral conditions as in equation (6.5) below. It is important to mention this result because there are many empirical relations which attempt to show a relation between drag coefficient and wind speed, such as equation (6.4) below from Hsu (1986). Fig 3 shows the change of drag coefficient C_d with wind speed at different roughness Z_0. The values for C_d ($=C_M*C_M$ as shown in Eq. 3.15) are all constant at a designated Z_0 whatever the wind speed is. On the other hand, the roughness Z_0 is not dependent directly on the increasing wind speed either in the UNCOUPLED model or in the COUPLED model. It is dependent on wind profile with height (in the UNCOUPLED model) and sea states, such as wave age (in the COUPLED model). It is necessary to point out that the wave age also not depends directly on wind speed. The wave age will be change with time under a constant wind speed. Therefore, empirical relationships between drag coefficient and wind speed should not be imposed upon a model without a great amount of care, or inconsistencies will result.

Fig. 4 shows the variation of the coefficient of heat exchange C_MC_T with wind speed. The coefficient of heat exchange C_MC_T (as seen in Eqs. 3.16, 3.17) also depends mainly on roughness Z_0 according to the boundary layer model at a desired anemometer level Z_a under neutral conditions.

Figs. 5 and 6 show the friction velocity U_* and flux of momentum FM change with increasing wind speed at different designated roughness Z_o respectively.

In the unstable case, Fig. 7-10 show the changes of corresponding drag coefficient C_d, coefficient of heat exchange $C_M C_T$, friction velocity U_* and flux of momentum FM at different temperature differences. The Fig. 11 is for flux of sensible heat FS. It is interested to find from Figs.7-10 that the drag coefficient C_d, the coefficient of heat exchange $C_M C_T$, the friction velocity U_* and the flux of momentum FM are largely insensitive to the magnitude of the temperature differences at high winds. The flux of sensible heat FS, as shown in Fig. 11, is sensitive to temperature differences at all wind speeds.

Fig. 12 shows the change of drag coefficient C_d with wave age at different roughness Z_o in the neutral case. It is seen that the drag coefficient is unchangeable under designated roughness not only for wind speed but also for wave age. However, the drag coefficient is indirectly changed with wave age through roughness. It will be shown that the drag coefficient is decreased when the wave age increases, and in turn, the roughness increases, as the sea state evolves and matures.

Fig. 13-15 show the changes of coefficient of heat exchange, friction velocity and flux of momentum with wave age respectively.

Fig. 16-19 show the variation of the drag coefficient, and the coefficient of heat exchange, the friction velocity and the flux of momentum respectively at different temperature difference with wave age. Fig. 20 is for the case of flux of sensible heat. From these figures, it will be seen that the drag coefficient, the coefficient of heat exchange and the flux of sensible heat change under unstable case, especially under older wave age conditions. It is also interested that only the flux of sensible heat is sensitive for the younger waves.

4. COUPLED ONE-POINT MODEL

Our COUPLED ONE-POINT MODEL is essential for duration-limited waves, evolving in response to forcing by wind that is initiated at an initial time. For a very large ocean, observations at very large fetch ($>> 10^3$ km) will not experience advective effects. We assume that

$$\underline{C}_g \cdot \nabla E(f,\theta) << \varphi_{in} + \varphi_{nl} + \varphi_{ds} \qquad (4.1)$$

then, Eq.(3.1) may be written as follows :

$$\frac{\partial E(f,\theta)}{\partial t} \cong \varphi_{in} + \varphi_{nl} + \varphi_{ds} \qquad (4.2)$$

which is valid for growing windsea spectra at large fetch and we

can use this simple coupled model to explore some basic characteristics in comparison with the corresponding uncoupled model.

First of all, we assume that the wind speed and direction are unchanged with time. The peak frequency will be obtained through the wave model. If a first guess roughness z_0 is assumed, the friction velocity U_* or drag coefficient C_d will be obtained from the boundary layer model. Therefore, a 'new' roughness is calculated using the Charnock formula (2.1) in the uncoupled model and Eq.(2.5) in the coupled model. If this 'new' roughness is within allowable error relative to the old roughness, we may proceed to the next time step in the simulation. Otherwise we must iterate, and using C_d, U_* and the wave model recompute the peak frequency. The boundary layer model then leads to a new estimates for C_d and U_*. Thence, Eq. (2.5) leads to a re-estimate of the roughness.

Fig. 21a-c show the change of roughness z_0 with wave age at different constant wind speed V_{10}=10 m/s (Fig.21a), V_{10}=20 m/s (Fig.21b) and V_{10}=30 m/s (Fig.21c). It is seen that the roughness is decreased with increasing wave age under constant wind speed. This indicates that the roughness is not a direct function of wind speed. As we have pointed out in section 3.3, the drag coefficient is a function of only roughness under neutral conditions. The drag coefficient C_d also is changed with changed roughness even when the wind speed keeps constant in the coupled model.

Fig. 22a-c show the change of roughness z_0 with time at different constant wind speed V_{10}=10 m/s (Fig.22a), V_{10}=20 m/s (Fig.22b) and V_{10}=30 m/s (Fig.22c). It is very interested to see from Figures 21 and 22 that Wu's roughness formula Eq.(2.1) is the same as Smith's formula Eq.(2.5) at wave age about 26 in wind speed V_{10}=10 m/s, 20 m/s cases and takes about 17 hours at V_{10}=10 m/s and 22 hours at V_{10}=20 m/s case. However at V_{10}=30 m/s even in 100 hours (see fig. 21c and 22c) Wu's formula has no crossover with that of Smith. This seems to indicate that the Wu's formula is suitable only at older wave age. It seems unsuitable for younger waves, especially under very strong wind speed as simulated by the coupled model. Alternately the integration grid used in this computation is probably not adequate to model 30 m/s winds.

Fig. 23a-c and 25a-c show the change of drag coefficient C_d and friction velocity U_* with wave age. Fig. 24a-c, 26a-c show their changes with time respectively. In these figures, the a, b and c represent wind speed at V_{10}=10 m/s, V_{10}=20 m/s and V_{10}=30 m/s respectively. It can be seen that in the coupled model the drag coefficient and friction velocity change at constant wind speed condition and they have a same value with uncoupled corresponding cases at wave age at about 23 under V_{10}=10 m/s and V_{10}=20 m/s (see Figs. 23a, 23b and 25a, 25b). This is corresponding to about 14 hours at V_{10}=10 m/s (see Figs. 24a and 26a) and about 19 hours at V_{10}=20 m/s (see Figs. 24b and 26b). The

coupled model never return to Wu's case when the wind speed is at V_{10}=30 m/s (see Figs. 23c and 25c), even after 100 hours (see Figs. 24c and 26c), which may be a problem of the computational grid that needs further work.

Fig. 27a-c show the change of forecasted significant wave height H_s with time at constant wind speed using logarithmic coordinate for V_{10}=10 m/s (Fig.27a), V_{10}=20 m/s (Fig.27b) and V_{10}= 30 m/s (Fig.27c) respectively. Fig. 28a-c is the same with Fig. 27a-c, but using linear coordinates. All calculations mentioned above are under the neutral stable condition. The differences in forecasted significant wave height by means of the coupled and uncoupled models are obvious, especially under strong wind speed.

From table 1, we can see that the maximum difference between using coupled and uncoupled model for the forecasted significant wave height reaches about three meters under strong wind at the neutral stable case.

In the unstable case, the influences of instability on the changes for roughness Z_o, drag coefficient C_d, coefficient of heat exchange C_MC_T and friction velocity with wave age are shown on Figs. 29a-c to 32a-c respectively. The signs a, b, c on these figures are expressed at wind speed V_{10}=10 m/s, V_{10}=20 m/s and V_{10}=30 m/s respectively. The DT on these figures is the difference between air temperature T_a and sea surface temperature T_s ($DT=T_a-T_s$).

In the unstable case, the differences in forecasted significant wave height between the coupled and uncoupled model are more obvious. Fig. 33a-b show the differences under various conditions. In these figures, the $DT=T_a-T_s$, $DQ=Q_a-Q_s$ at wind speed V_{10}=20 m/s. The influences of unstable conditions are greater in coupled model (Fig.33b) than the corresponding ones in the uncoupled model (Fig.33a).

Another important fact, which influences the forecasted significant wave height, is the selection of anemometer level Z_a, Z_a=10 meter is used in this paper except where noted. Fig. 34a-b shows the differences at V_{10}=30 m/s (Fig.34a for log coordinate and 34b for linear coordinate). The maximum difference is about 3.5 meter between Z_a=5 m and 50 m). Table 2 shows corresponding forecasted significant wave height at various cases.

Fig. 35a-b show the change of spectral density with frequency at different time for coupled model (Fig.35a) and uncoupled (Fig.35b) respectively. From these figures we can seen the peak frequency is decreasing with increasing time, so that the wave age will increase and the roughness will decrease with time.

The vertical profile of wind speed with time is unchanged in the uncoupled model. In the coupled model due to the changes of roughness and friction velocity the vertical profile of wind speed changes with time. Figs. 36a-c (log coordinate) and 37a-c (linear

coordinate) show these variations corresponding to wind speed V_{10}=10 m/s (36a,37a), V_{10}=20 m/s (36b,37b) and V_{10}=30 m/s (36c,37c) and t=10, 20 and 30 hours respectively.

5. COUPLED WIND-SEA MODEL

In this paper, the uncoupled model is the third generation **WAM** model (Hasselmann et al., 1989). In this wave model the spectral energy balance equation (Eq.3.1) is integrated for wind-generated waves in time for duration-limited growth and the roughness is calculated by Wu's formula Eq. (2.1). Since the roughness is a constant at constant wind speed and it is independent on sea states, such as wave age, significant wave height etc, we call it an uncoupled model. In the coupled model, the roughness is calculated by Smith's formula Eq. (2.5) and it is changed as the wave age changes, even at constant wind speed. The coupled method is described in section **4** (one-point model).

The model's grid is selected in the northwest Atlantic, on a transverse Mercator projection with an assumed equator at 51°W and a grid spacing of 119 km near Halifax, Nova Scotia. The grid consists of 160 points of which 139 are water points, at which model parameters are generated. These grids coincide with the coarse grids of the Canadian Spectral Ocean Wave Model (CSOWM). Fig. 38a shows the coarse grid of the CSOWM covering the northwest Atlantic. The points in a box with thick line are used in this model. Fig. 38b shows the grids we used in this report. The sign " ▸ " is the location of buoy number **44138** and sign " • " for **44139**.

The input data for every grid point are as follows :

1. WDDR—— wind direction.
2. WDSP—— wind speed.
3. ZANG—— the zenith.
4. ALAT—— the latitude of grids.
5. ALONG—— the longitude of grids.
6. DEPTH—— the water depth

The main output two dimension (x and y direction) data are as follows :

1. USTYX——two dimensional friction velocity (every 12 hours).
2. Z0YX——two dimensional roughness (every 12 hours).
3. CDYX——two dimensional drag coefficient (every 12 hours).
4. FPYX——two dimensional peak frequency (every 12 hours).
5. HTYX——two dimensional forecasted significant wave height (every 12 hours).
6. FQYX——two dimensional flux of momentum (every 12 hours).
7. FVYX——two dimensional flux of latent heat (every 12 hours).
8. FCYX——two dimensional flux of sensible heat (every 12 hours).
9. FL3 ——two dimensional frequency-direction spectrum, which is printed out at any time you want.

You must write FL3, USTYX, Z0YX and FPYX at the last time step when you want to continue to calculate the next time step and change some parameters related with time in this model.

6. A MECHANISM OF IMPACT ON FLUXES OF MOMENTUM, SENSIBLE HEAT AND LATENT HEAT

What does the drag coefficient (C_d) depends on ? There are several empirical formulae about the relationship between C_d and wind speed V_{10} at 10 meters above the sea level. As we discussed in section 3.3, the drag coefficient C_d depends mainly on the roughness Z_0 rather than the wind speed at a desired anemometer level Z_a under neutral condition in this model. It (C_d) is unchanged at a designated roughness Z_0 although the wind speed may be increasing. It is also noticed that the roughness Z_0 is a function of friction velocity U^* and wave age rather than wind speed and that the roughness Z_0 can also be changed under constant wind speed. This seems to indicate that the drag coefficient C_d is not a direct function of wind speed.

Therefore, the drag coefficient (C_d), which influences the fluxes of momentum, heat and water vapour, depends on

1. the changes of wind speed with height $\left(\frac{\partial U}{\partial z}\right)$, not the wind speed itself at 10 meters.
2. Sea states, such as wave height, wave age and so on.
3. the thermal conditions or instability.

We use $$C_d = C_d(Z_0, Z_{0T}) \qquad (6.1)$$

where $$Z_0 = Z_0(U^*, \text{SEA STATE}) \qquad (6.2)$$

Z_{0T} is expressed as thermal conditions

U^* is the friction velocity

IN NEUTRAL OR STABLE CASES, the drag coefficient only depends on **ROUGHNESS** Z_0, which means

$$C_d = C_d\,(Z_0) \qquad (6.3)$$

HSU has a relationship between C_{d10} and V_{10} (Hsu, 1986 Eq. 35).

$$C_{d10} = \left\{\frac{0.4}{14.56 - \ell n\ V_{10}}\right\}^2 \qquad (6.4)$$

but, according to Hsu's Eq.(7) and (8) in the same paper under neutral condition, we have:

$$C_d = \left(\frac{U^*}{U_z}\right)^2 = \left\{\frac{\kappa}{ln\left(\frac{z}{z_0}\right)}\right\}^2 \qquad (6.5)$$

which shows that the drag coefficient C_d also only depends on roughness Z_0 at desired level Z.

In this paper we discuss only the case $Z_0 = Z_{0T}$. The general expression and characteristics of the thermal roughness Z_{0T} will be discussed in another paper. The coefficient of heat exchange calculated by Eq.(3.21) shows that it is also only dependent on roughness Z_0 in the neutral stable cases and at a designated level Z_a.

In the unstable case, from Eqs. (3.15) to (3.17) and from Eqs. (3.22) to (3.29) it is seen that although these expressions are more complex, the drag coefficient C_d and the coefficient of heat exchange C_MC_T are also the functions of roughness Z_0 (or thermal roughness Z_{0T}) directly and indirectly at a designated level Z_a.

The precise calculations of the drag coefficient and the coefficient of heat exchange are very important and complex. They will directly influence the calculations of momentum, sensible heat and latent heat fluxes. There is a reaction of the sea state (wave age) on roughness, and the roughness changes with changing sea state. As we discussed above, the fluxes of momentum, sensible heat and latent heat will change with changing sea state.

Figs. 39a-c to 42a-c show the various fluxes calculated by our coupled one-point model at constant wind speed . Fig. 39a-c shows momentum flux changes with wave age under neutral stable case at different wind speed V_{10}=10 m/s (fig.39a), V_{10}=20 m/s (Fig.39b) and V_{10}=30 m/s (Fig.39c). Fig. 40 shows the same but with time and the a, b, and c on figures are the same as described in Fig. 39a-c.

Figs. 41a-c show the same as in Fig. 39a-c, but in the unstable case. Fig. 42a-c show the same as in Fig. 41a-c, but for the flux of sensible heat. The DT on these figures are the difference between air and sea surface temperature ($DT=T_a-T_s$). It is seen that these fluxes are no longer a constant as calculated by uncoupled model at constant wind speed.

Table 3 lists estimates for these different cases for fluxes of momentum, sensible heat and latent heat. Under special cases, such as T_a-T_s=20 degrees or Q_a-Q_s=20 g/kg or both, these fluxes can change by a factor two. This may be useful to study the suddenly developing cyclone over the eastern coast of Canada and it seems to be worthy to couple the coupled wind-sea model with an atmospheric model to consider the changing roughness with changing sea state.

7. AN EXAMPLE FOR UNCOUPLED AND COUPLED MODEL

As a example, we use the uncoupled and coupled models mentioned above for one-point and wind-sea models. The wind data are provided by Recherche en Prévision Numérique (RPN) every three hours for the CAL/VAL period from Nov. 8 to 25, 1991. The hourly wind data are obtained by linear interpolation. The time step is 20 minutes for the one-point models and one hour for wind-sea models. The buoy data are provided by Atmospheric Environment Services (AES) in Bedford Nova Scotia.

7.1 One-point model

Fig. 43 shows the observations at buoy station number 44138 for winds (Fig.43a) and temperatures (Fig.43b). Fig. 44a shows the comparisons of observational wave heights (solid line) with the ones calculated by uncoupled model (dotted line) and coupled model (dashed line). It is seen that the forecasted significant wave heights calculated by the coupled model are closer to the observations than the ones calculated by the uncoupled model. It is interesting to notice from Fig.44b that if we use a weighted wind speed V as follows :

$$V = \left(V_{ave} \times 2.0 + V_{gust}\right) / 3.0 \qquad (7.1)$$

the forecasted significant wave heights (dot dash line) are even closer to the observations (solid line) than either the ones calculated by coupled model (dashed line) or the ones calculated by uncoupled model (dotted line).

Fig. 45a, 45b and 46 are the same as Fig. 43a, 43b and 44a respectively but at buoy station 44139.

7.2 Wind-sea model

Two dimensional wind-sea uncoupled and coupled models are calculated using the wind data provided by RPN during the CAL/VAL period. The hindcast is done for Nov. 8-25, 1991. A cyclone was just over the region between Nova Scotia and Newfoundland on Nov. 15. Fig. 47a and 47b are the wind fields at that region for Nov. 15 and 16 respectively. Fig 48a and 48b are the wind speeds corresponding to Fig. 47a and 47b respectively.

Fig. 49 shows the forecasted significant wave heights with the uncoupled model (Fig.49a) and the coupled model (Fig.49b). It is worth noticing that the maximum wave height is 7.0 meters in the coupled model and 5.9 meters in uncoupled model. The observational maximum wave height is 7.1 meters in the cyclone region, where the wind direction and wind speed are changing rapidly and the wave age is very young. In other regions, the wave

age is older, so the forecasted significant wave heights in the coupled model are almost the same as the ones in uncoupled model.

Fig 50a and 50b show the forecasted significant wave heights at grid point number 1464 and 1465 (the coarse grid number of the Canadian Spectral Ocean Wave Model in northwest Atlantic region) near the buoy station number 44138 and Fig. 51a, 51b are at grid point number 1518 and 1519 near buoy station number 44139. The forecasted results are more in accord with observations, especially on Nov. 16, 1991. The maximum wave height in the coupled model is almost the same as the observations.

Figs. 52a-b to 54a-b show the distributions of fluxes for momentum (Fig.52a,b), sensible heat (Fig.53a,b) and latent heat (Fig.54a,b) on Nov. 16, 1991. The **a** and **b** on the figures correspond to the uncoupled model and coupled model cases respectively. It is seen from these figures that the fluxes of momentum, sensible heat and latent heat in the coupled model are higher in the cyclone region and almost the same in the other region as the fluxes in the uncoupled model.

7.3 Calibrations of wind

As mentioned in meteorology, the observational wind can not be directly used in a numerical weather forecast model, it is necessary to calibrate the wind according to some equilibrium relationships, such as geostrophic balance or thermal-wind balance which expresses the balance between geopotential height and wind field or the vector difference of wind and mean temperature field between two designated levels.

We have to find a balance state between sea state and the wind near the sea. The coupled wind-sea model makes it possible to do this kind of calibration. A forecasted or observational wind can be calibrated through changing the friction velocity U^* and roughness Z_o at a required level Z_a.

Fig. 55 shows that the observational winds (dotted line) and the calibrated winds (solid line) at buoy station number 44138. Fig. 56 is the same with Fig. 55, but at buoy station number 44139. It seems to be necessary that the calibrated wind rather than observational wind may be useful for data assimilation.

8. CONCLUSIONS AND DISCUSSION

1. The effects of sea states, such as wave age, on roughness in the boundary layer are very important for the improvement of the forecasted significant wave height. The **WAM** model developed by Hasselmann et al (1989) seems only to describe the **Fully-developed** wind sea at the cases where the **WAVE AGE** (C_p/U_*) is very old. If the wind speed is not so strong, the changes in predicted significant wave height between the coupled and uncoupled models is negligible. If the wind speed is very strong ($V_{10} \geq$ 30 m/s) or the wave age is very YOUNG, the reactions of sea state on the boundary layer and its coupling mechanisms are very important to improve the wave forecasts.

2 The drag coefficient C_d is a direct function of only roughness Z_o rather than wind speed under neutral case and the roughness is a function of friction velocity and wave age (as seen in Eq. 2.5) rather than wind speed in the coupled model. This indicates that the drag coefficient C_d is not a direct function of wind speed. C_d is changed when the roughness changes with wave age. Under very strong wind speed conditions, such as 30 m/s, the drag coefficient can change by a factor two.

3. The effects of the sea states, such as wave age, on fluxes of momentum, sensible and latent heat are also very important. The fluxes are changed not only by the differences of temperature and water vapour between sea surface and air, but also by transfer coefficients, which are changed with roughness and thermal conditions rather than wind speed. The roughness is changed with vertical wind profile and wave age, so that the coefficients are changed with changing wave age. This may be very important for simulating the CANADIAN ATLANTIC STORMS over the east coast of Canada.

4. It may be very important in doing the four-dimensional data assimilation to use coupled wind-sea models, which make the sea states, such as wave age, and vertical wind profile reach a balance state with corresponding atmospheric boundary layer model values. This is a very important condition in doing data assimilation, especially in estimating the wind over sea surface.

9. ACKNOWLEDGEMENT

The Federal Panel on Energy Research and Development (PERD) of Canada provided funding for this research. The Northern Cod Fund supported L. Wang's visit to BIO.

10. REFERENCES

Charnock, H.: 1955, Wind stress on a water surface, *Quart.J. Roy. Meteorol. Soc.*, **81**, 639-640.

Charnock, H., 1958: A note on empirical wind wave formulae, *Q. J. R. Meteorol. Soc.*, **84**, 443-447.

Delage, Y., 1988a: The positioning of the lowest levels in the boundary layer of atmospheric circulation models, *Atmosphere-Ocean*, **26**, No. 3, 329-340.

Delage, Y., 1988b: A parameterization of the stable atmospheric boundary layer, *Boundary Layer Meteorology*, **43**, 365-381.

Donelan, M.A.: 1990, Air-Sea Interaction, in B. LeMehaute and D. Hanes(Eds.), *The Sea: Ideas and observations on Progress in the Study of the Seas*, Vol.9, to be published by Wiley-Interscience, New York.

Donelan, M.A., F.W. Dobson., S.D. Smith and R.J. Anderson, 1993: On the dependence of sea surface roughness on wave development. *J. Phys. Oceanogr.*, **23**, 2143-2149.

Geernaert, G. L., S. E. Larsen, and F. Hansen, 1987: Measurements of the wind stress, heat flux, and turbulence intensity during storm condition over the North Sea, *J. Geopgys. Res.*, **92**, 13,129-13,139.

Hasselmann, K., 1961: On the nonlinear energy transfer in a gravity-wave spectrum. Part 1. General theory, *J. Fluid Mech.*, **12**, 481-500.

Hasselmann, K., T.P. Barnett, E. Bouws, H. Carlson, D.E. Cartwright, K. Enke, J.A. Ewing, H. Gienapp, D.E. Hasselmann, A. Meerburg, P. Müller, D.J. Olbers, K. Richter, W. Swell and H. Walden, 1973: Measurements of wind wave-growth and swell decay during the Joint North Sea Wave Project (JONSWAP). *Dtsch. Hydrogr. Z.*, Suppl. A, **80**, (12).

Hasselmann, K., 1974: On the spectral dissipation of ocean waves due to white-capping. *Bound.-Layer Meteor.* **6**, 107-127.

Hasselmann, S., K. Hasselmann, G. K. Komen, P. Janssen, J. A. Ewing, and V. Cardone, 1989: The **WAM** model - A third generation ocean wave prediction model, *J. Phys. Ocean.*, **18**, 1775-1810.

Hsu, S. A., 1974: A dynamic roughness equation and its application to wind stress determination at the Air-Sea interface, *J. Phys. Ocean.*, **4**, 116-120.

Hsu, S. A., 1986: A mechanism for the increase of wind stress (drag) coefficient with wind speed over water surface: A parametric model, *J. Phys. Ocean.*, **16**, 144-150.

Janssen.P.A.M.: 1989, Wave induced stress and the drag of air flow over sea waves, *J. Phys. Ocean.*, **19**, 745-754.

Maat, N., C. Kraan and W.A. Oost, 1991: The roughness of wind waves, *Boundary-Layer Meteorology,* **54**, 89-103.

Nordeng, T. E., 1991: On the wave age dependent drag coefficient and roughness length at sea, *J. Geophys. Res.*, **96**, No. C4, 7167-7174.

Smith, S.D., R.J. Anderson., W.A. Oost., N.M. Kraan., J. DeCosmo., K.B. Katsaros., K.L. Davidson., K. Bumke., L. Hasse., and H.M. Chadwick., 1992: Sea surface wind stress and drag coefficient: The HEXOS results. *Boundary-Layer Meteorology*. **60**, 109-142.

Snyder, R., F. Dobson, J. Elliott, and R. Long, 1981 : Array measurements of atmospheric pressure fluctuations above gravity waves, *J. Fluid Mech.*, **102**, 1-90.

Toba, Y. and Koga, M.: 1986, A parameter describing overall conditions of wave breaking whitecapping, Sea-Spray production and wind stress, in E. C. Monahan and G. Mac Niocaill (Eds), *Oceanic Writecaps,* D. Reidel, pp. 37-47.

Toba, Y., N.Iida, H. Kawamura, N. Ebuchi, and I.S. Jones, 1990: Wave dependence on sea surface wind stress, *J. Phys. Oceanogr.*, **20**, 705-721.

Wu, J.: 1980, Wind stress coefficients over sea surface near neutral conditions. A revisit, *j. Phys. Ocean.*, **10**, 727-740.

TABLE 1 : FORECASTING WAVE HEIGHT (in neutral case)

WIND SPEED (m/s)	10	20	30	40	50
t=10 hours					
UNCOUPLED	1.14	3.06	4.21	8.56	11.10
COUPLED	1.31	3.49	5.86	9.32	13.00
t=20 hours					
UNCOUPLED	1.45	5.44	9.03	13.80	16.30
COUPLED	1.60	6.40	12.00	16.90	19.20
t=30 hours					
UNCOUPLED	1.62	7.34	11.90	15.50	16.60
COUPLED	1.73	7.94	13.90	17.40	19.50
t=40 hours					
UNCOUPLED	1.75	8.65	13.40	15.50	16.60
COUPLED	1.83	9.09	14.30	17.40	19.90
t=50 hours					
UNCOUPLED	1.86	9.63	13.60	15.50	16.60
COUPLED	1.93	10.00	14.30	17.50	19.90

TABLE 2. FORECASTING SIGNIFICANT WAVE HEIGHT AT VARIOUS ZA

TIME (hours)	10	20	30	40	50
Za=5	5.74	10.80	13.60	14.30	14.30
Za=10	5.43	9.69	12.30	13.50	13.60
Za=20	5.11	8.67	11.10	12.60	12.90
Za=50	4.79	7.98	10.10	11.60	12.30

TABLE 3. FLUXES OF MOMENTUM, SENSIBLE HEAT AND LATENT HEAT

	DT=0 DQ=0	DT=20 DQ=0	DT=0 DQ=20	DT=20 DQ=20
FLUX OF MOMENTUM				
UNCOUPLED MODEL	1.1614	1.2033	1.1926	1.2188
COUPLED MODEL	2.0648	2.1578	2.1219	2.1898
FLUX OF SENSIBLE HEAT				
UNCOUPLED MODEL	0	1.2927	0	1.3126
COUPLED MODEL	0	2.3196	0	2.3608
FLUX OF LATENT HEAT				
UNCOUPLED MODEL	0	0	0.7519	0.7801
COUPLED MODEL	0	0	1.3377	1.4031

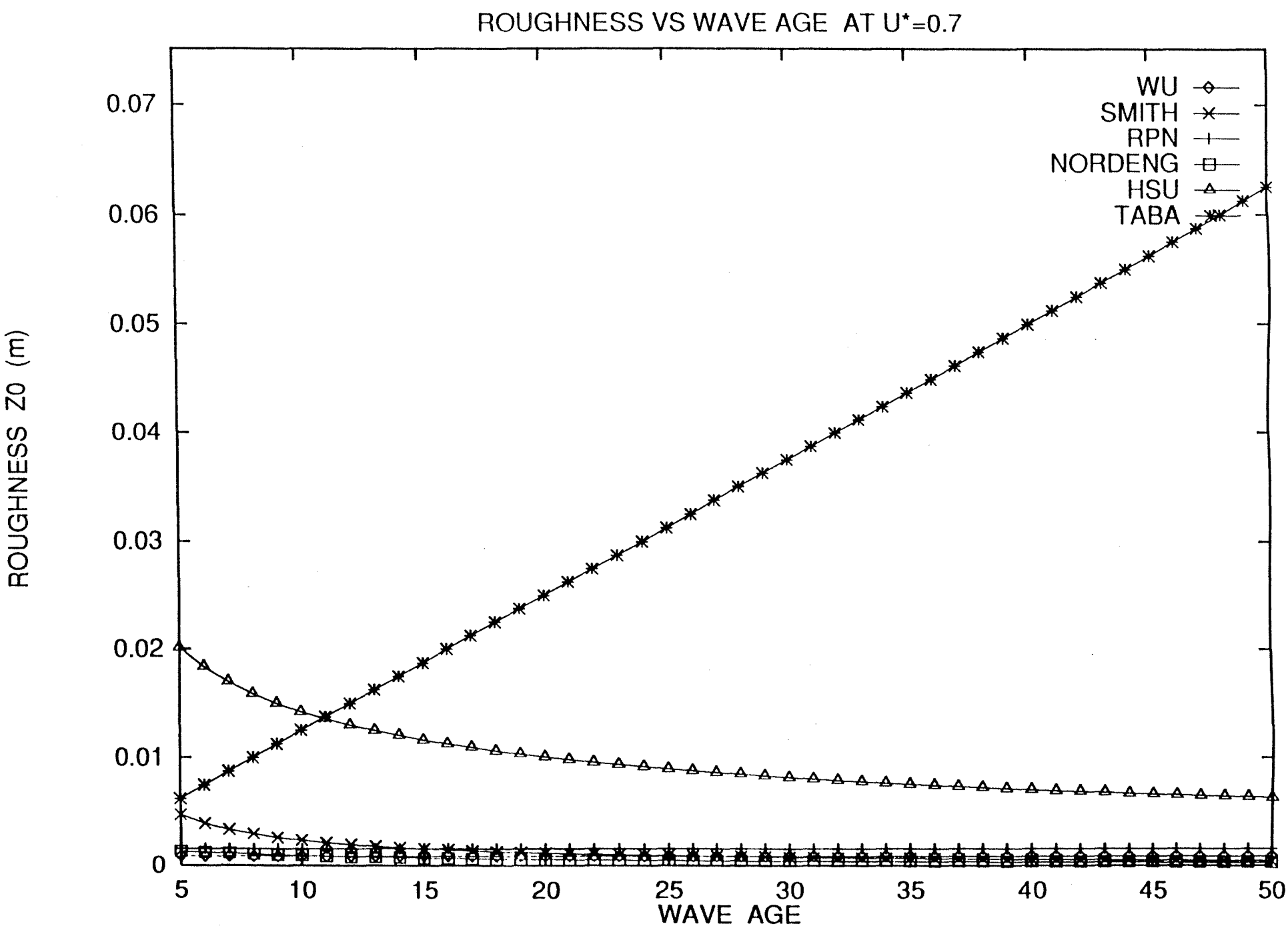
ROUGHNESS VS WAVE AGE AT U*=0.7
WU
SMITH
RPN
NORDENG
HSU
TABA
ROUGHNESS Z0 (m)
0.07
0.06
0.05
0.04
0.03
0.02
0.01
0
5
10
15
20
25
30
35
40
45
50
WAVE AGE

Fig.1a

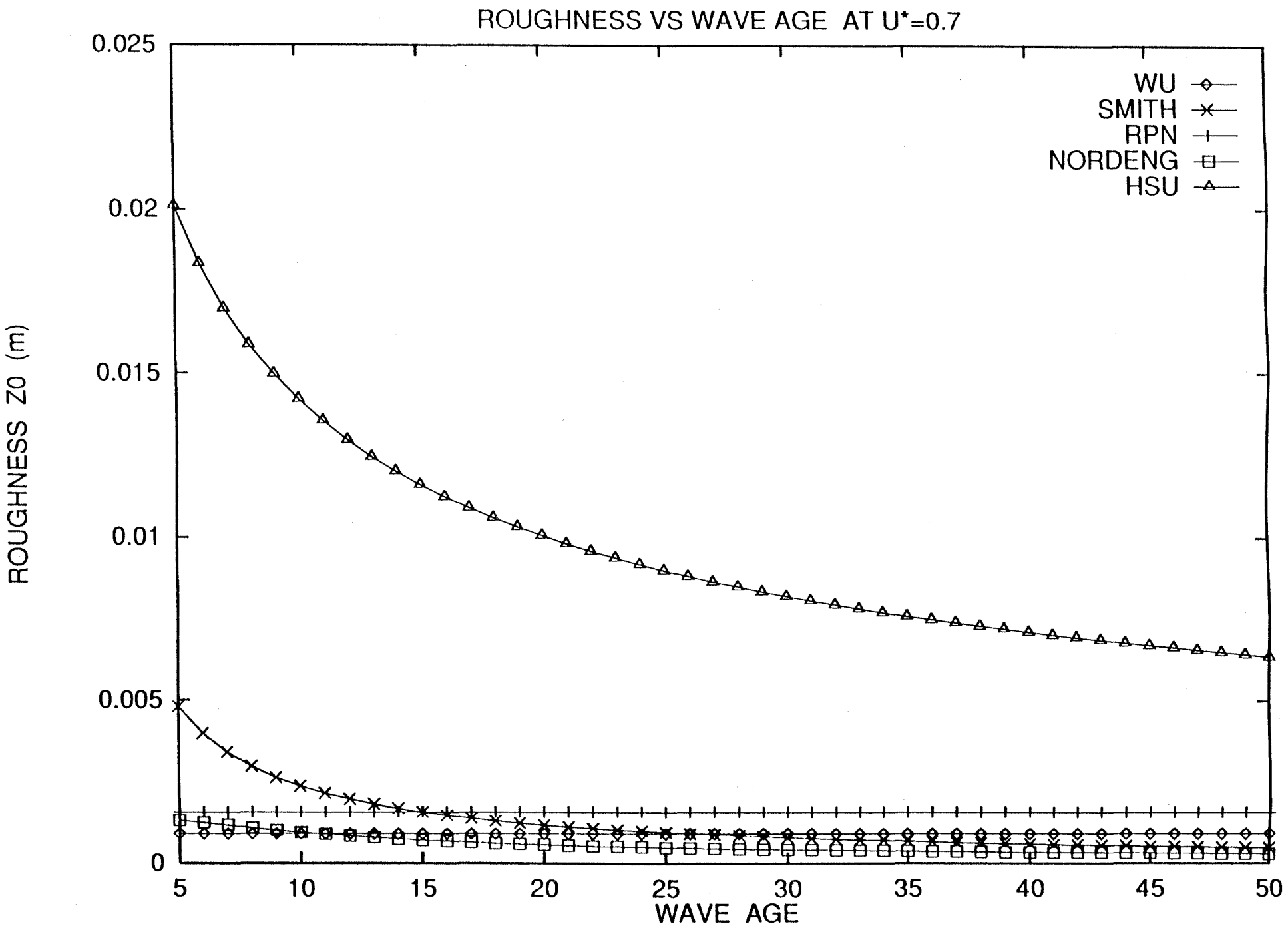
ROUGHNESS VS WAVE AGE AT U*=0.7
ROUGHNESS Z0 (m)
0.025
0.02
0.015
0.01
0.005
0
5
10
15
20
25
30
35
40
45
50
WAVE AGE
WU
SMITH
RPN
NORDENG
HSU

Fig.1b

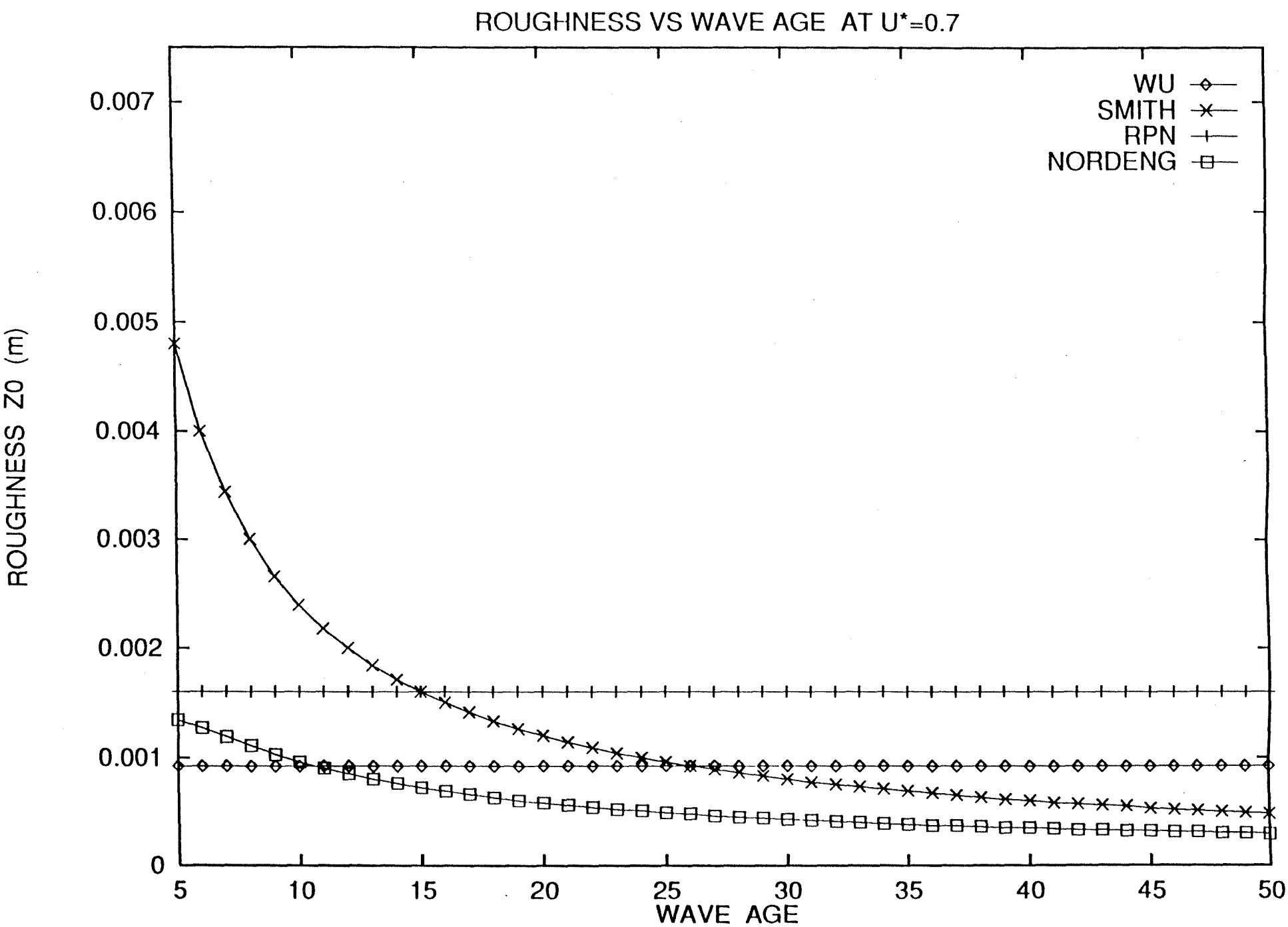
ROUGHNESS VS WAVE AGE AT U*=0.7
WU
SMITH
RPN
NORDENG
ROUGHNESS Z0 (m)
0.007
0.006
0.005
0.004
0.003
0.002
0.001
0
5
10
15
20
25
30
35
40
45
50
WAVE AGE

Fig.1c

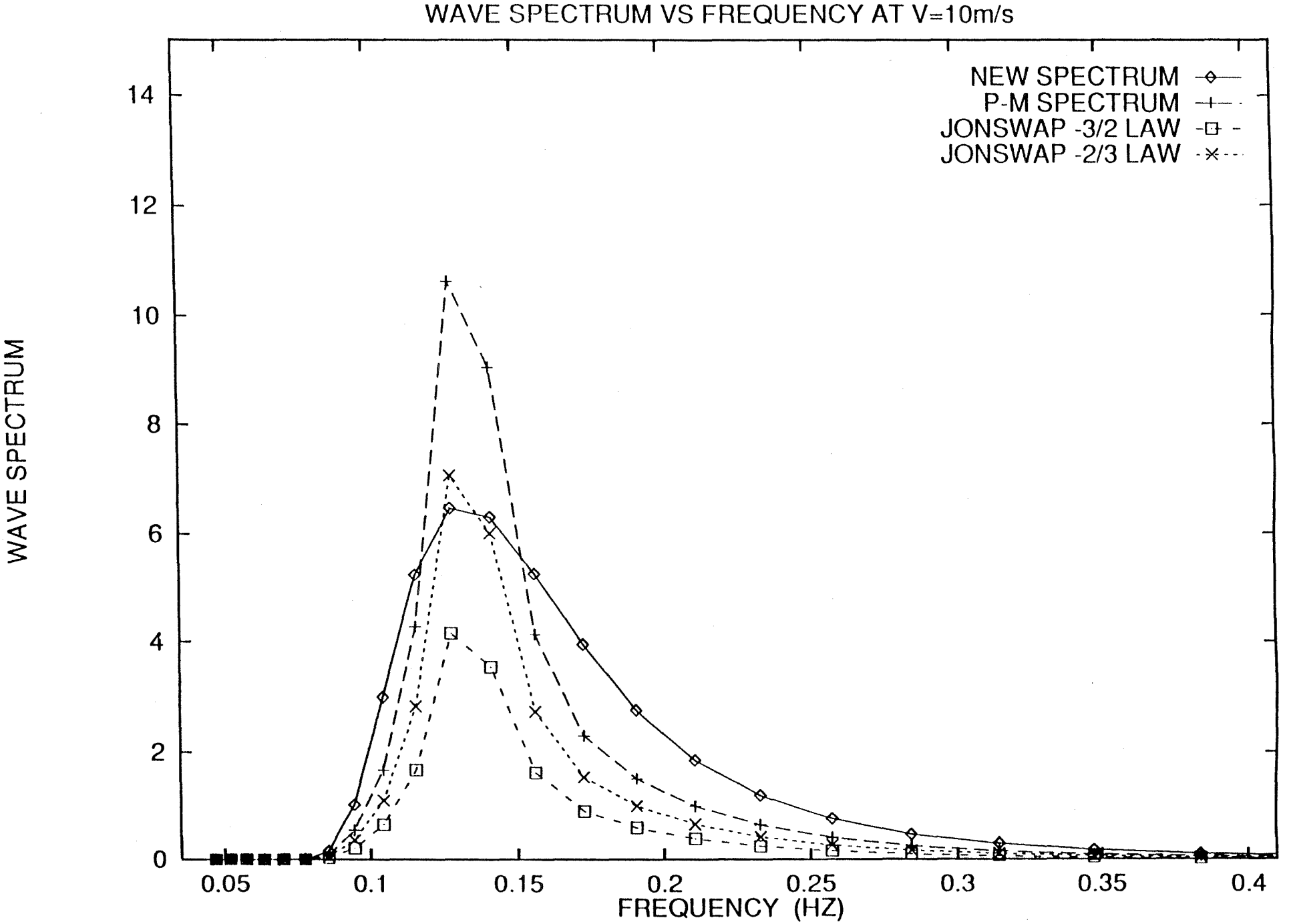
WAVE SPECTRUM VS FREQUENCY AT V=10m/s
NEW SPECTRUM
P-M SPECTRUM
JONSWAP -3/2 LAW
JONSWAP -2/3 LAW
WAVE SPECTRUM
FREQUENCY (HZ)
0
2
4
6
8
10
12
14
0.05
0.1
0.15
0.2
0.25
0.3
0.35
0.4

Fig.2a

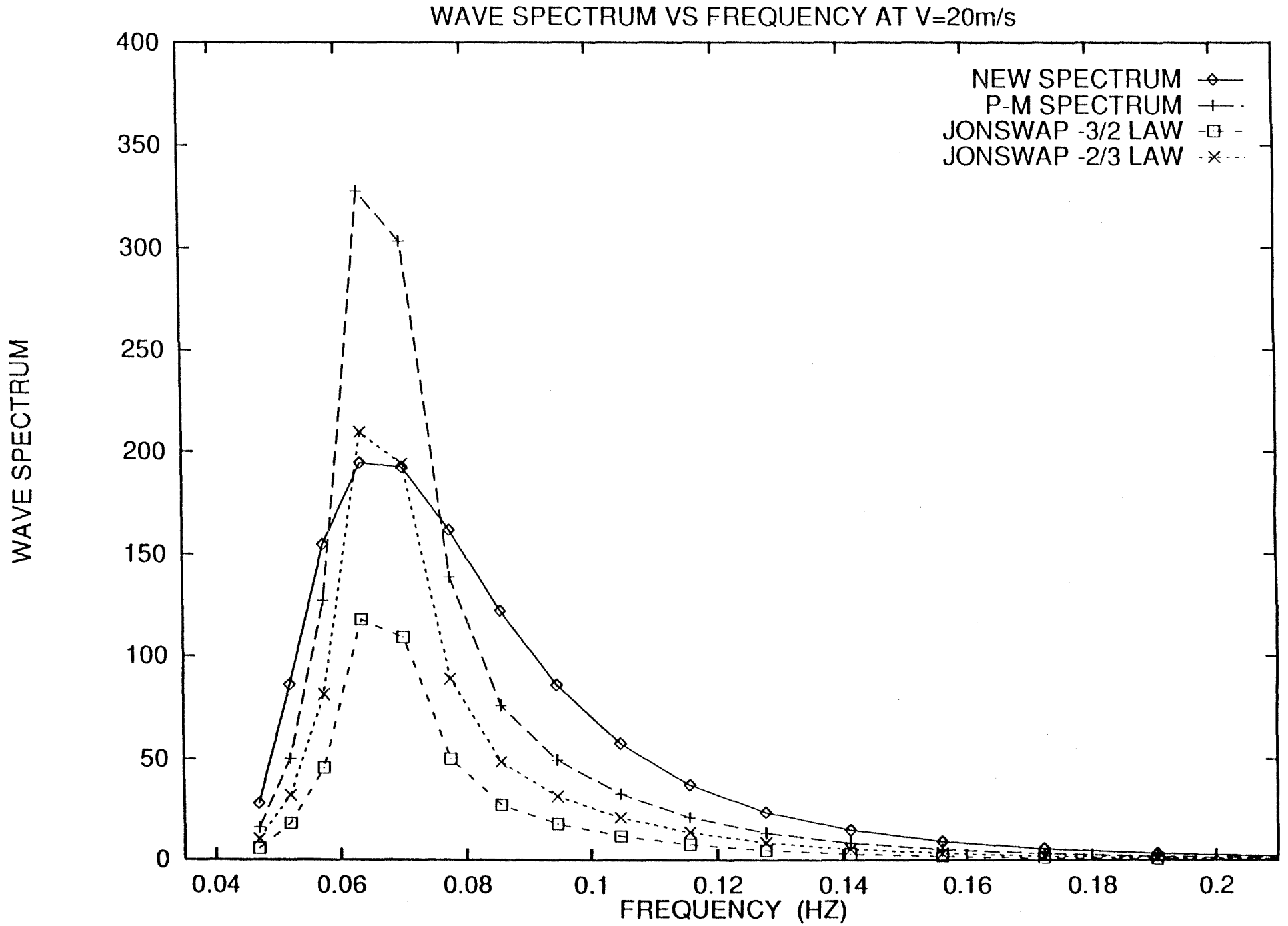
WAVE SPECTRUM VS FREQUENCY AT V=20m/s
NEW SPECTRUM
P-M SPECTRUM
JONSWAP -3/2 LAW
JONSWAP -2/3 LAW
WAVE SPECTRUM
FREQUENCY (HZ)
400
350
300
250
200
150
100
50
0
0.04
0.06
0.08
0.1
0.12
0.14
0.16
0.18
0.2

Fig.2b

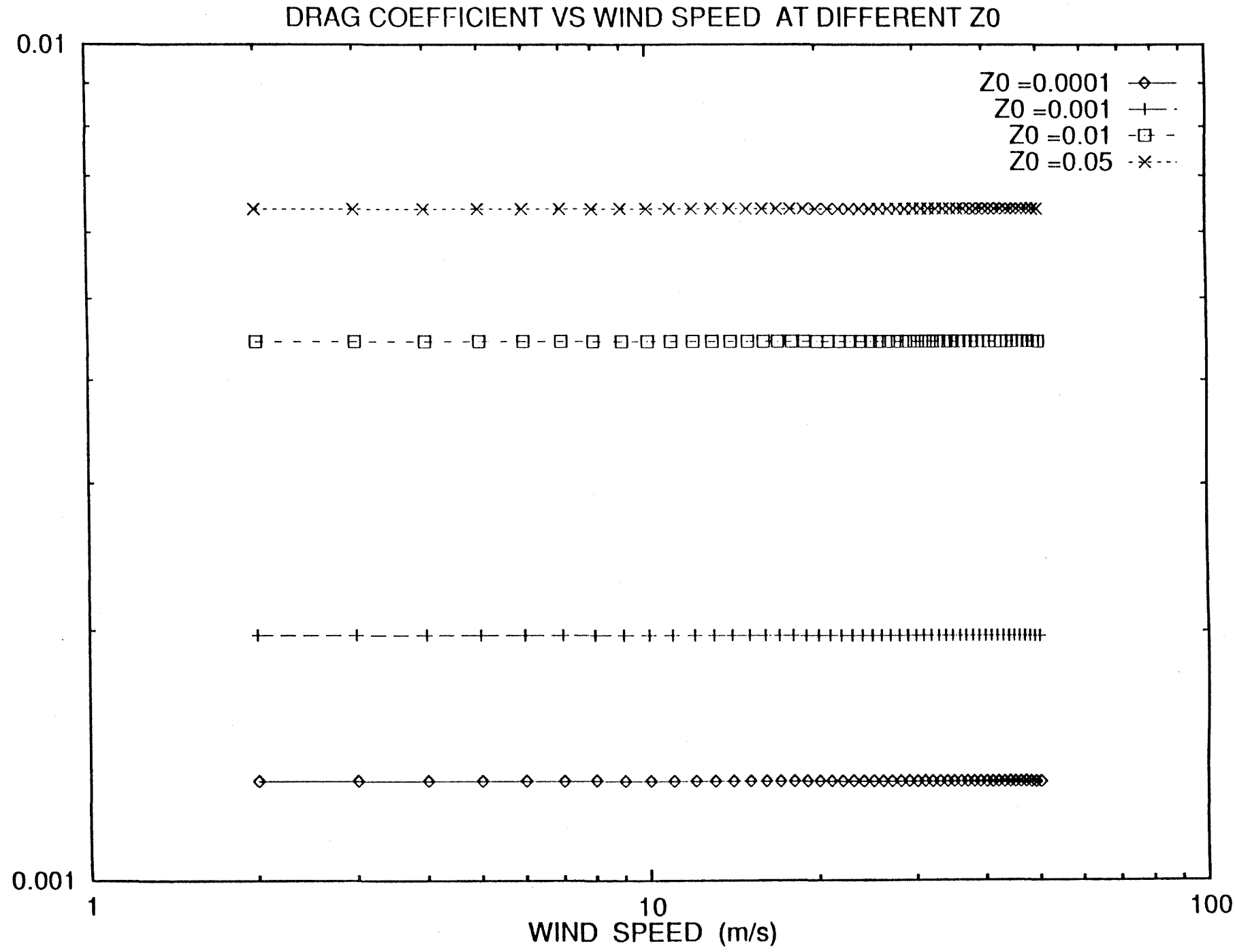
DRAG COEFFICIENT VS WIND SPEED AT DIFFERENT Z0
0.01
0.001
1
10
100
WIND SPEED (m/s)
DRAG COEFFICIENT CD
Z0 =0.0001
Z0 =0.001
Z0 =0.01
Z0 =0.05

Fig.3

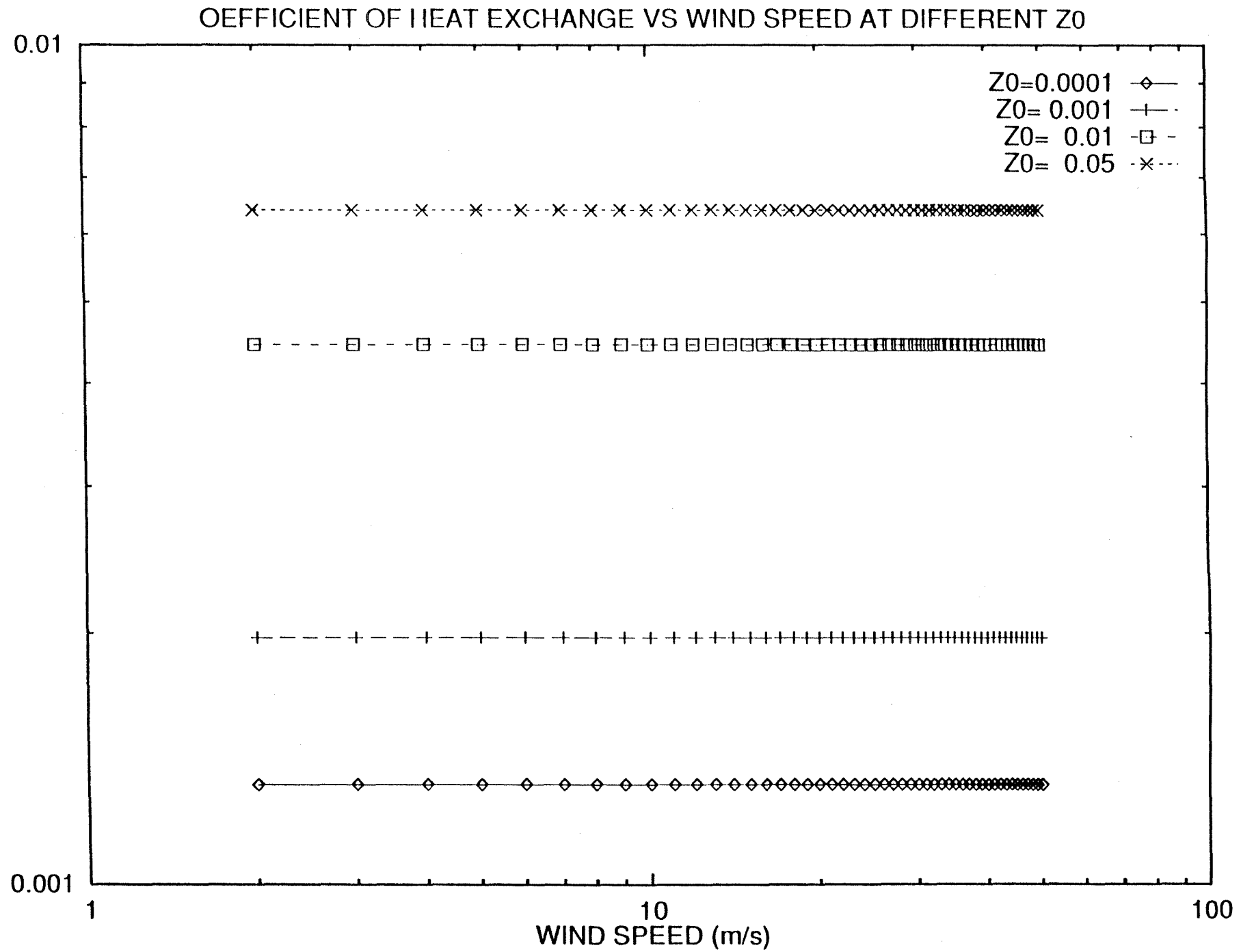
OEFFICIENT OF HEAT EXCHANGE VS WIND SPEED AT DIFFERENT Z0
COEFFICIENT OF HEAT EXCHANGE CMCT
0.01
0.001
1
10
100
WIND SPEED (m/s)
Z0=0.0001
Z0= 0.001
Z0= 0.01
Z0= 0.05

Fig.4

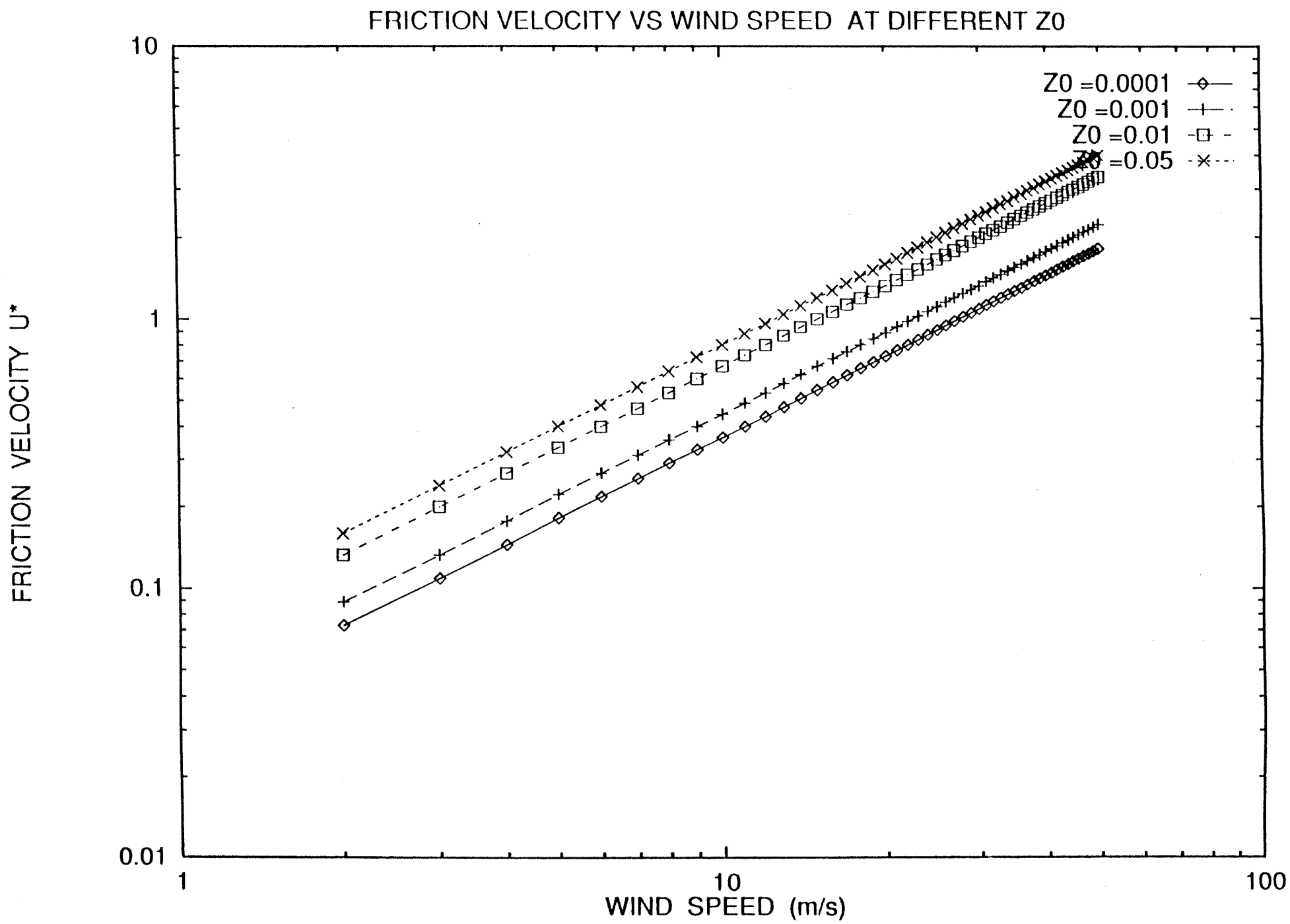
FRICTION VELOCITY VS WIND SPEED AT DIFFERENT Z0
FRICTION VELOCITY U*
WIND SPEED (m/s)
10
1
0.1
0.01
1
10
100
Z0 =0.0001
Z0 =0.001
Z0 =0.01
Z0 =0.05

F' - 5

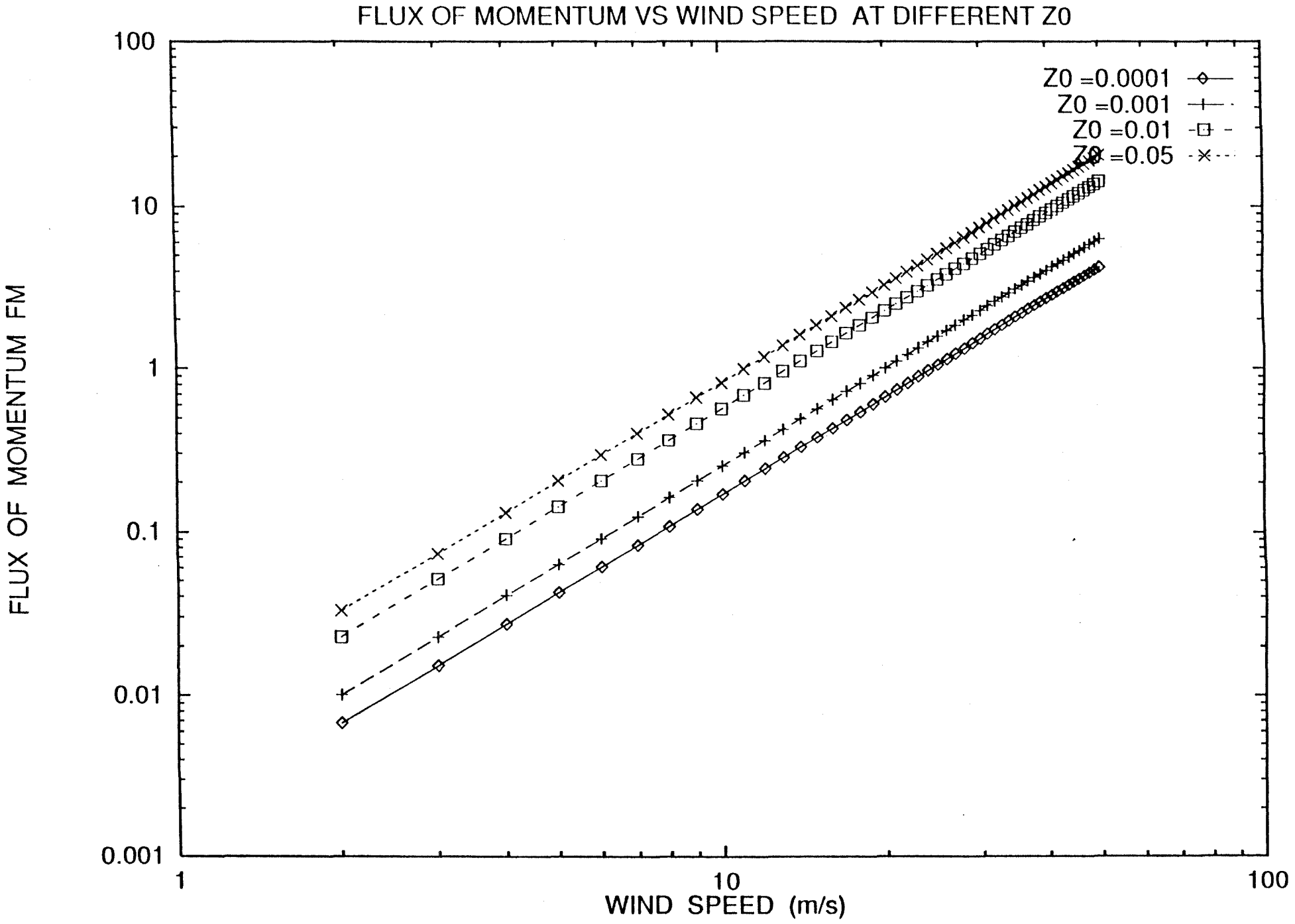
FLUX OF MOMENTUM VS WIND SPEED AT DIFFERENT Z0
FLUX OF MOMENTUM FM
WIND SPEED (m/s)
Z0 =0.0001
Z0 =0.001
Z0 =0.01
Z0 =0.05
100
10
1
0.1
0.01
0.001
1
10
100

Fig. 6

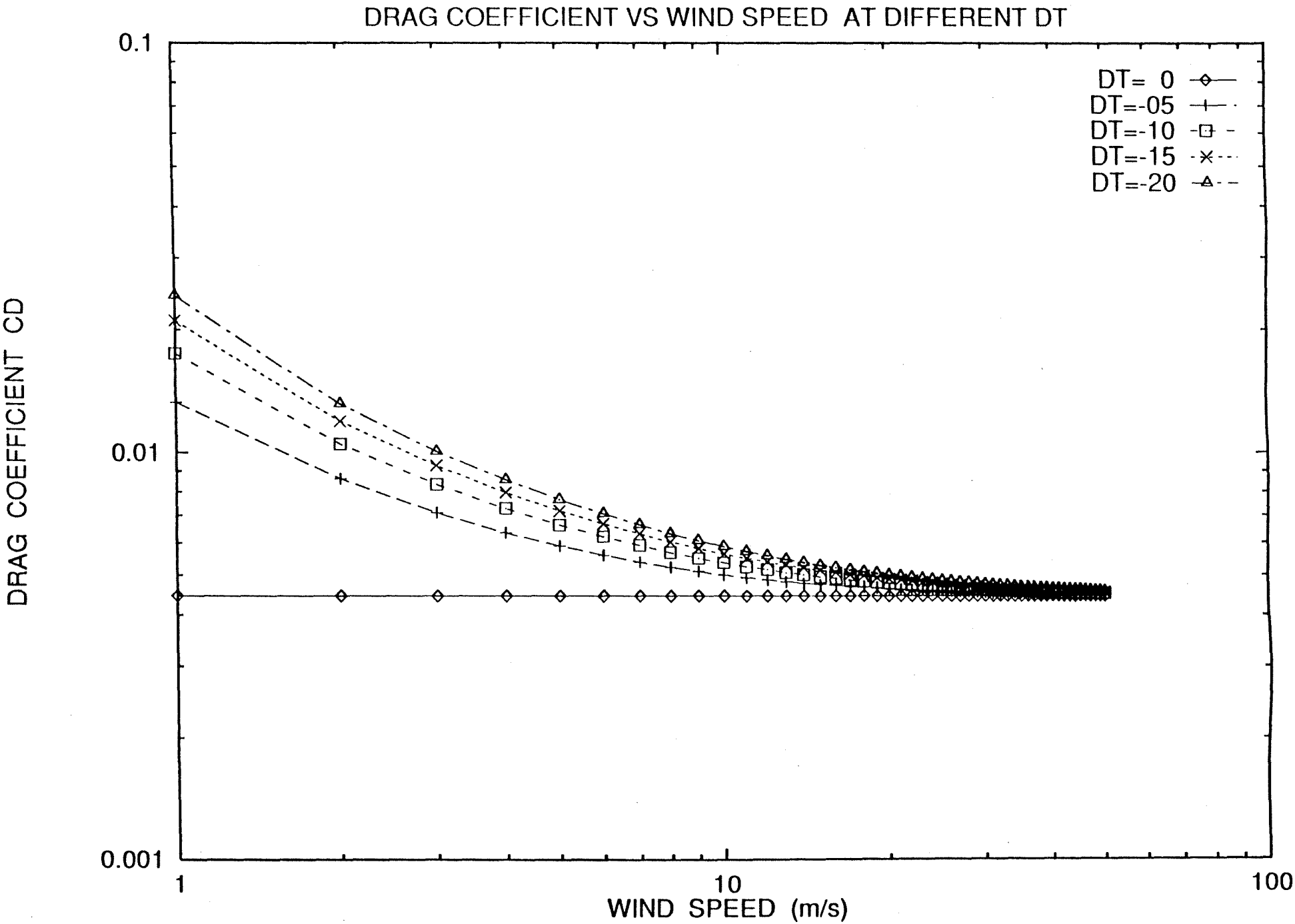
DRAG COEFFICIENT VS WIND SPEED AT DIFFERENT DT
DRAG COEFFICIENT CD
0.1
0.01
0.001
1
10
100
WIND SPEED (m/s)
DT= 0
DT=-05
DT=-10
DT=-15
DT=-20

Fig.7

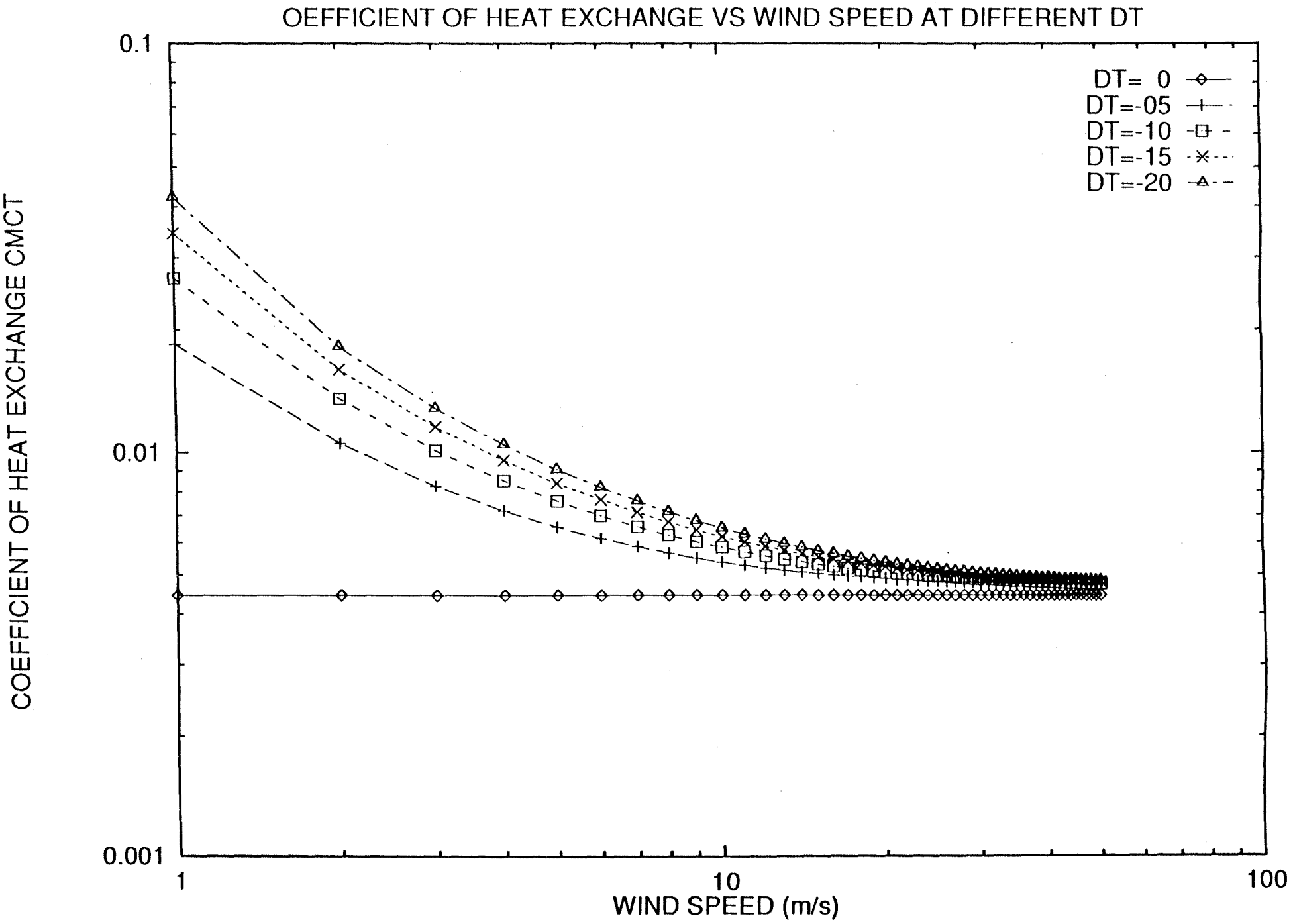
OEFFICIENT OF HEAT EXCHANGE VS WIND SPEED AT DIFFERENT DT
COEFFICIENT OF HEAT EXCHANGE CMCT
0.1
0.01
0.001
1
10
100
WIND SPEED (m/s)
DT= 0
DT=-05
DT=-10
DT=-15
DT=-20

Fig.8

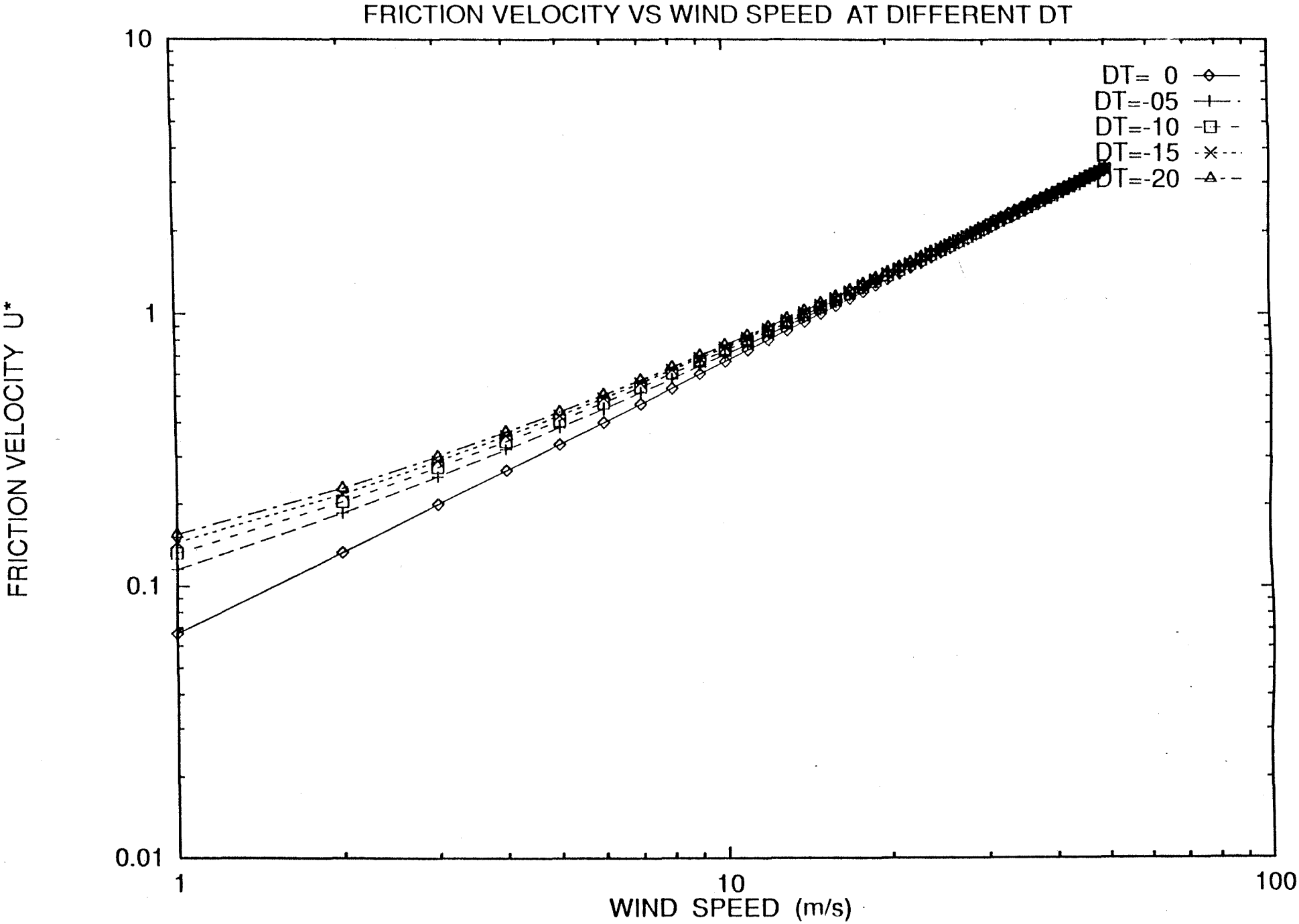
FRICTION VELOCITY VS WIND SPEED AT DIFFERENT DT
FRICTION VELOCITY U*
WIND SPEED (m/s)
10
1
0.1
0.01
1
10
100
DT= 0
DT=-05
DT=-10
DT=-15
DT=-20

Fig. 9

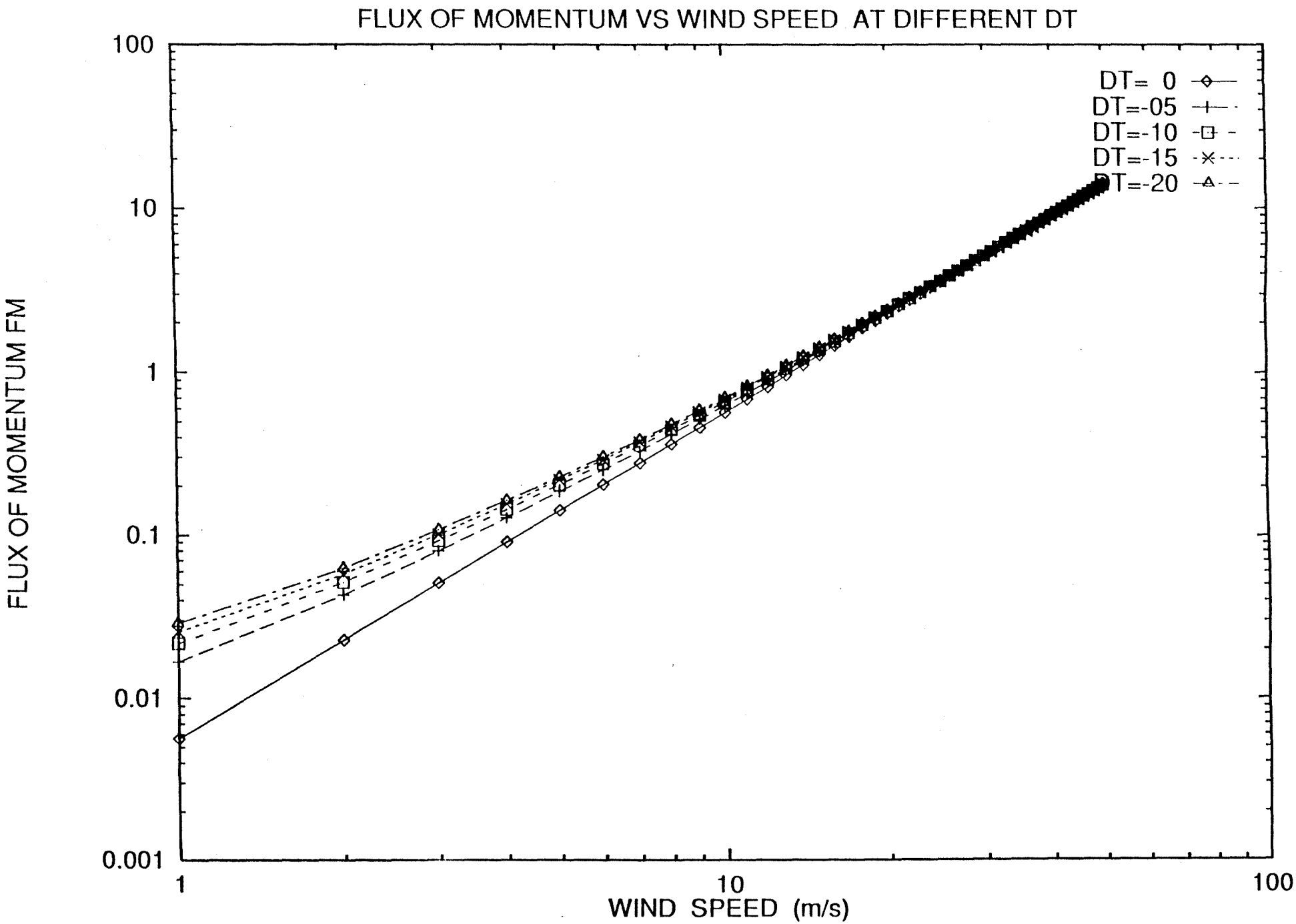
FLUX OF MOMENTUM VS WIND SPEED AT DIFFERENT DT
FLUX OF MOMENTUM FM
WIND SPEED (m/s)
100
10
1
0.1
0.01
0.001
1
10
100
DT= 0
DT=-05
DT=-10
DT=-15
DT=-20

Fig.10

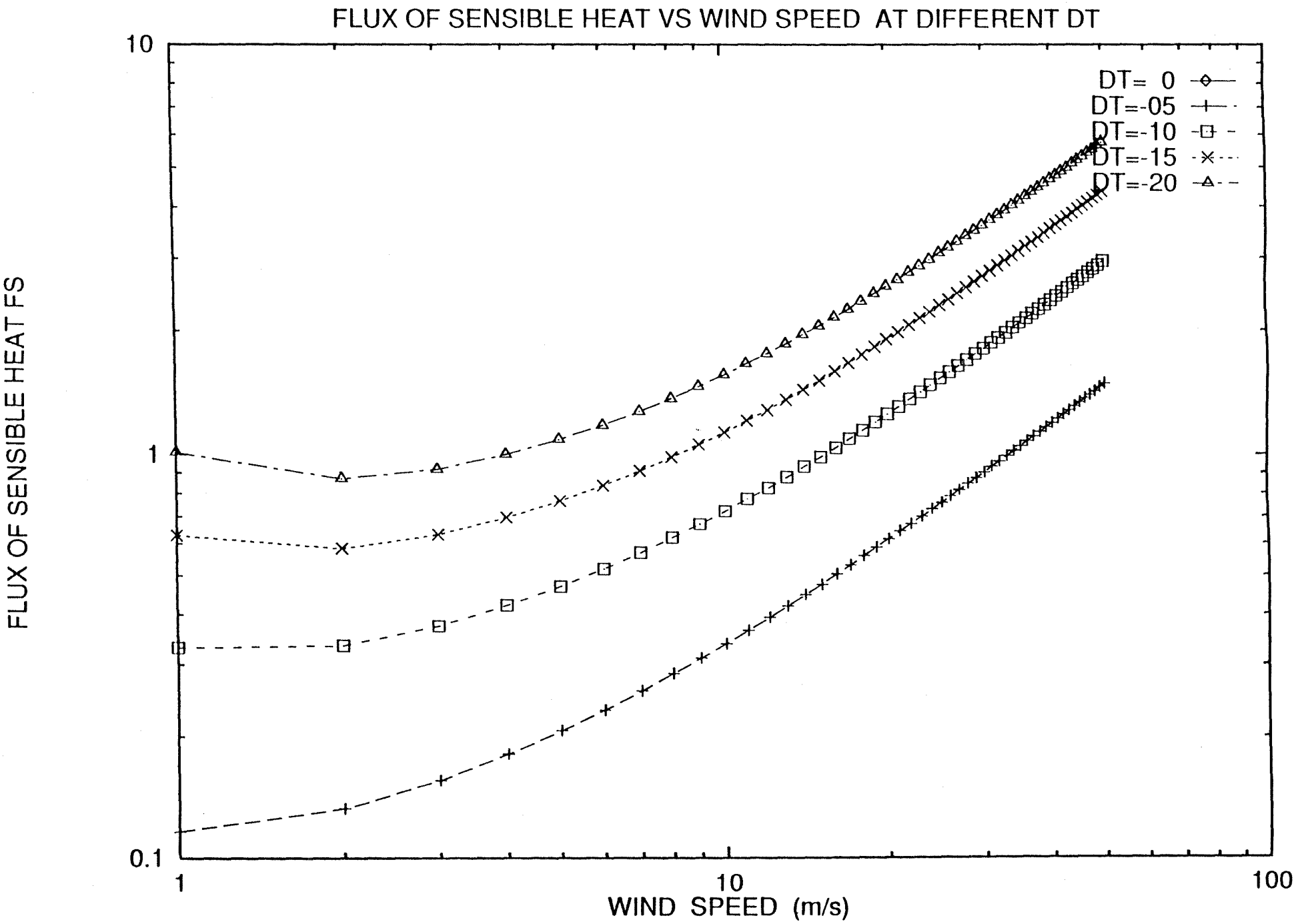
FLUX OF SENSIBLE HEAT VS WIND SPEED AT DIFFERENT DT
FLUX OF SENSIBLE HEAT FS
WIND SPEED (m/s)
10
1
0.1
1
10
100
DT= 0
DT=-05
DT=-10
DT=-15
DT=-20

Fig.11

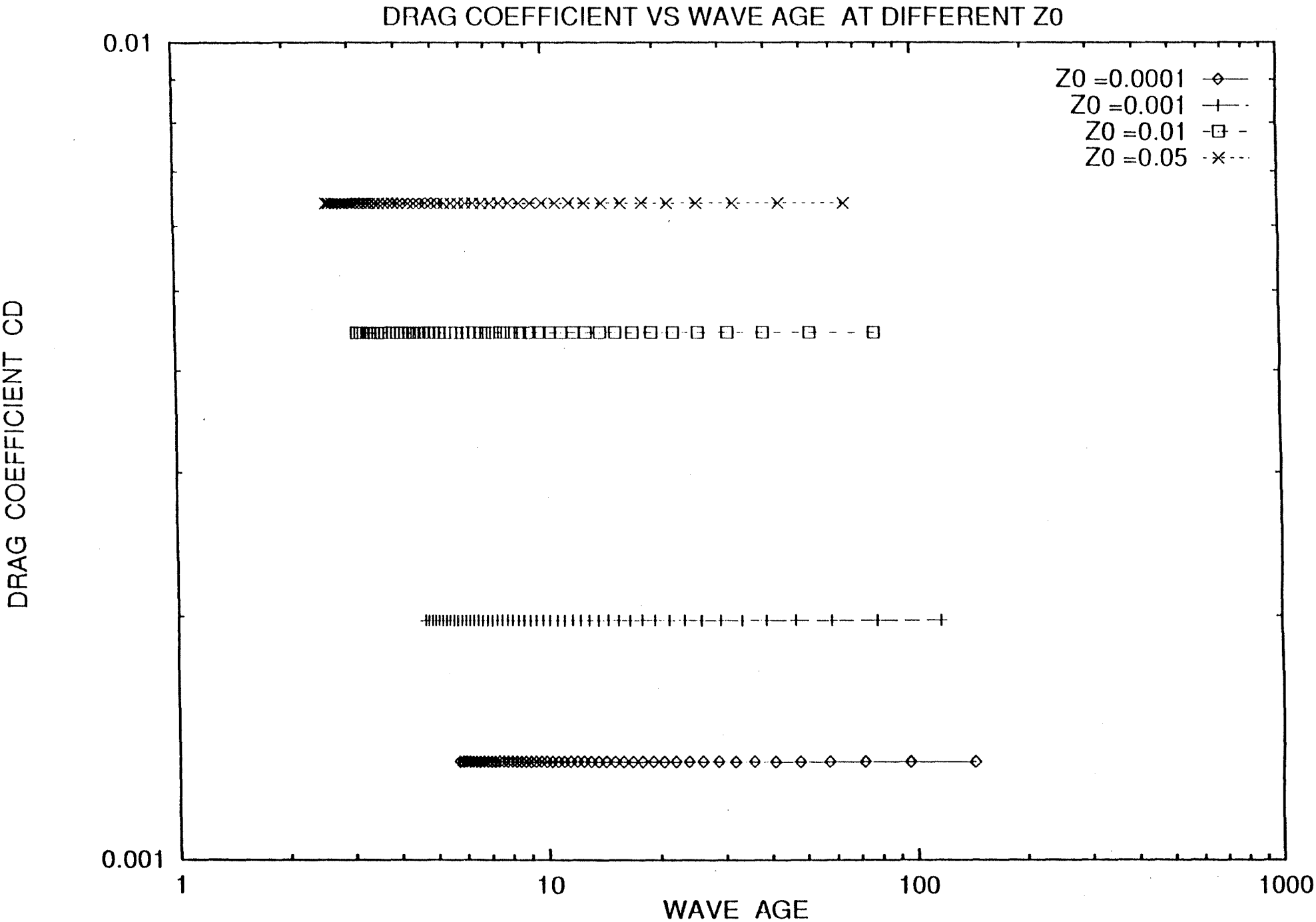
DRAG COEFFICIENT VS WAVE AGE AT DIFFERENT Z0
0.01
0.001
DRAG COEFFICIENT CD
1
10
100
1000
WAVE AGE
Z0 =0.0001
Z0 =0.001
Z0 =0.01
Z0 =0.05

Fig.12

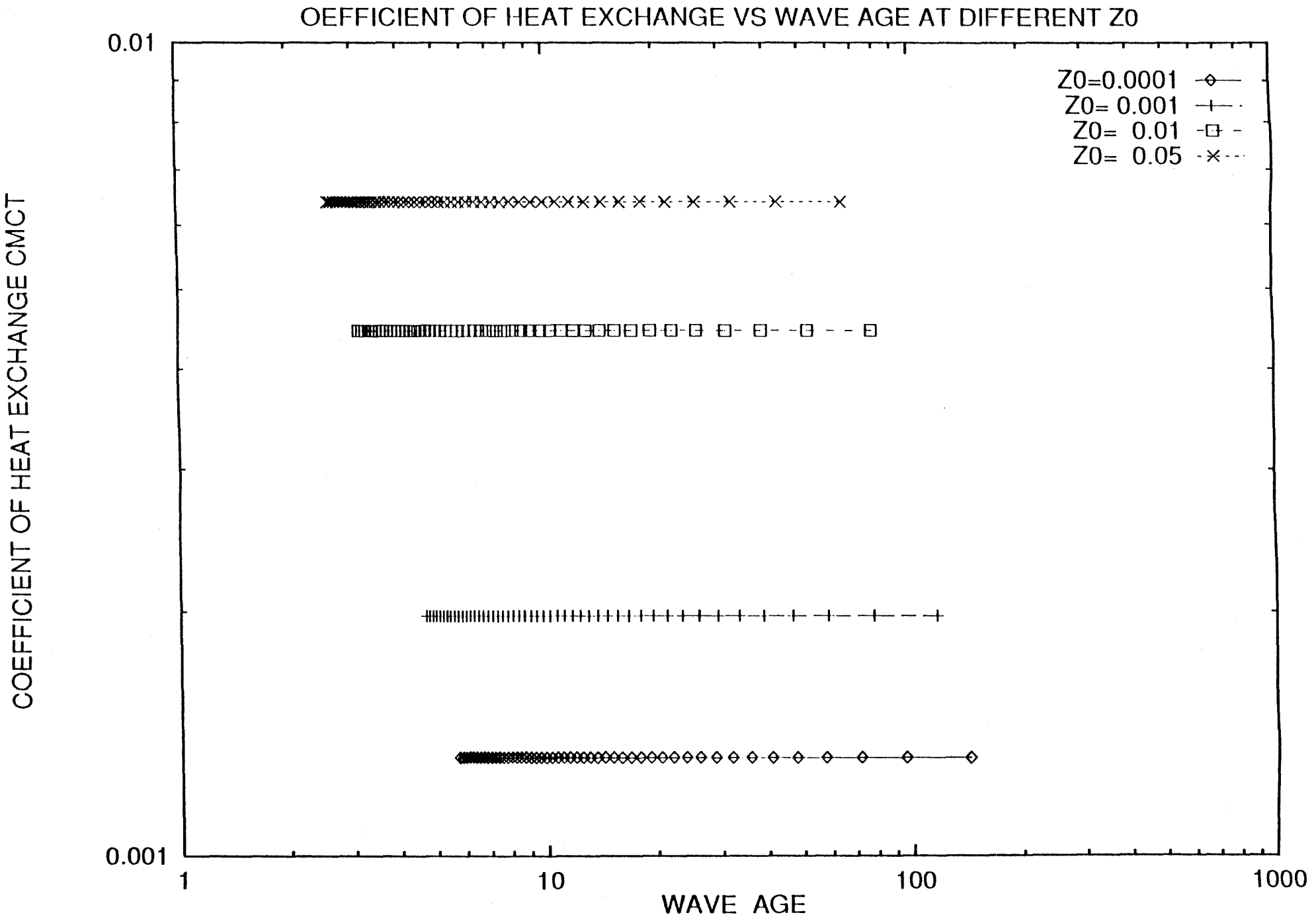
OEFFICIENT OF HEAT EXCHANGE VS WAVE AGE AT DIFFERENT Z0
0.01
0.001
1
10
100
1000
WAVE AGE
COEFFICIENT OF HEAT EXCHANGE CMCT
Z0=0.0001
Z0= 0.001
Z0= 0.01
Z0= 0.05

Fig.13

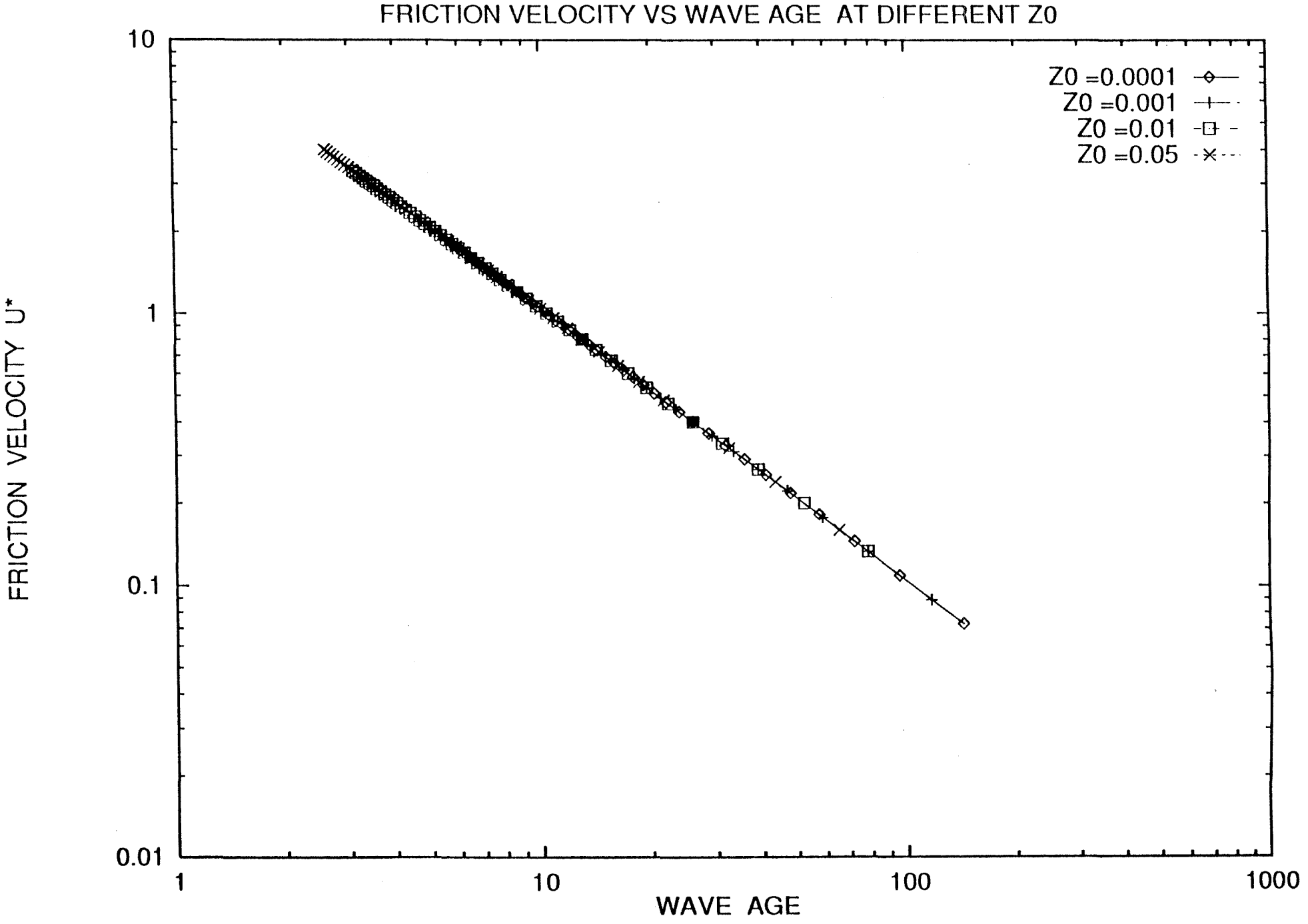
FRICTION VELOCITY VS WAVE AGE AT DIFFERENT Z0
Z0 =0.0001
Z0 =0.001
Z0 =0.01
Z0 =0.05
FRICTION VELOCITY U*
10
1
0.1
0.01
1
10
100
1000
WAVE AGE

Fig.14

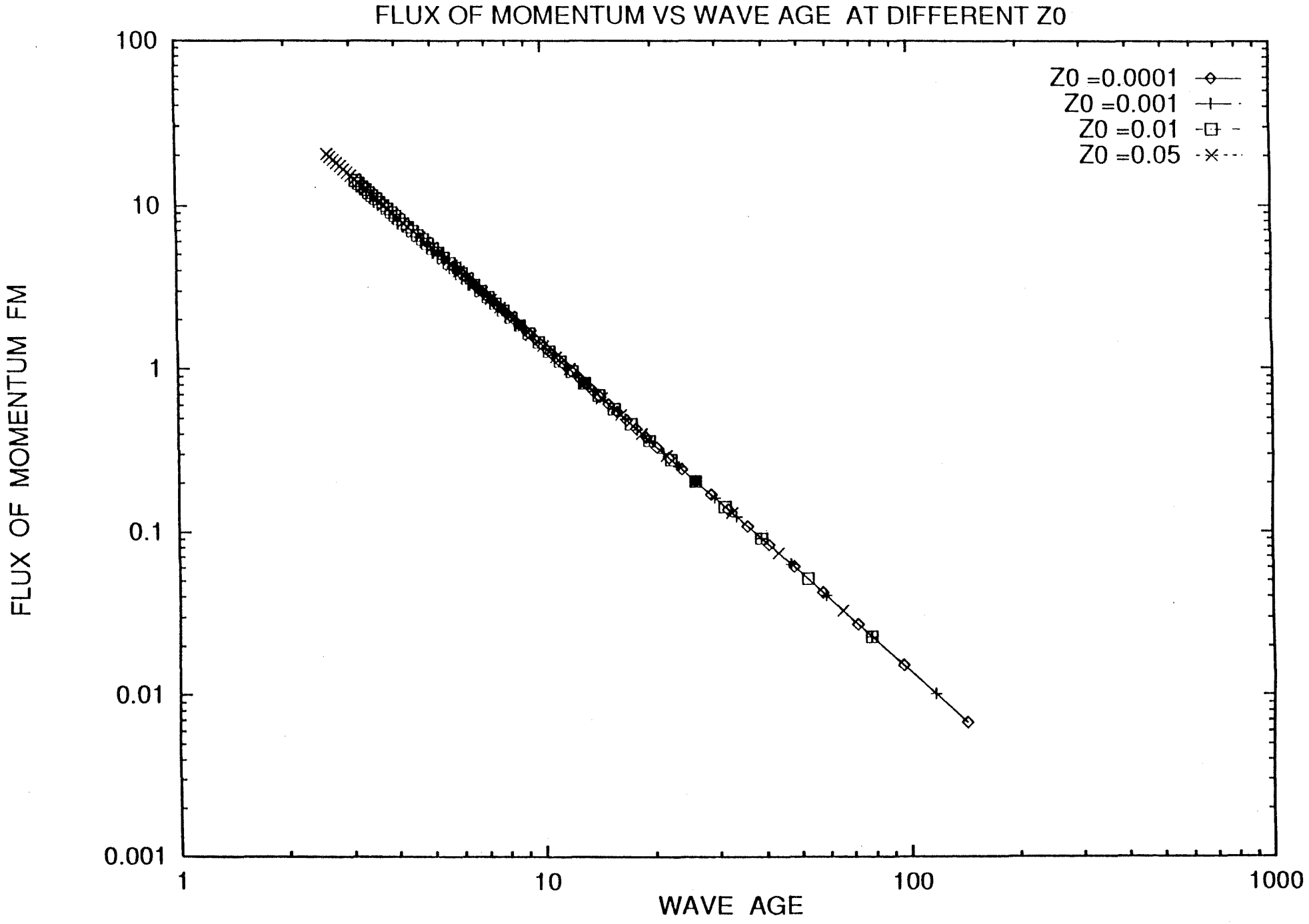
FLUX OF MOMENTUM VS WAVE AGE AT DIFFERENT Z0
Z0 =0.0001
Z0 =0.001
Z0 =0.01
Z0 =0.05
FLUX OF MOMENTUM FM
WAVE AGE
100
10
1
0.1
0.01
0.001
1
10
100
1000

Fig.15

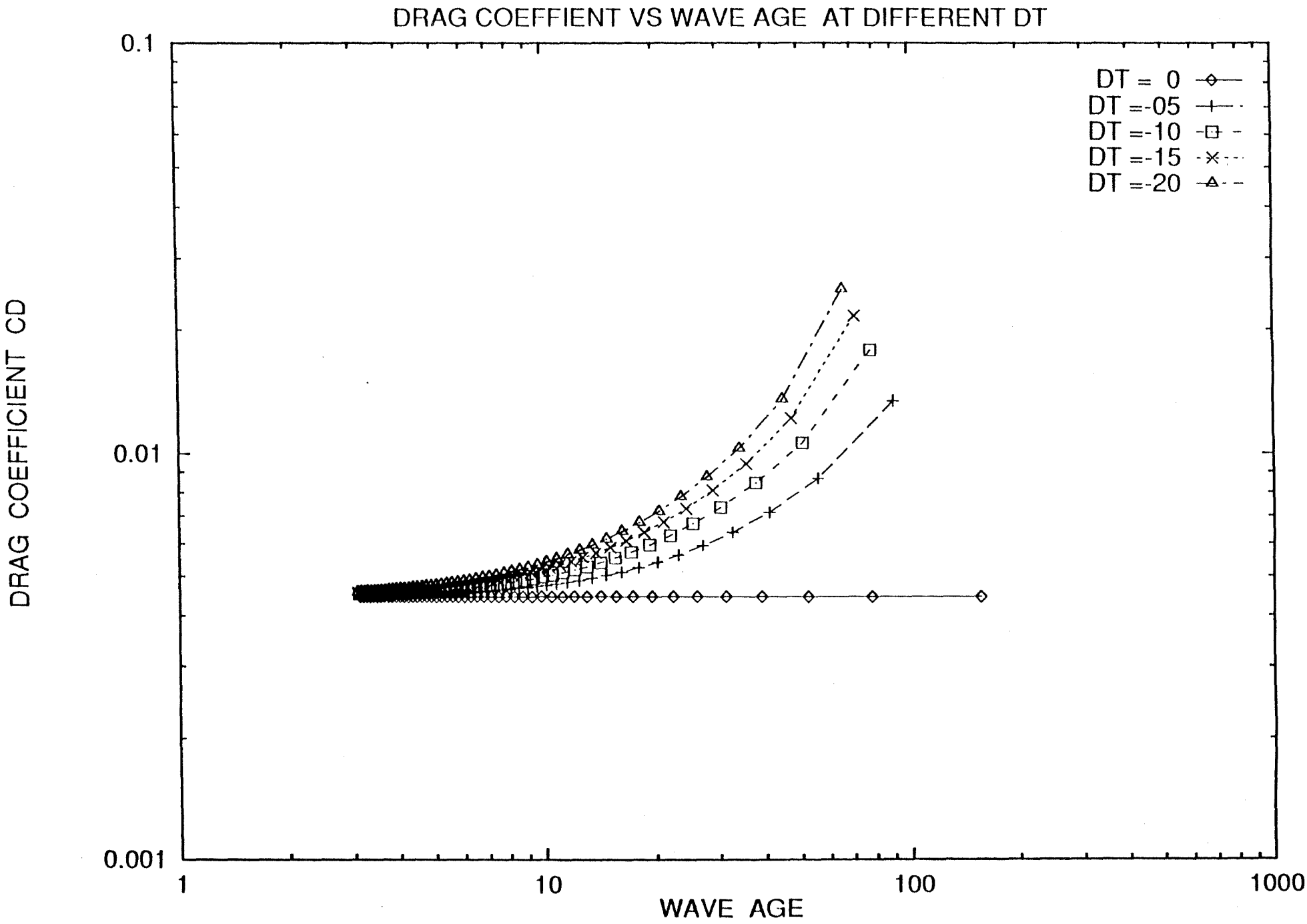
DRAG COEFFIENT VS WAVE AGE AT DIFFERENT DT
DRAG COEFFICIENT CD
0.1
0.01
0.001
1
10
100
1000
WAVE AGE
DT = 0
DT =-05
DT =-10
DT =-15
DT =-20

Fig.16

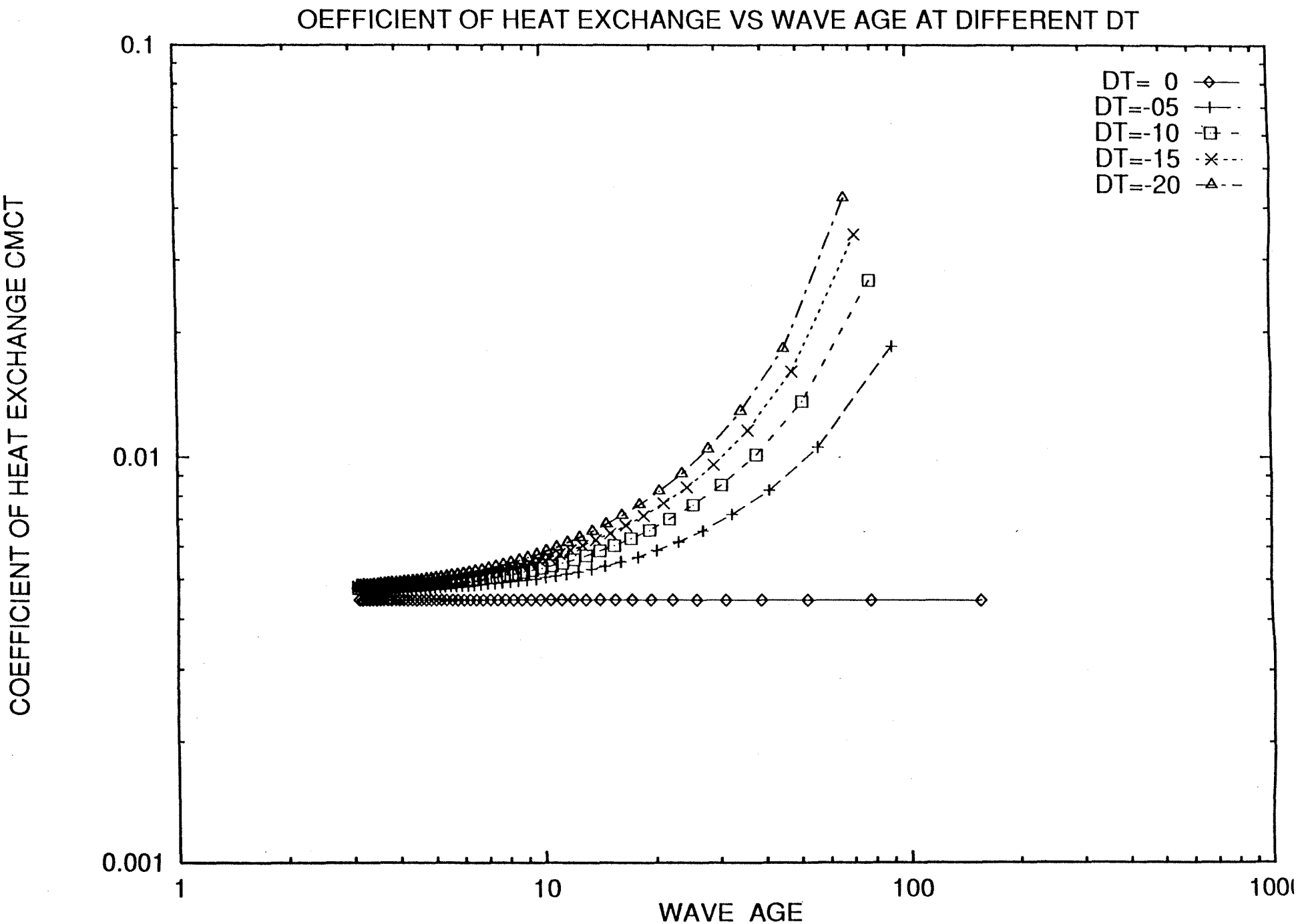
OEFFICIENT OF HEAT EXCHANGE VS WAVE AGE AT DIFFERENT DT
COEFFICIENT OF HEAT EXCHANGE CMCT
0.1
0.01
0.001
1
10
100
100
WAVE AGE
DT= 0
DT=-05
DT=-10
DT=-15
DT=-20

Fig.17

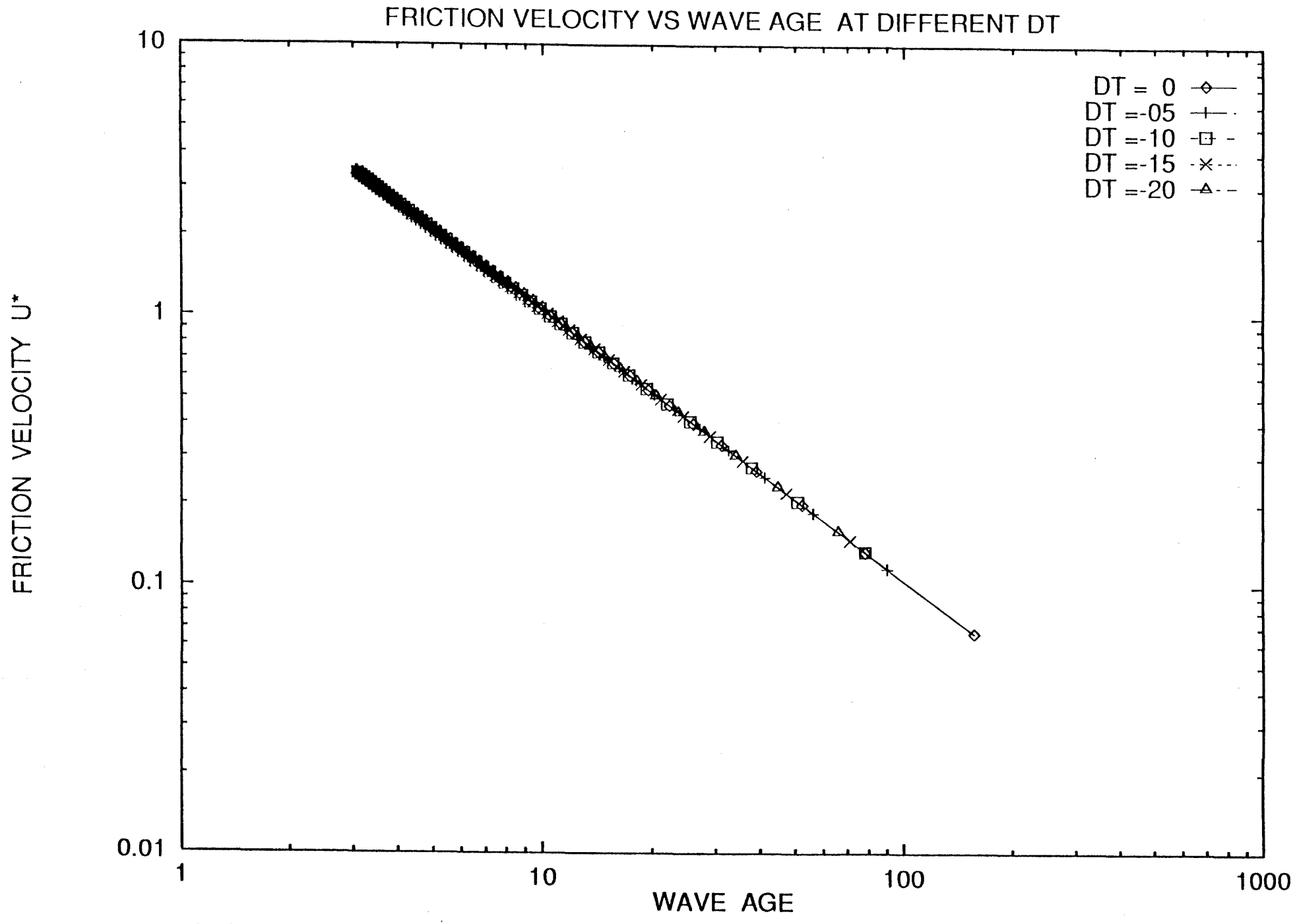
FRICTION VELOCITY VS WAVE AGE AT DIFFERENT DT
DT = 0
DT =-05
DT =-10
DT =-15
DT =-20
FRICTION VELOCITY U*
WAVE AGE
10
1
0.1
0.01
1
10
100
1000

Fig.18

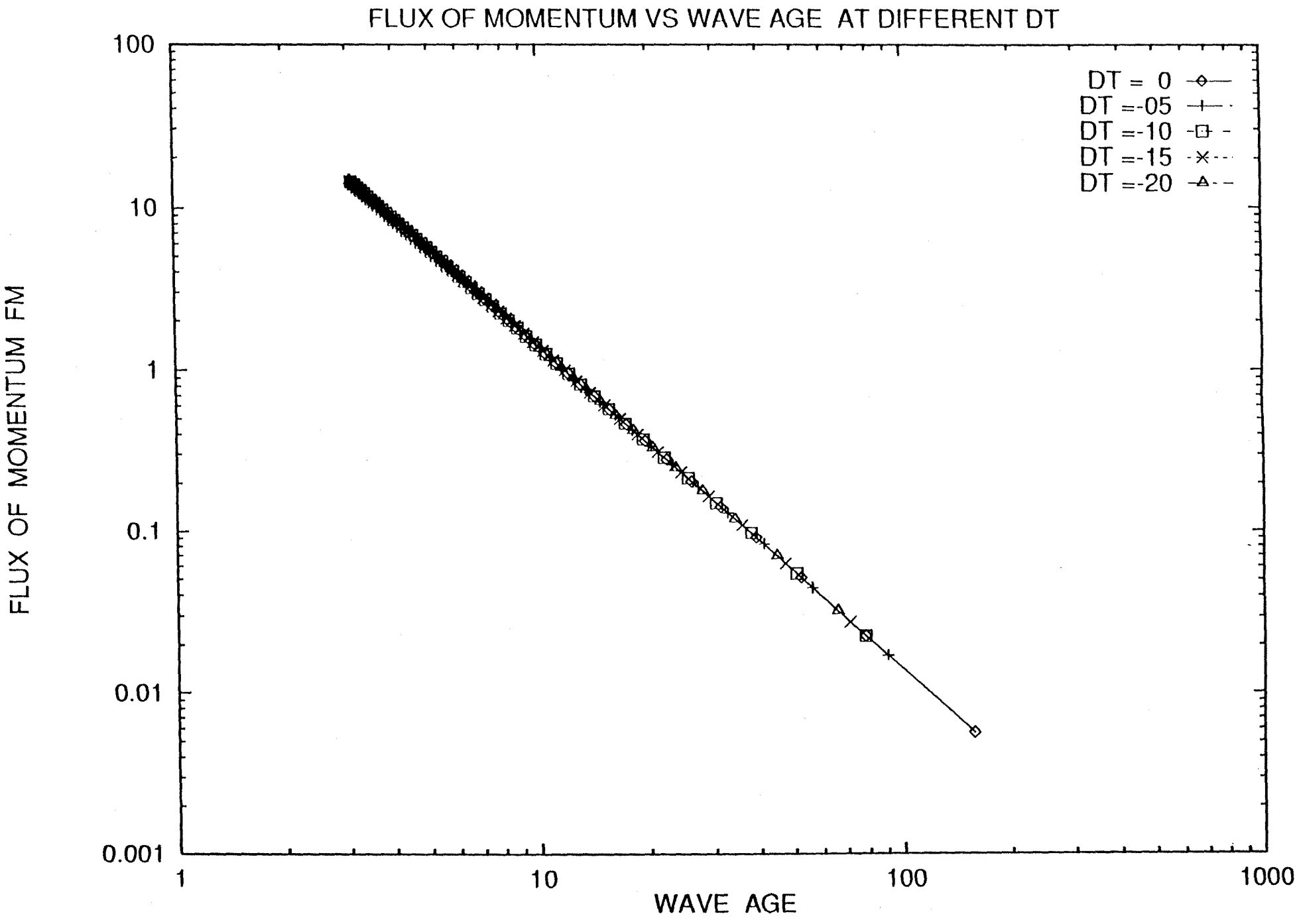
FLUX OF MOMENTUM VS WAVE AGE AT DIFFERENT DT
DT = 0
DT =-05
DT =-10
DT =-15
DT =-20
FLUX OF MOMENTUM FM
WAVE AGE
100
10
1
0.1
0.01
0.001
1
10
100
1000

Fig.19

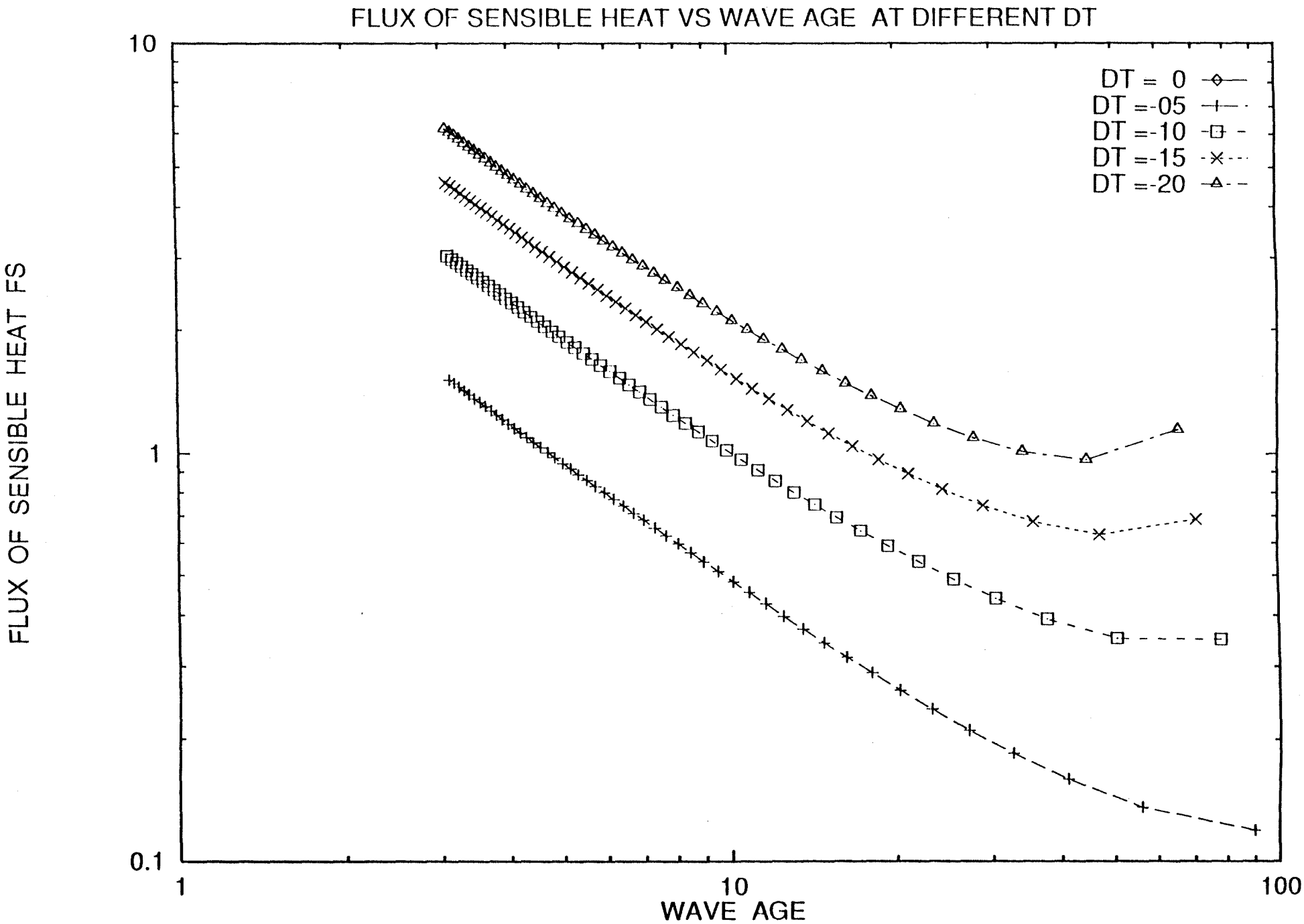
FLUX OF SENSIBLE HEAT VS WAVE AGE AT DIFFERENT DT
FLUX OF SENSIBLE HEAT FS
WAVE AGE
10
1
0.1
1
10
100
DT = 0
DT =-05
DT =-10
DT =-15
DT =-20

Fig.20

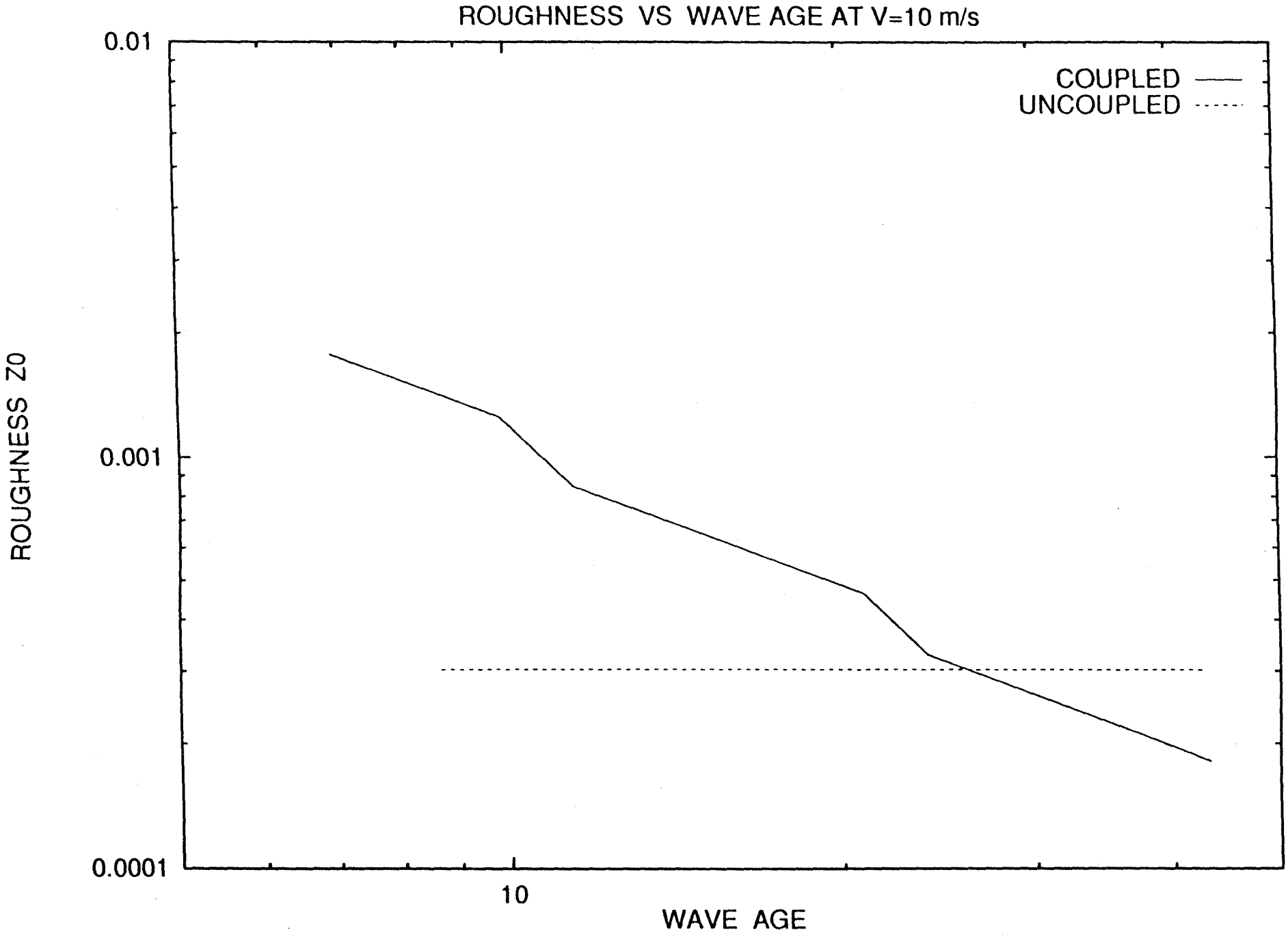
ROUGHNESS VS WAVE AGE AT V=10 m/s
COUPLED
UNCOUPLED
0.01
0.001
0.0001
ROUGHNESS Z0
10
WAVE AGE

Fig.21a

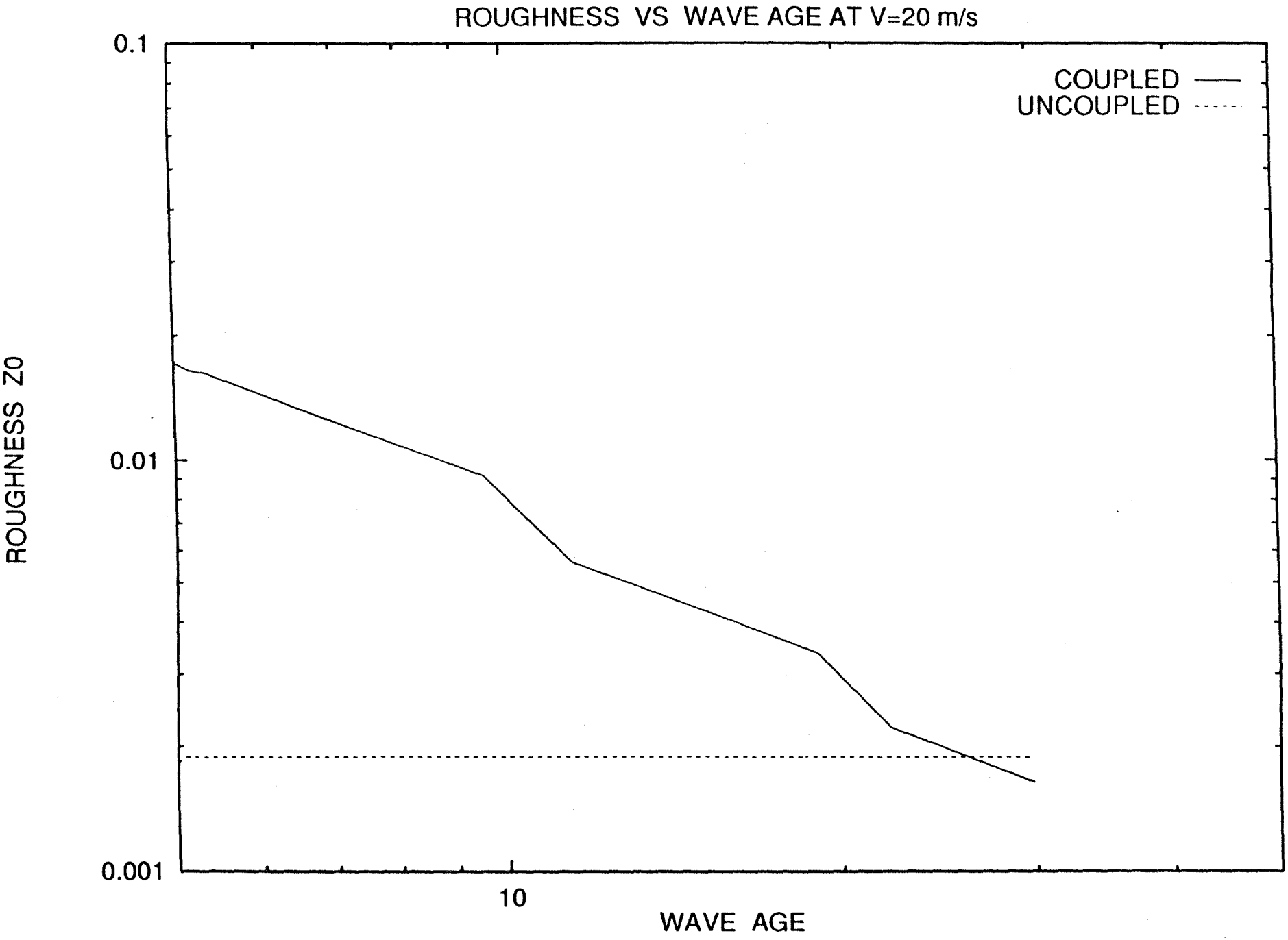
ROUGHNESS VS WAVE AGE AT V=20 m/s
COUPLED
UNCOUPLED
ROUGHNESS Z0
0.1
0.01
0.001
10
WAVE AGE

Fig. 21b

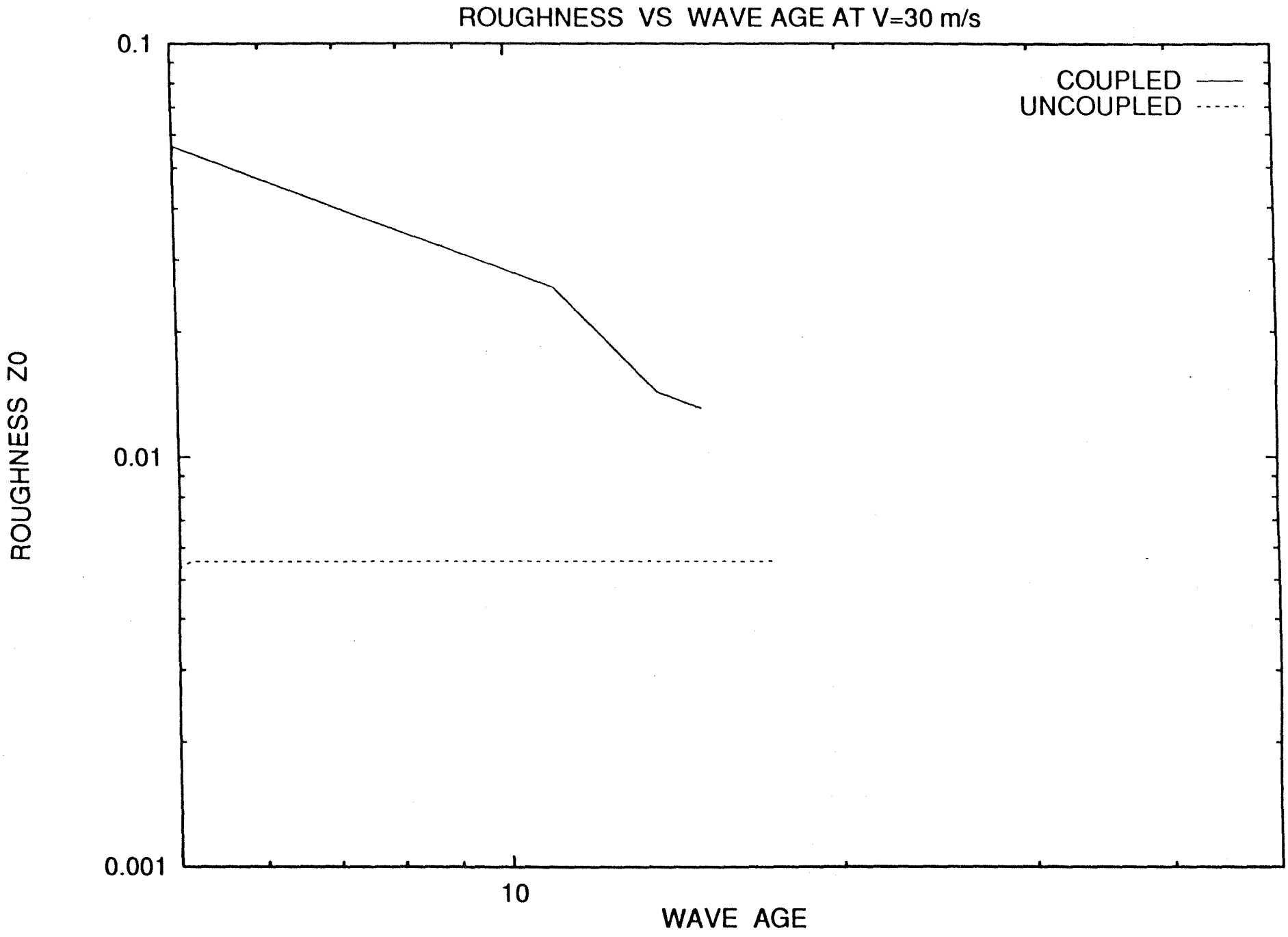
ROUGHNESS VS WAVE AGE AT V=30 m/s
COUPLED
UNCOUPLED
ROUGHNESS Z0
0.1
0.01
0.001
10
WAVE AGE

Fig.21c

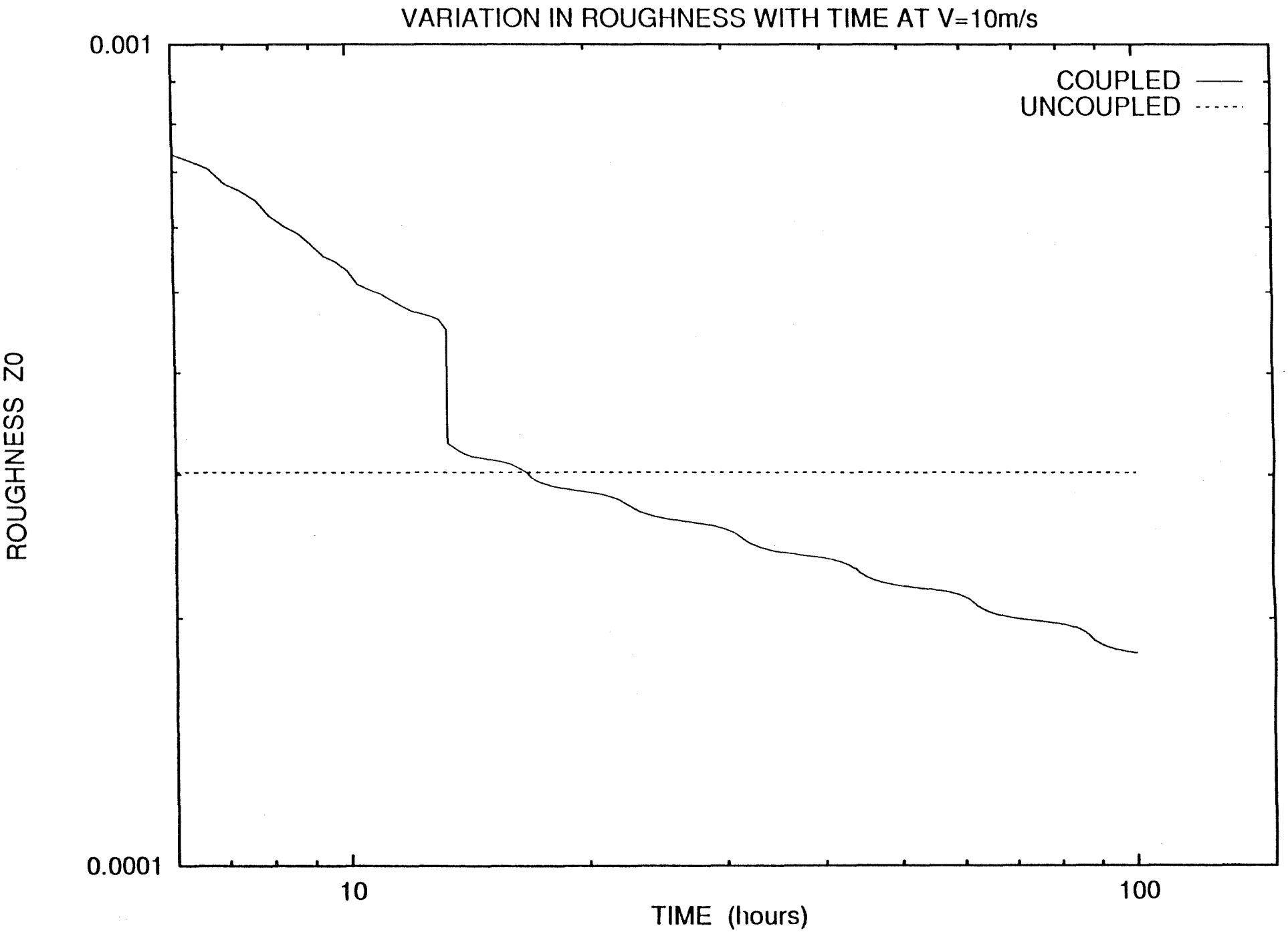
VARIATION IN ROUGHNESS WITH TIME AT V=10m/s
0.001
0.0001
COUPLED
UNCOUPLED
ROUGHNESS Z0
10
100
TIME (hours)

Fig.22a

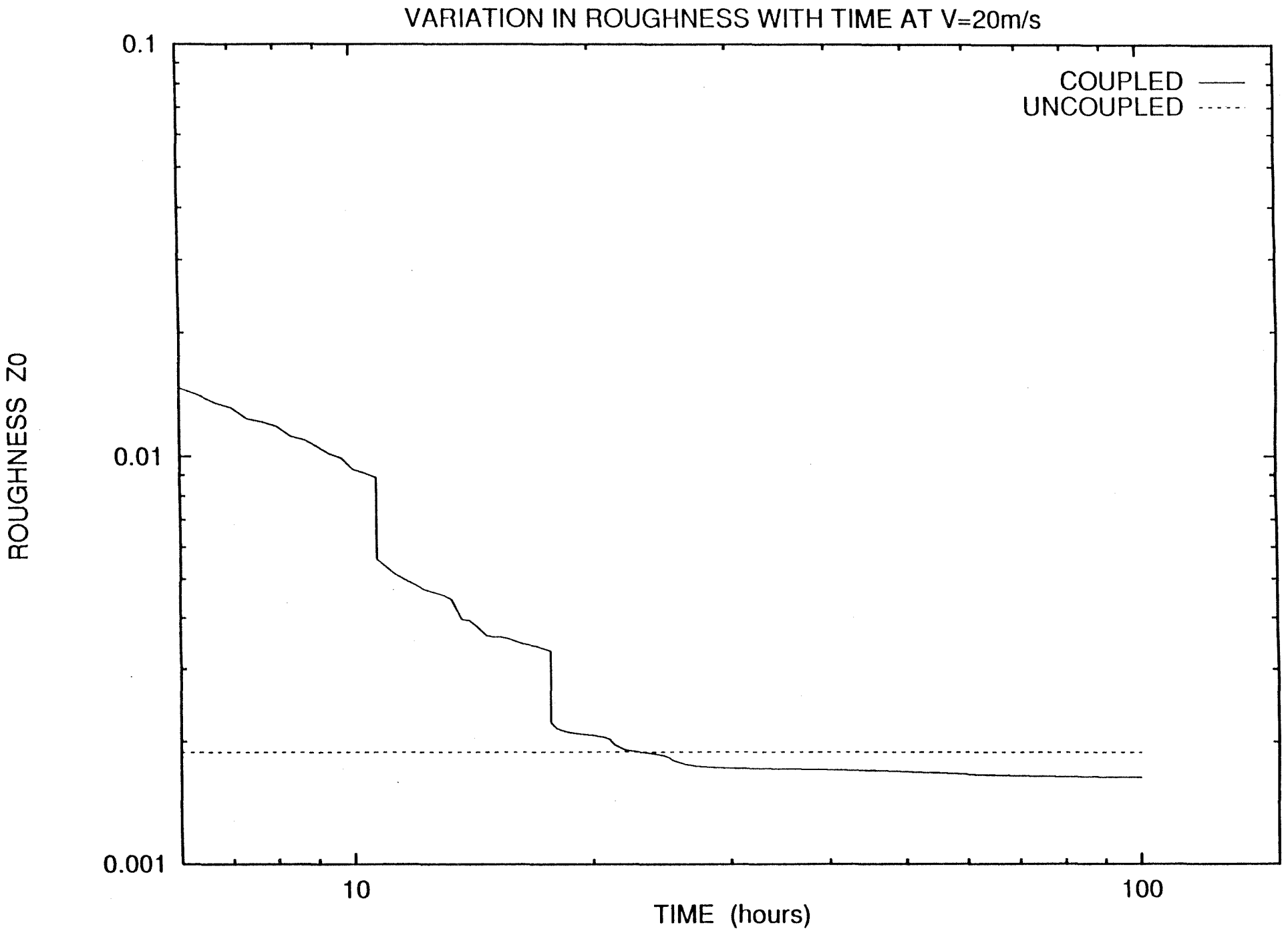
VARIATION IN ROUGHNESS WITH TIME AT V=20m/s
COUPLED
UNCOUPLED
ROUGHNESS Z0
0.1
0.01
0.001
10
100
TIME (hours)

Fig.22b

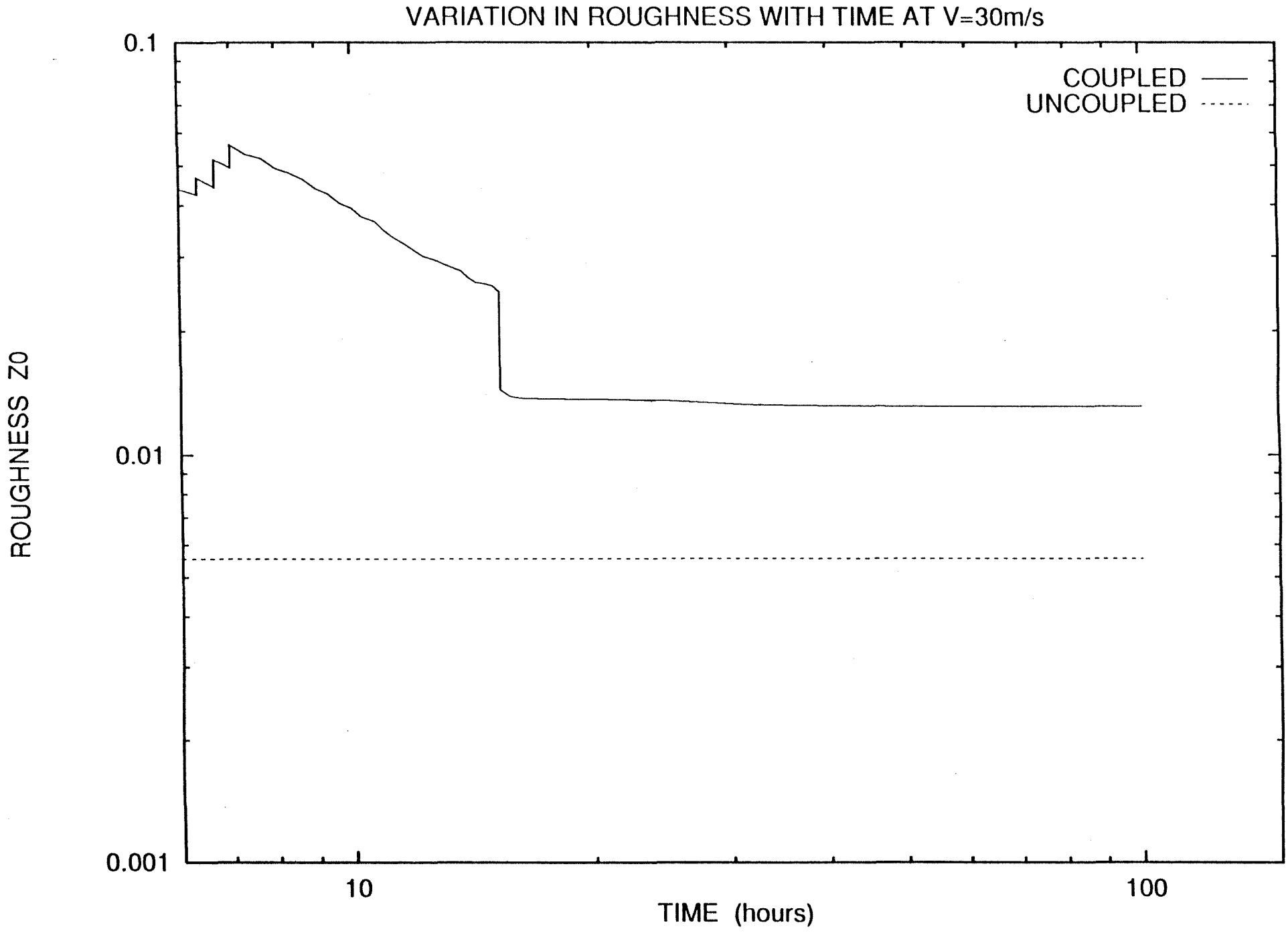
VARIATION IN ROUGHNESS WITH TIME AT V=30m/s
COUPLED
UNCOUPLED
ROUGHNESS Z0
0.1
0.01
0.001
10
100
TIME (hours)

Fig.22c

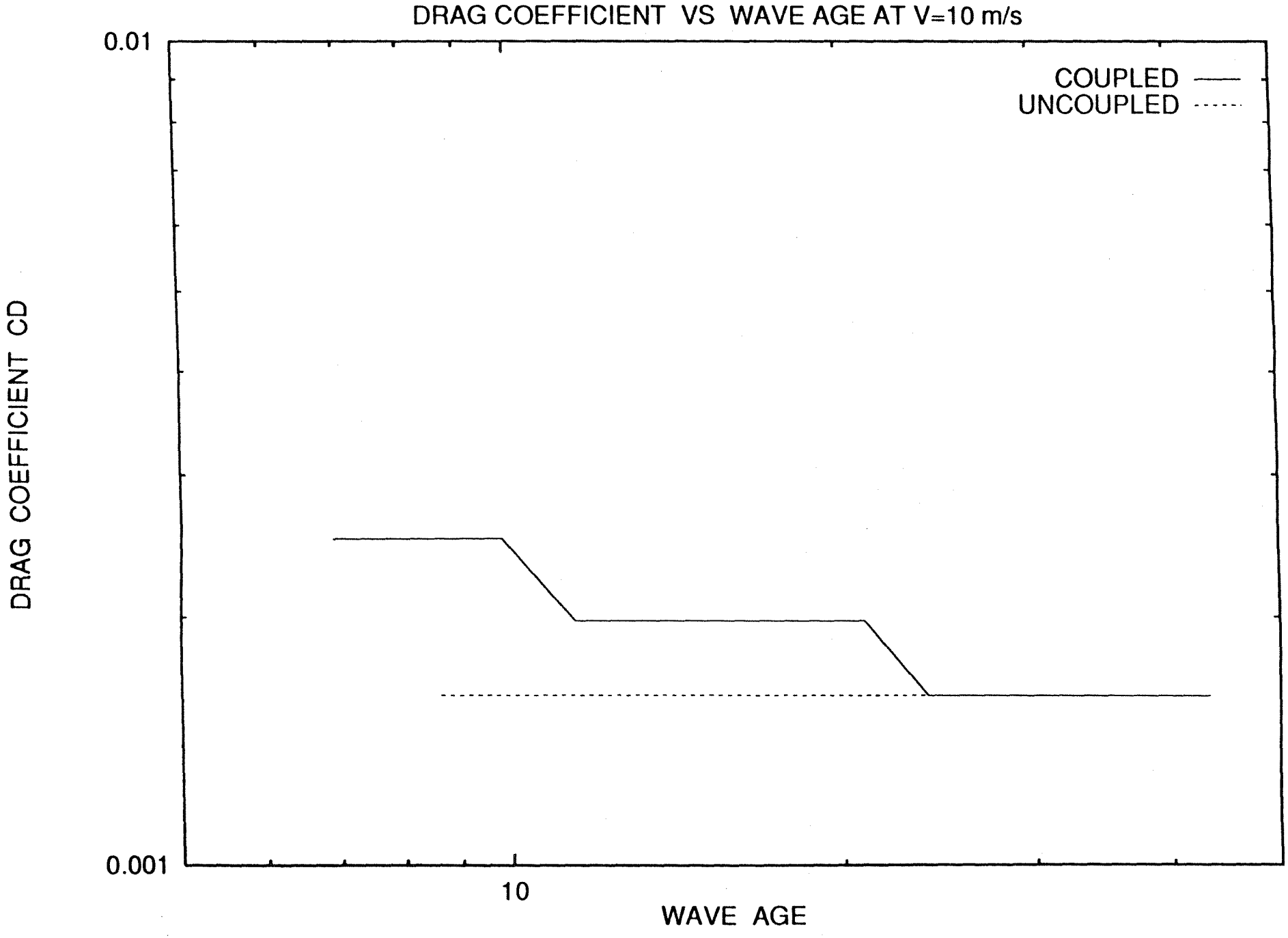
DRAG COEFFICIENT VS WAVE AGE AT V=10 m/s
0.01
0.001
COUPLED
UNCOUPLED
DRAG COEFFICIENT CD
10
WAVE AGE

Fig.23a

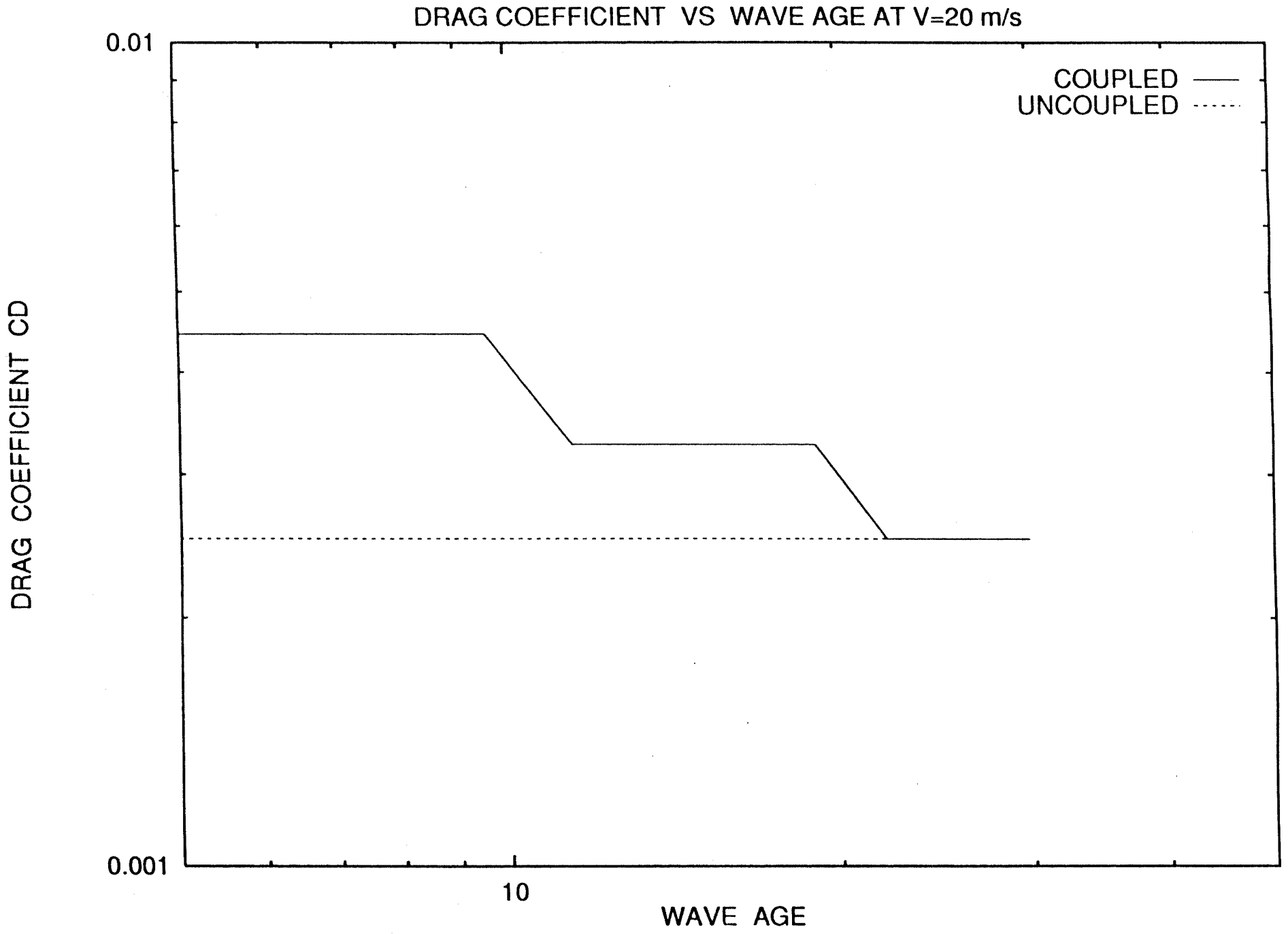
DRAG COEFFICIENT VS WAVE AGE AT V=20 m/s
0.01
0.001
COUPLED
UNCOUPLED
DRAG COEFFICIENT CD
10
WAVE AGE

Fig.23b

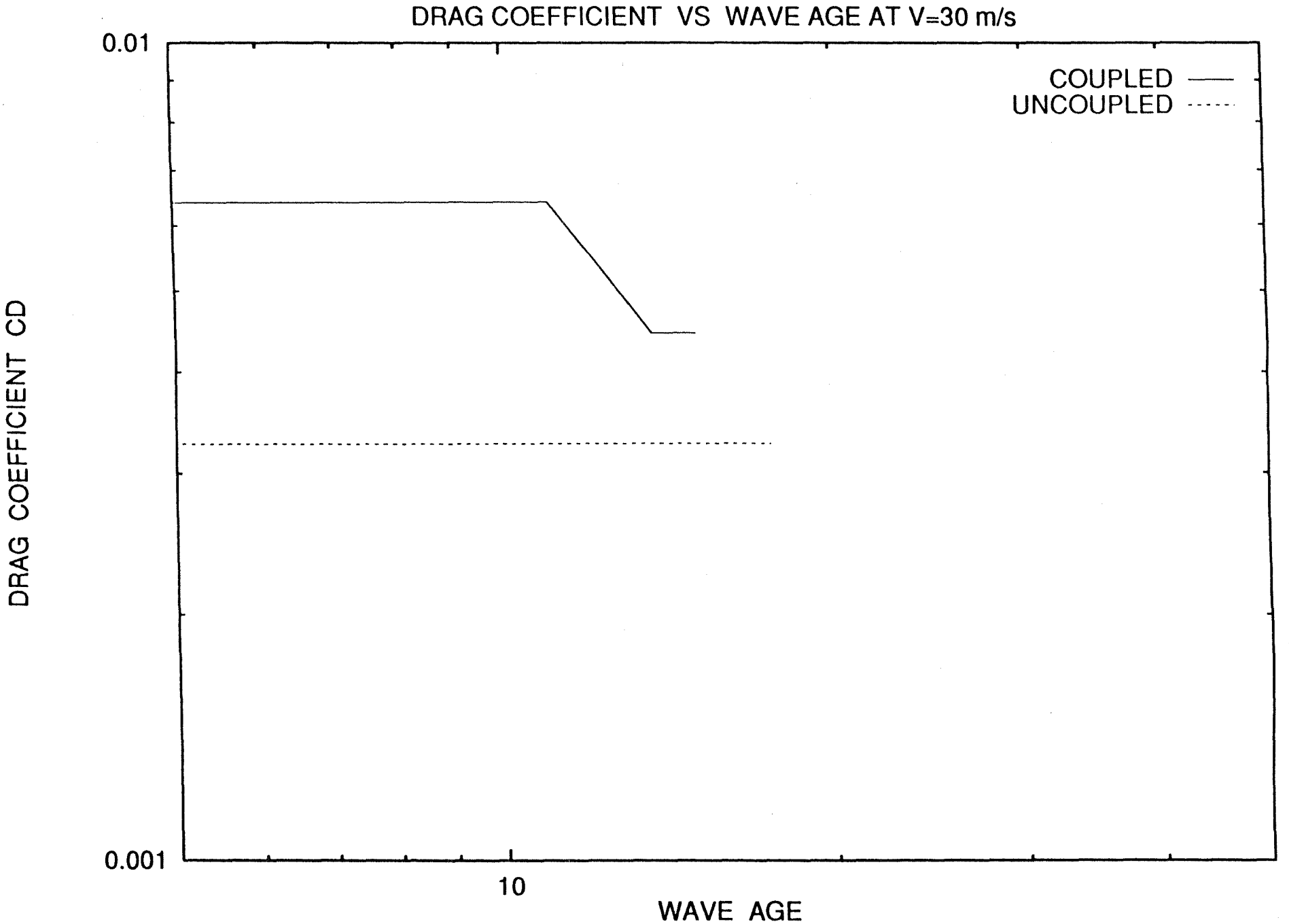
DRAG COEFFICIENT VS WAVE AGE AT V=30 m/s
0.01
0.001
10
COUPLED
UNCOUPLED
DRAG COEFFICIENT CD
WAVE AGE

Fig. 23c

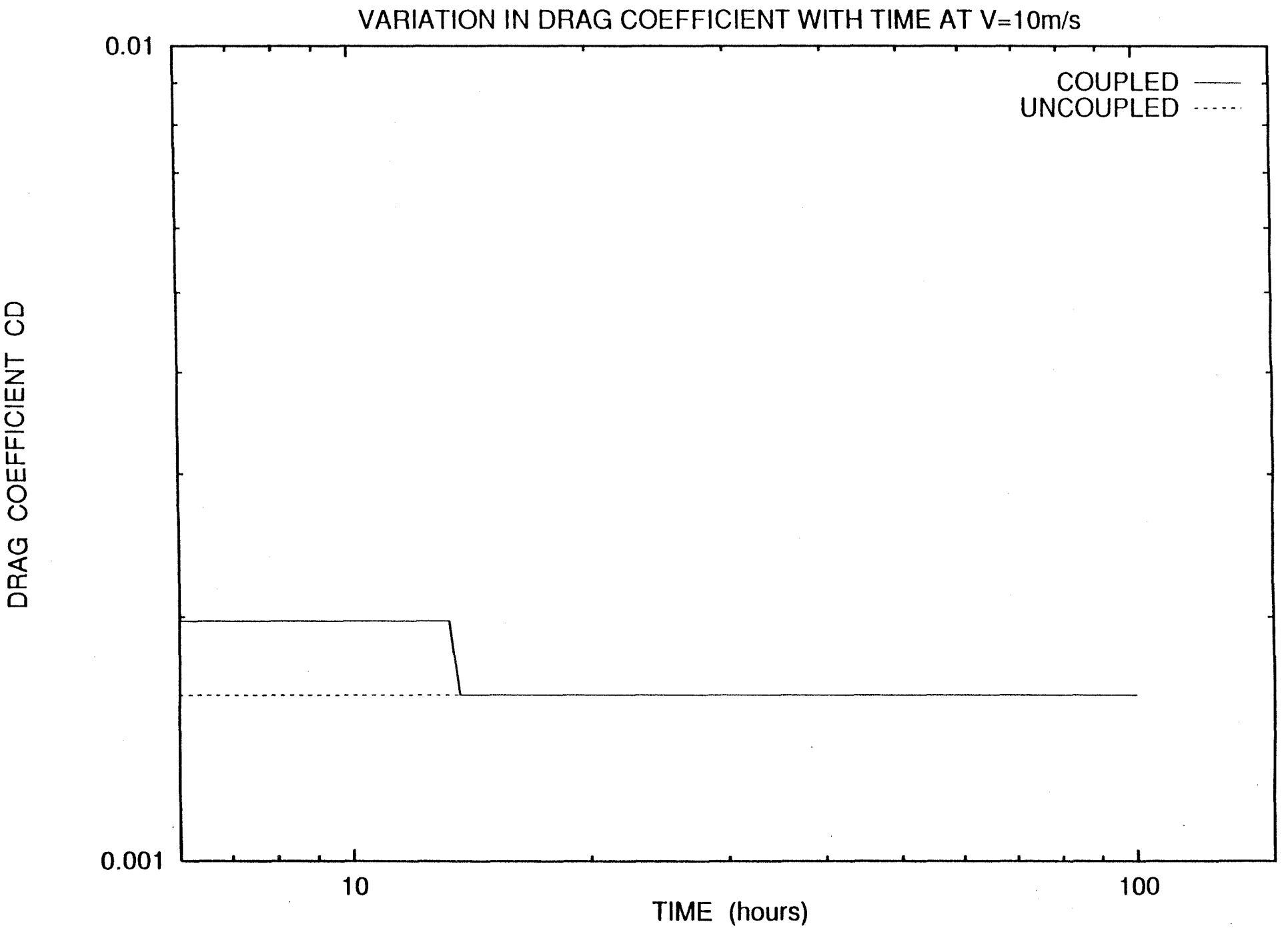
VARIATION IN DRAG COEFFICIENT WITH TIME AT V=10m/s
0.01
0.001
COUPLED
UNCOUPLED
DRAG COEFFICIENT CD
10
100
TIME (hours)

Fig.24a

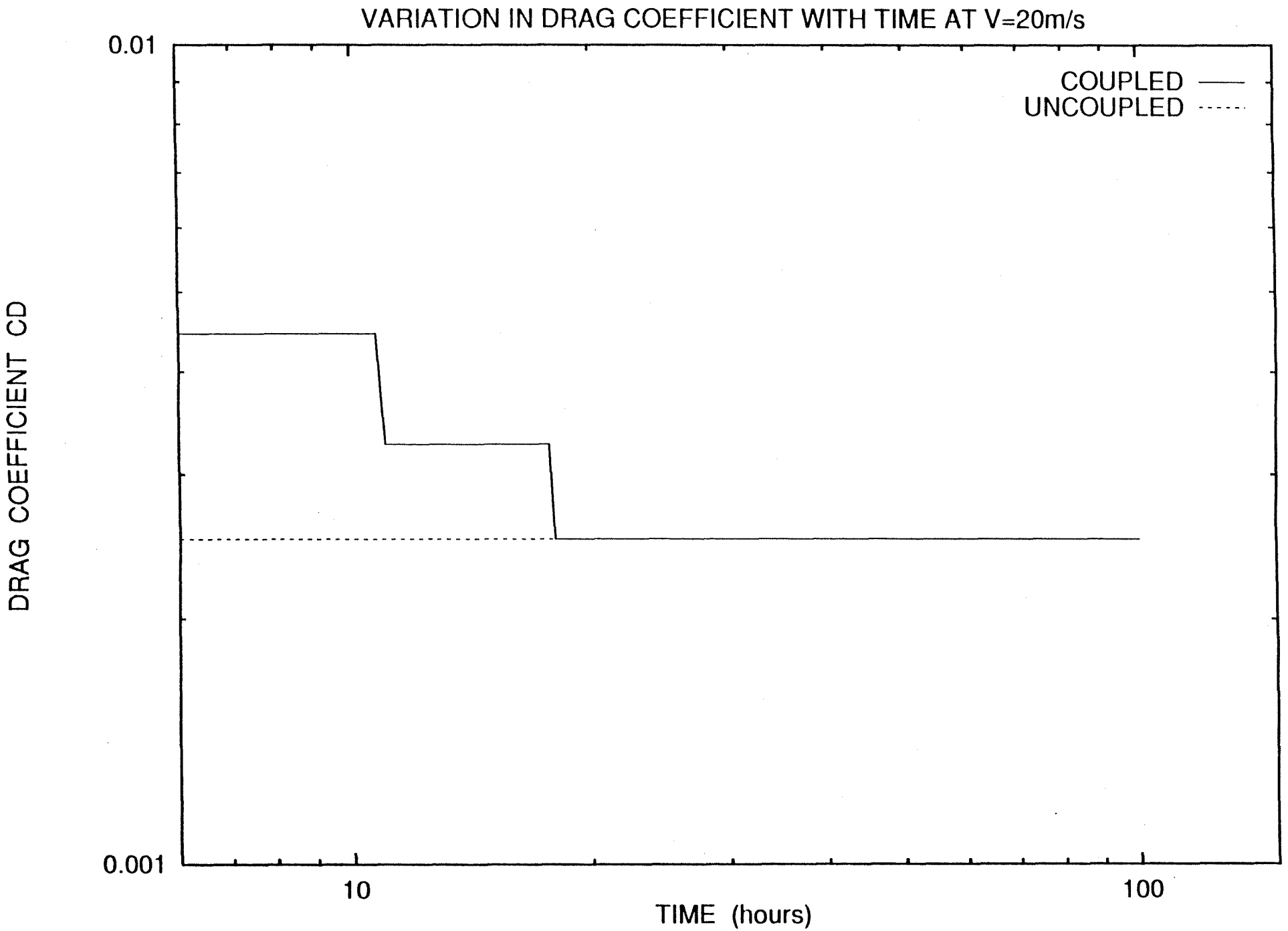
VARIATION IN DRAG COEFFICIENT WITH TIME AT V=20m/s
0.01
0.001
COUPLED
UNCOUPLED
DRAG COEFFICIENT CD
10
100
TIME (hours)

Fig.24b

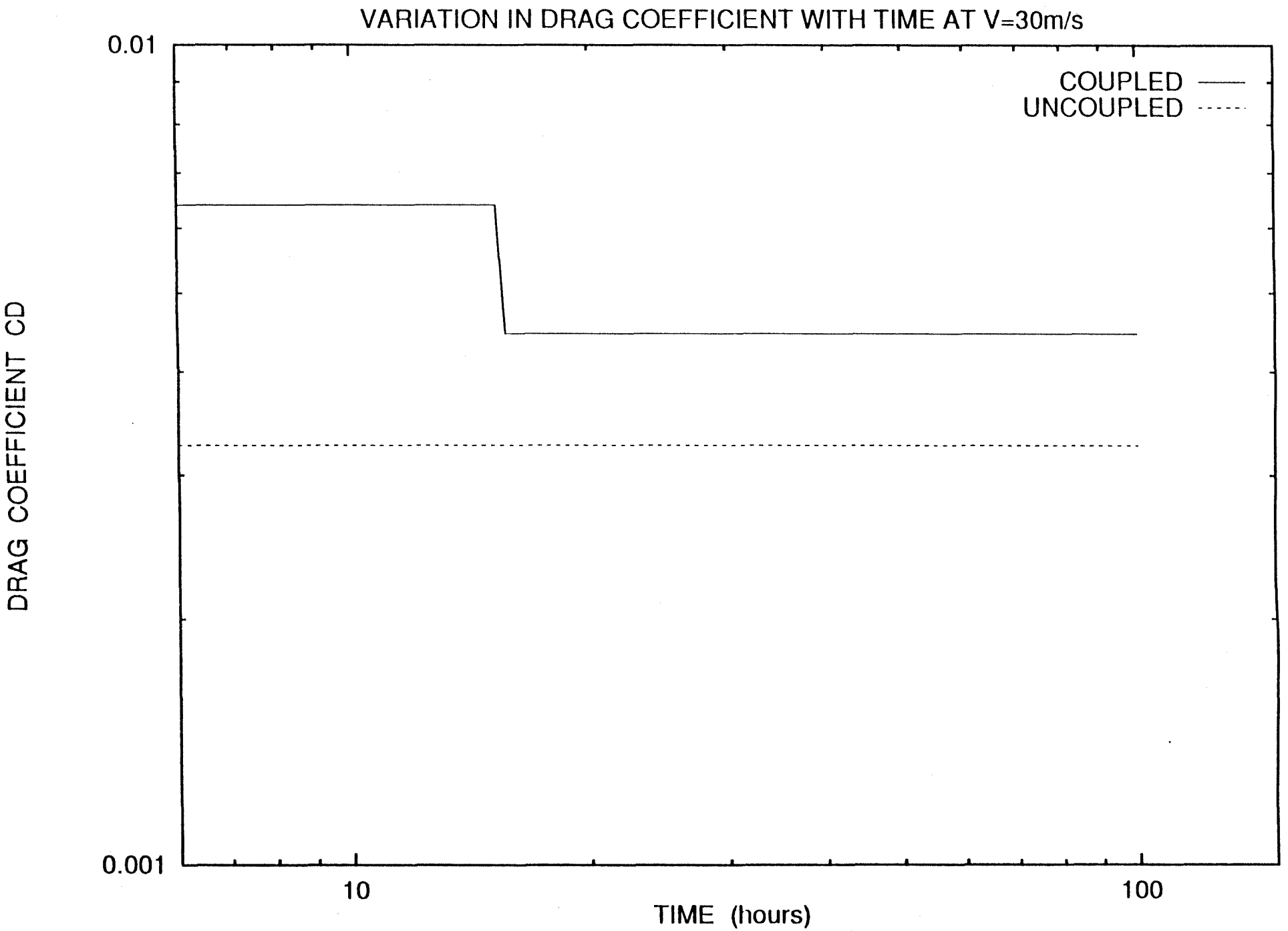
VARIATION IN DRAG COEFFICIENT WITH TIME AT V=30m/s
0.01
0.001
COUPLED
UNCOUPLED
DRAG COEFFICIENT CD
10
100
TIME (hours)

Fig.24c

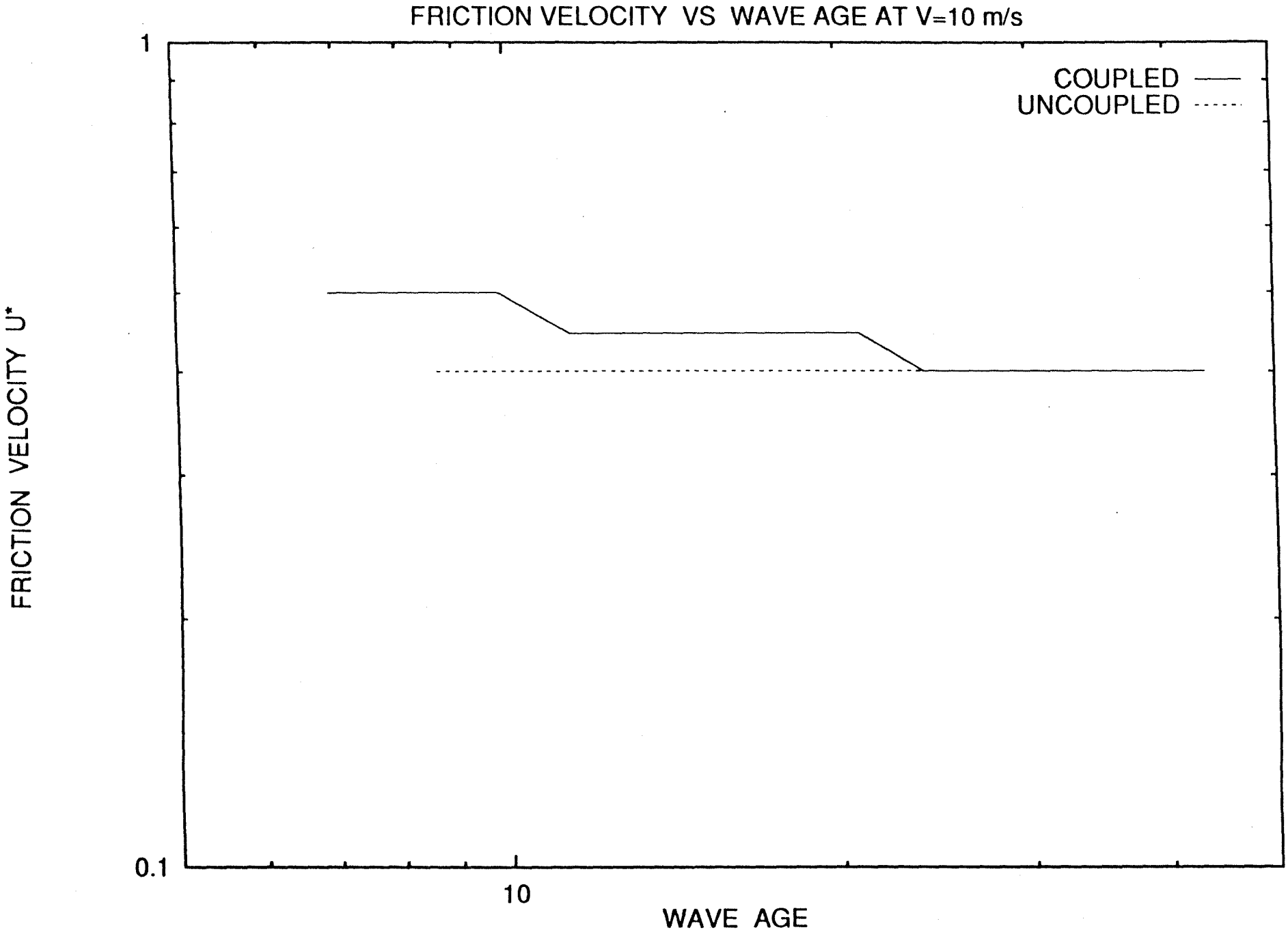
FRICTION VELOCITY VS WAVE AGE AT V=10 m/s
COUPLED
UNCOUPLED
FRICTION VELOCITY U*
1
0.1
10
WAVE AGE

Fig.25a

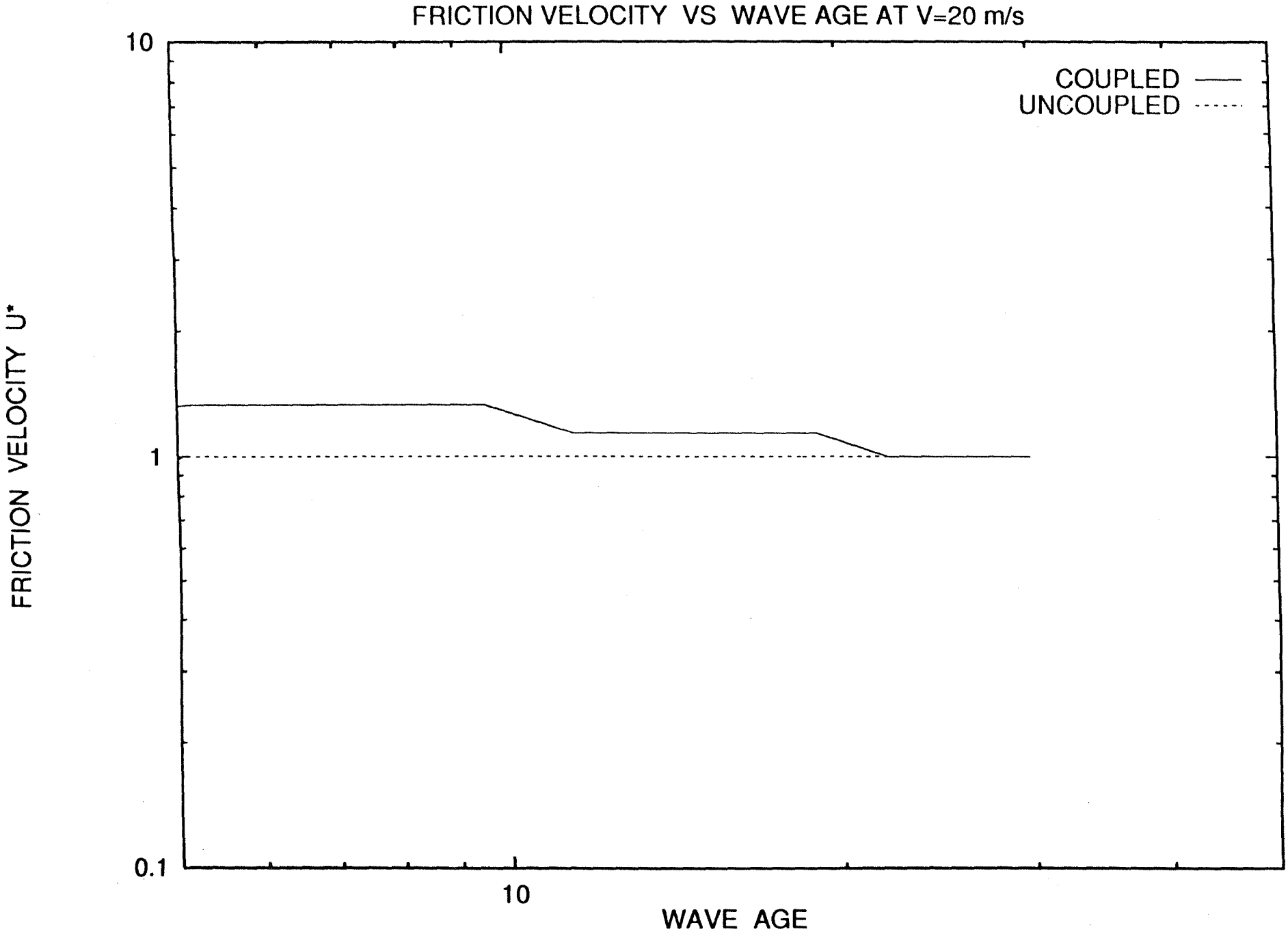
FRICTION VELOCITY VS WAVE AGE AT V=20 m/s
COUPLED
UNCOUPLED
FRICTION VELOCITY U*
10
1
0.1
10
WAVE AGE

Fig.25b

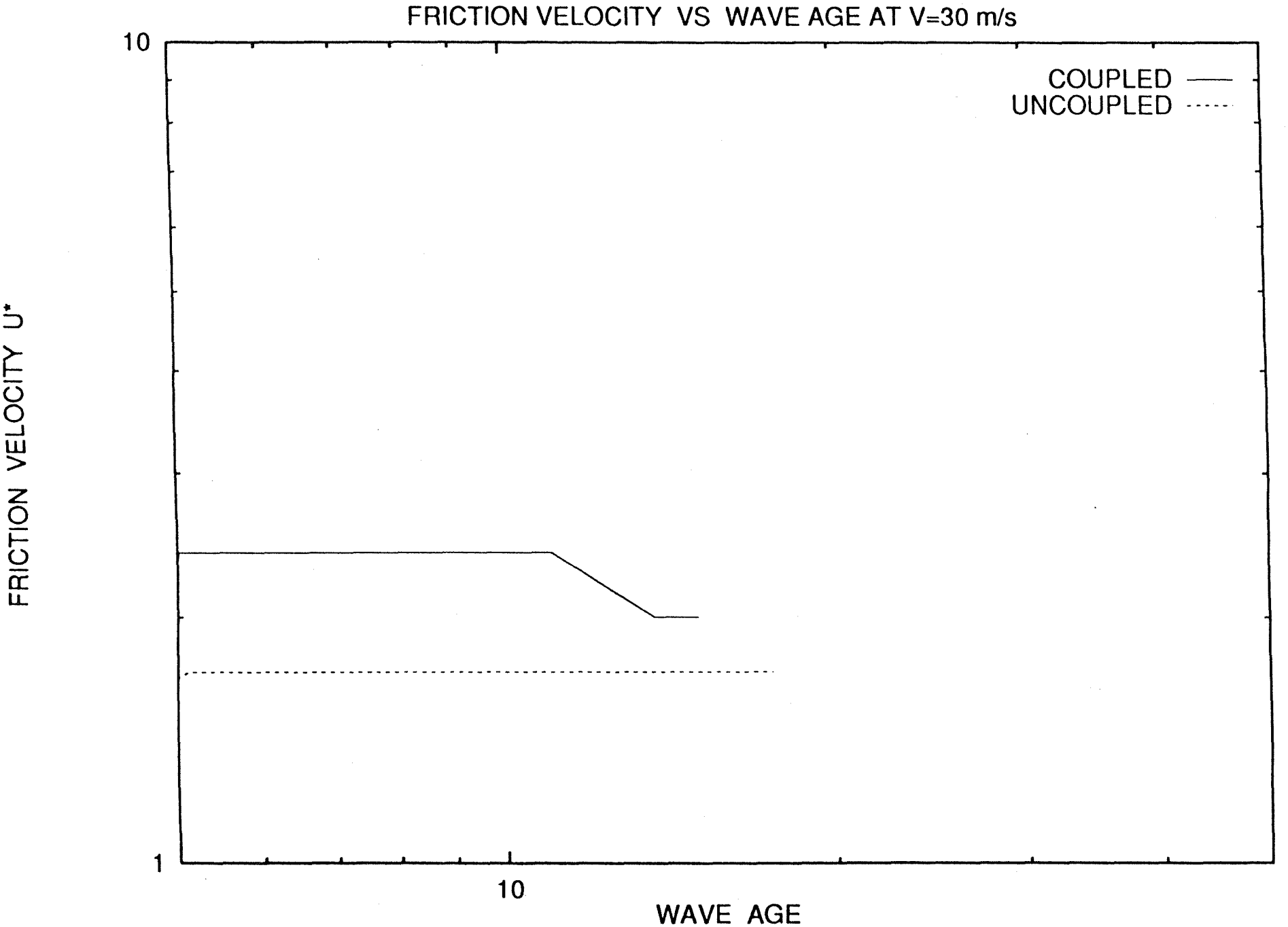
FRICTION VELOCITY VS WAVE AGE AT V=30 m/s
10
1
10
COUPLED
UNCOUPLED
FRICTION VELOCITY U*
WAVE AGE

Fig.25c

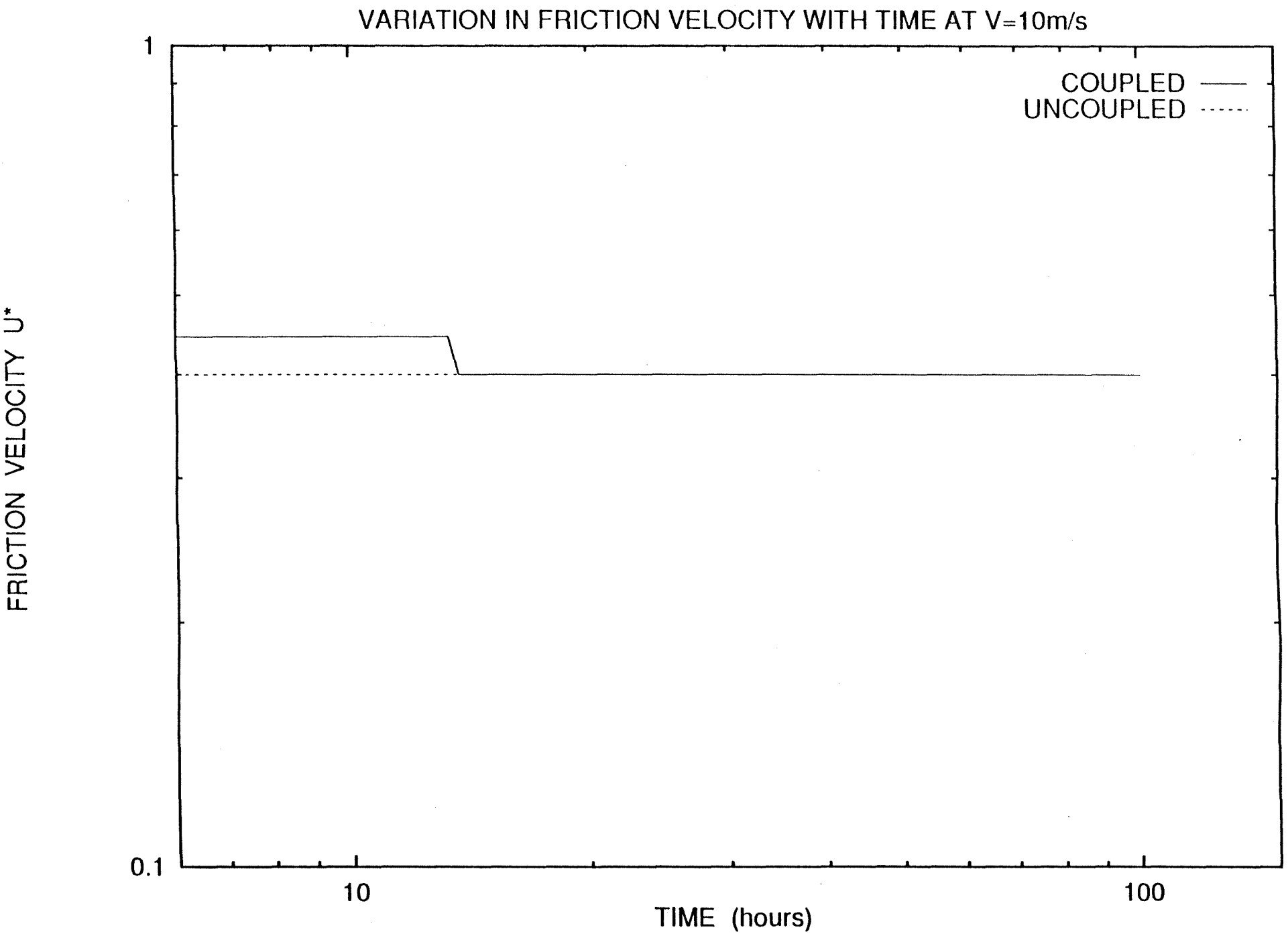
VARIATION IN FRICTION VELOCITY WITH TIME AT V=10m/s
COUPLED
UNCOUPLED
FRICTION VELOCITY U*
1
0.1
10
100
TIME (hours)

Fig.26a

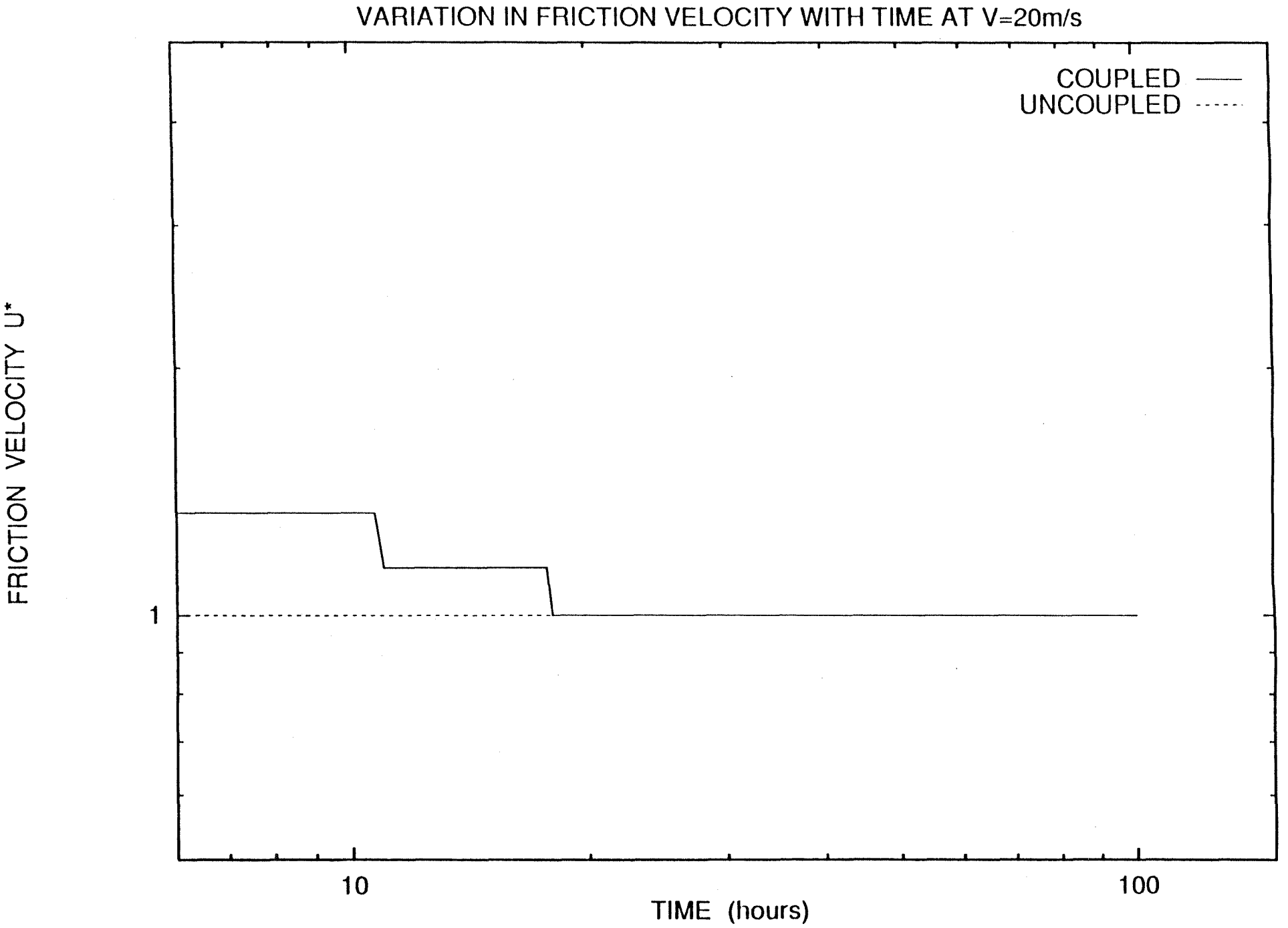
VARIATION IN FRICTION VELOCITY WITH TIME AT V=20m/s
COUPLED
UNCOUPLED
FRICTION VELOCITY U*
1
10
100
TIME (hours)

Fig. 26b

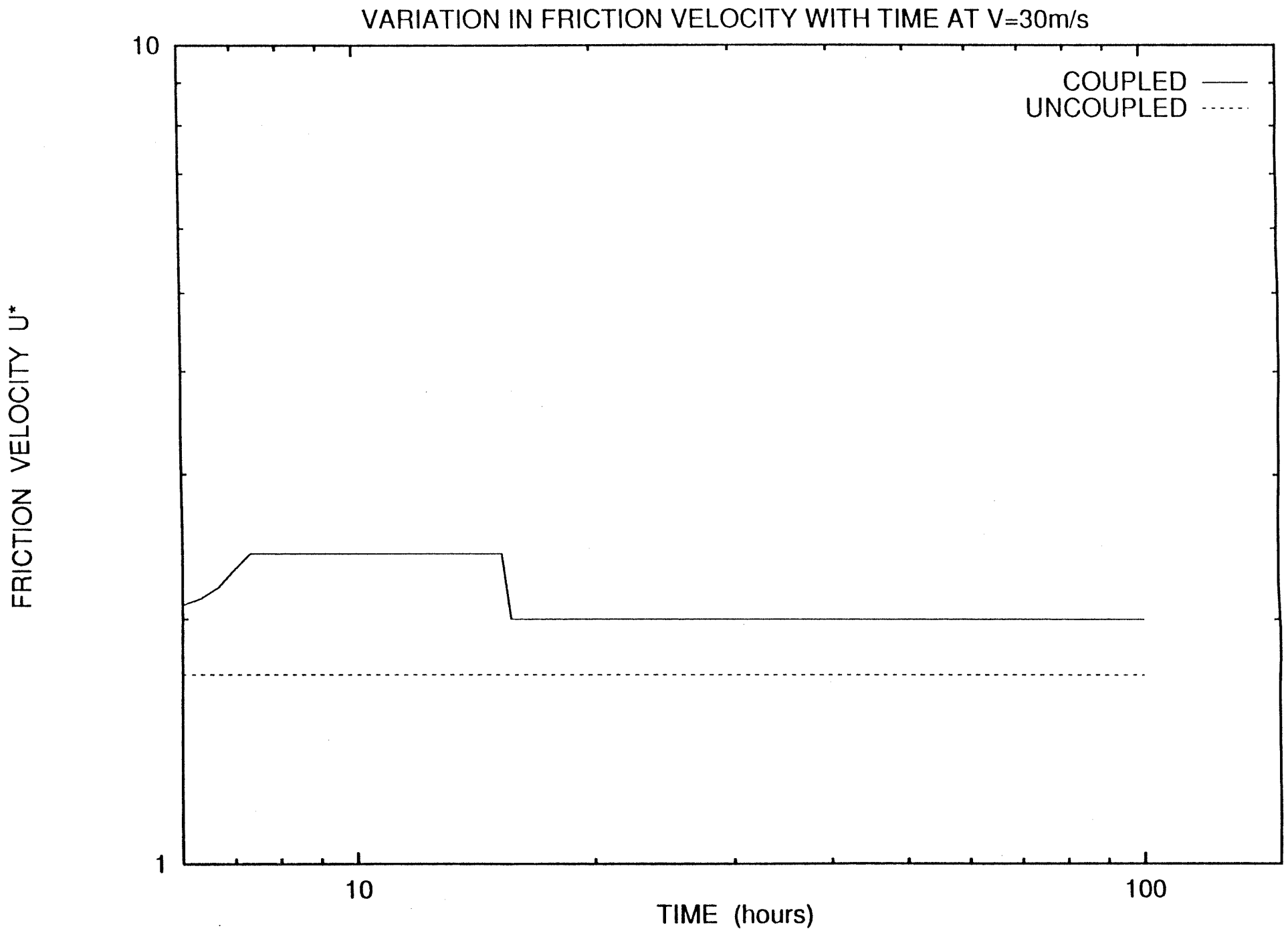
VARIATION IN FRICTION VELOCITY WITH TIME AT V=30m/s
10
1
COUPLED
UNCOUPLED
FRICTION VELOCITY U*
10
100
TIME (hours)

Fig.26c

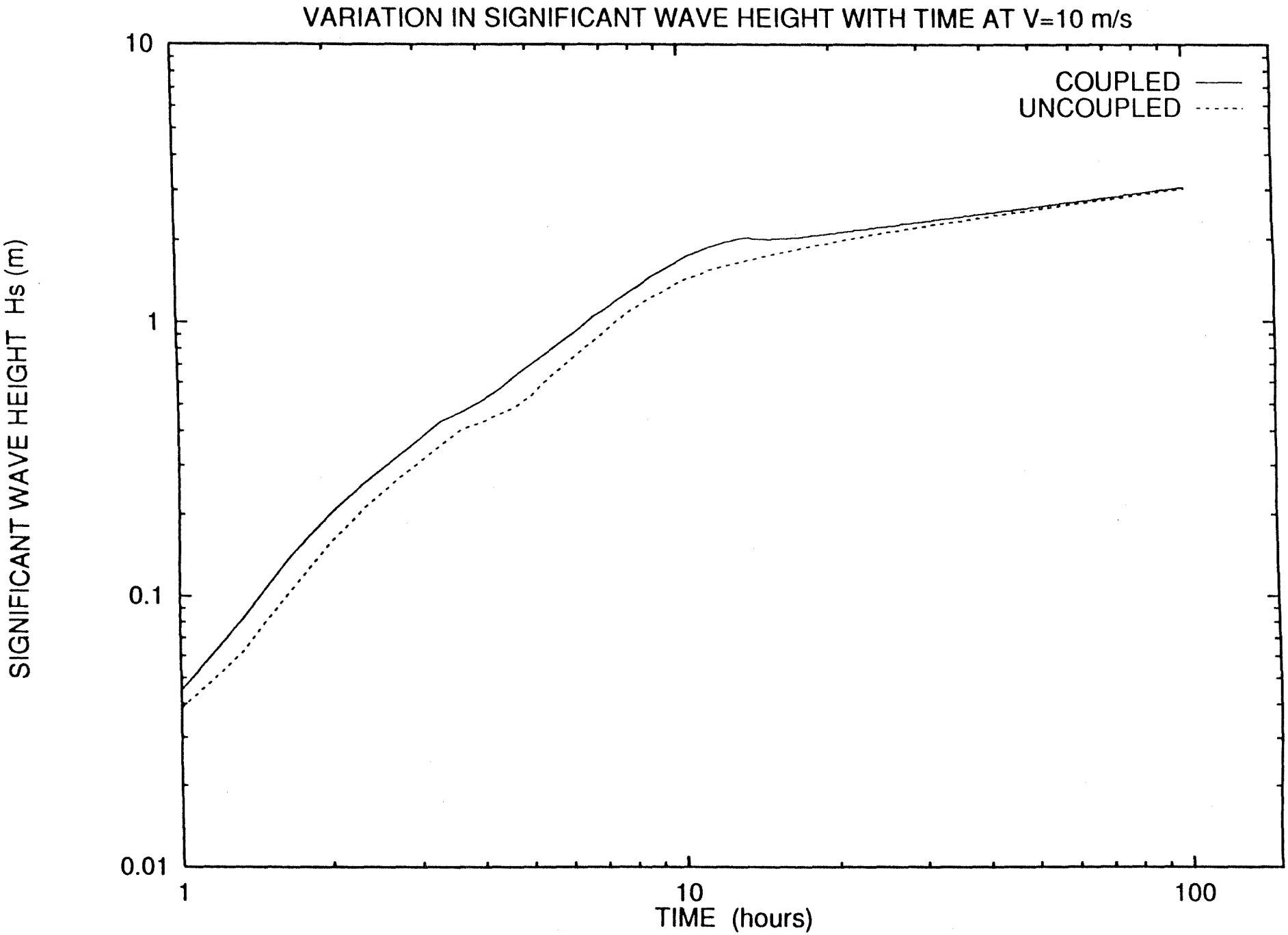
VARIATION IN SIGNIFICANT WAVE HEIGHT WITH TIME AT V=10 m/s
COUPLED
UNCOUPLED
SIGNIFICANT WAVE HEIGHT Hs (m)
10
1
0.1
0.01
1
10
100
TIME (hours)

Fig.27a

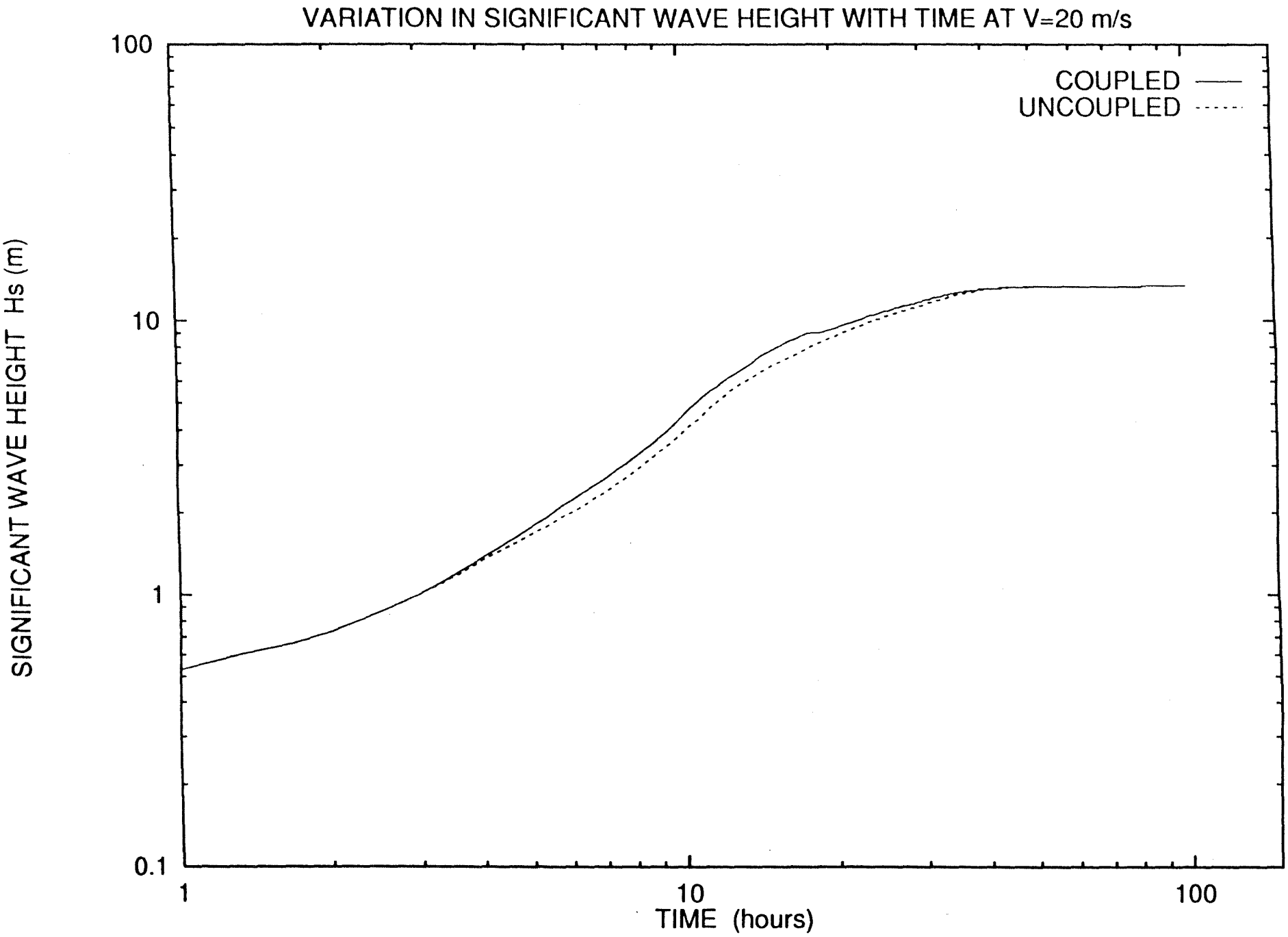
VARIATION IN SIGNIFICANT WAVE HEIGHT WITH TIME AT V=20 m/s
COUPLED
UNCOUPLED
SIGNIFICANT WAVE HEIGHT Hs (m)
100
10
1
0.1
1
10
100
TIME (hours)

Fig.27b

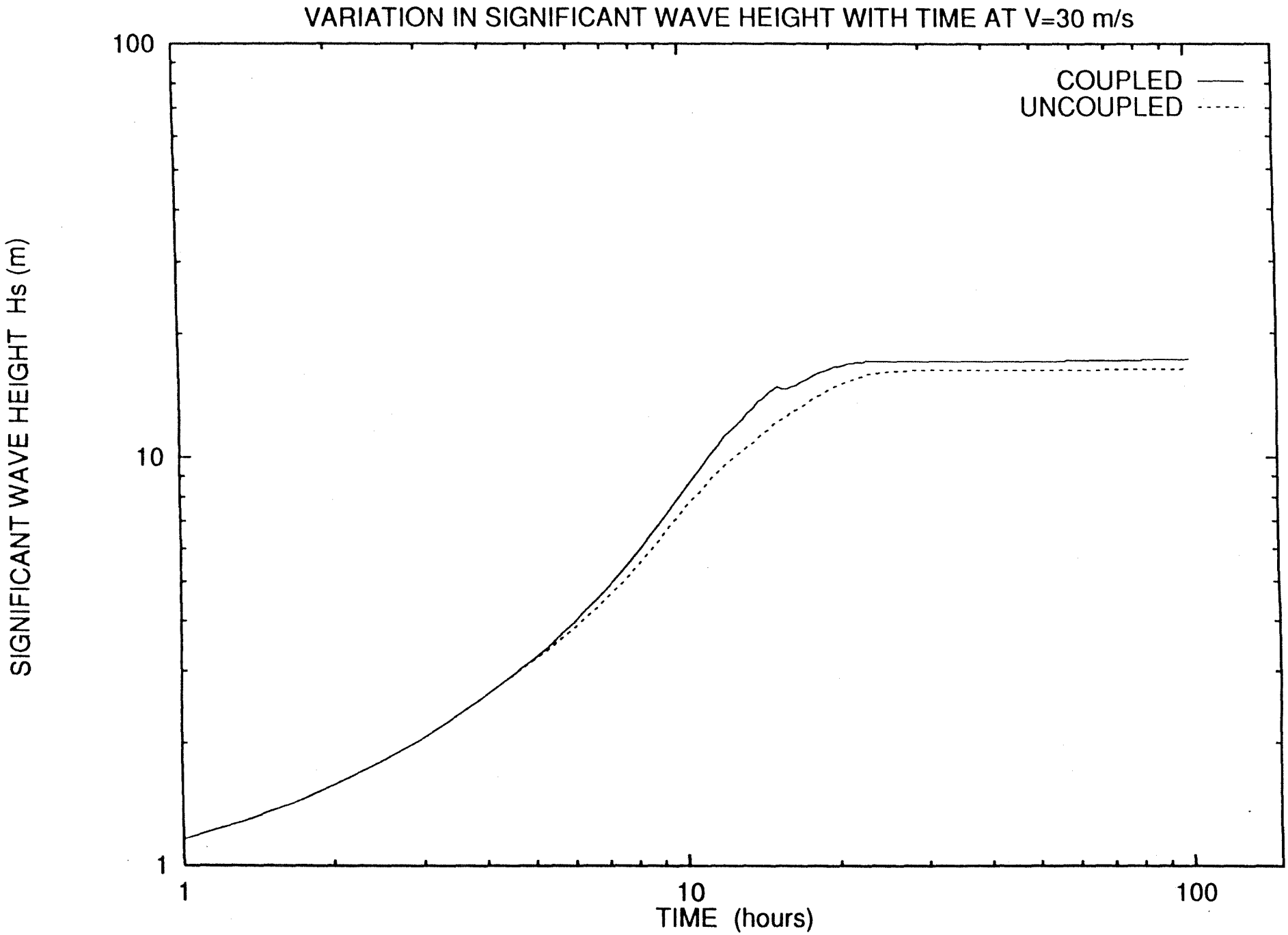
VARIATION IN SIGNIFICANT WAVE HEIGHT WITH TIME AT V=30 m/s
COUPLED
UNCOUPLED
SIGNIFICANT WAVE HEIGHT Hs (m)
100
10
1
1
10
100
TIME (hours)

Fig.27c

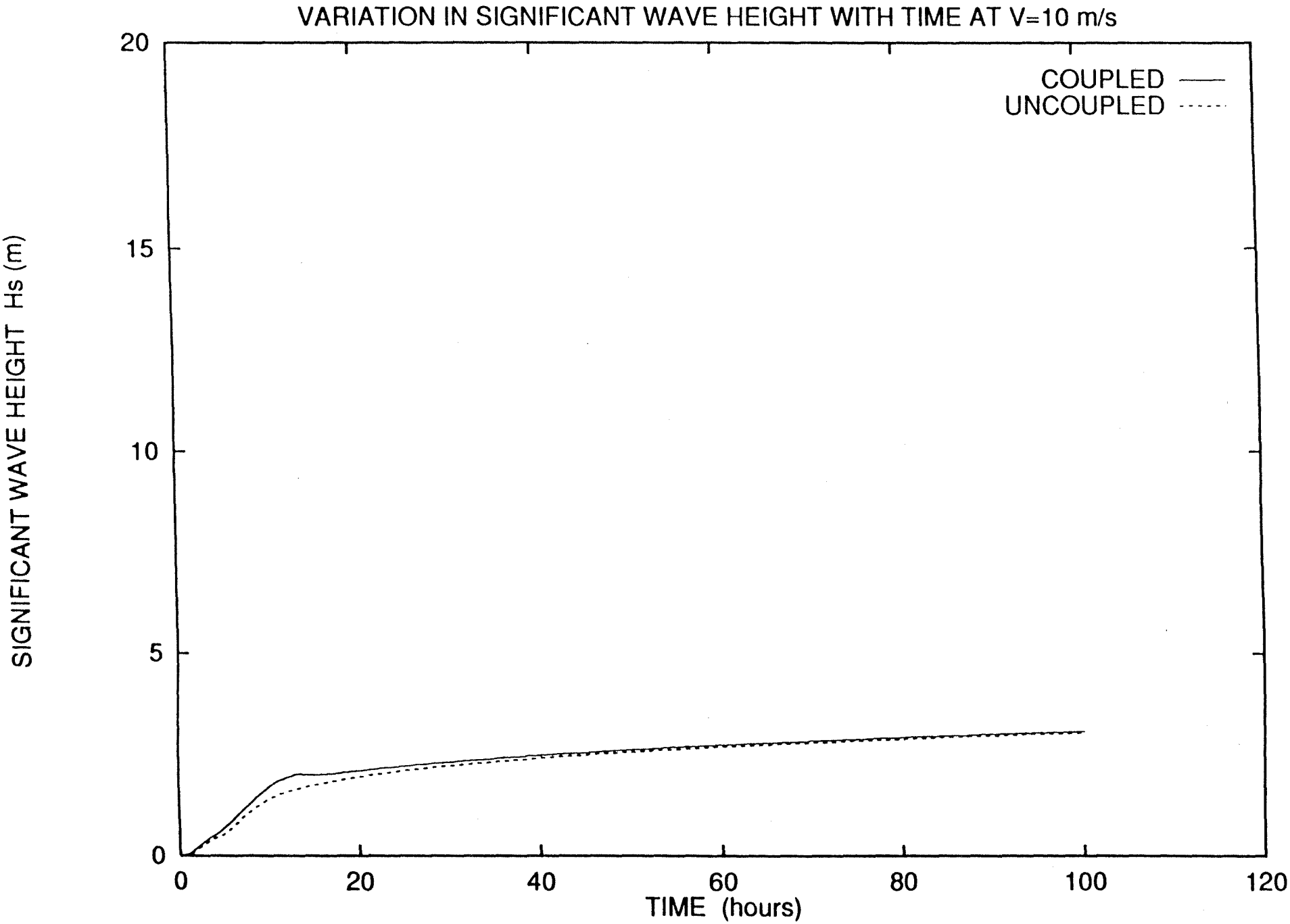
VARIATION IN SIGNIFICANT WAVE HEIGHT WITH TIME AT V=10 m/s
COUPLED
UNCOUPLED
SIGNIFICANT WAVE HEIGHT Hs (m)
20
15
10
5
0
0
20
40
60
80
100
120
TIME (hours)

Fig.28a

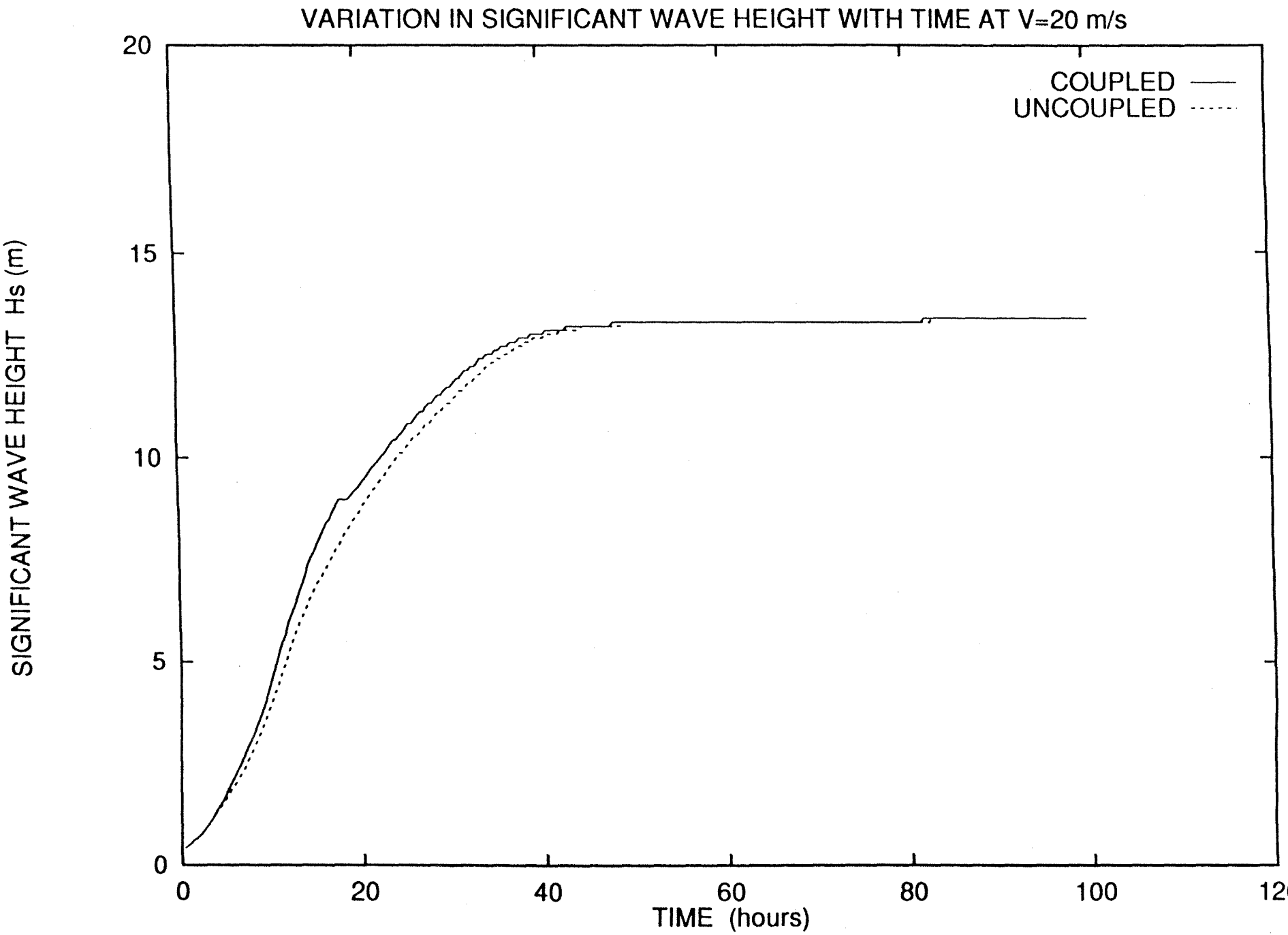
VARIATION IN SIGNIFICANT WAVE HEIGHT WITH TIME AT V=20 m/s
COUPLED
UNCOUPLED
SIGNIFICANT WAVE HEIGHT Hs (m)
TIME (hours)
0
5
10
15
20
0
20
40
60
80
100
120

Fig.28b

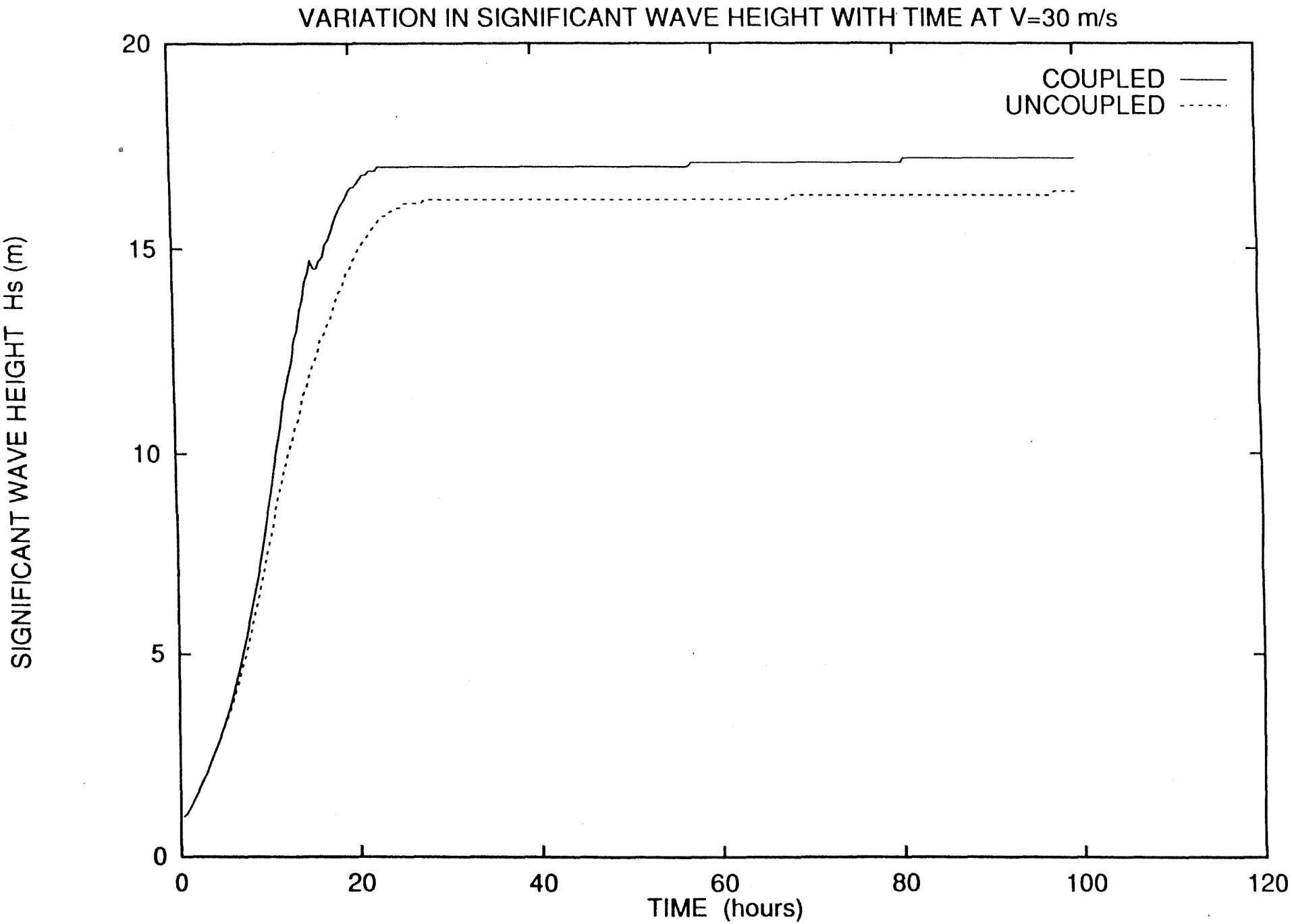
VARIATION IN SIGNIFICANT WAVE HEIGHT WITH TIME AT V=30 m/s
COUPLED
UNCOUPLED
SIGNIFICANT WAVE HEIGHT Hs (m)
TIME (hours)
0
5
10
15
20
0
20
40
60
80
100
120

Fig.28c

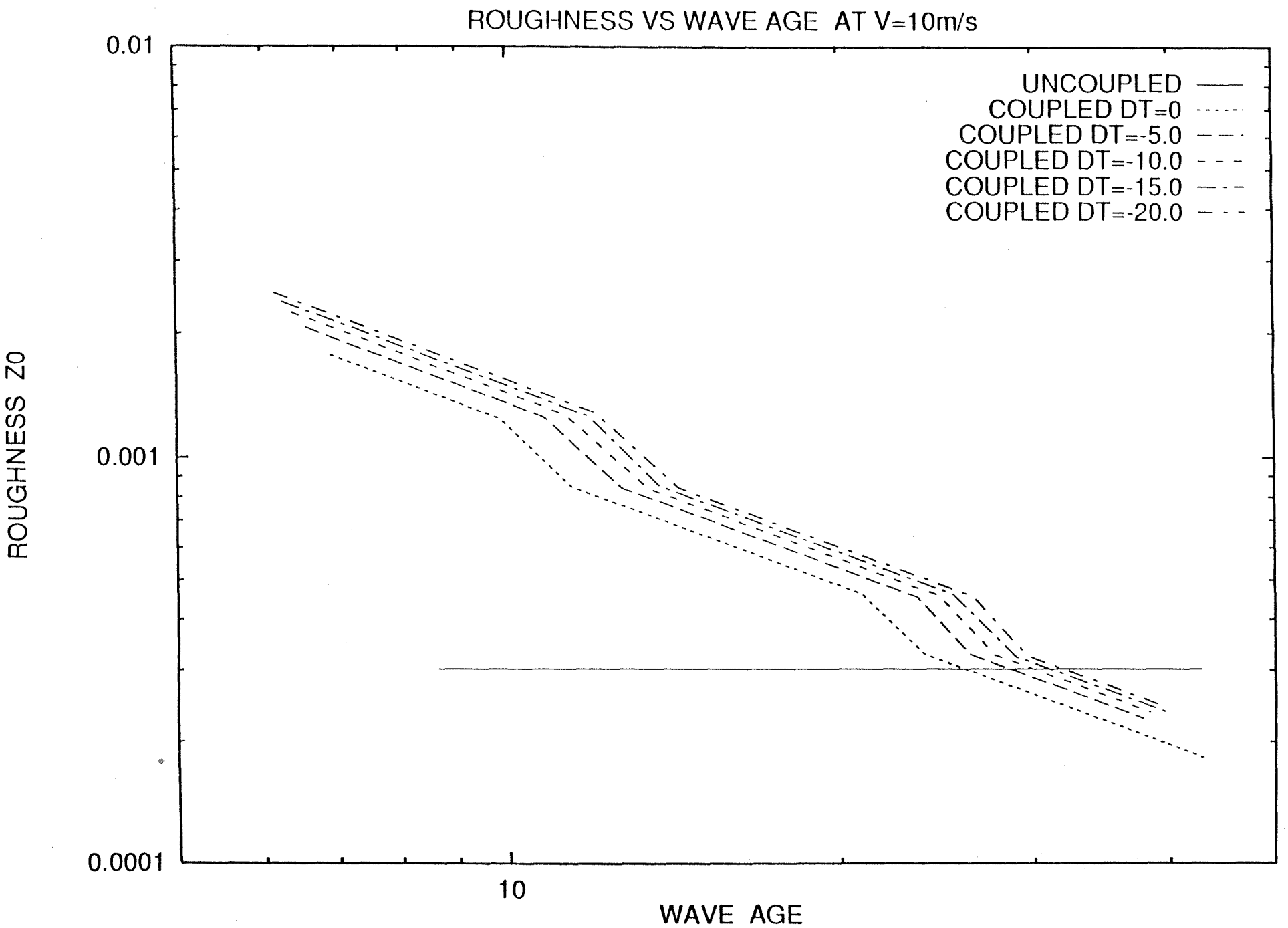
ROUGHNESS VS WAVE AGE AT V=10m/s
0.01
0.001
0.0001
ROUGHNESS Z0
10
WAVE AGE
UNCOUPLED
COUPLED DT=0
COUPLED DT=-5.0
COUPLED DT=-10.0
COUPLED DT=-15.0
COUPLED DT=-20.0

Fig.29a

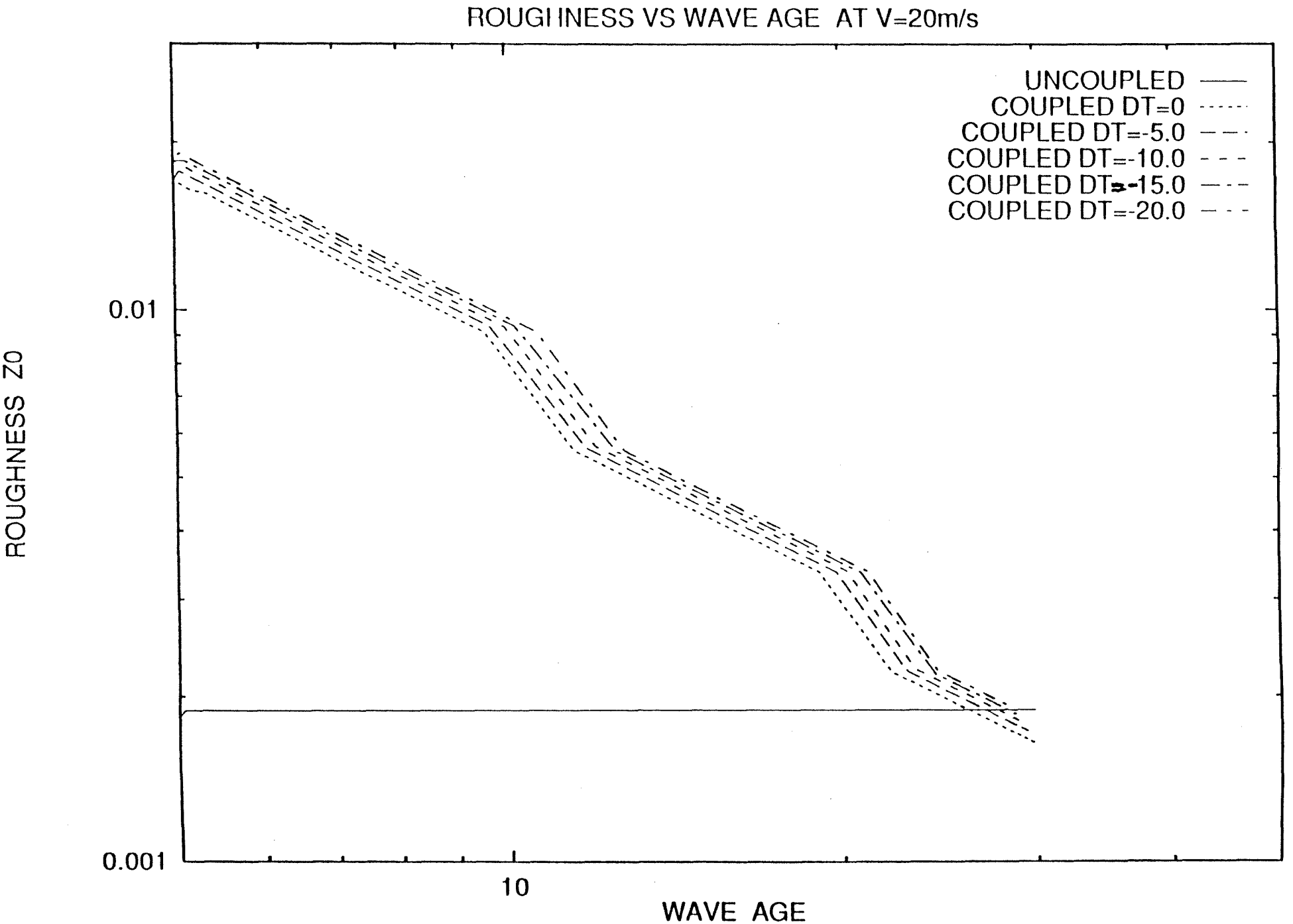
ROUGHINESS VS WAVE AGE AT V=20m/s
UNCOUPLED
COUPLED DT=0
COUPLED DT=-5.0
COUPLED DT=-10.0
COUPLED DT=-15.0
COUPLED DT=-20.0
0.01
0.001
ROUGHNESS Z0
10
WAVE AGE

Fig.29b

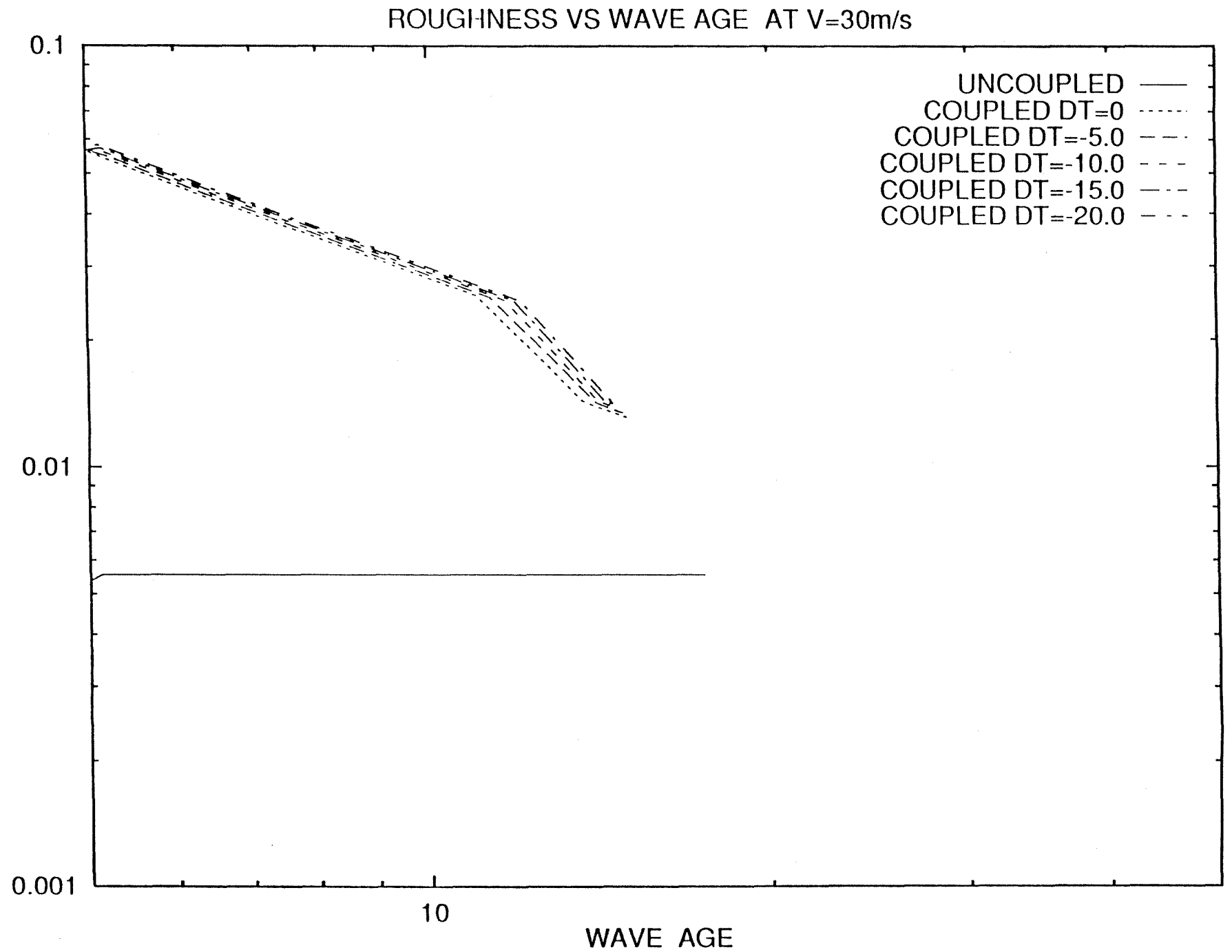
ROUGHNESS VS WAVE AGE AT V=30m/s
0.1
0.01
0.001
10
ROUGHNESS Z0
WAVE AGE
UNCOUPLED
COUPLED DT=0
COUPLED DT=-5.0
COUPLED DT=-10.0
COUPLED DT=-15.0
COUPLED DT=-20.0

Fig. 29c

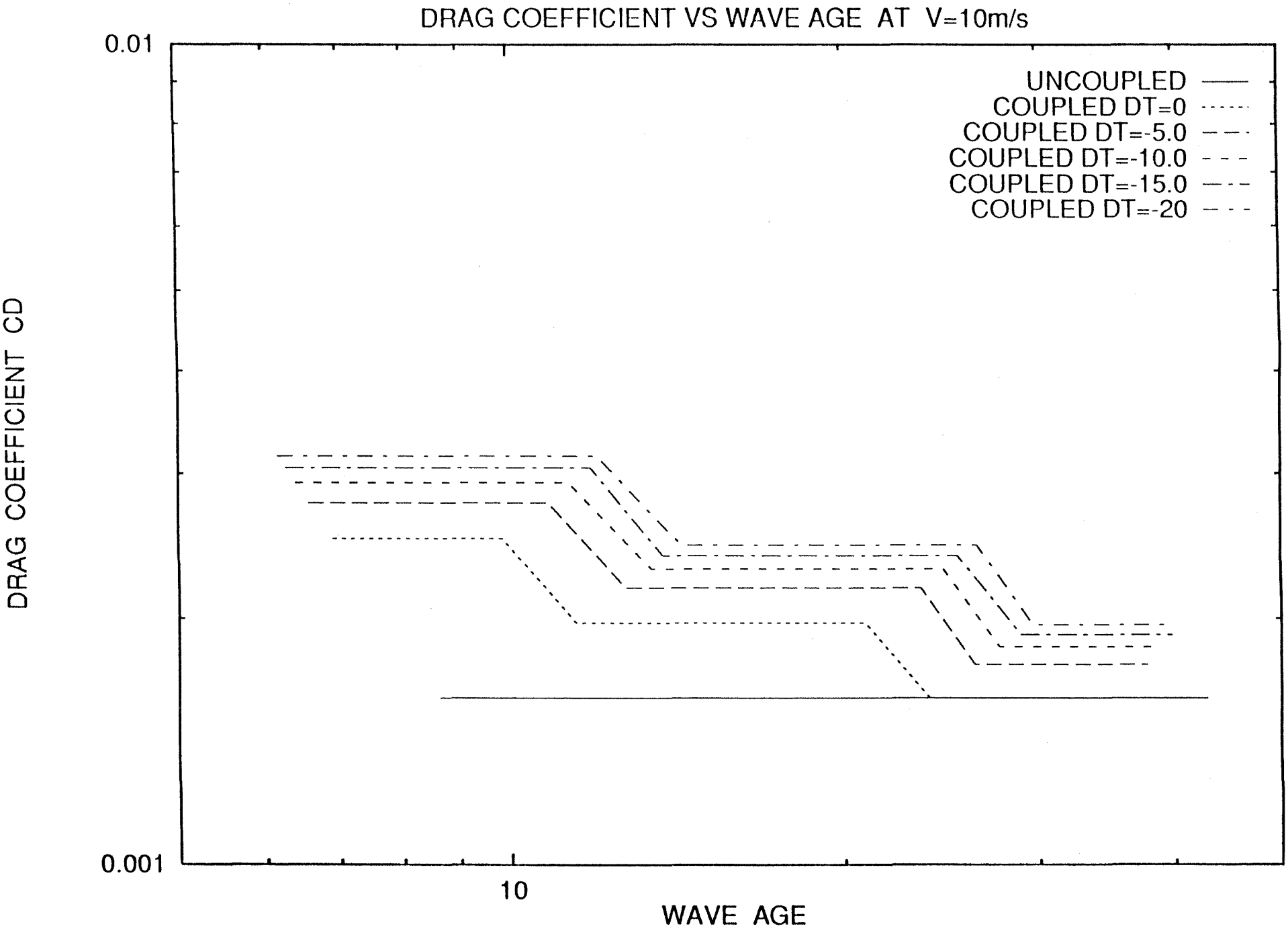
DRAG COEFFICIENT VS WAVE AGE AT V=10m/s
0.01
0.001
10
WAVE AGE
DRAG COEFFICIENT CD
UNCOUPLED
COUPLED DT=0
COUPLED DT=-5.0
COUPLED DT=-10.0
COUPLED DT=-15.0
COUPLED DT=-20

Fig. 30a

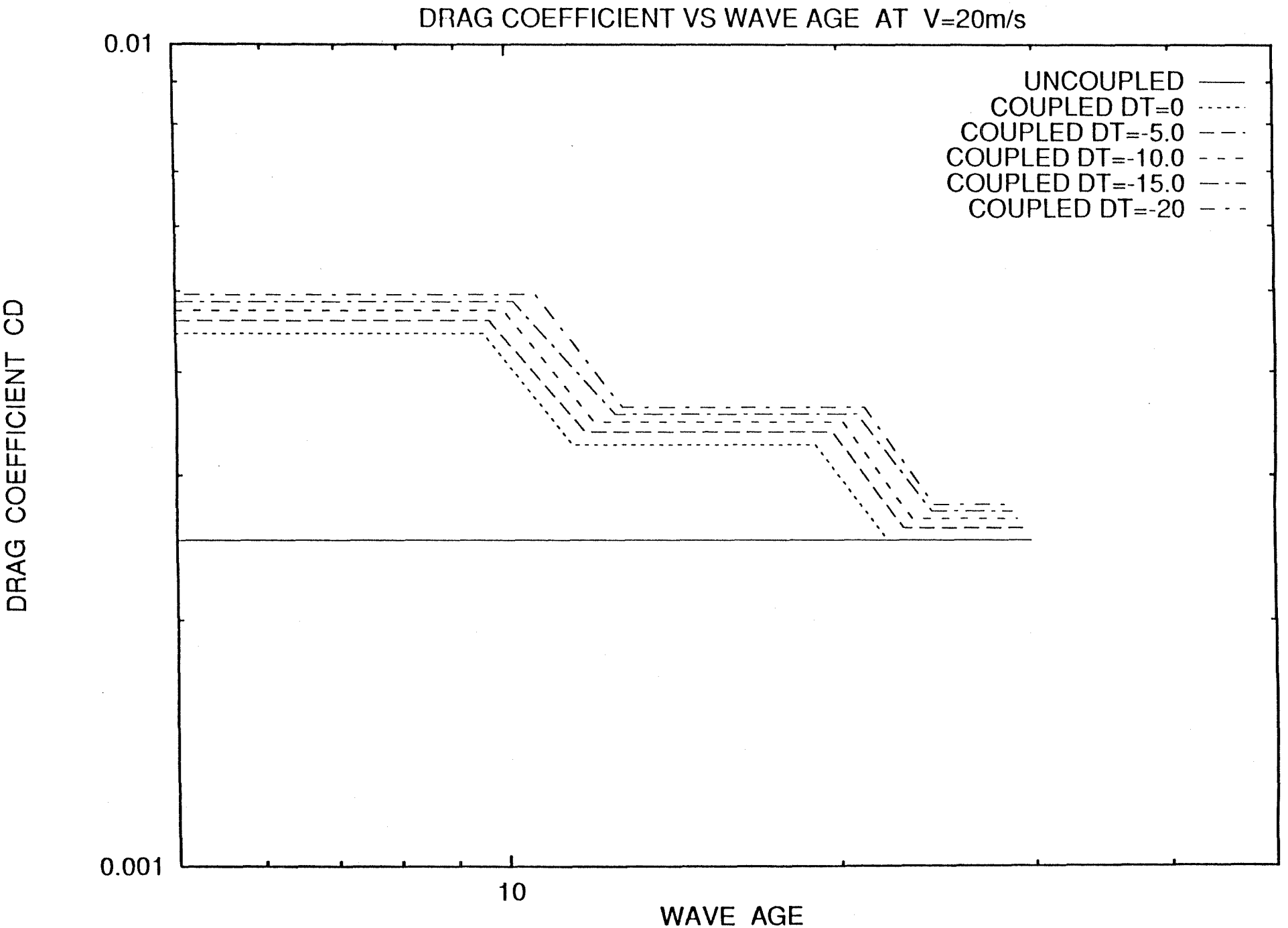
DRAG COEFFICIENT VS WAVE AGE AT V=20m/s
0.01
0.001
10
WAVE AGE
DRAG COEFFICIENT CD
UNCOUPLED
COUPLED DT=0
COUPLED DT=-5.0
COUPLED DT=-10.0
COUPLED DT=-15.0
COUPLED DT=-20

F' 30b

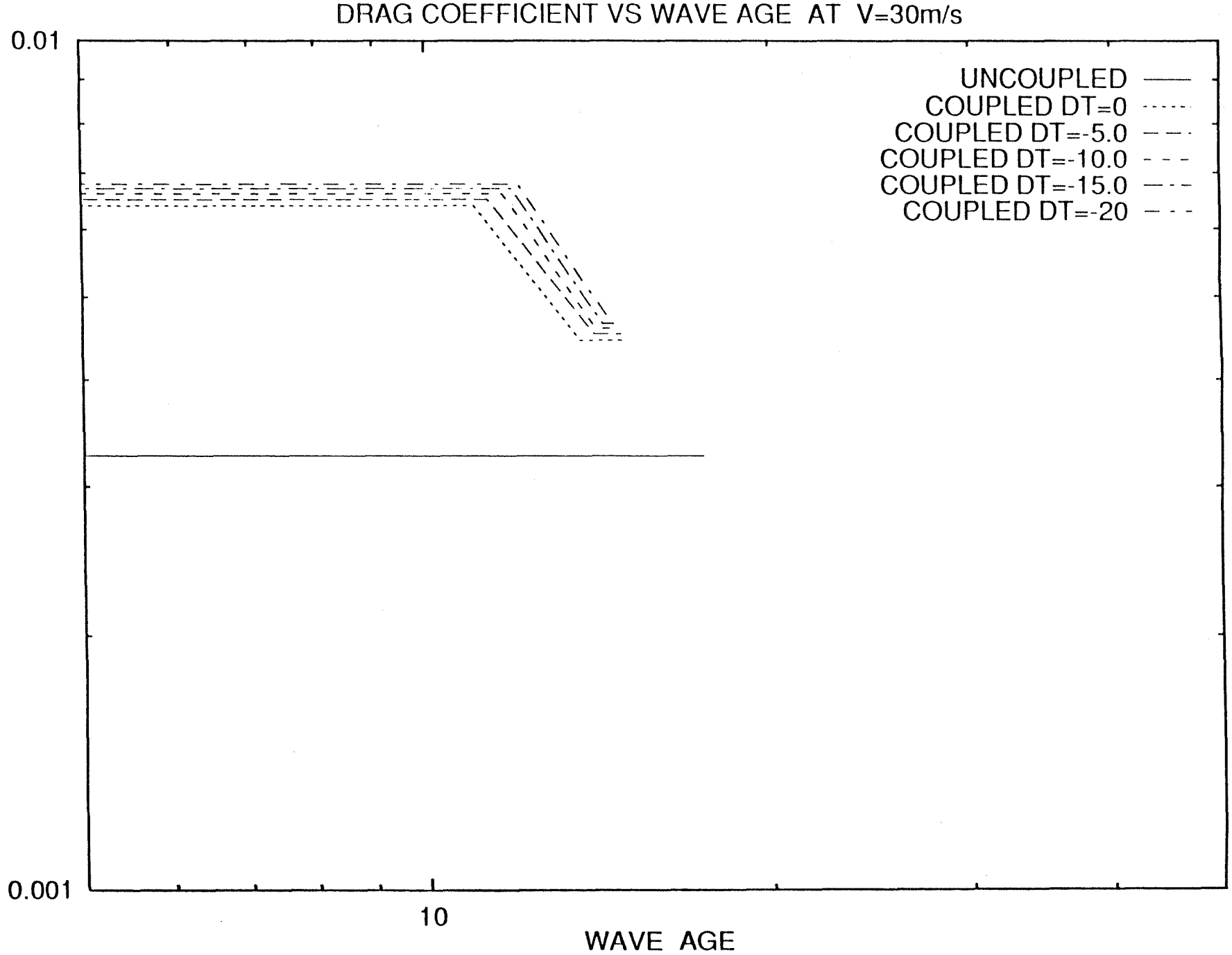
DRAG COEFFICIENT VS WAVE AGE AT V=30m/s
0.01
0.001
10
WAVE AGE
DRAG COEFFICIENT CD
UNCOUPLED
COUPLED DT=0
COUPLED DT=-5.0
COUPLED DT=-10.0
COUPLED DT=-15.0
COUPLED DT=-20

Fig.30c

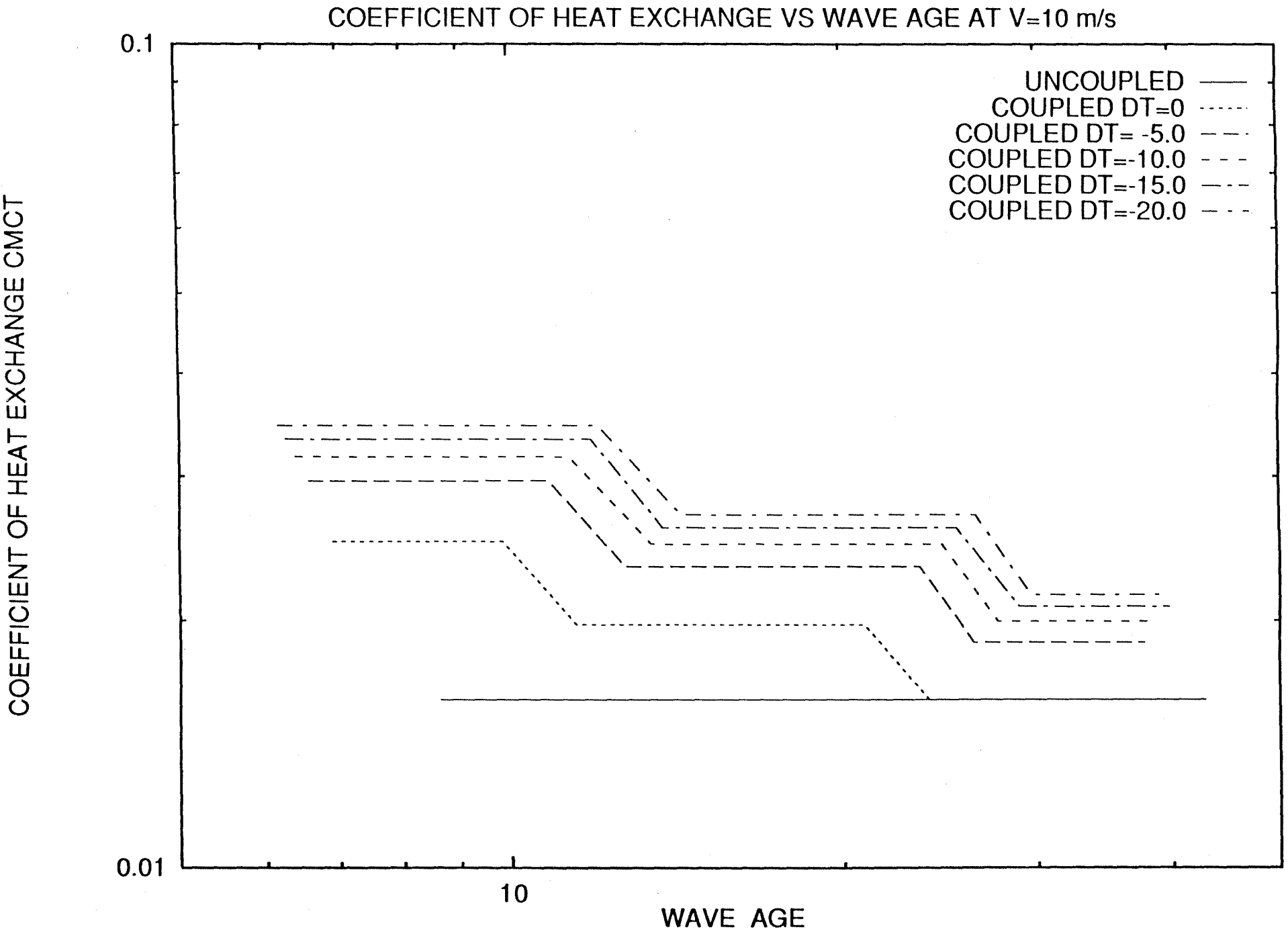
COEFFICIENT OF HEAT EXCHANGE VS WAVE AGE AT V=10 m/s
0.1
0.01
10
WAVE AGE
COEFFICIENT OF HEAT EXCHANGE CMCT
UNCOUPLED
COUPLED DT=0
COUPLED DT= -5.0
COUPLED DT=-10.0
COUPLED DT=-15.0
COUPLED DT=-20.0

Fig. 31a

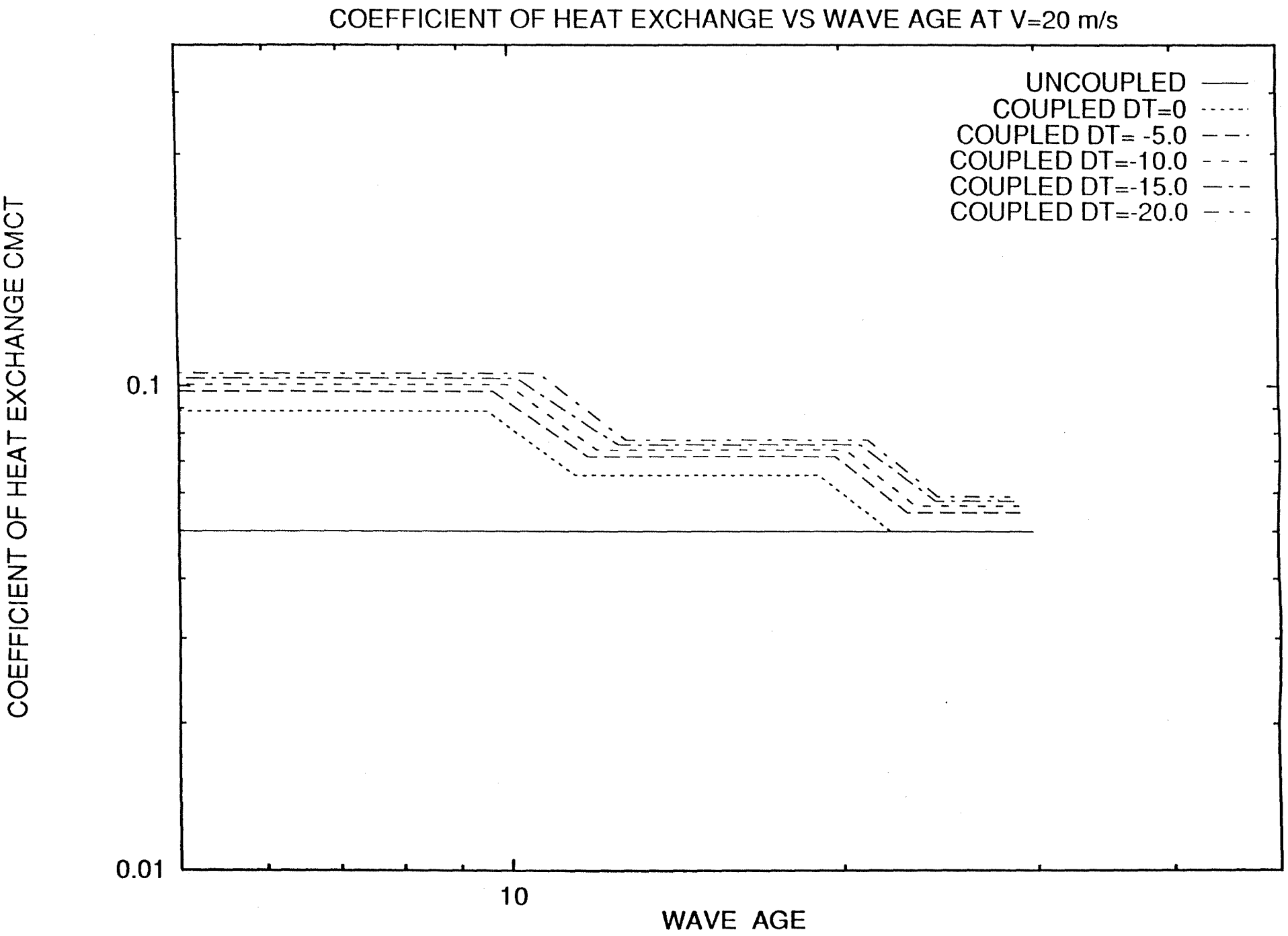
COEFFICIENT OF HEAT EXCHANGE VS WAVE AGE AT V=20 m/s
UNCOUPLED
COUPLED DT=0
COUPLED DT= -5.0
COUPLED DT=-10.0
COUPLED DT=-15.0
COUPLED DT=-20.0
COEFFICIENT OF HEAT EXCHANGE CMCT
0.1
0.01
10
WAVE AGE

Fig. 31b

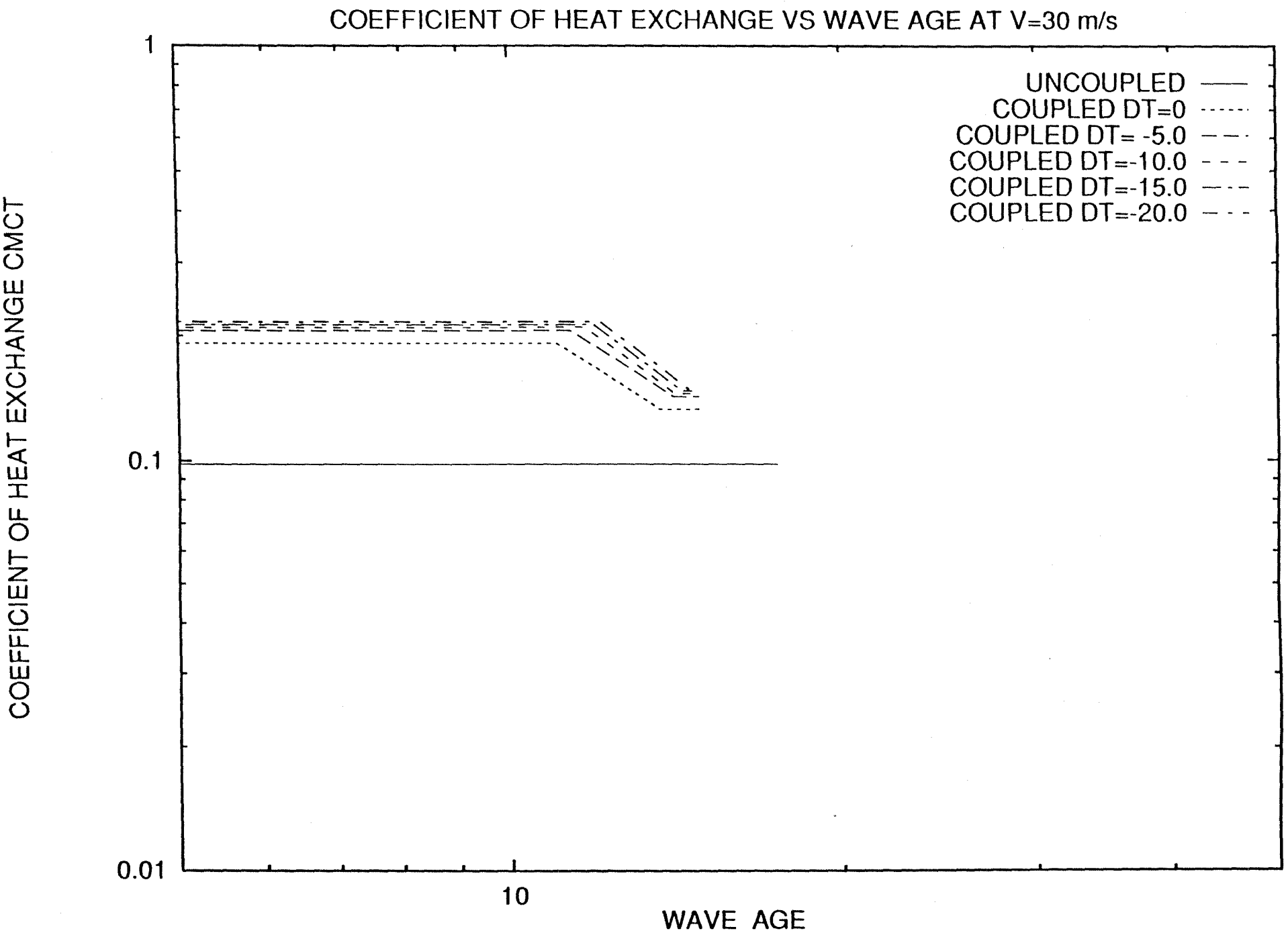
COEFFICIENT OF HEAT EXCHANGE VS WAVE AGE AT V=30 m/s
UNCOUPLED
COUPLED DT=0
COUPLED DT= -5.0
COUPLED DT=-10.0
COUPLED DT=-15.0
COUPLED DT=-20.0
COEFFICIENT OF HEAT EXCHANGE CMCT
1
0.1
0.01
10
WAVE AGE

Fig.31c

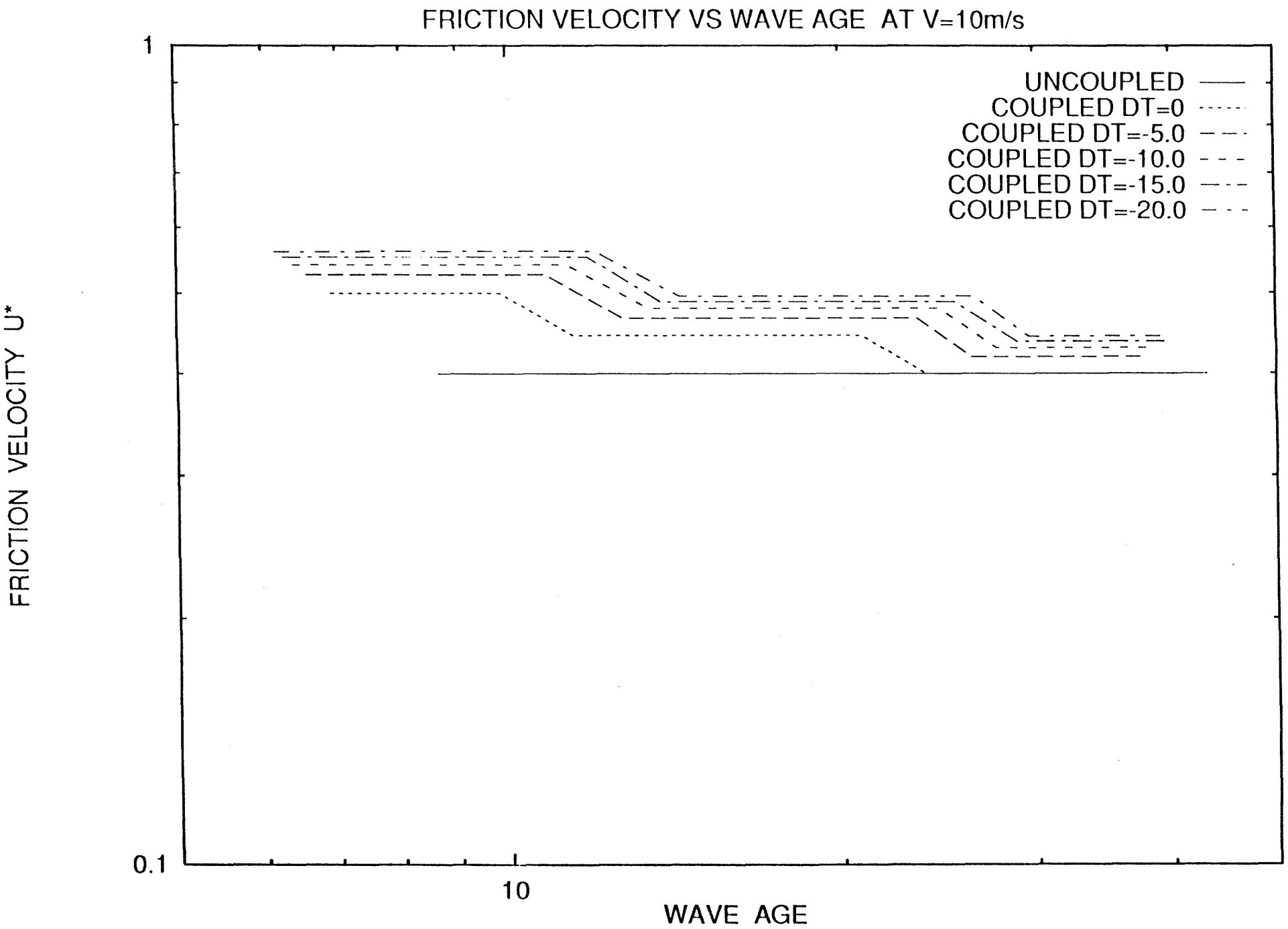
FRICTION VELOCITY VS WAVE AGE AT V=10m/s
1
0.1
10
WAVE AGE
FRICTION VELOCITY U*
UNCOUPLED
COUPLED DT=0
COUPLED DT=-5.0
COUPLED DT=-10.0
COUPLED DT=-15.0
COUPLED DT=-20.0

Fig. 32a

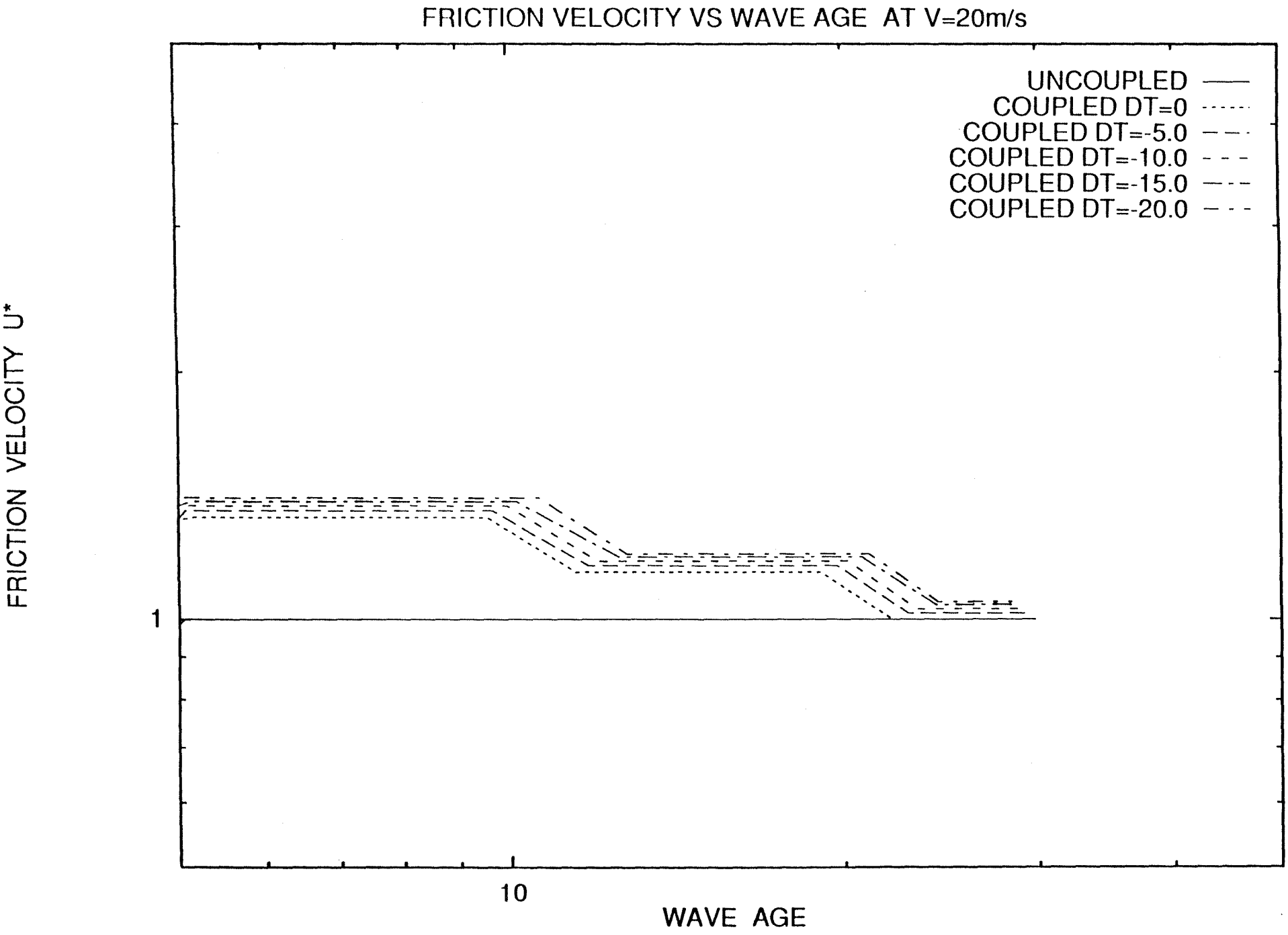
FRICTION VELOCITY VS WAVE AGE AT V=20m/s
UNCOUPLED
COUPLED DT=0
COUPLED DT=-5.0
COUPLED DT=-10.0
COUPLED DT=-15.0
COUPLED DT=-20.0
FRICTION VELOCITY U*
1
10
WAVE AGE

Fig. 32b

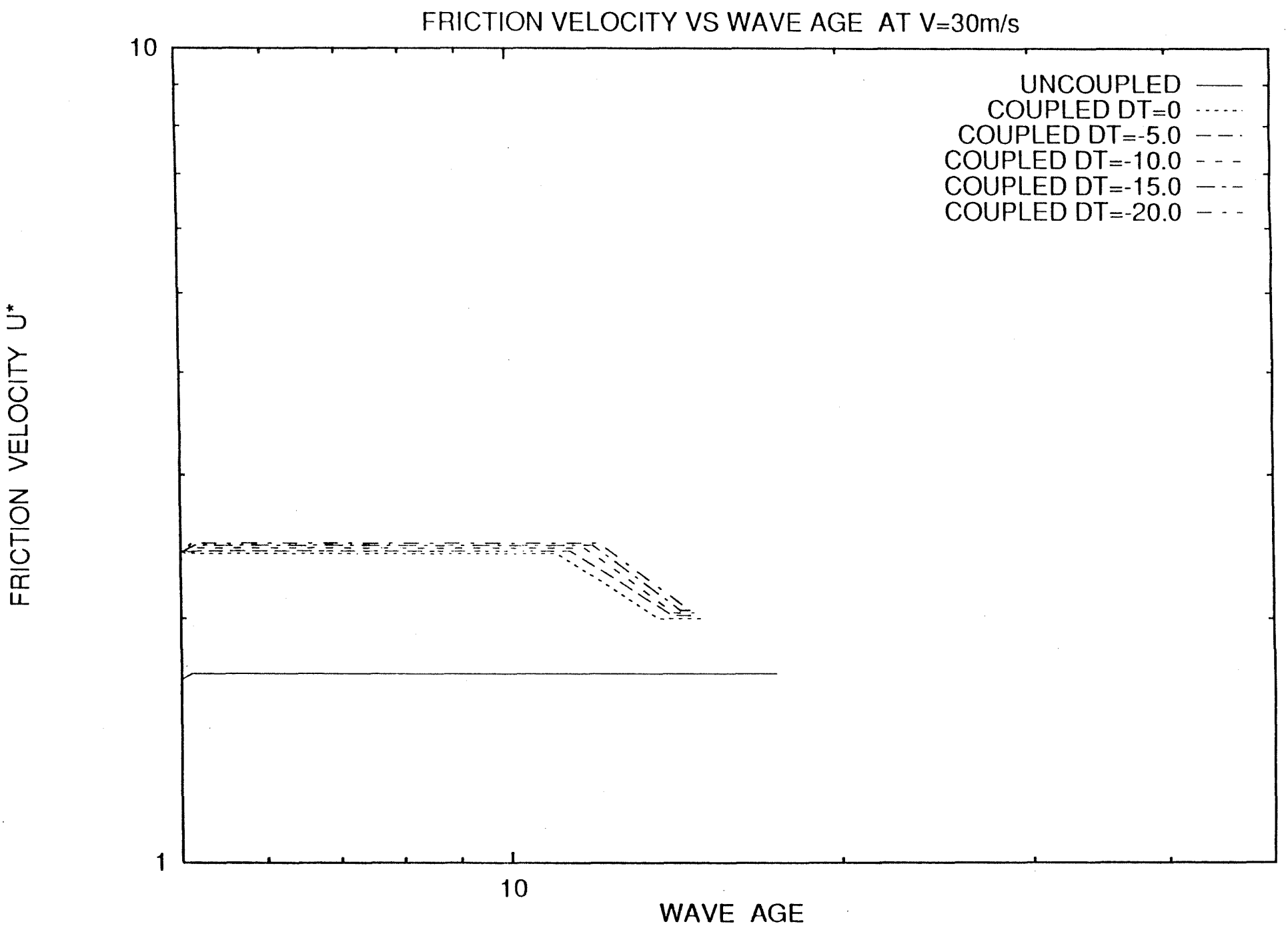
FRICTION VELOCITY VS WAVE AGE AT V=30m/s
10
1
10
FRICTION VELOCITY U*
WAVE AGE
UNCOUPLED
COUPLED DT=0
COUPLED DT=-5.0
COUPLED DT=-10.0
COUPLED DT=-15.0
COUPLED DT=-20.0

Fig. 32c

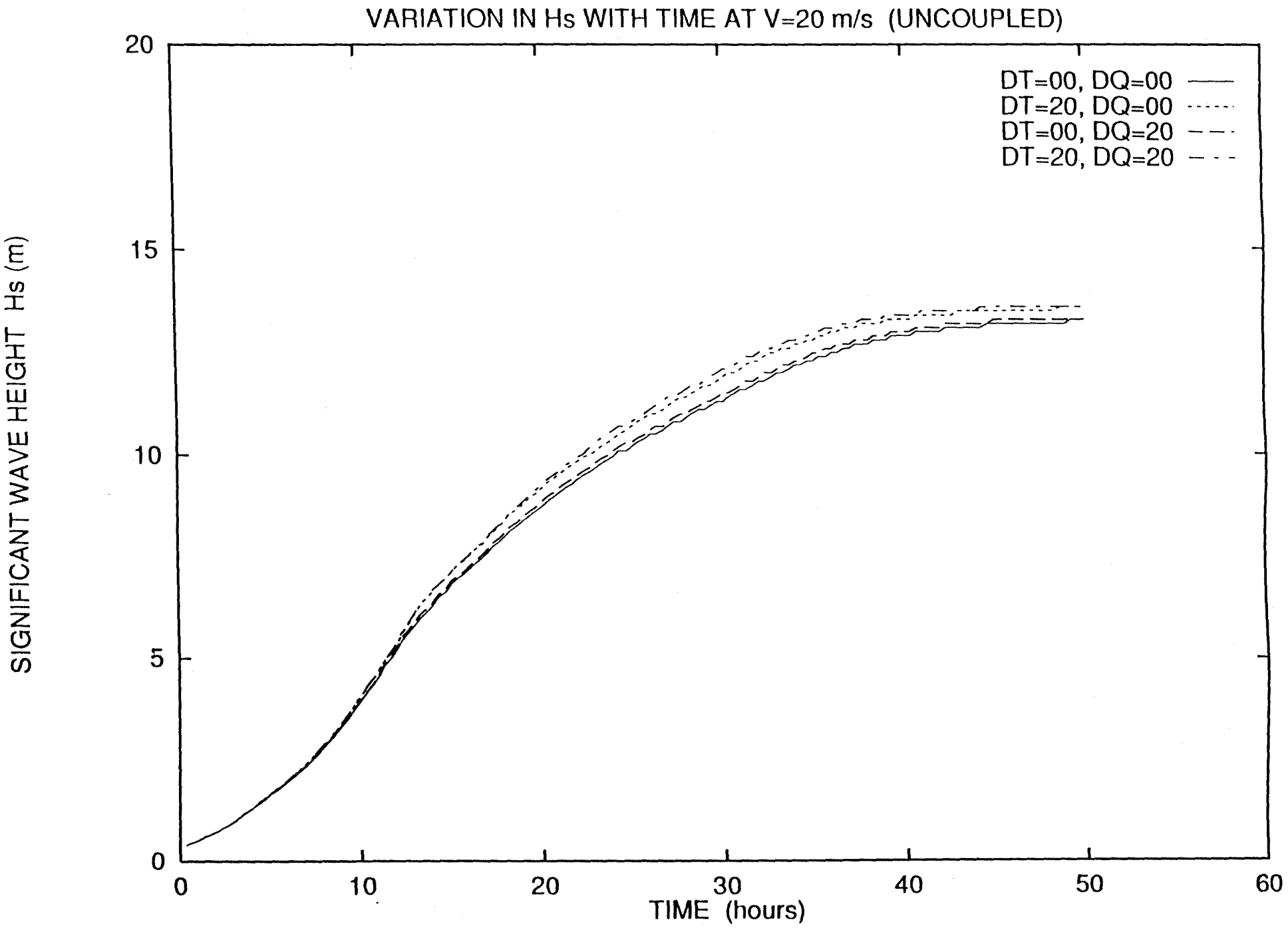
VARIATION IN Hs WITH TIME AT V=20 m/s (UNCOUPLED)
DT=00, DQ=00
DT=20, DQ=00
DT=00, DQ=20
DT=20, DQ=20
SIGNIFICANT WAVE HEIGHT Hs (m)
TIME (hours)
0
5
10
15
20
0
10
20
30
40
50
60

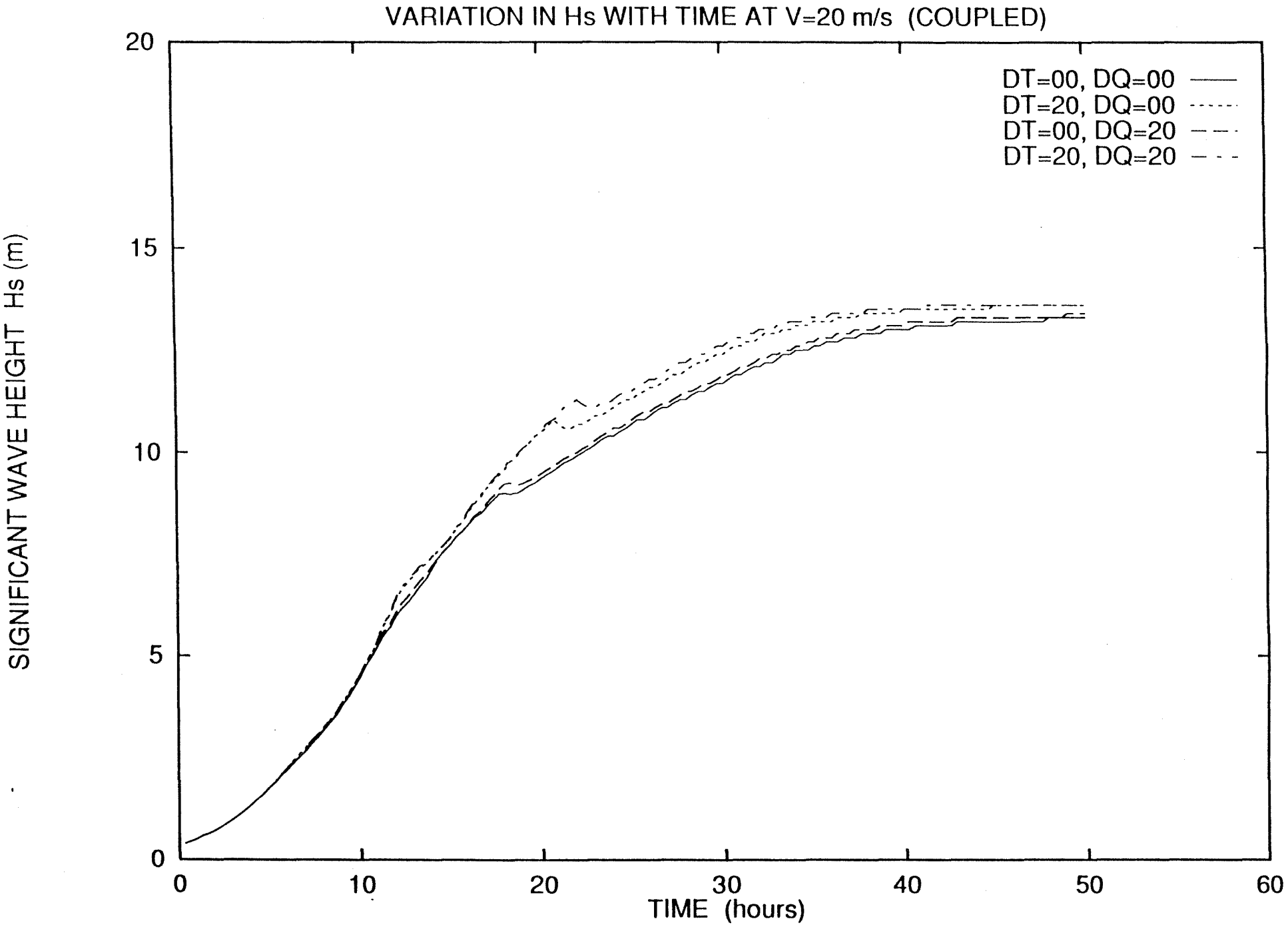
VARIATION IN Hs WITH TIME AT V=20 m/s (COUPLED)
DT=00, DQ=00
DT=20, DQ=00
DT=00, DQ=20
DT=20, DQ=20
SIGNIFICANT WAVE HEIGHT Hs (m)
TIME (hours)
0
5
10
15
20
0
10
20
30
40
50
60

Fig.33b

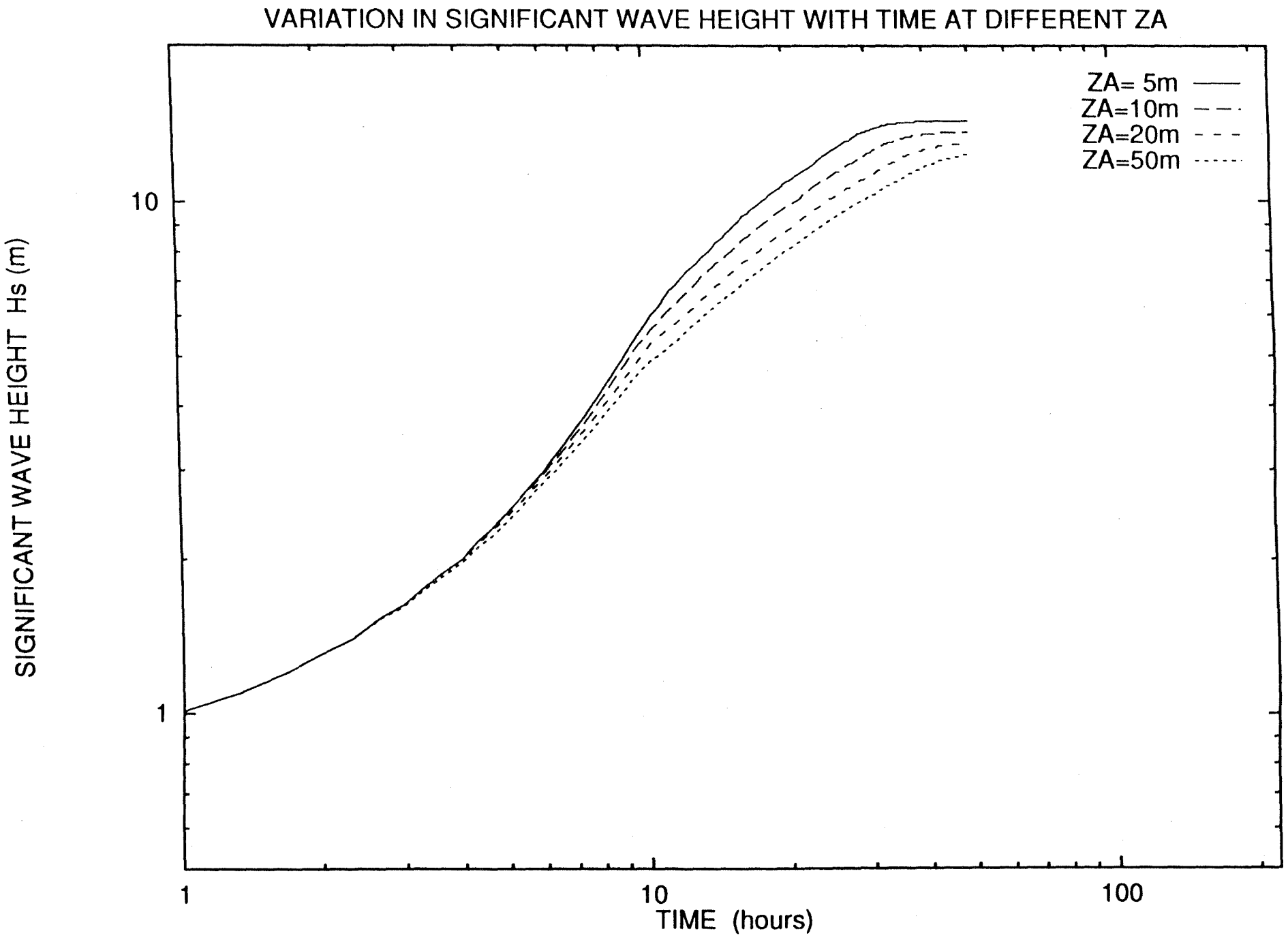
VARIATION IN SIGNIFICANT WAVE HEIGHT WITH TIME AT DIFFERENT ZA
ZA= 5m
ZA=10m
ZA=20m
ZA=50m
SIGNIFICANT WAVE HEIGHT Hs (m)
10
1
1
10
100
TIME (hours)

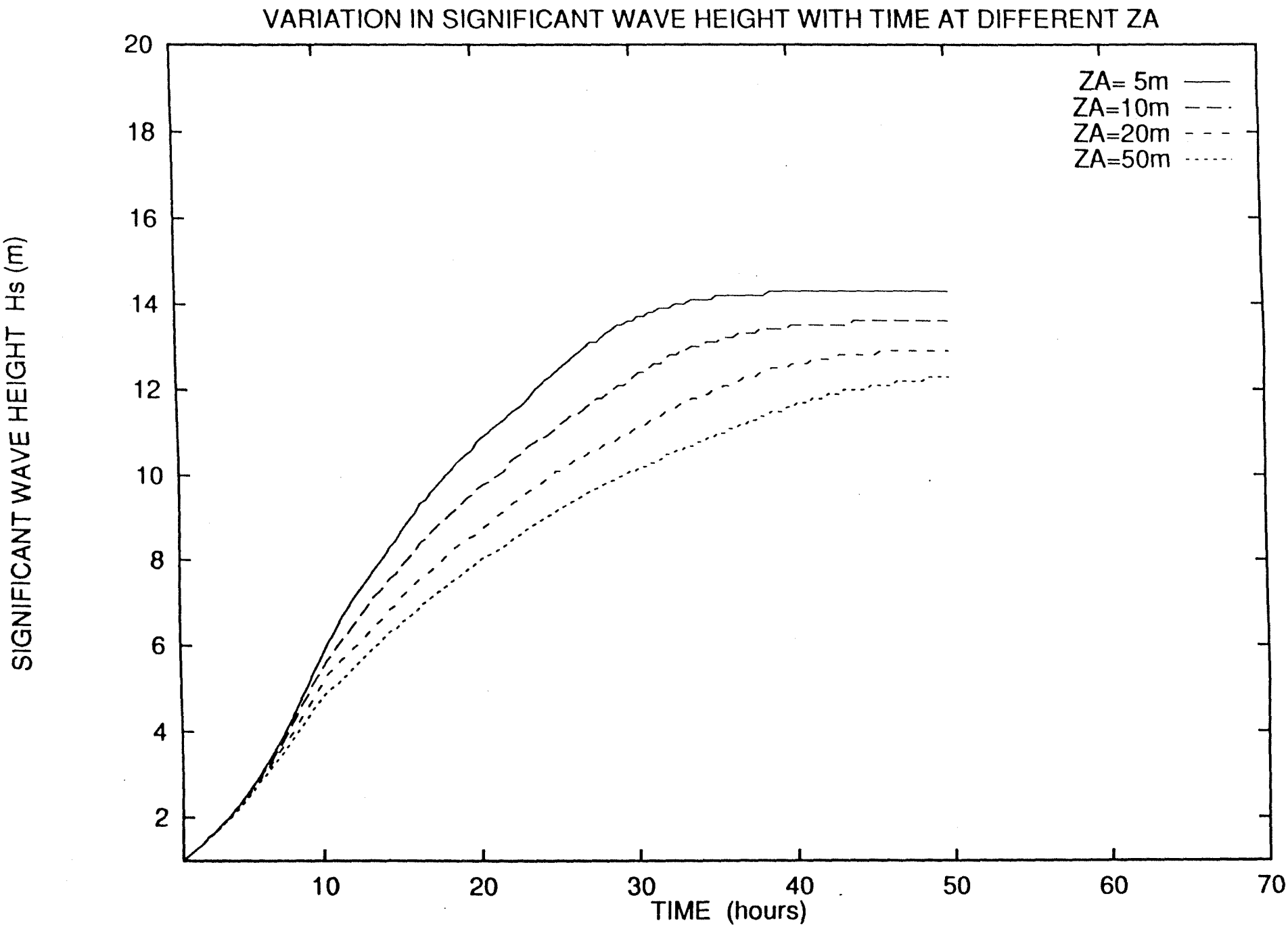
VARIATION IN SIGNIFICANT WAVE HEIGHT WITH TIME AT DIFFERENT ZA
SIGNIFICANT WAVE HEIGHT Hs (m)
TIME (hours)
ZA= 5m
ZA=10m
ZA=20m
ZA=50m
20
18
16
14
12
10
8
6
4
2
10
20
30
40
50
60
70

Fig. 34b

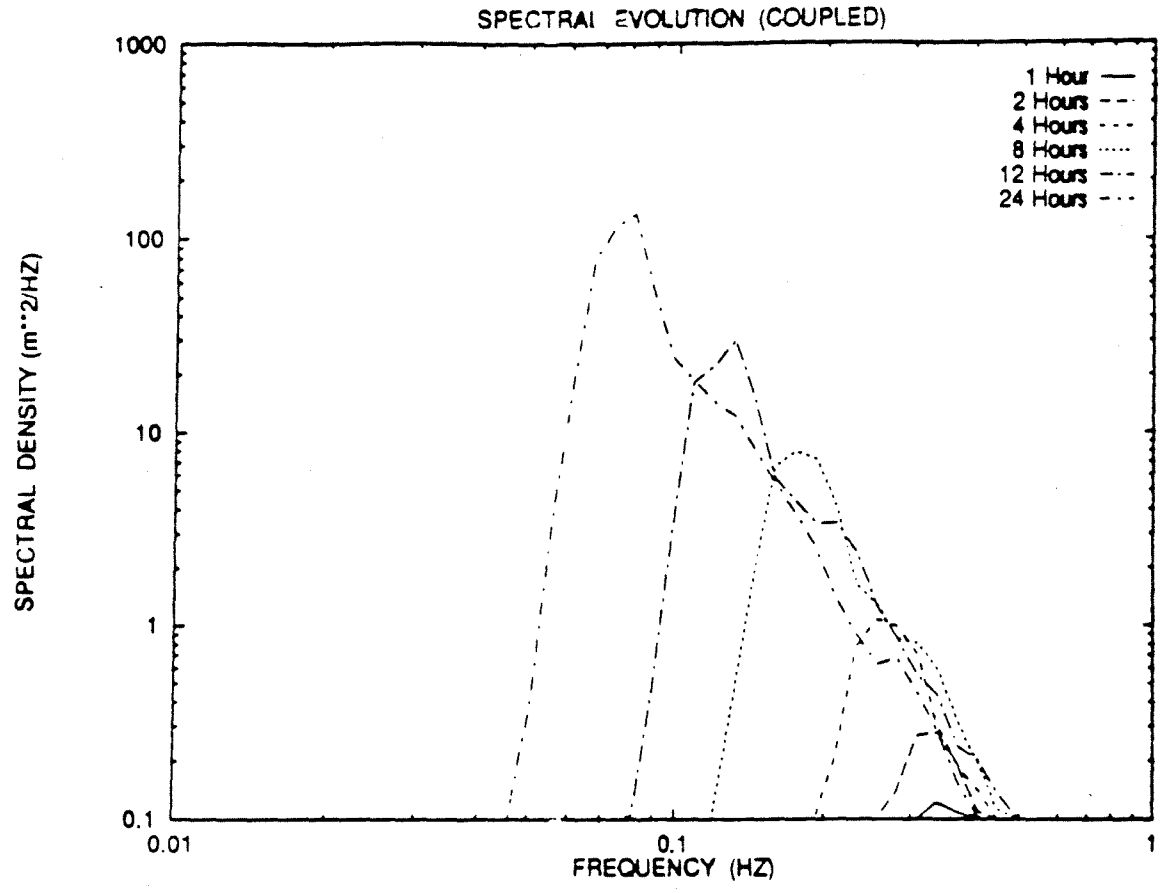

Fig.35a

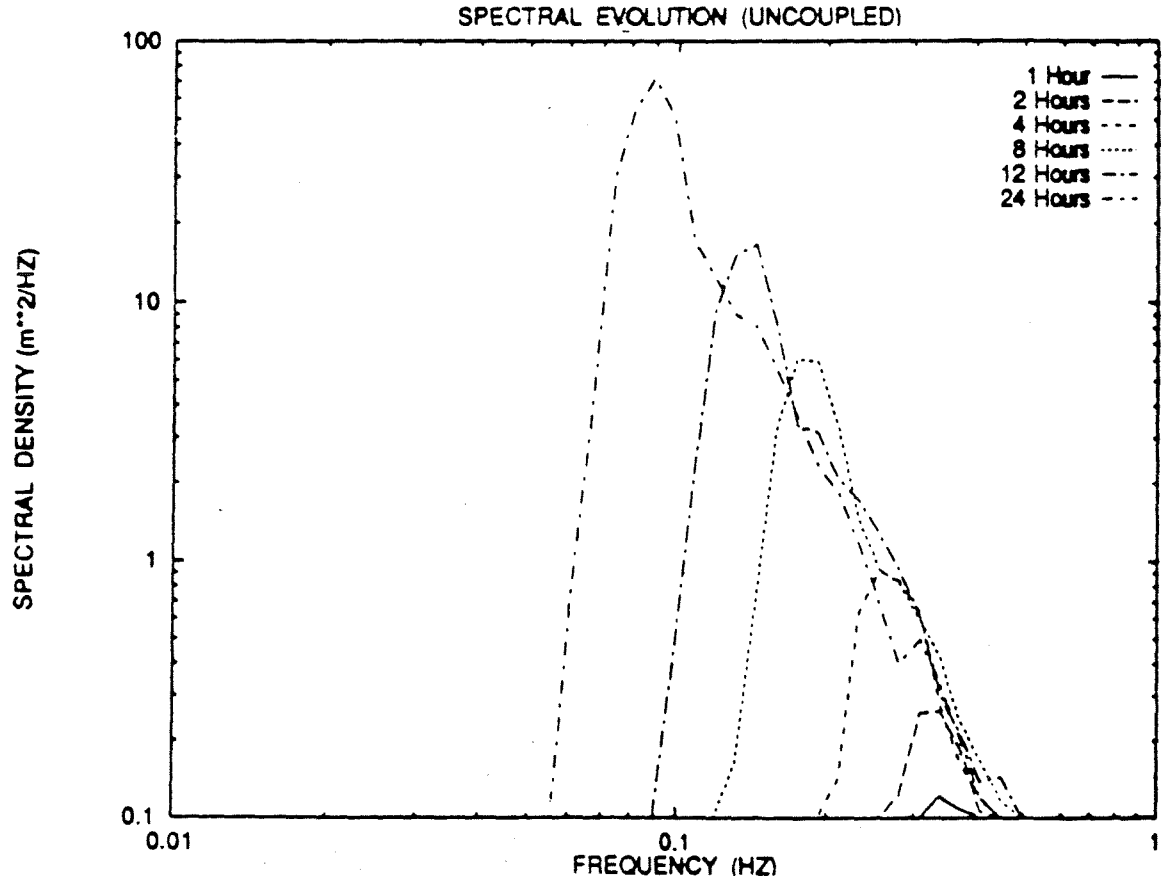

Fig.35b

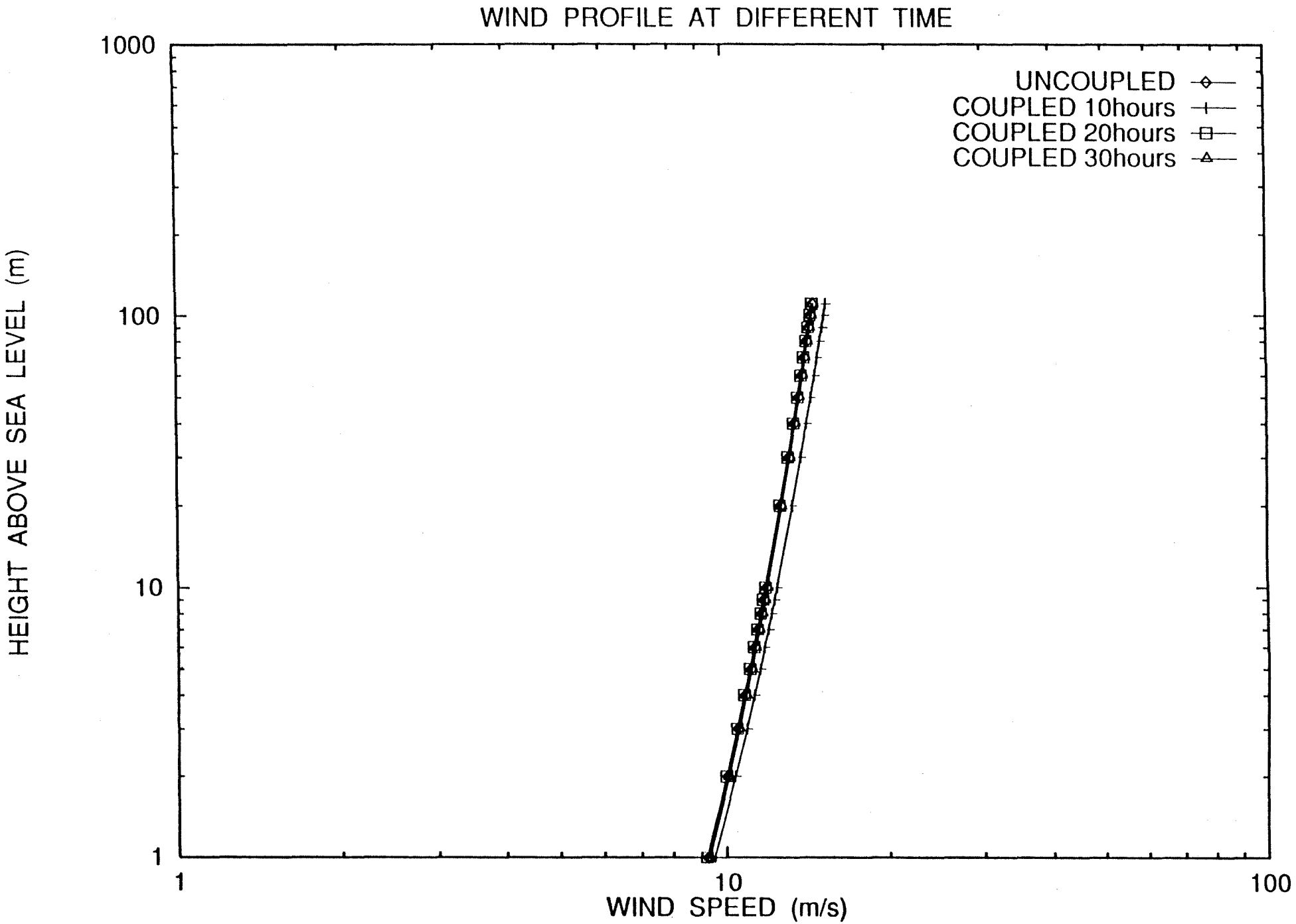
WIND PROFILE AT DIFFERENT TIME
UNCOUPLED
COUPLED 10hours
COUPLED 20hours
COUPLED 30hours
HEIGHT ABOVE SEA LEVEL (m)
1000
100
10
1
1
10
100
WIND SPEED (m/s)

Fig.36a

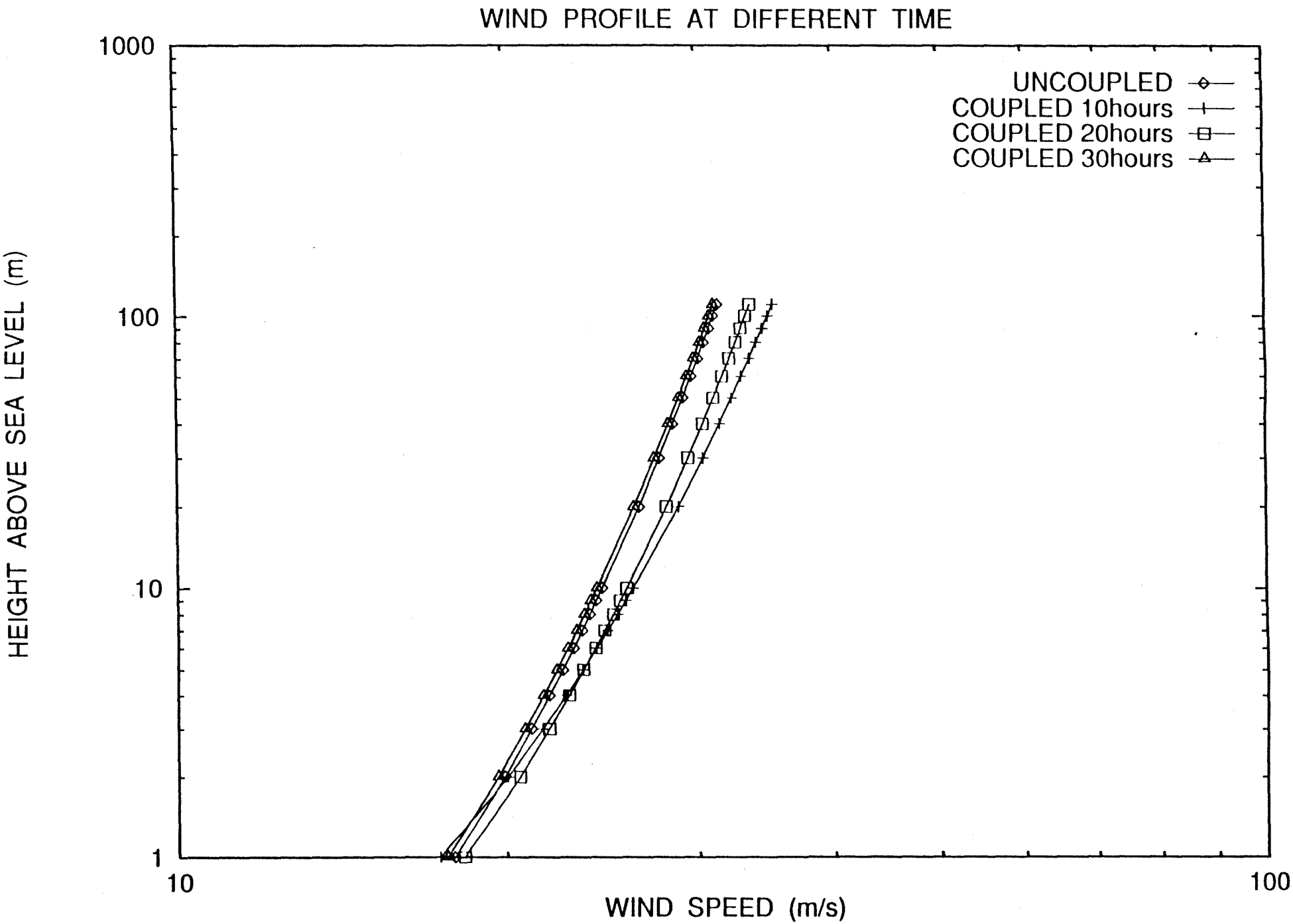
WIND PROFILE AT DIFFERENT TIME
UNCOUPLED
COUPLED 10hours
COUPLED 20hours
COUPLED 30hours
HEIGHT ABOVE SEA LEVEL (m)
1000
100
10
1
10
100
WIND SPEED (m/s)

Fig.36b

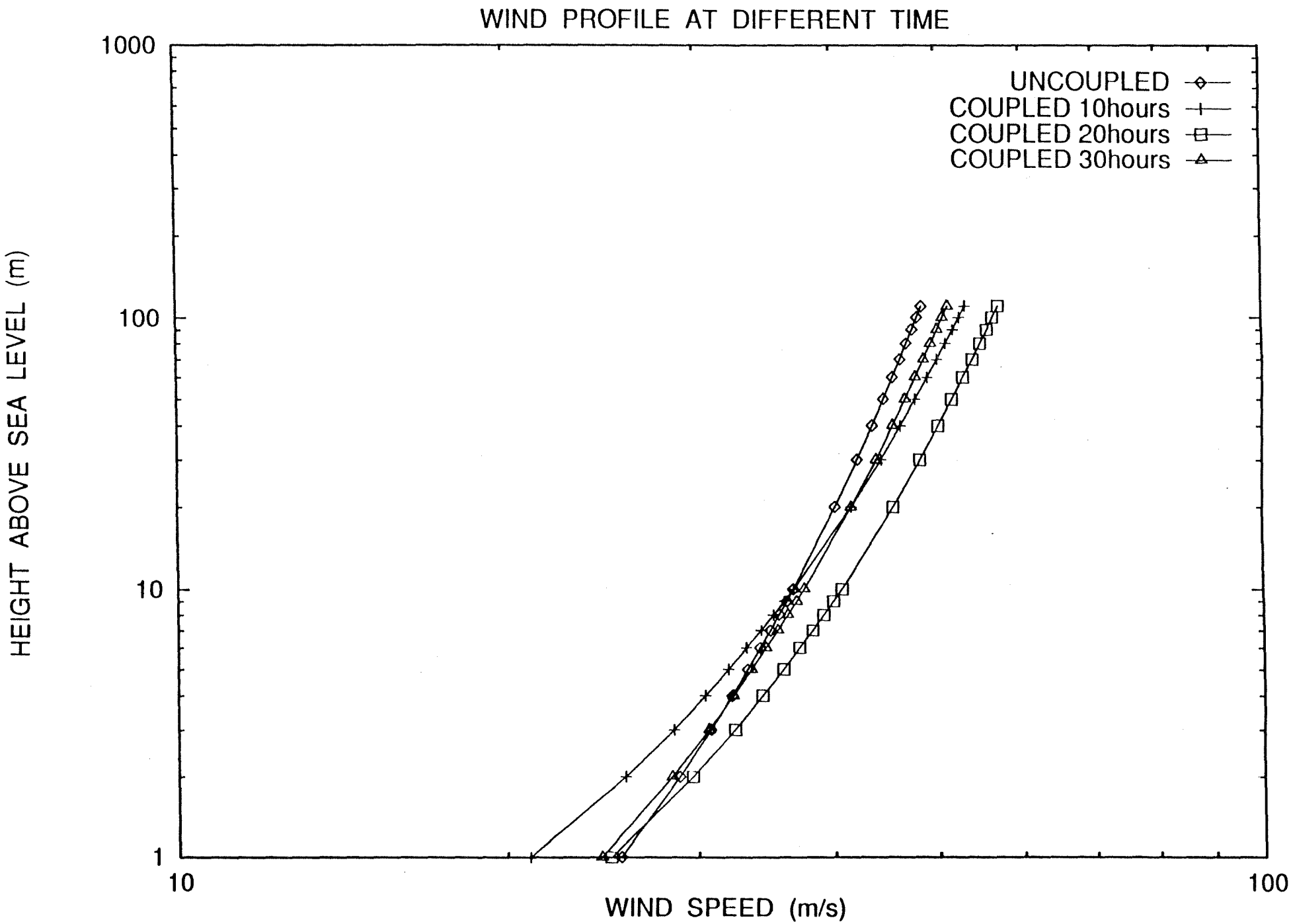
WIND PROFILE AT DIFFERENT TIME
UNCOUPLED
COUPLED 10hours
COUPLED 20hours
COUPLED 30hours
HEIGHT ABOVE SEA LEVEL (m)
1000
100
10
1
10
100
WIND SPEED (m/s)

Fig.36c

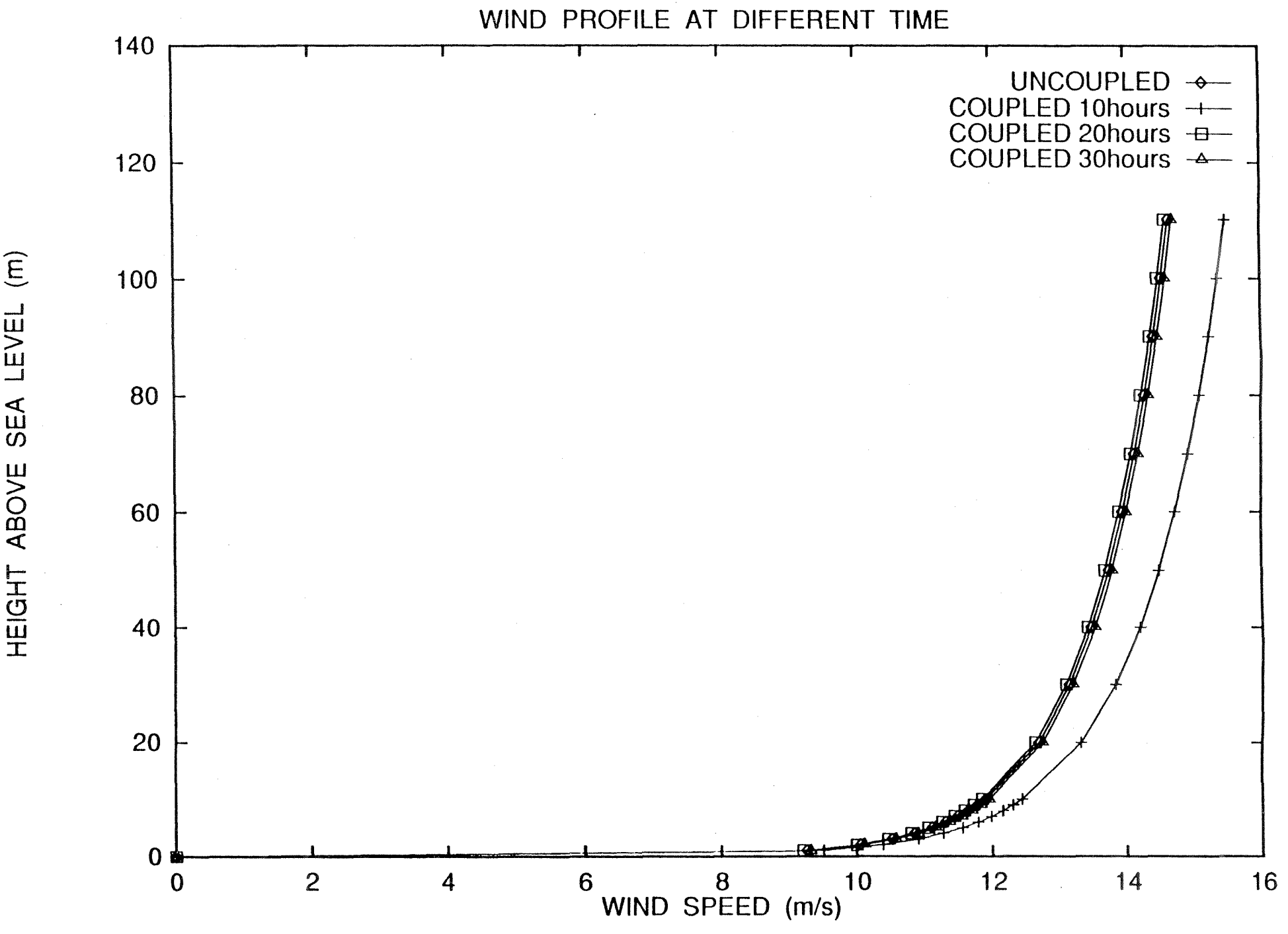
WIND PROFILE AT DIFFERENT TIME
UNCOUPLED
COUPLED 10hours
COUPLED 20hours
COUPLED 30hours
HEIGHT ABOVE SEA LEVEL (m)
WIND SPEED (m/s)
0
20
40
60
80
100
120
140
0
2
4
6
8
10
12
14
16

Fig.37a

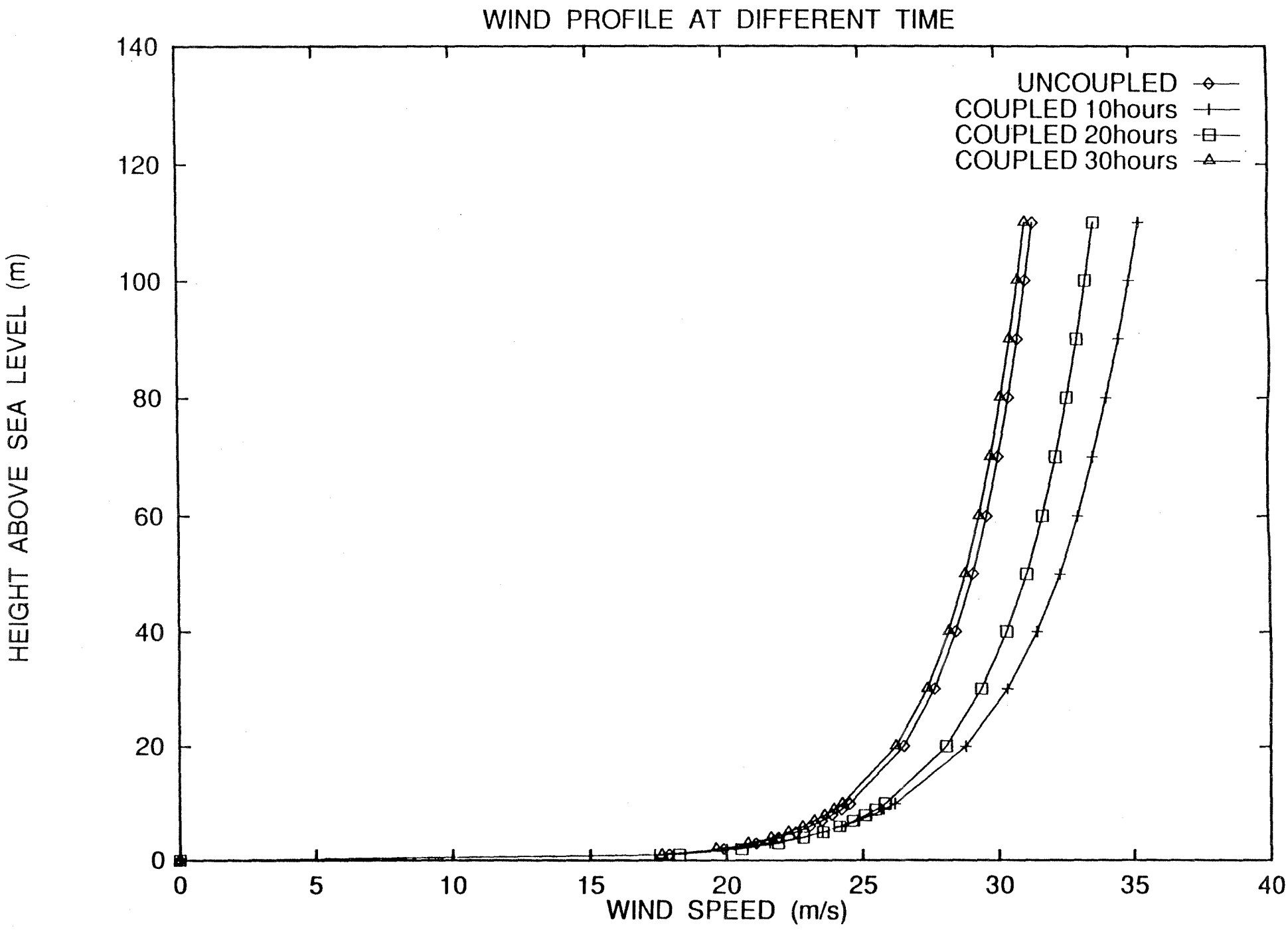
WIND PROFILE AT DIFFERENT TIME
UNCOUPLED
COUPLED 10hours
COUPLED 20hours
COUPLED 30hours
HEIGHT ABOVE SEA LEVEL (m)
WIND SPEED (m/s)
0
20
40
60
80
100
120
140
0
5
10
15
20
25
30
35
40

Fig. 37b

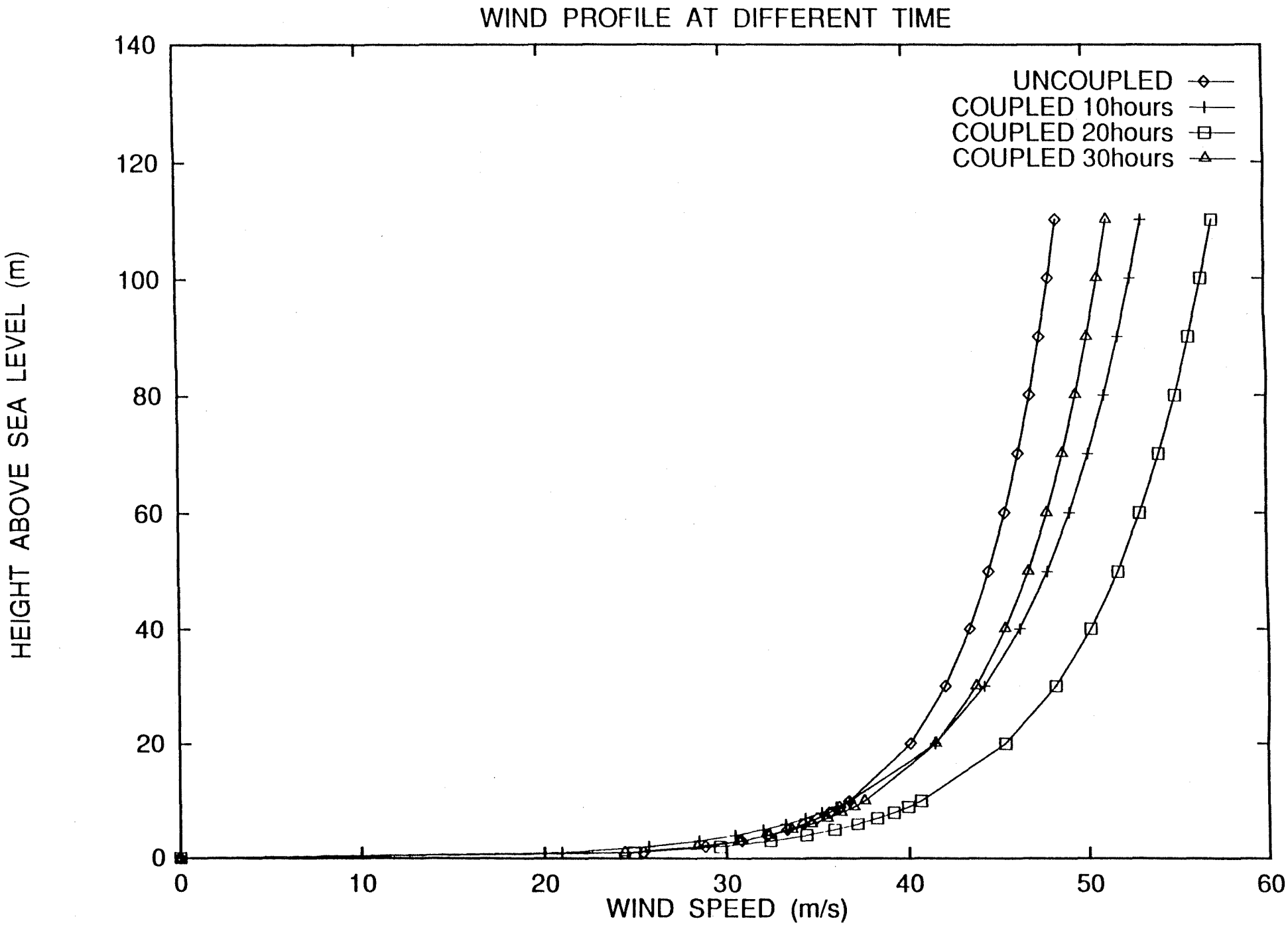
WIND PROFILE AT DIFFERENT TIME
UNCOUPLED
COUPLED 10hours
COUPLED 20hours
COUPLED 30hours
HEIGHT ABOVE SEA LEVEL (m)
WIND SPEED (m/s)
0
20
40
60
80
100
120
140
0
10
20
30
40
50
60

Fig.37c
rl /a

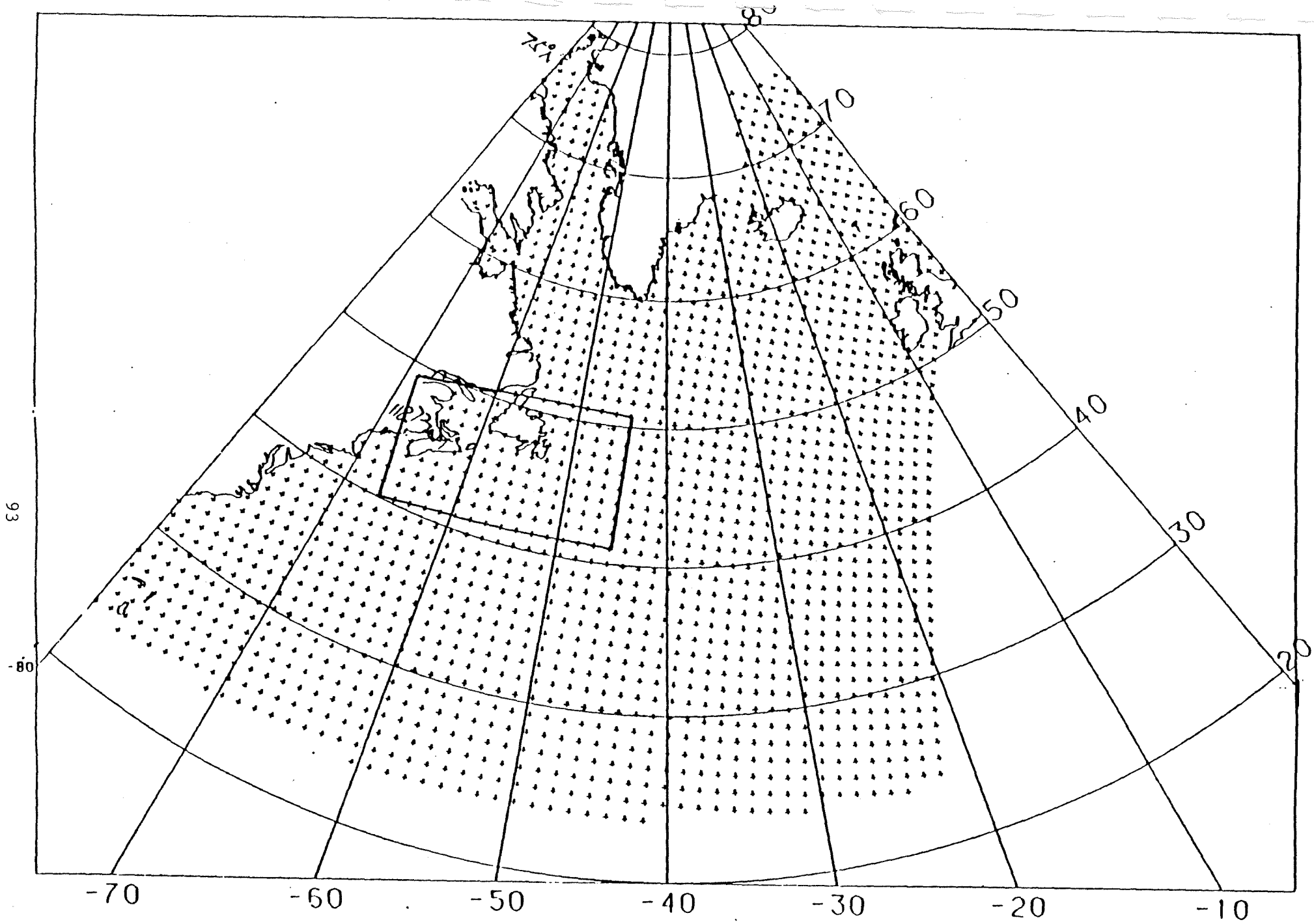

Fig. 38a

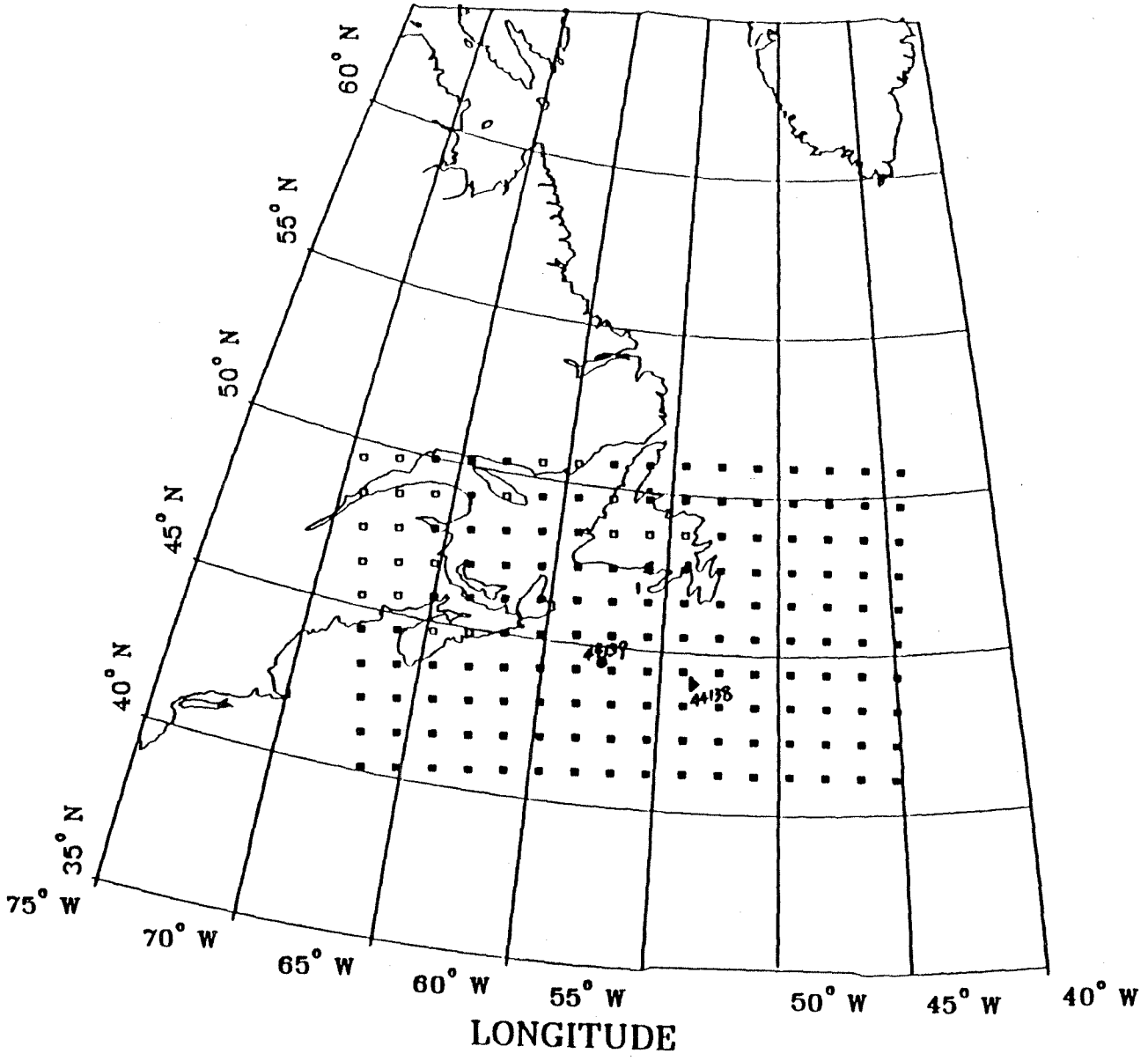
LATITUDE
60° N
55° N
50° N
45° N
40° N
35° N
75° W
70° W
65° W
60° W
55° W
50° W
45° W
40° W
LONGITUDE
44139

Fig. 3[illegible]

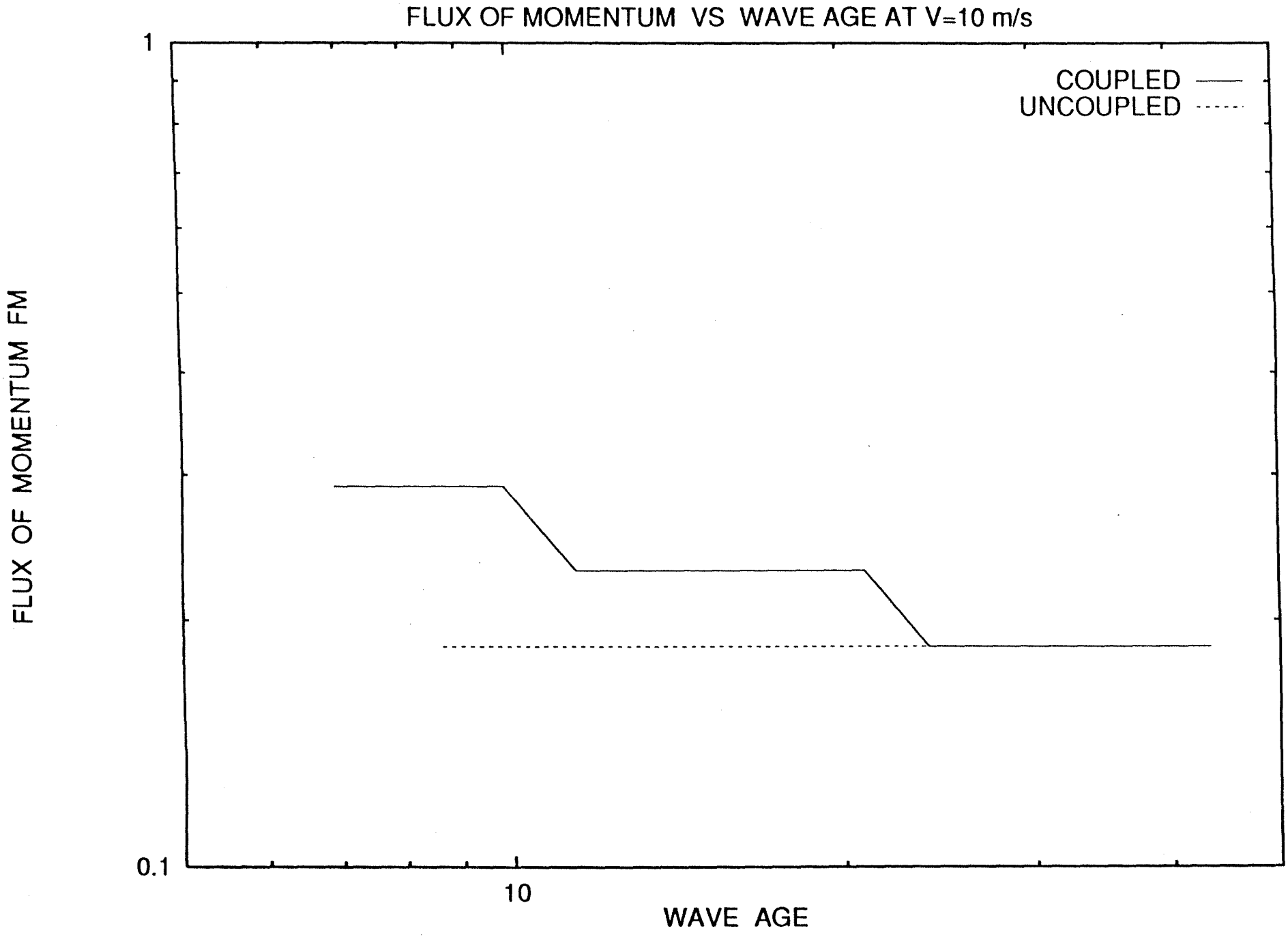
FLUX OF MOMENTUM VS WAVE AGE AT V=10 m/s
COUPLED
UNCOUPLED
FLUX OF MOMENTUM FM
1
0.1
10
WAVE AGE

Fig.39a

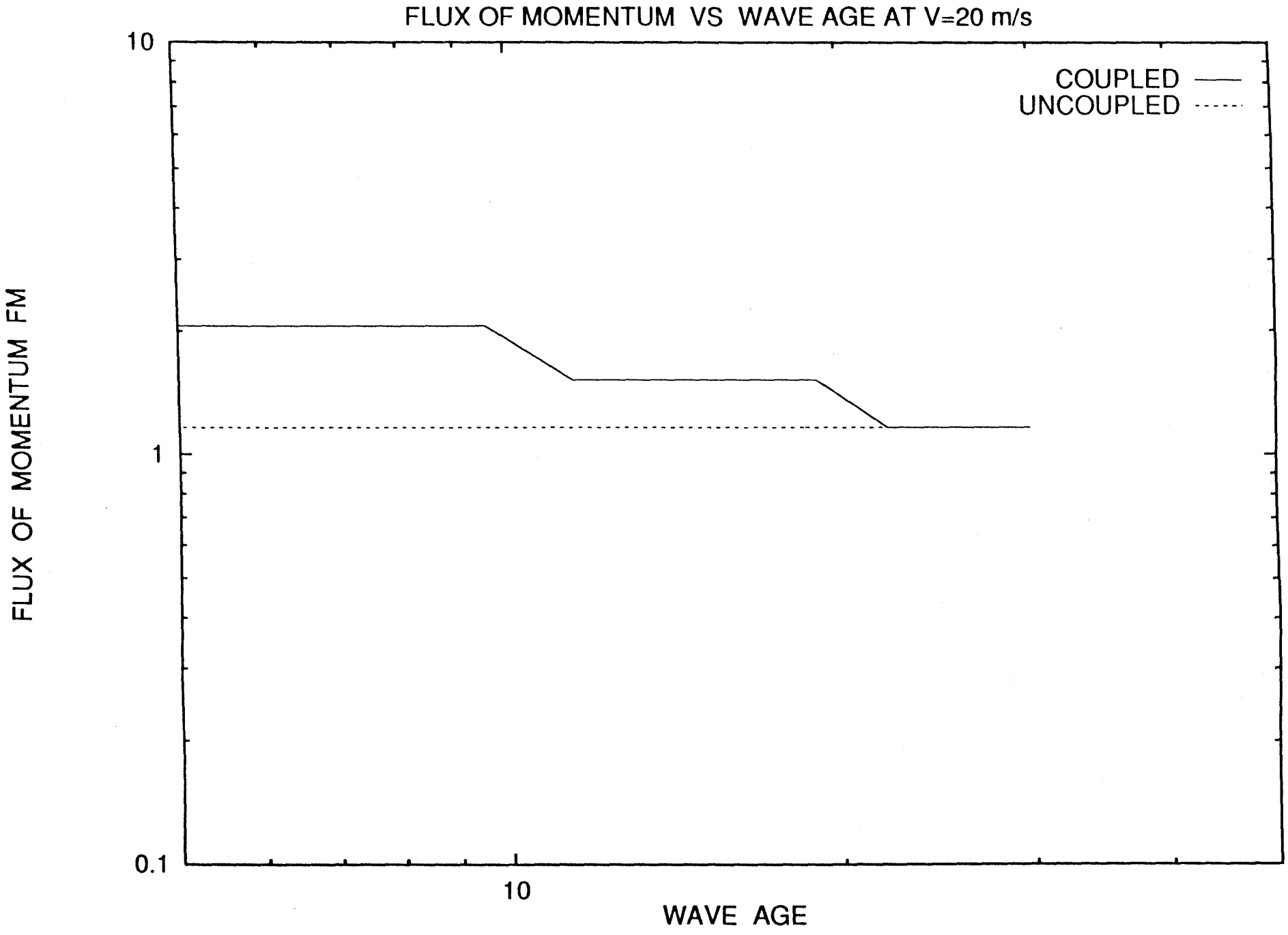
FLUX OF MOMENTUM VS WAVE AGE AT V=20 m/s
COUPLED
UNCOUPLED
FLUX OF MOMENTUM FM
10
1
0.1
10
WAVE AGE

Fig. 39b

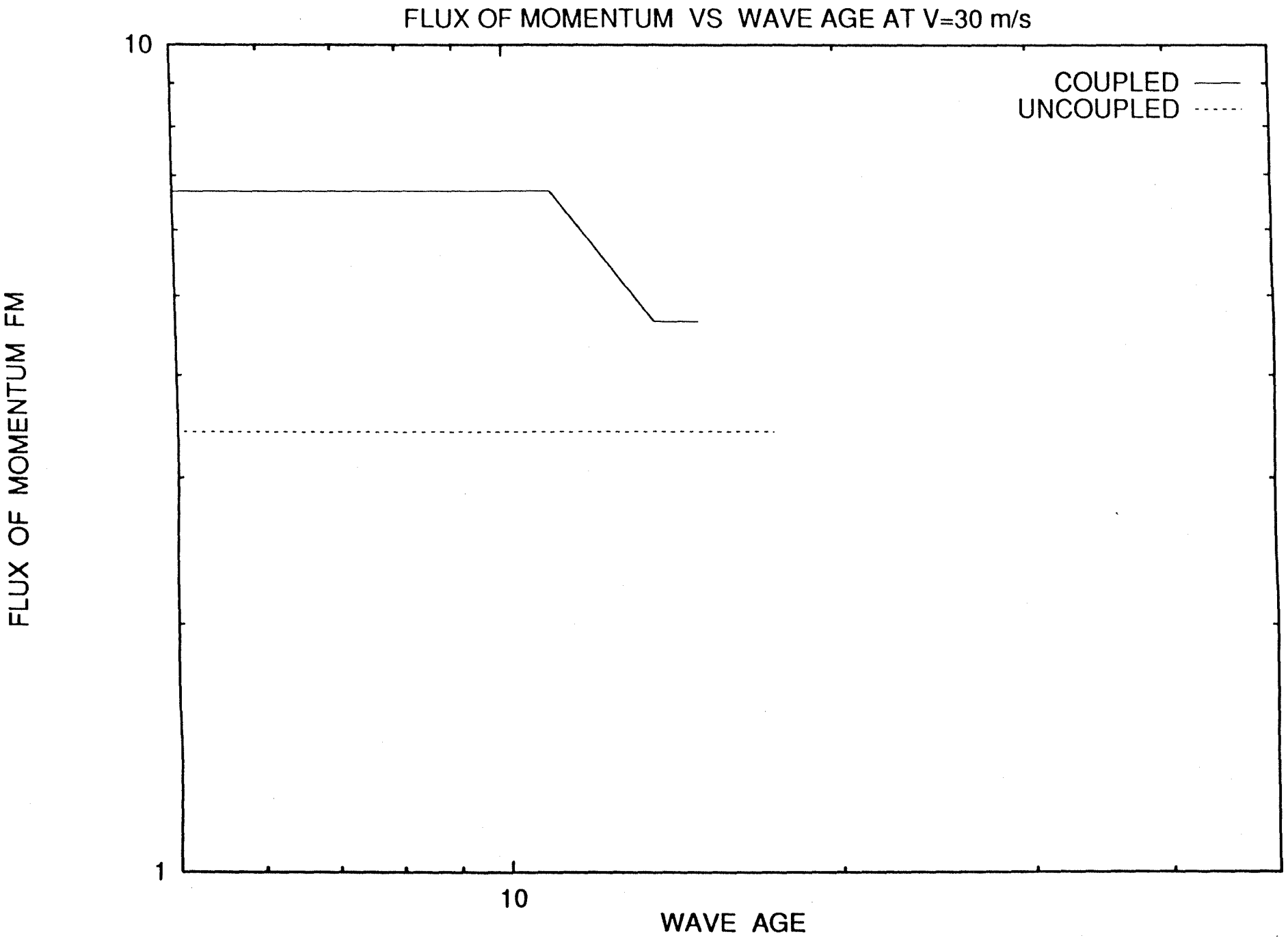
FLUX OF MOMENTUM VS WAVE AGE AT V=30 m/s
COUPLED
UNCOUPLED
FLUX OF MOMENTUM FM
10
1
10
WAVE AGE

Fig.39c

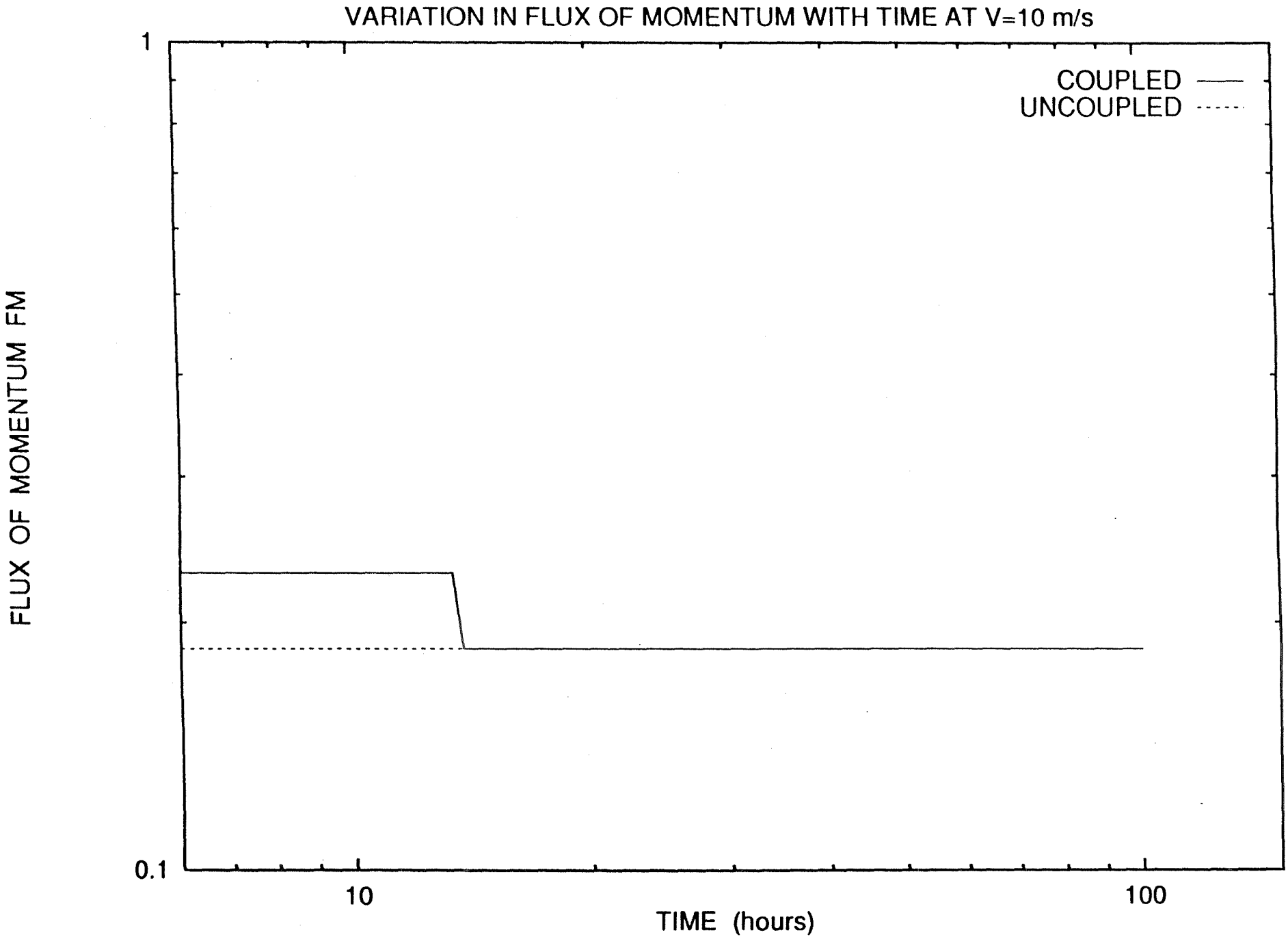
VARIATION IN FLUX OF MOMENTUM WITH TIME AT V=10 m/s
COUPLED
UNCOUPLED
FLUX OF MOMENTUM FM
1
0.1
10
100
TIME (hours)

Fig.40a

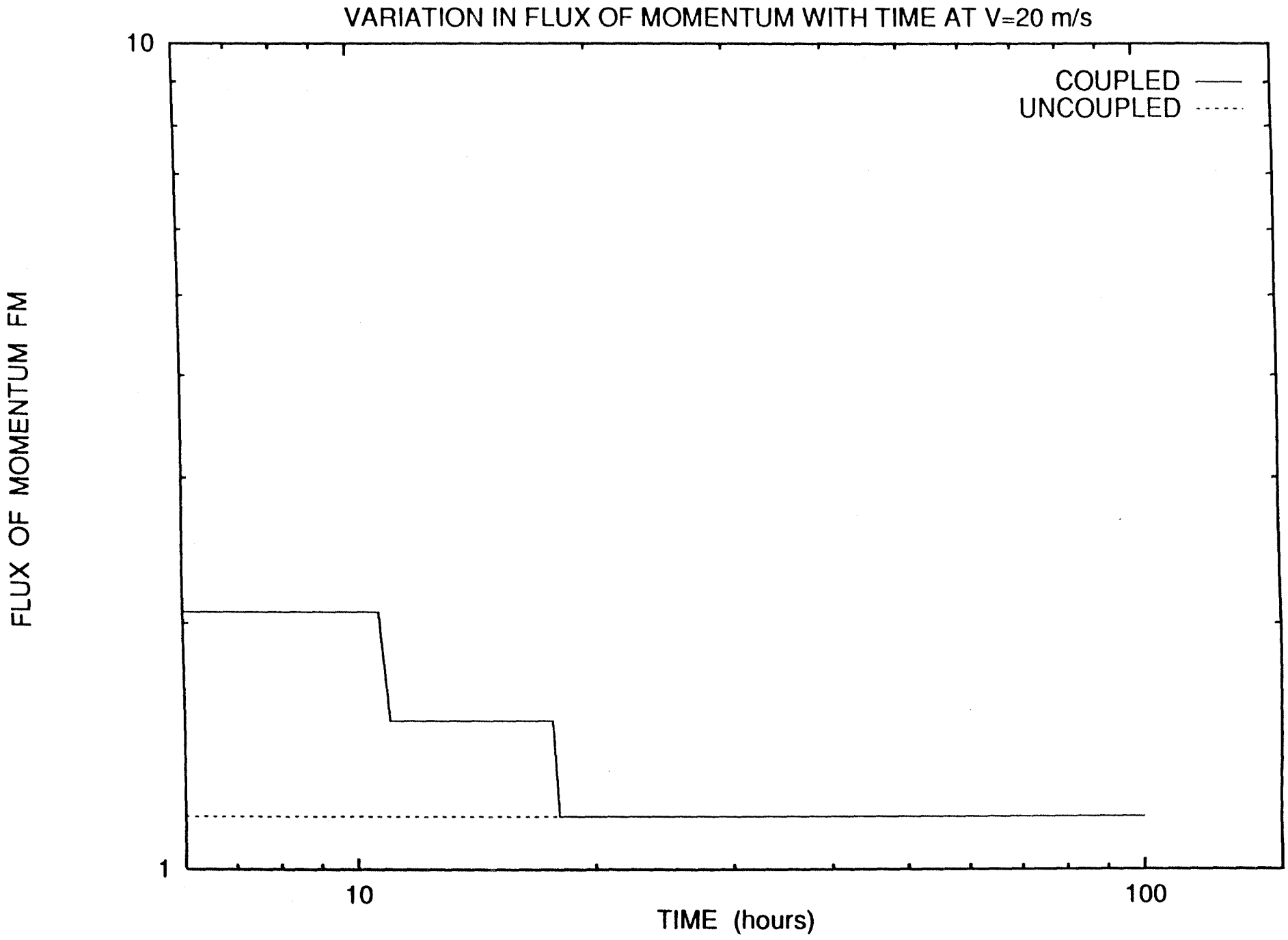
VARIATION IN FLUX OF MOMENTUM WITH TIME AT V=20 m/s
10
1
10
100
COUPLED
UNCOUPLED
FLUX OF MOMENTUM FM
TIME (hours)

Fig.40b

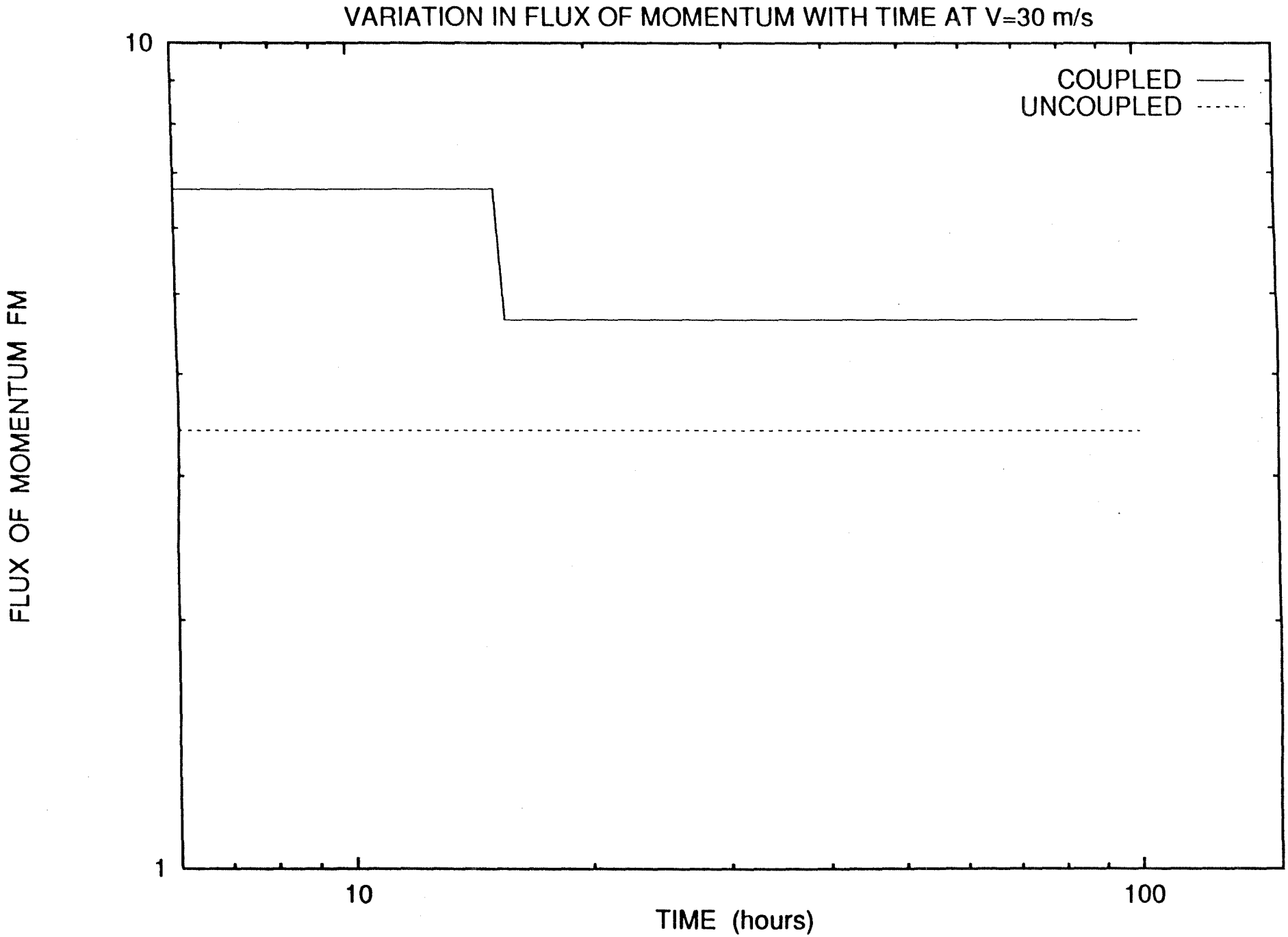
VARIATION IN FLUX OF MOMENTUM WITH TIME AT V=30 m/s
10
1
10
100
TIME (hours)
FLUX OF MOMENTUM FM
COUPLED
UNCOUPLED

Fig.40c

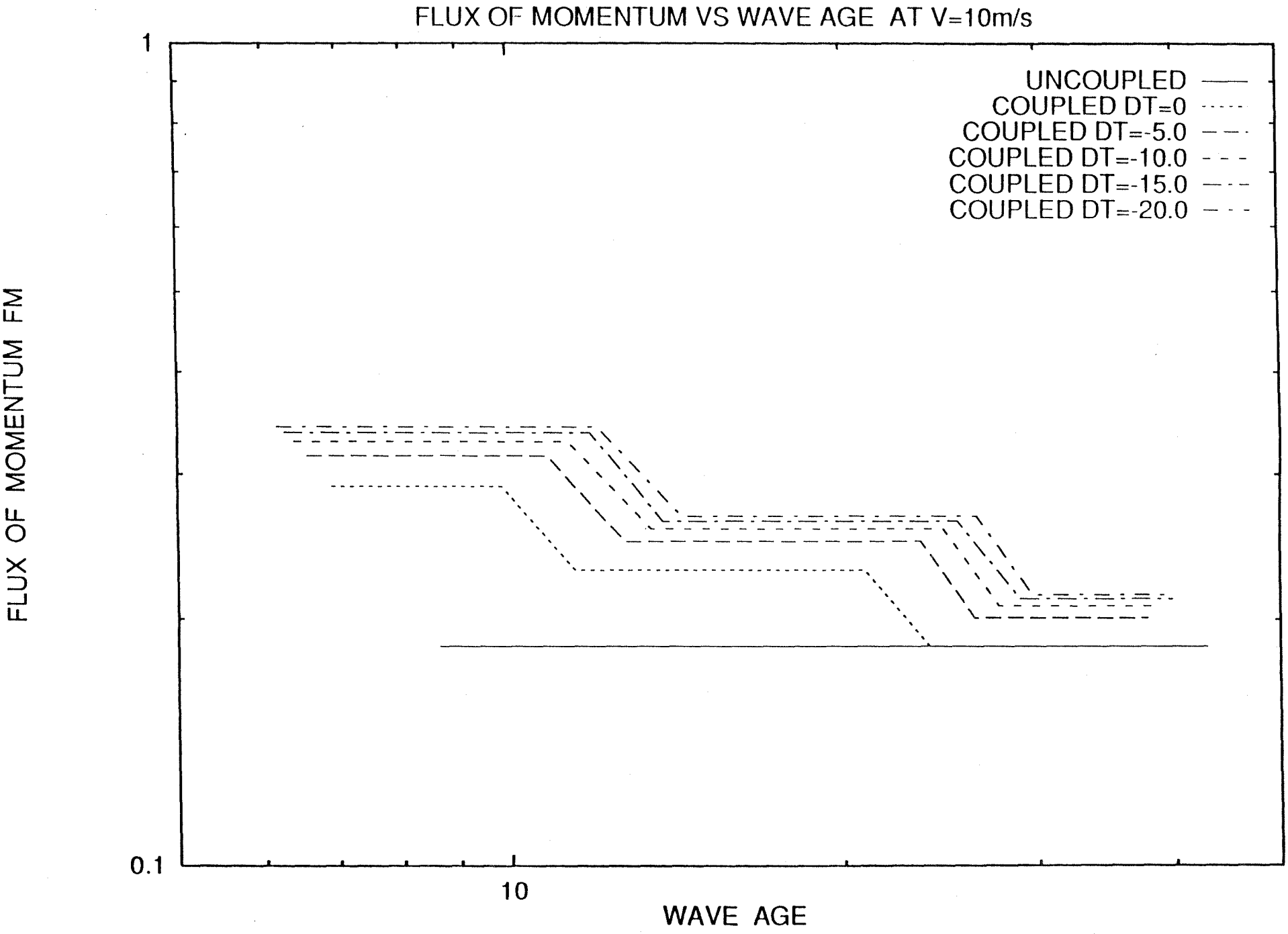
FLUX OF MOMENTUM VS WAVE AGE AT V=10m/s
1
0.1
10
WAVE AGE
FLUX OF MOMENTUM FM
UNCOUPLED
COUPLED DT=0
COUPLED DT=-5.0
COUPLED DT=-10.0
COUPLED DT=-15.0
COUPLED DT=-20.0

Fig.41a

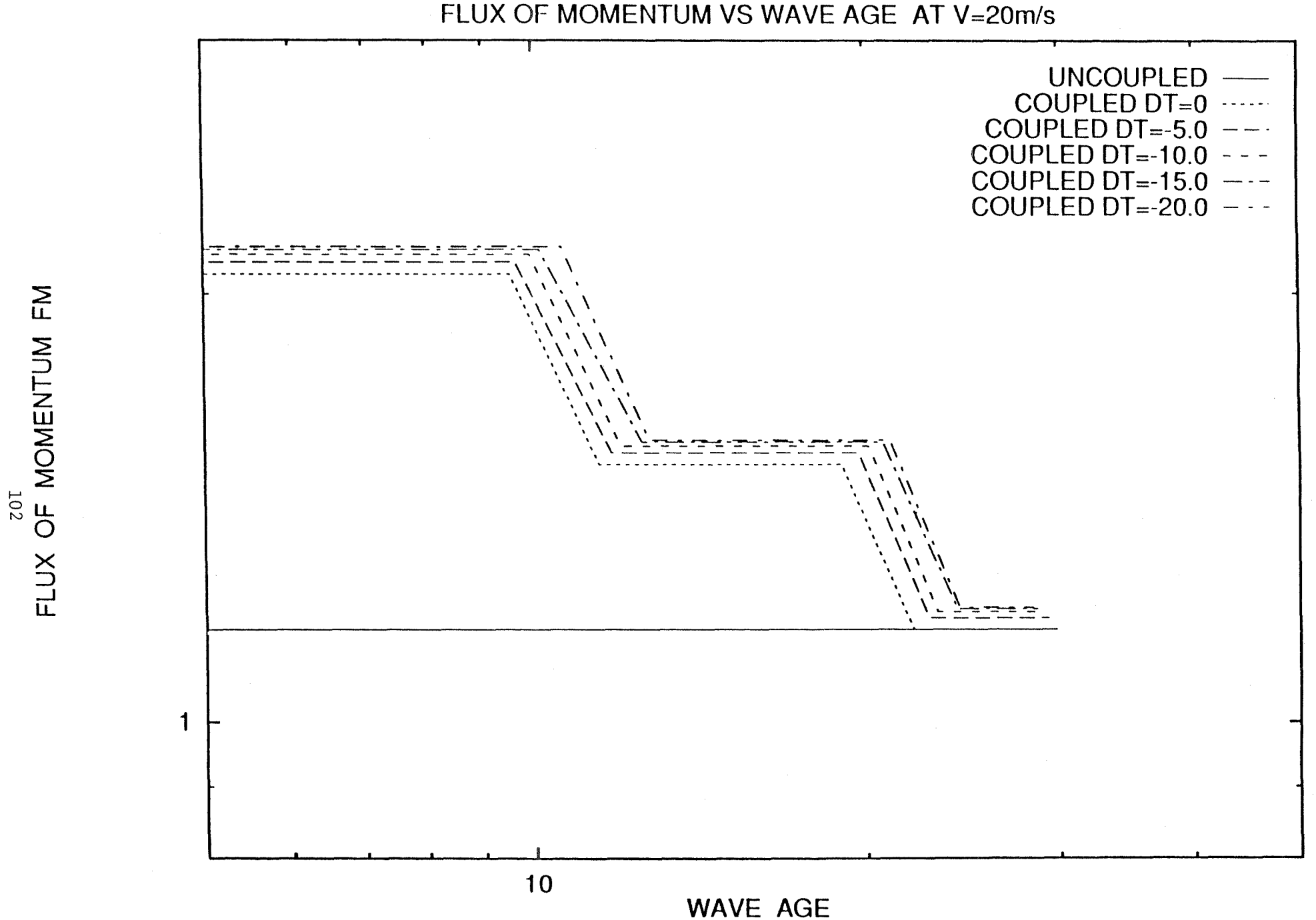
FLUX OF MOMENTUM VS WAVE AGE AT V=20m/s
UNCOUPLED
COUPLED DT=0
COUPLED DT=-5.0
COUPLED DT=-10.0
COUPLED DT=-15.0
COUPLED DT=-20.0
FLUX OF MOMENTUM FM
102
1
10
WAVE AGE

Fig.41b

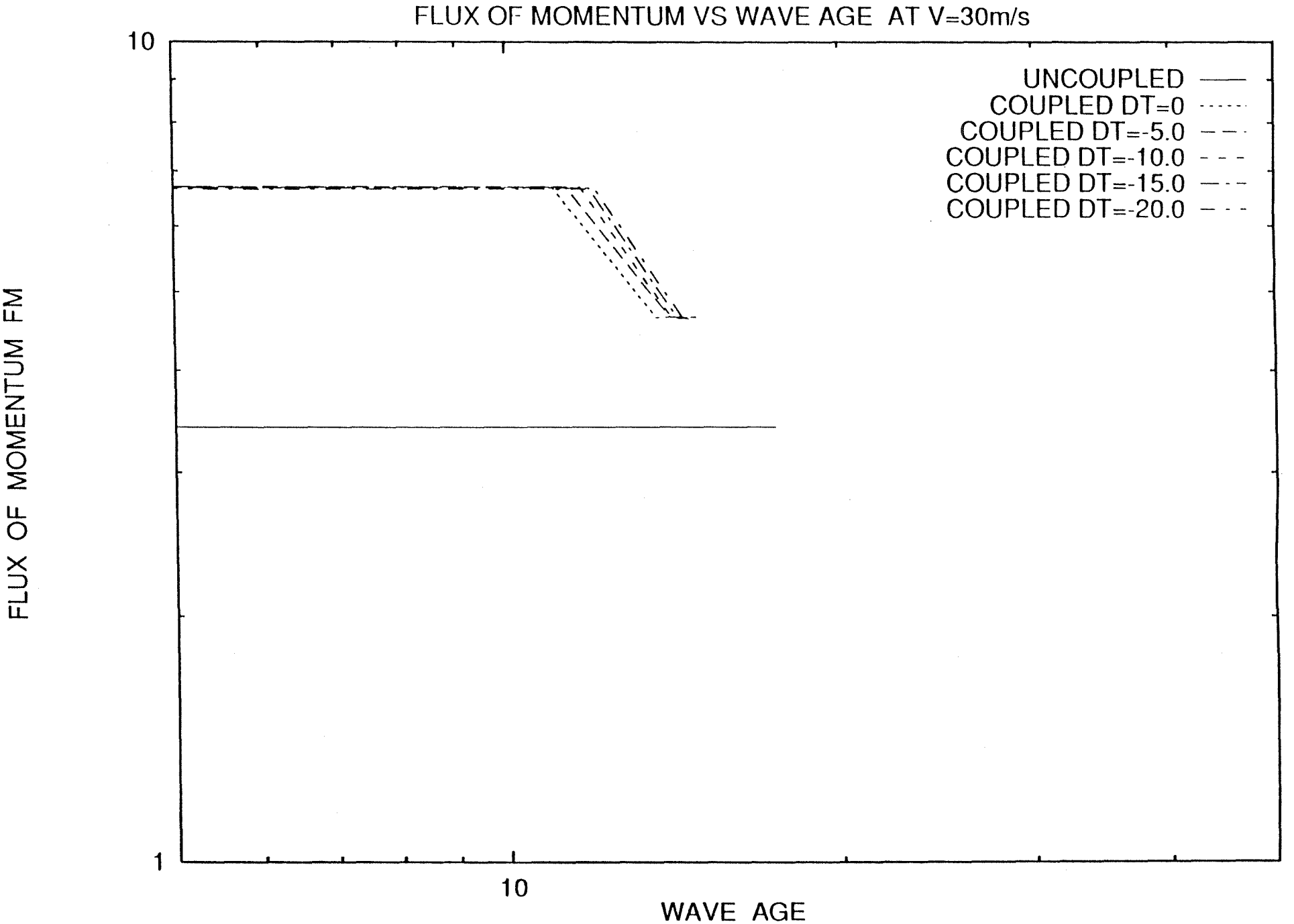
FLUX OF MOMENTUM VS WAVE AGE AT V=30m/s
10
1
10
WAVE AGE
FLUX OF MOMENTUM FM
UNCOUPLED
COUPLED DT=0
COUPLED DT=-5.0
COUPLED DT=-10.0
COUPLED DT=-15.0
COUPLED DT=-20.0

Fig.41c

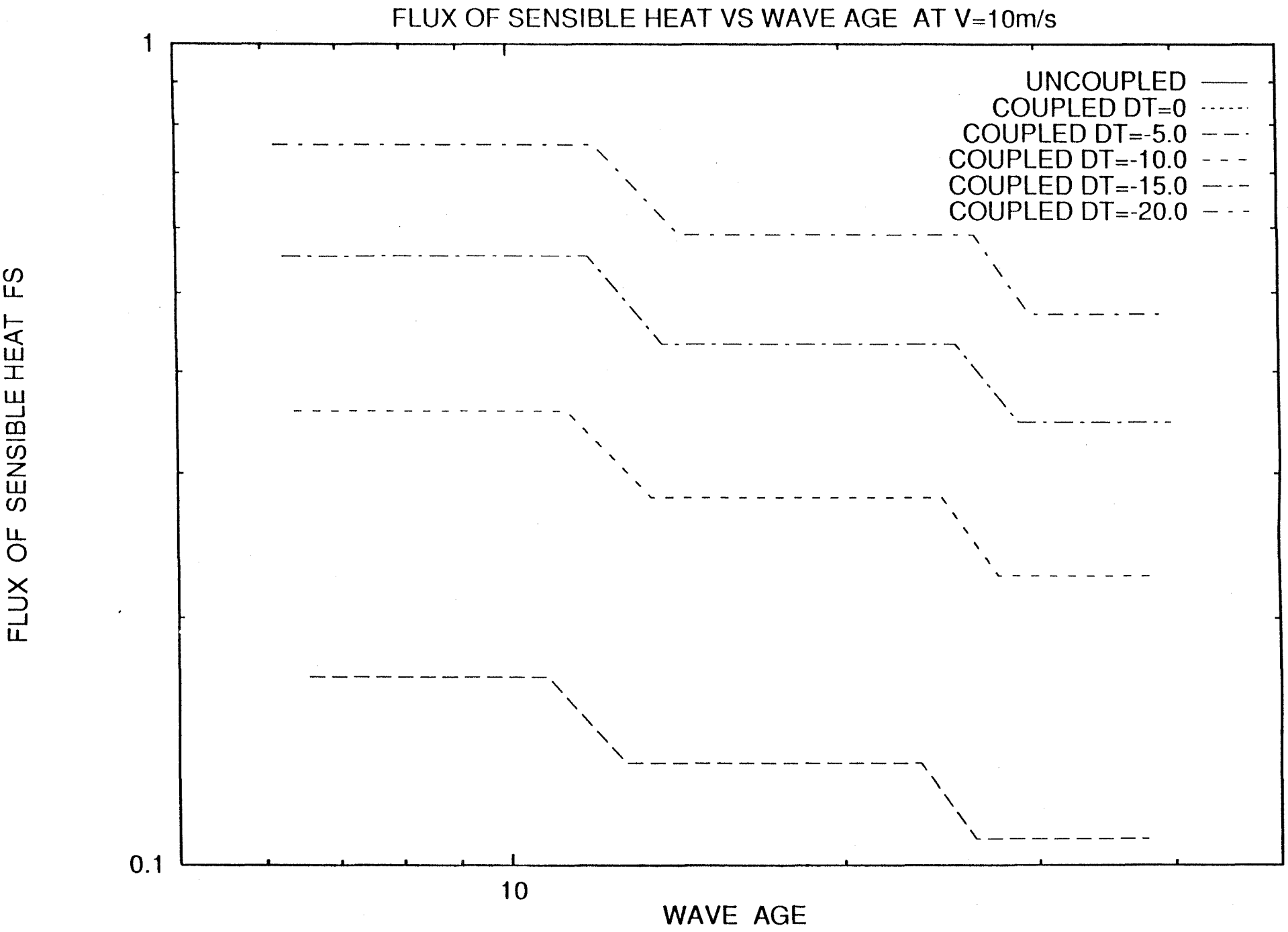
FLUX OF SENSIBLE HEAT VS WAVE AGE AT V=10m/s
1
0.1
10
WAVE AGE
FLUX OF SENSIBLE HEAT FS
UNCOUPLED
COUPLED DT=0
COUPLED DT=-5.0
COUPLED DT=-10.0
COUPLED DT=-15.0
COUPLED DT=-20.0

Fig.42a

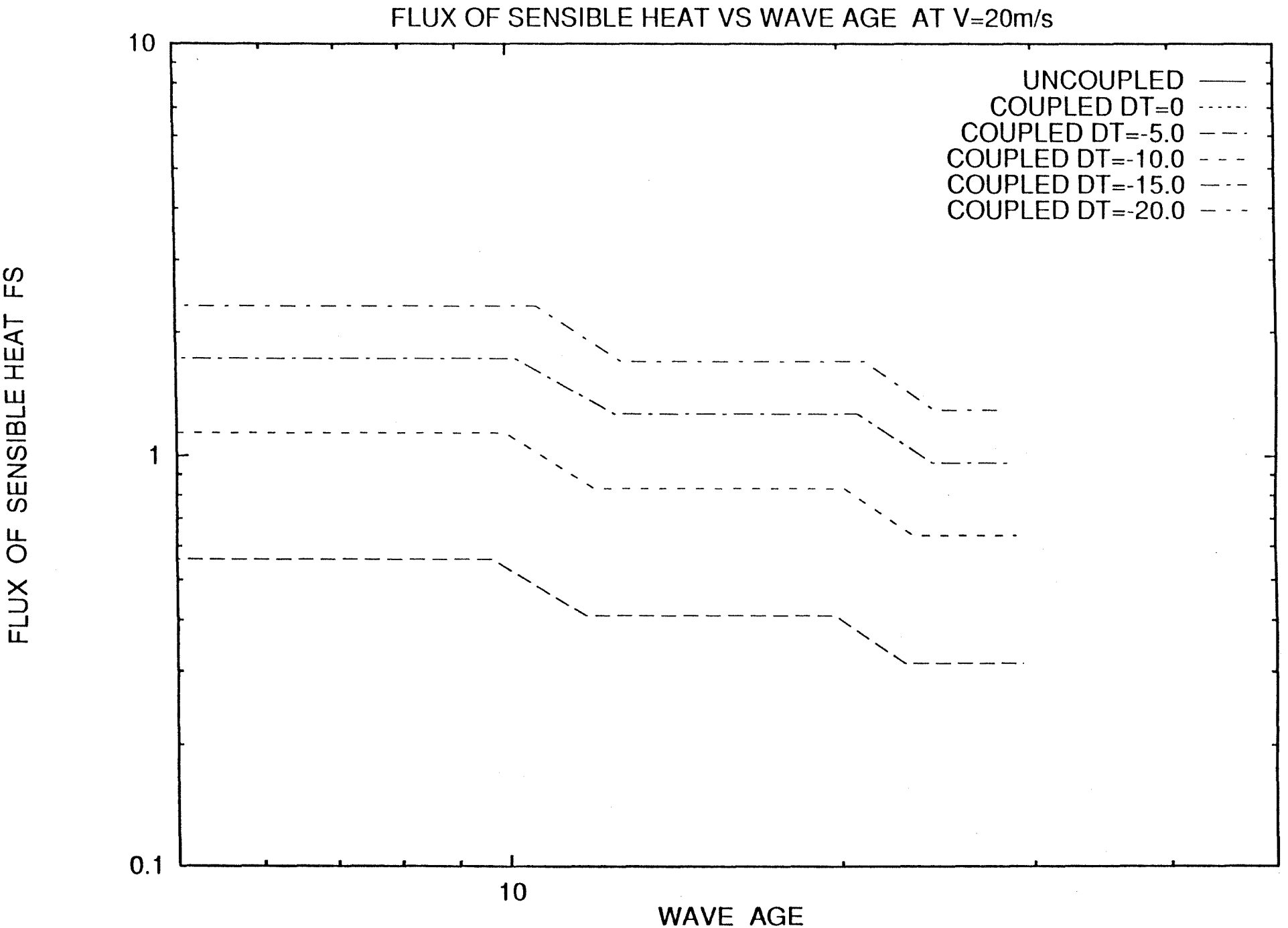
FLUX OF SENSIBLE HEAT VS WAVE AGE AT V=20m/s
UNCOUPLED
COUPLED DT=0
COUPLED DT=-5.0
COUPLED DT=-10.0
COUPLED DT=-15.0
COUPLED DT=-20.0
FLUX OF SENSIBLE HEAT FS
10
1
0.1
10
WAVE AGE

Fig.42b

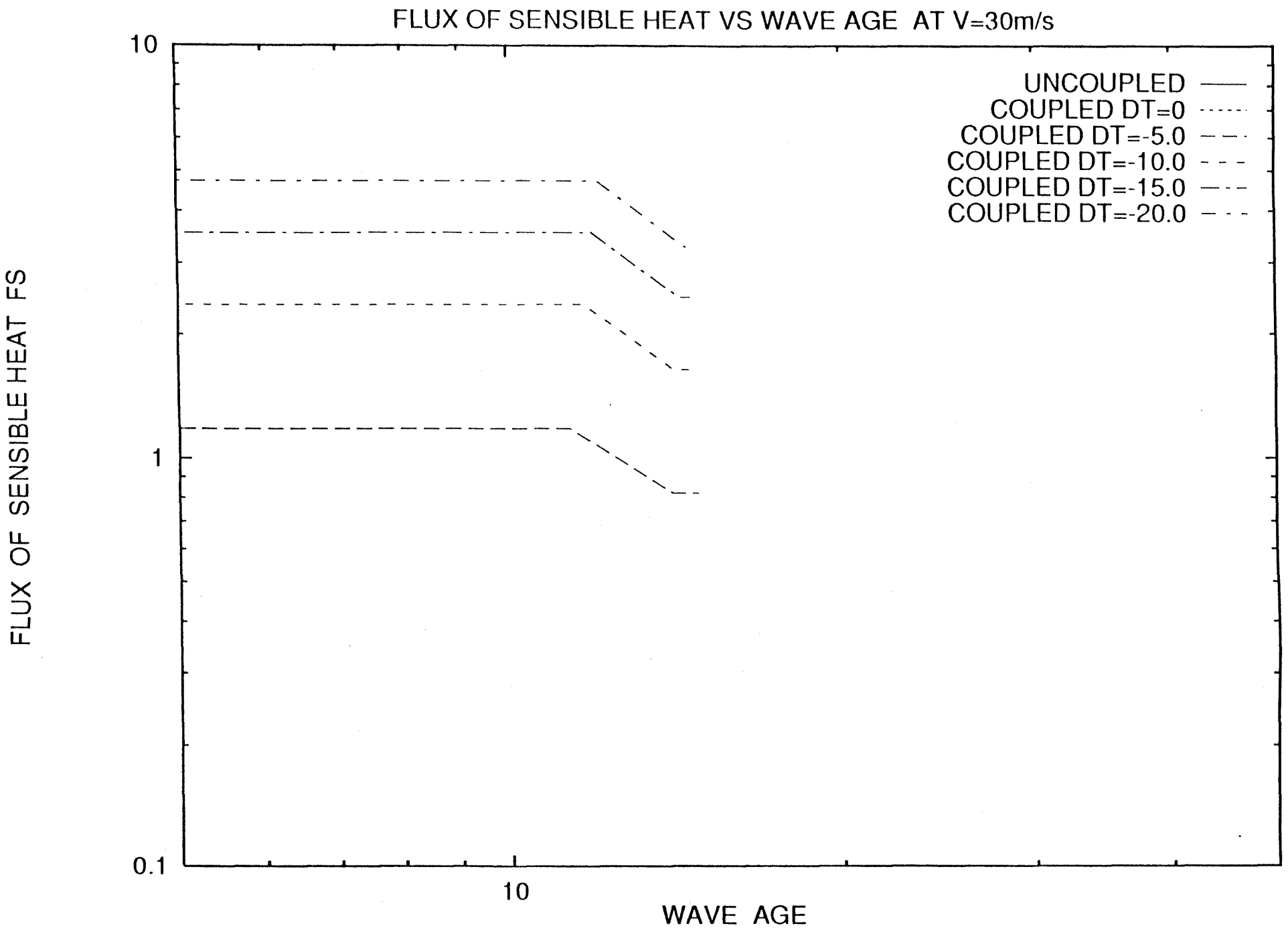
FLUX OF SENSIBLE HEAT VS WAVE AGE AT V=30m/s
10
1
0.1
10
WAVE AGE
FLUX OF SENSIBLE HEAT FS
UNCOUPLED
COUPLED DT=0
COUPLED DT=-5.0
COUPLED DT=-10.0
COUPLED DT=-15.0
COUPLED DT=-20.0

Fig.42c

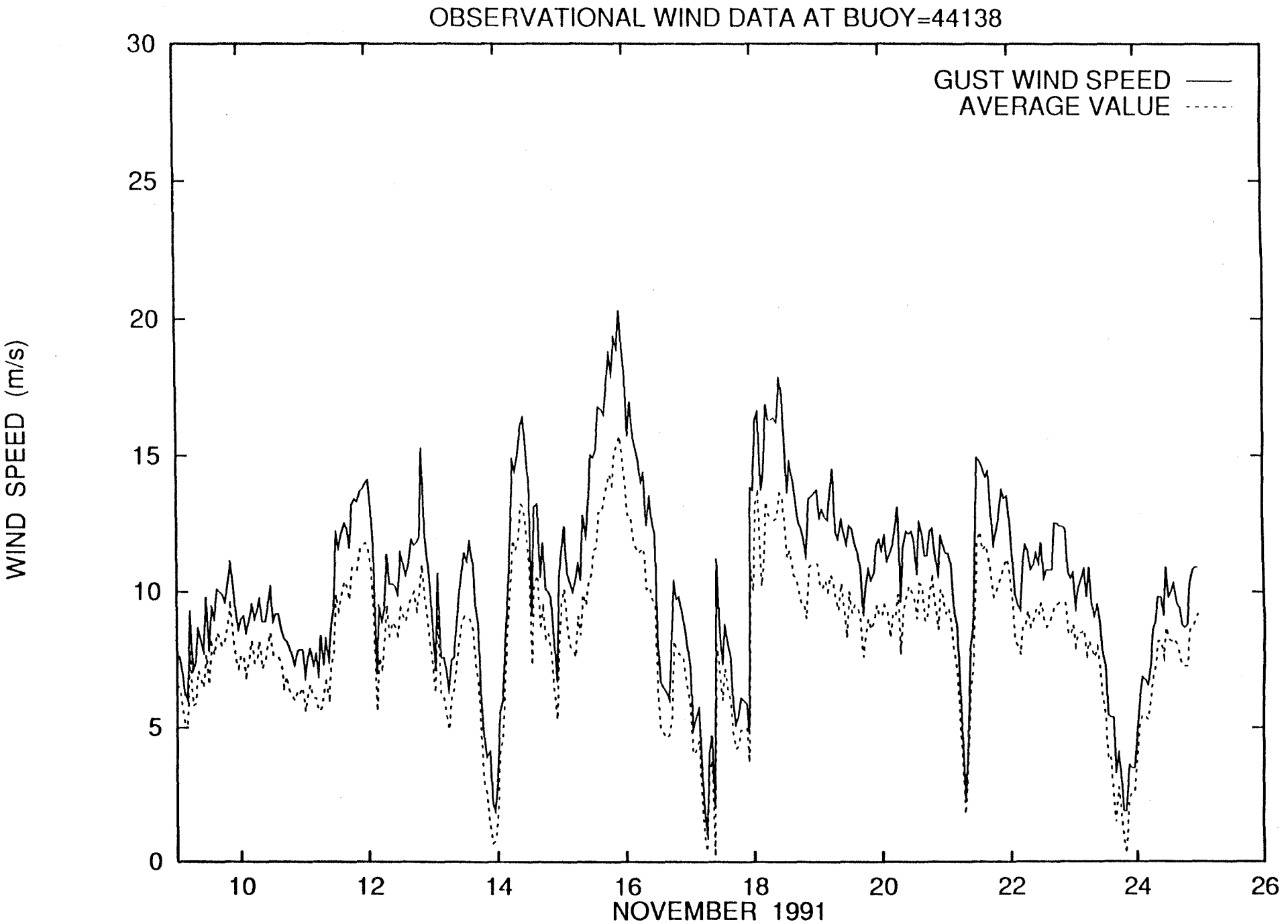
OBSERVATIONAL WIND DATA AT BUOY=44138
GUST WIND SPEED
AVERAGE VALUE
WIND SPEED (m/s)
0
5
10
15
20
25
30
10
12
14
16
18
20
22
24
26
NOVEMBER 1991

Fig.43a

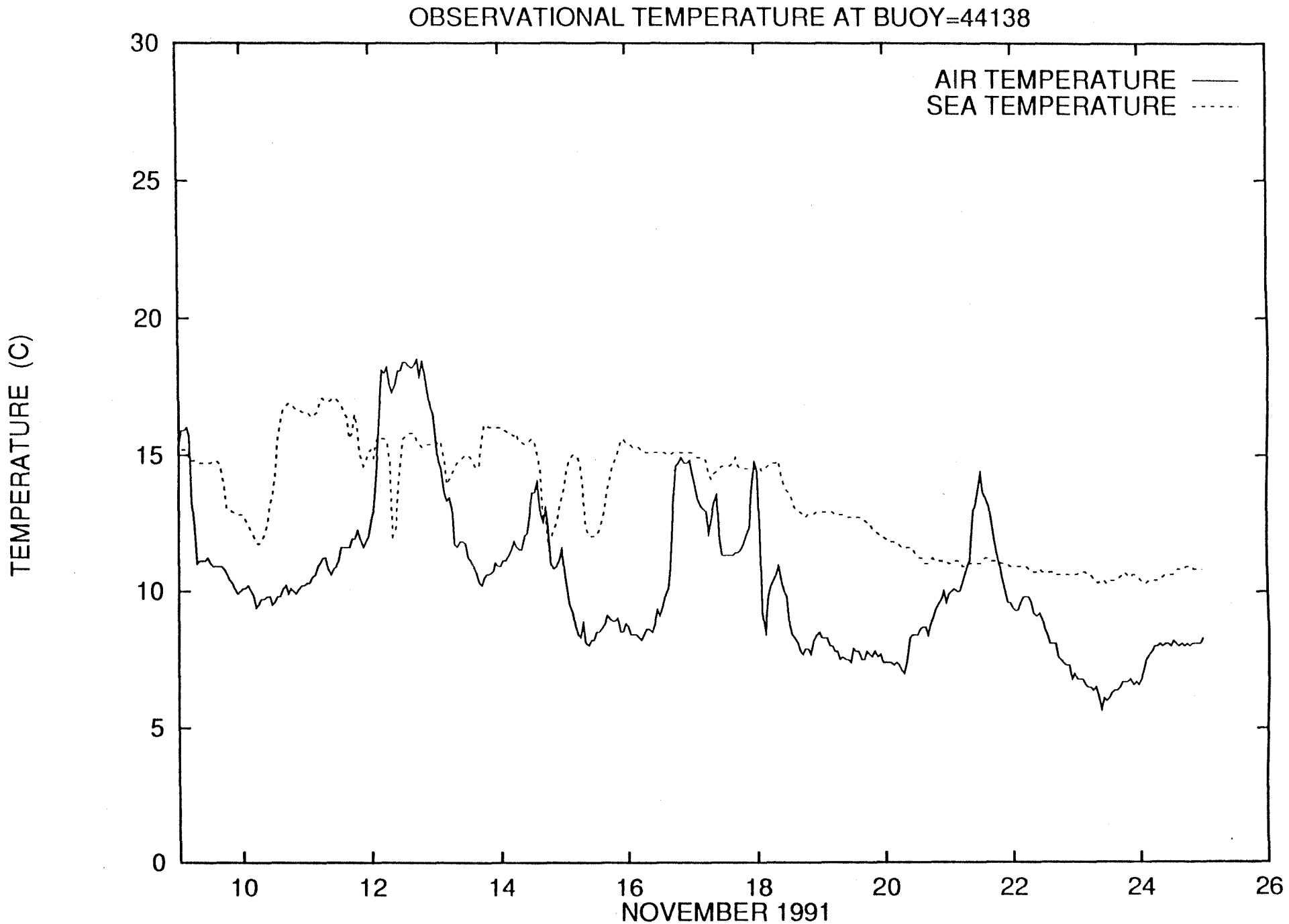
OBSERVATIONAL TEMPERATURE AT BUOY=44138
AIR TEMPERATURE
SEA TEMPERATURE
TEMPERATURE (C)
30
25
20
15
10
5
0
10
12
14
16
18
20
22
24
26
NOVEMBER 1991

Fig.43b

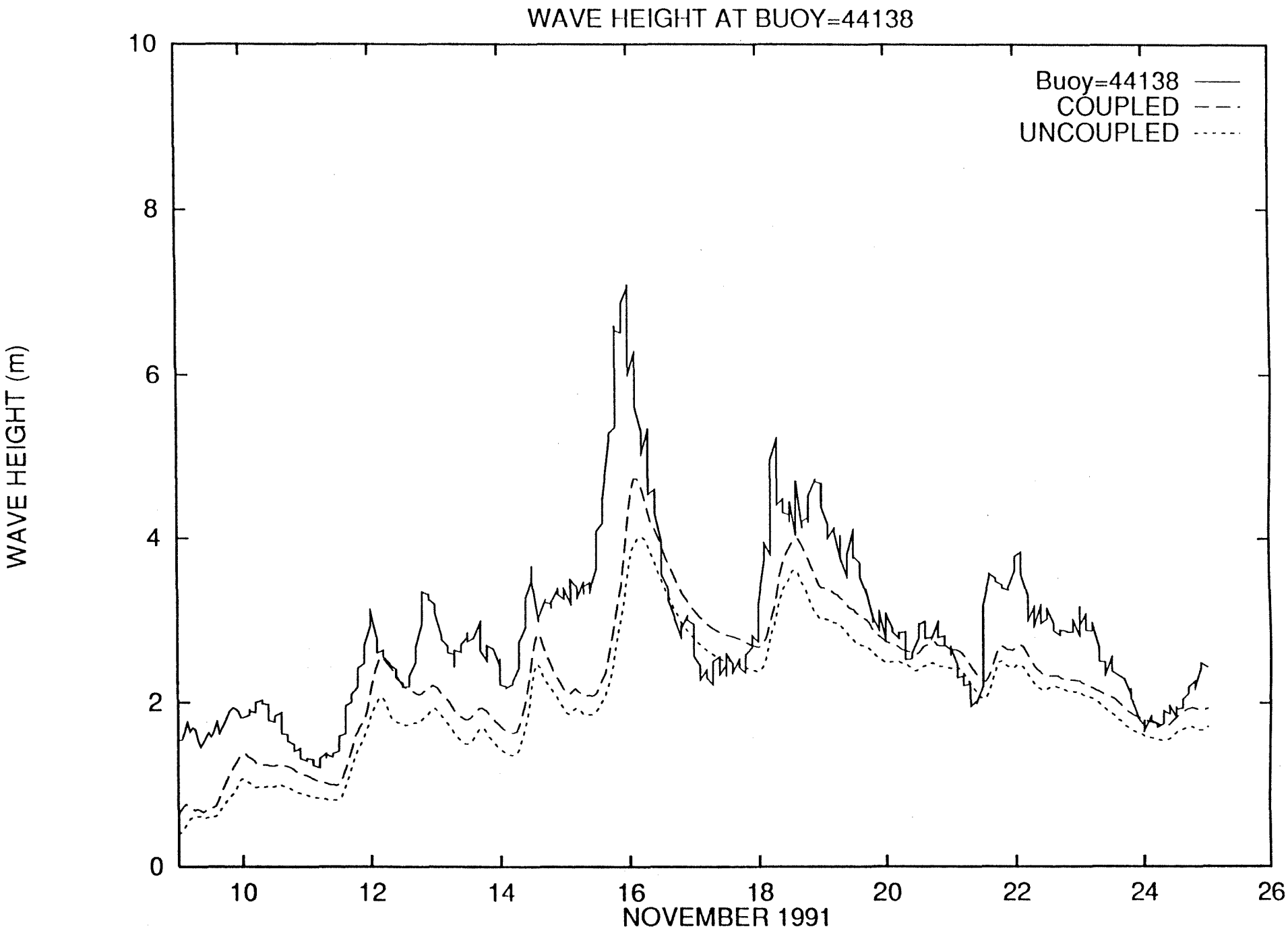
WAVE HEIGHT AT BUOY=44138
Buoy=44138
COUPLED
UNCOUPLED
WAVE HEIGHT (m)
0
2
4
6
8
10
10
12
14
16
18
20
22
24
26
NOVEMBER 1991

Fig.44a

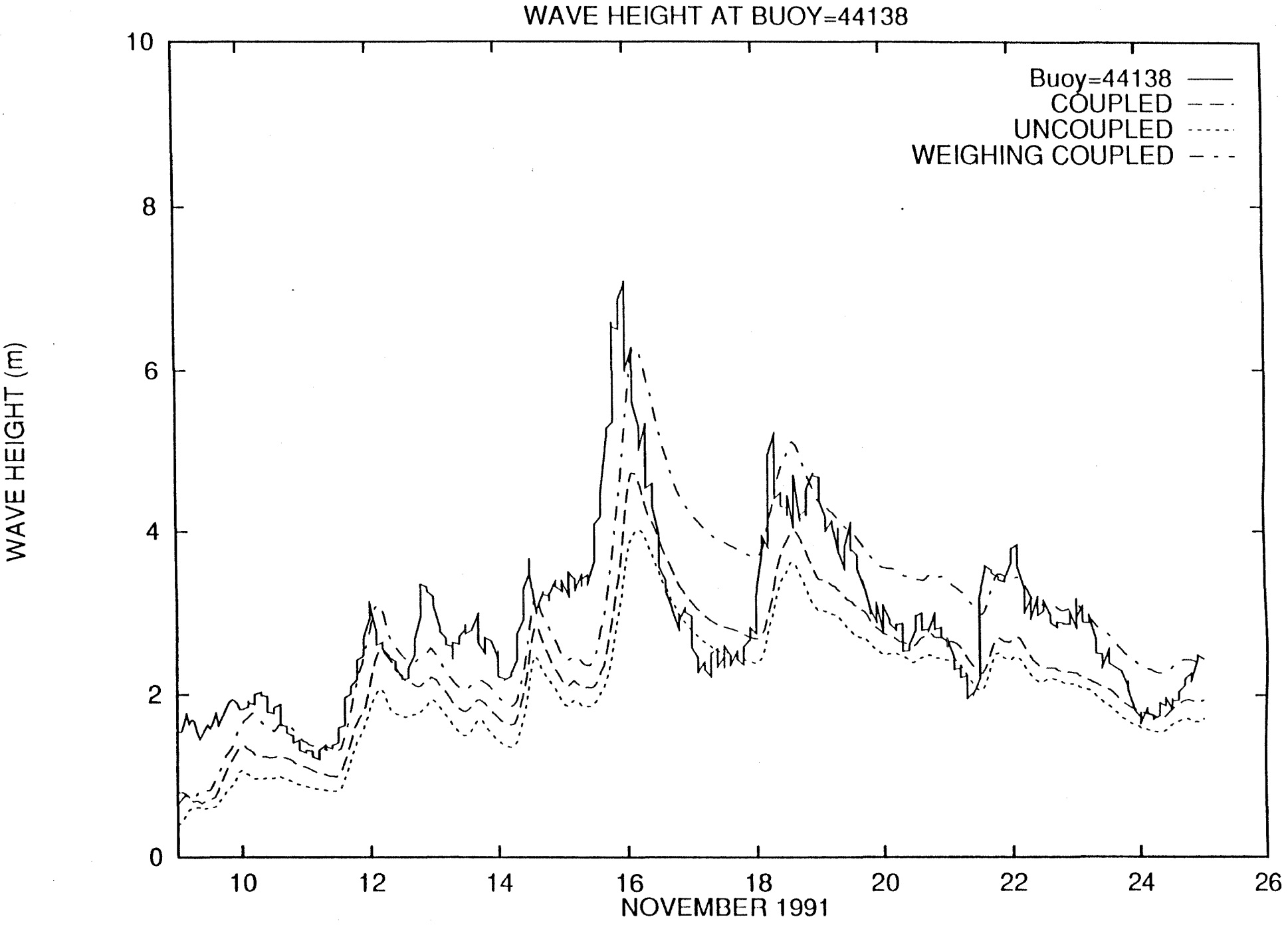
WAVE HEIGHT AT BUOY=44138
Buoy=44138
COUPLED
UNCOUPLED
WEIGHING COUPLED
WAVE HEIGHT (m)
0
2
4
6
8
10
10
12
14
16
18
20
22
24
26
NOVEMBER 1991

Fig.44b

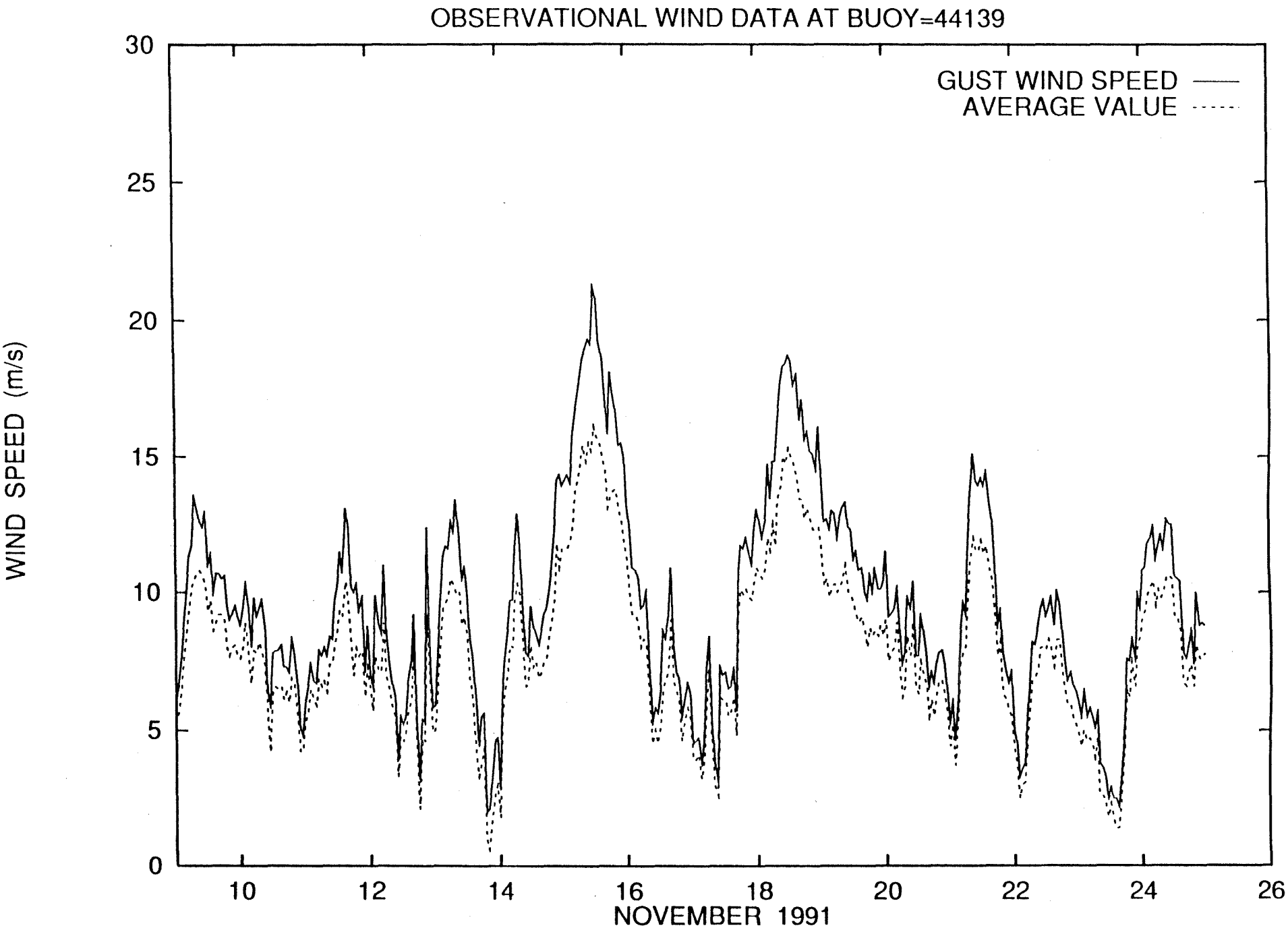
OBSERVATIONAL WIND DATA AT BUOY=44139
GUST WIND SPEED
AVERAGE VALUE
WIND SPEED (m/s)
30
25
20
15
10
5
0
10
12
14
16
18
20
22
24
26
NOVEMBER 1991

Fig.45a

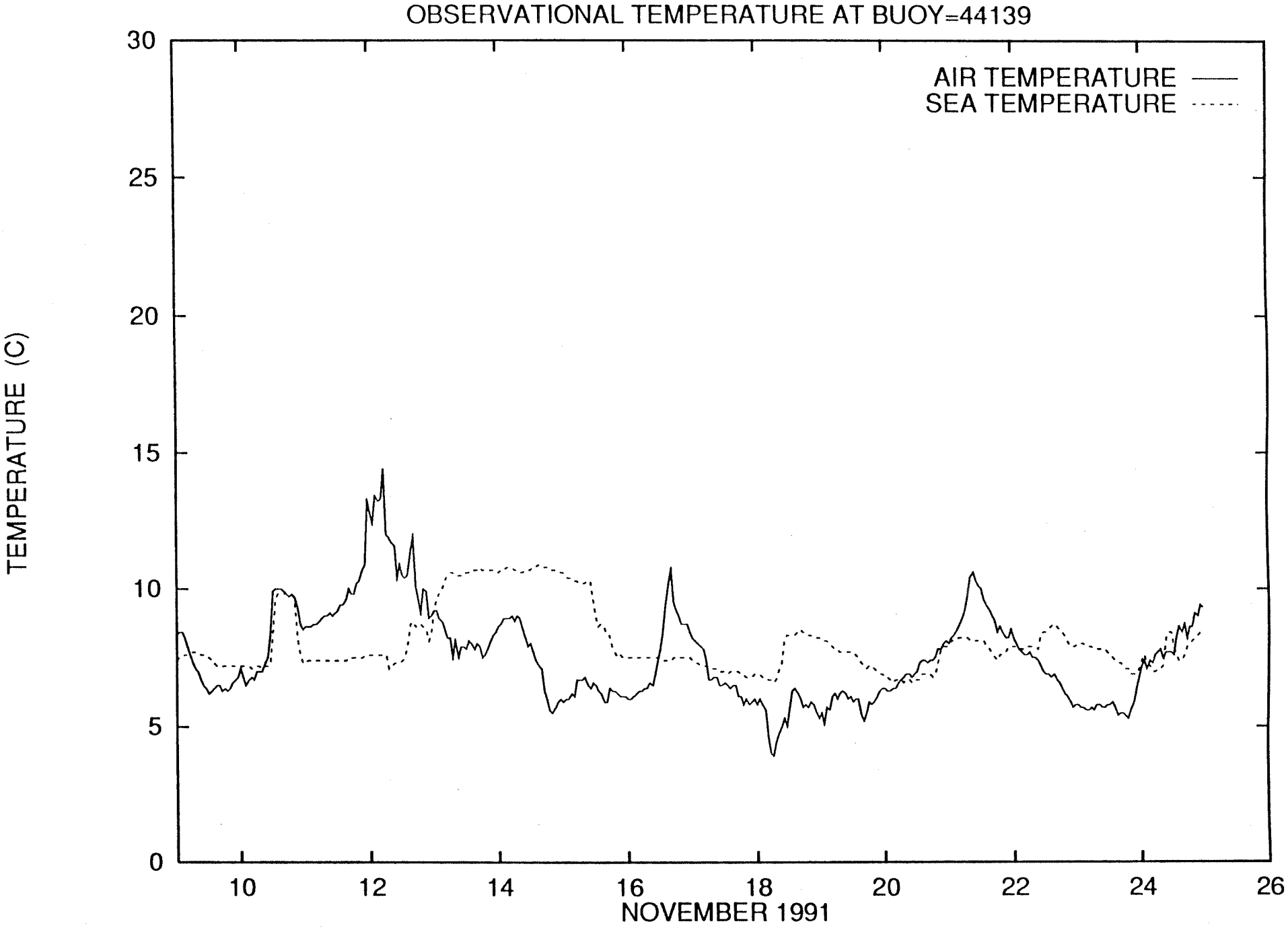
OBSERVATIONAL TEMPERATURE AT BUOY=44139
AIR TEMPERATURE
SEA TEMPERATURE
TEMPERATURE (C)
30
25
20
15
10
5
0
10
12
14
16
18
20
22
24
26
NOVEMBER 1991

Fig.45b

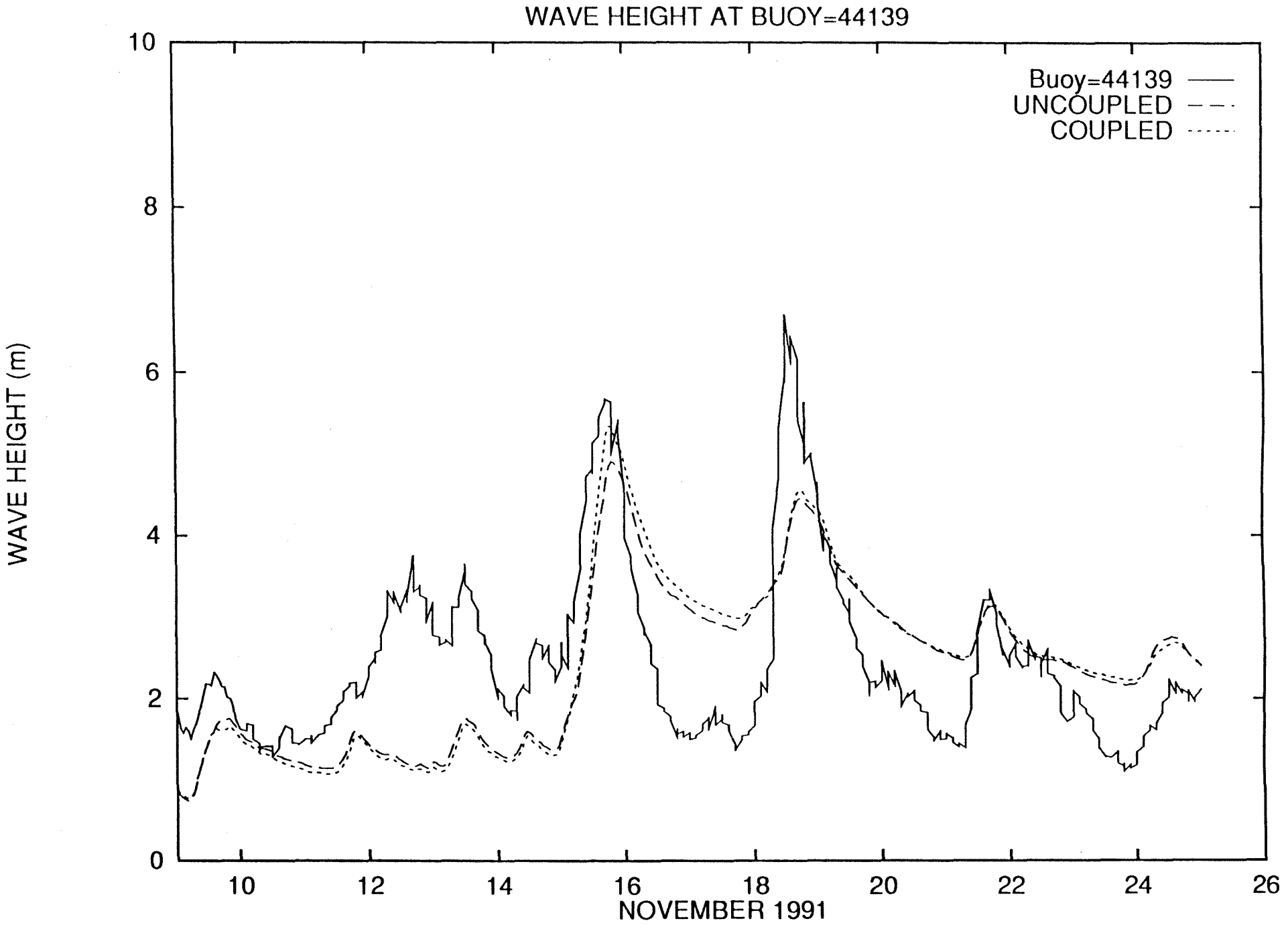
WAVE HEIGHT AT BUOY=44139
Buoy=44139
UNCOUPLED
COUPLED
WAVE HEIGHT (m)
0
2
4
6
8
10
10
12
14
16
18
20
22
24
26
NOVEMBER 1991

Fig.46

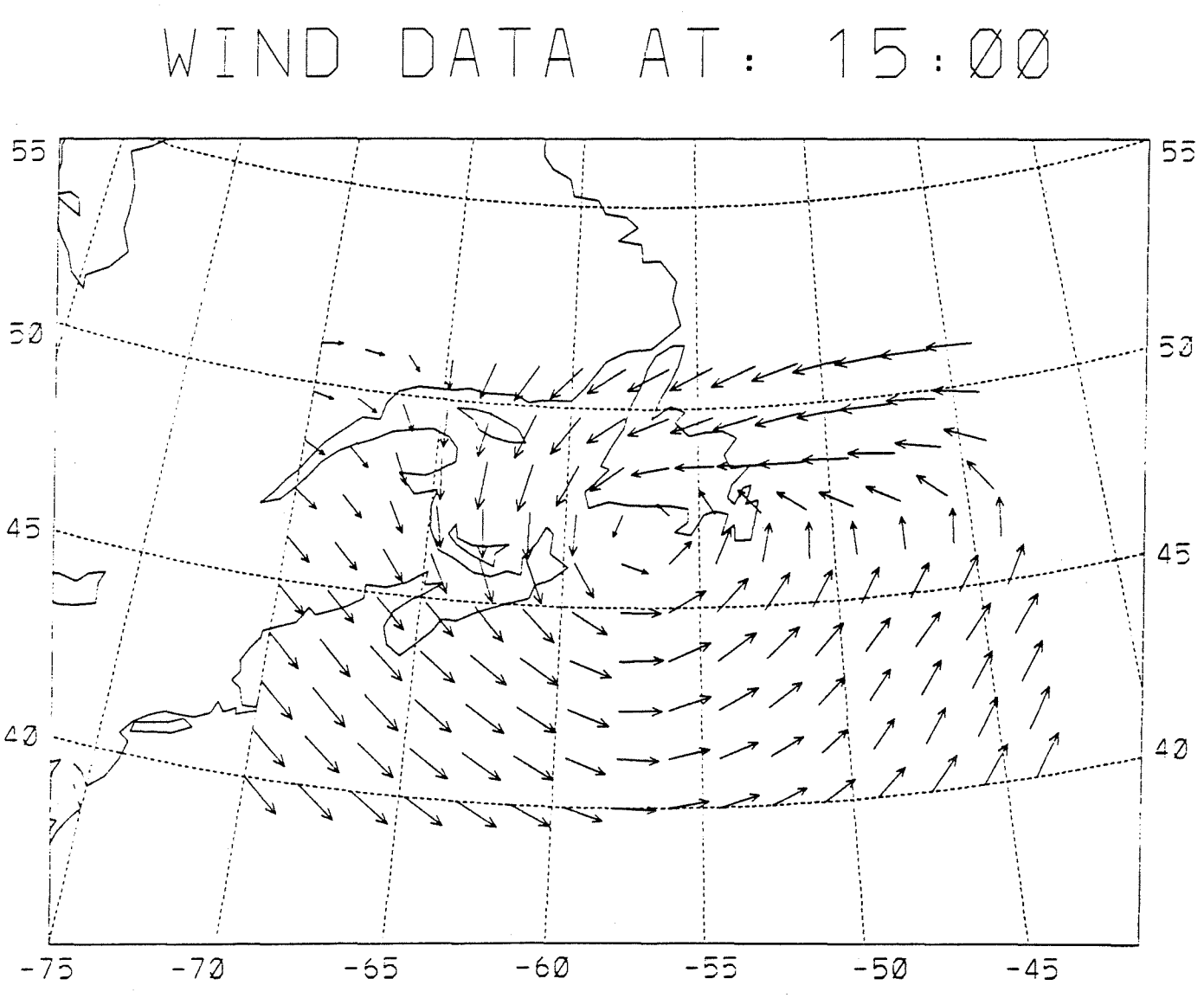
WIND DATA AT: 15:00
55
50
45
40
-75
-70
-65
-60
-55
-50
-45
0.265E+01
MAXIMUM VECTOR

Fig.47a

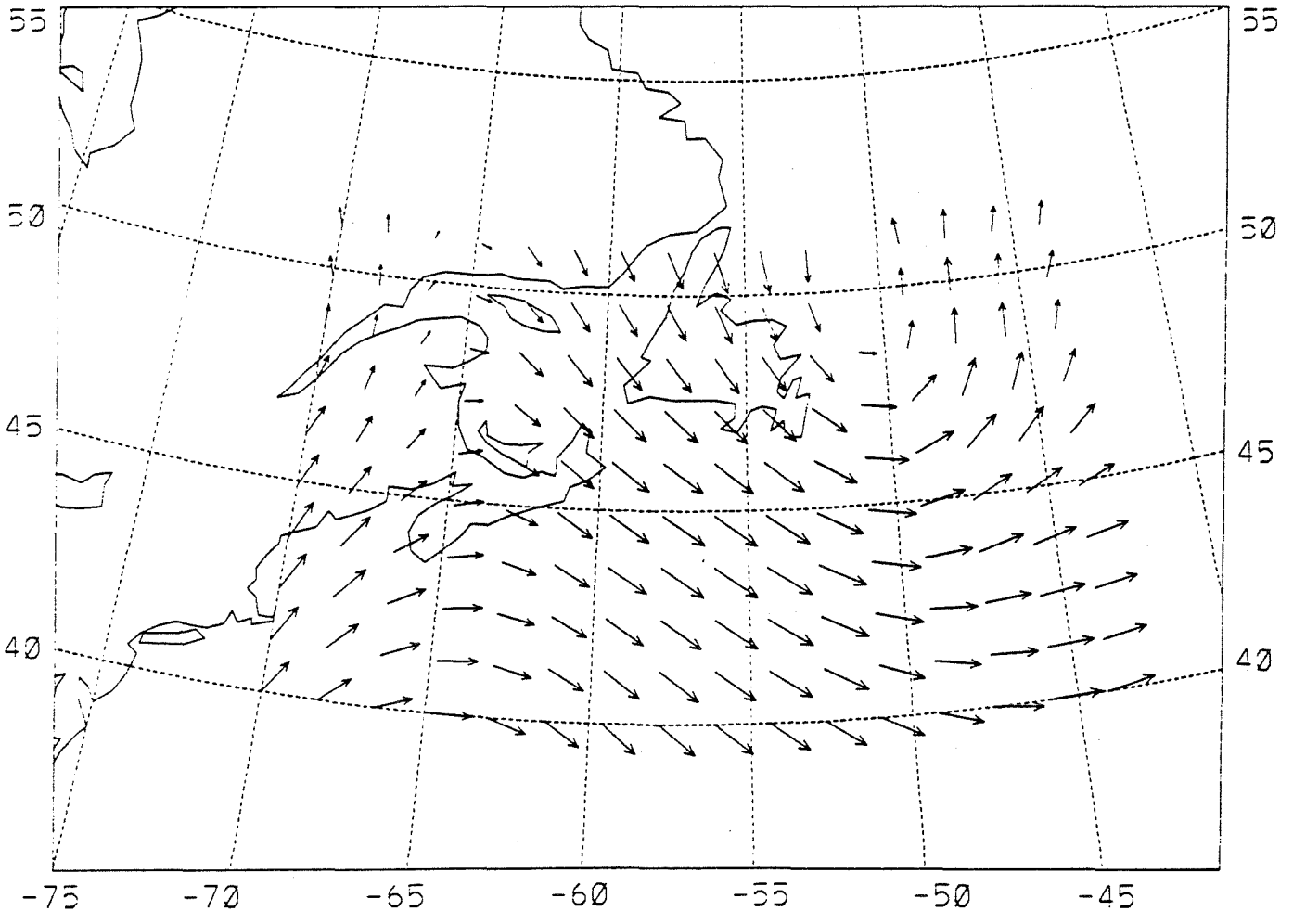
WIND DATA AT: 16:00
55
50
45
40
-75
-70
-65
-60
-55
-50
-45
0.286E-01
MAXIMUM VECTOR

Fig.47b

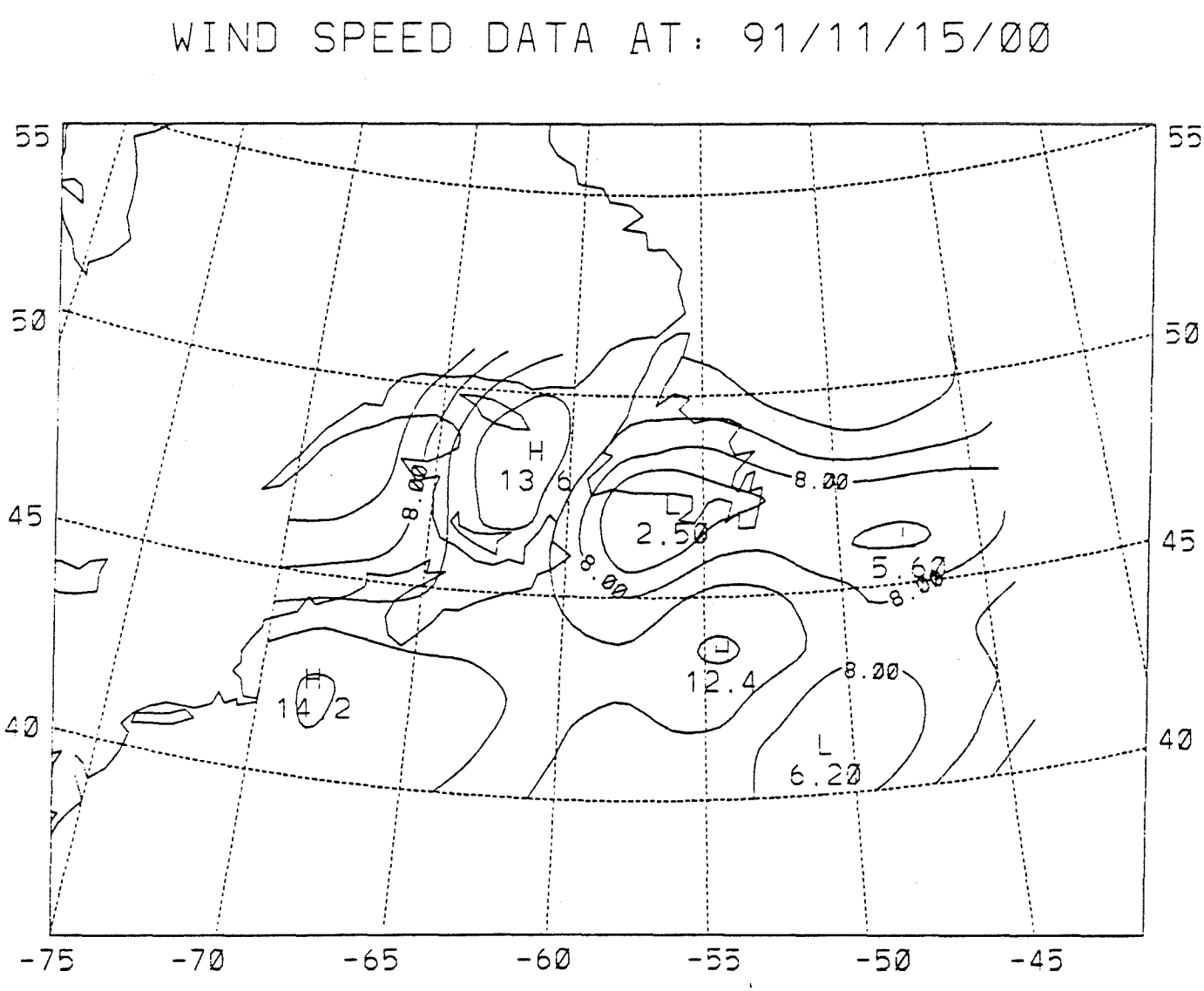

Fig.48a

CONTOUR FROM 6.0000 TO 28.000 CONTOUR INTERVAL OF 2.0000 PT(3,3)= 13.700

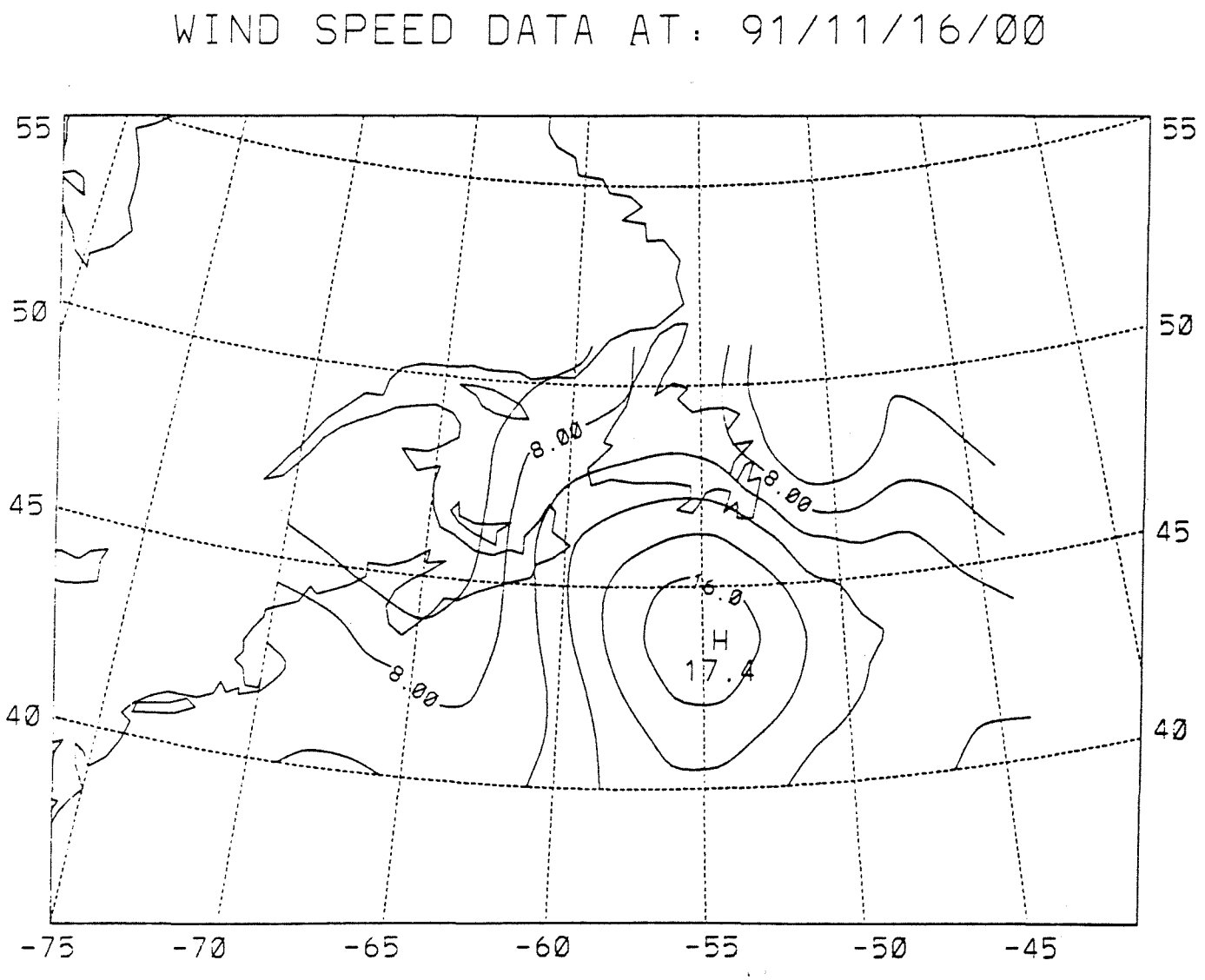

Fig.48b

CONTOUR FROM 6.0000 TO 28.000 CONTOUR INTERVAL OF 2.0000 PT(3,3)= 8.5000

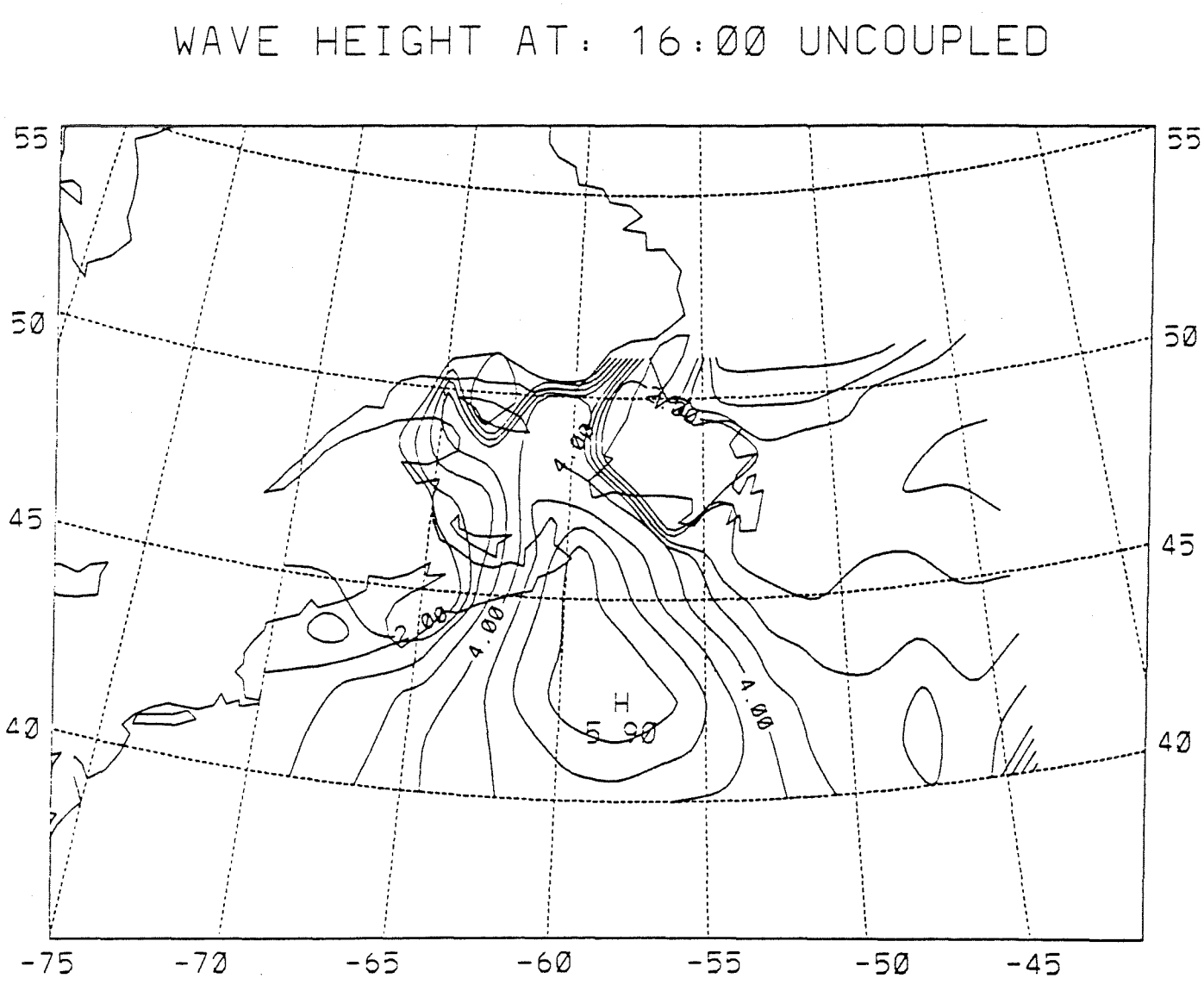

Fig.49a

CONTOUR FROM 2.0000 TO 8.0000 CONTOUR INTERVAL OF 0.50000 PT(3,3)= 3.2000

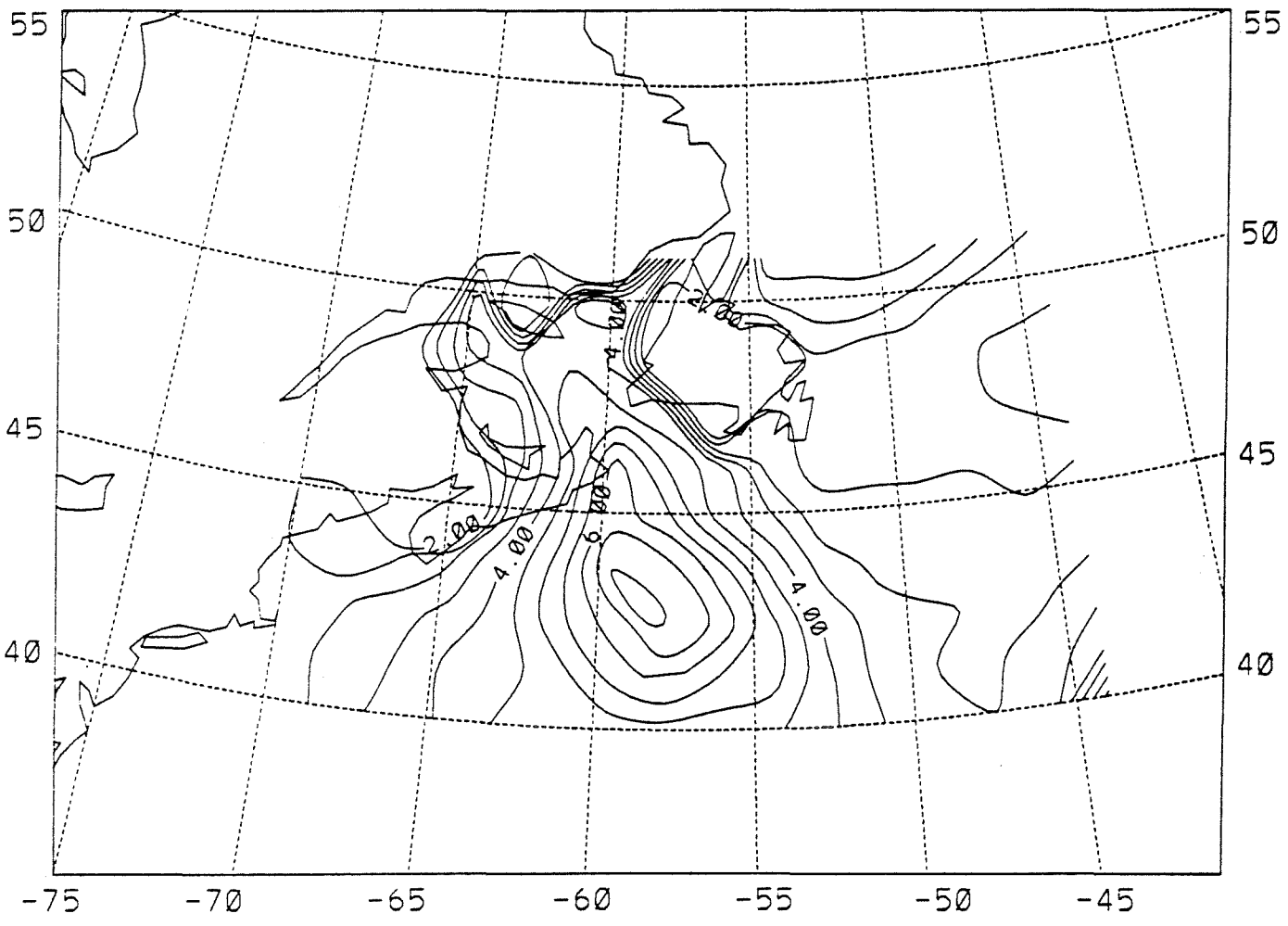

Fig.49b

CONTOUR FROM 2.0000 TO 8.0000 CONTOUR INTERVAL OF 0.50000 PT(3,3)= 3.2000

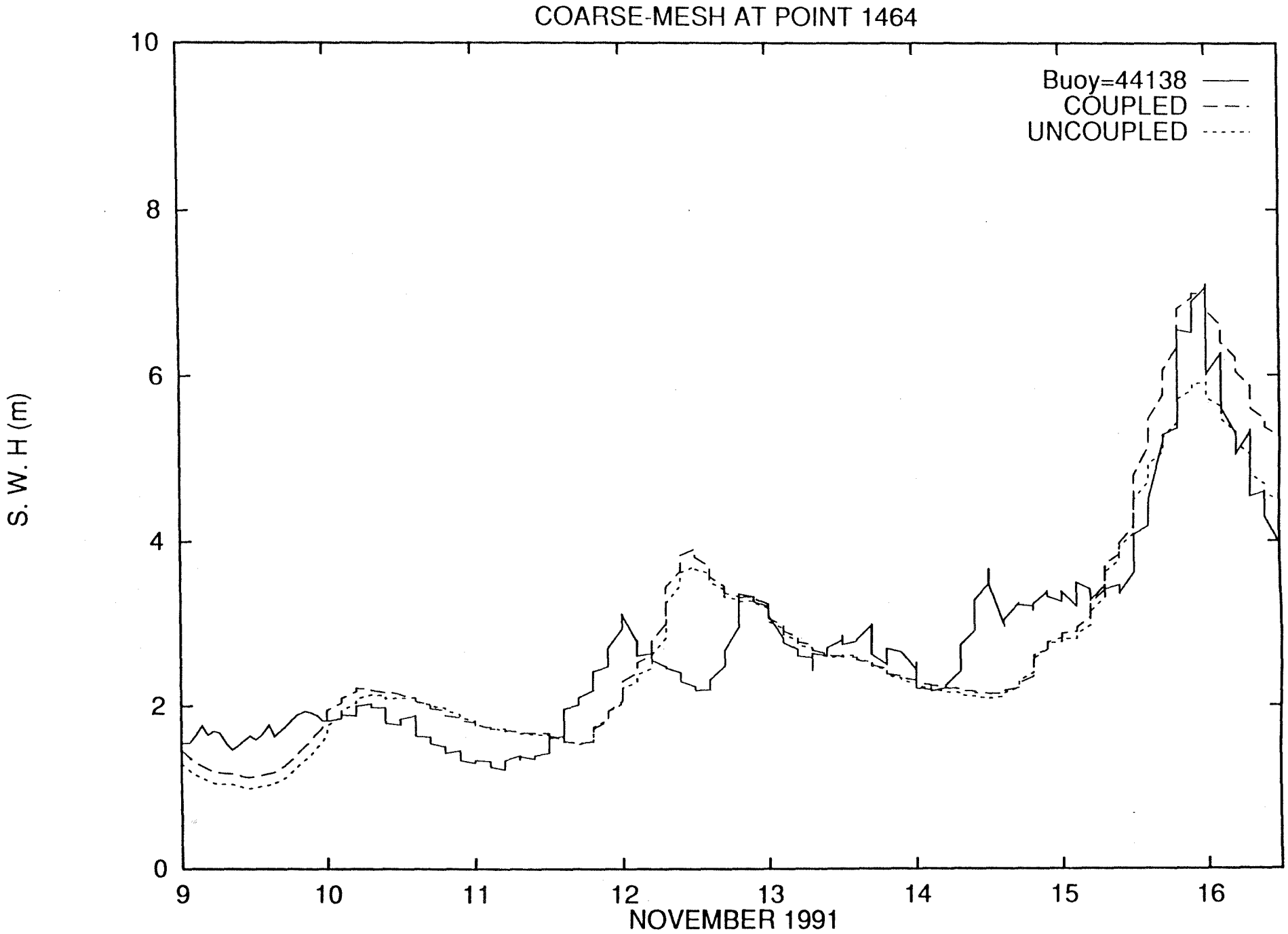
COARSE-MESH AT POINT 1464
Buoy=44138
COUPLED
UNCOUPLED
S. W. H (m)
0
2
4
6
8
10
9
10
11
12
13
14
15
16
NOVEMBER 1991

Fig.50a

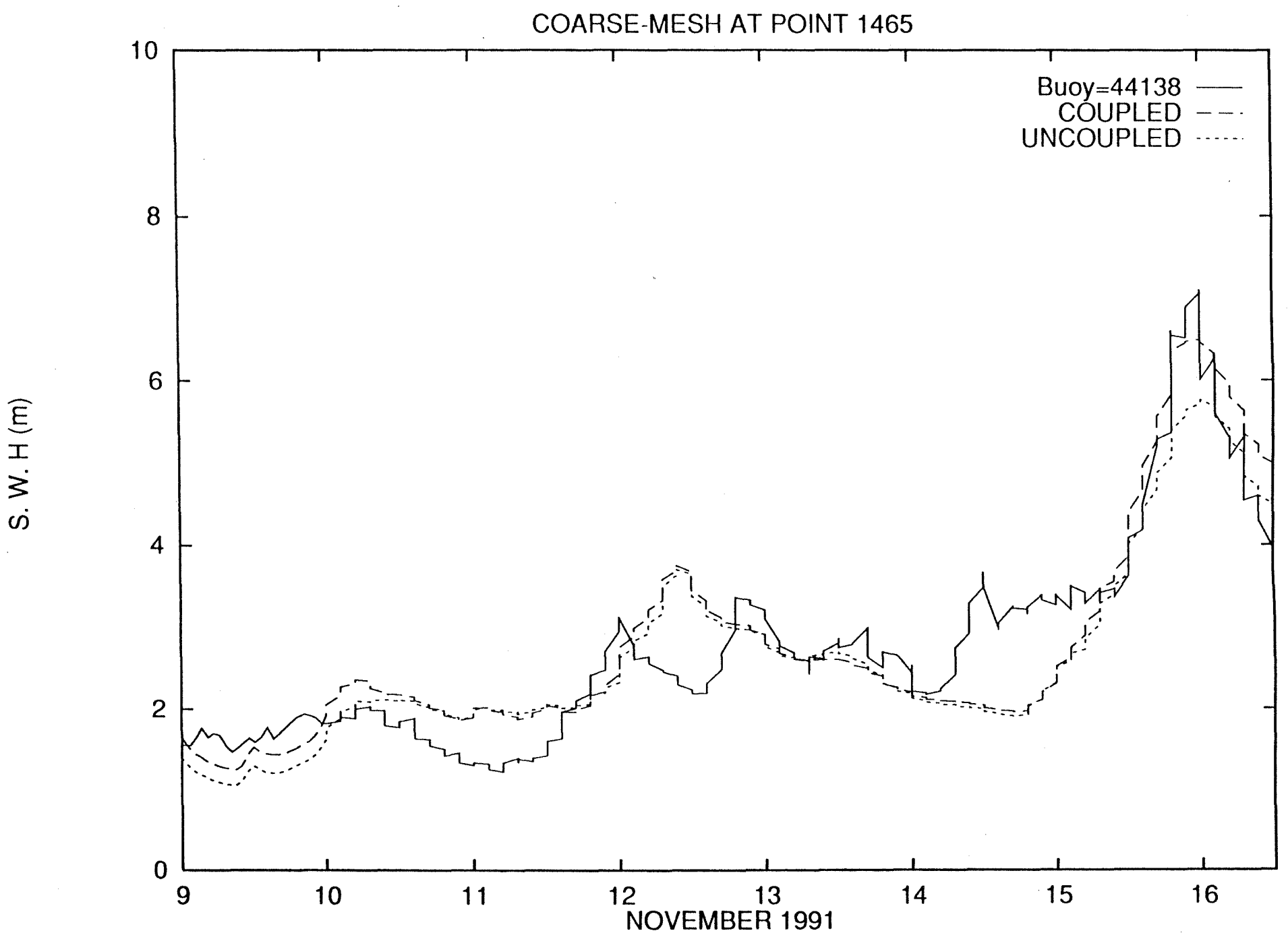
COARSE-MESH AT POINT 1465
Buoy=44138
COUPLED
UNCOUPLED
S. W. H (m)
0
2
4
6
8
10
9
10
11
12
13
14
15
16
NOVEMBER 1991

Fig.50b

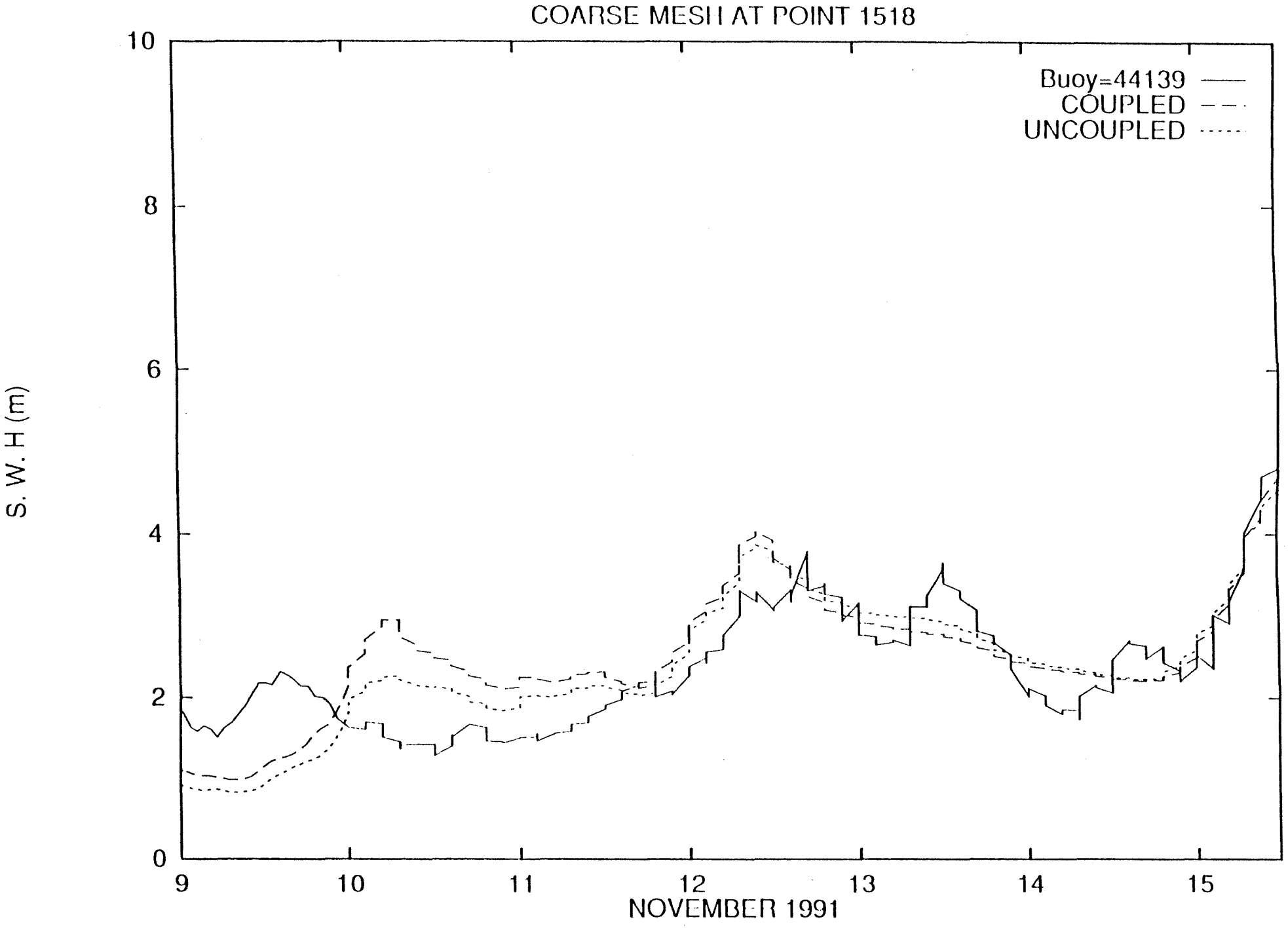
COARSE MESH AT POINT 1518
Buoy=44139
COUPLED
UNCOUPLED
S. W. H (m)
0
2
4
6
8
10
9
10
11
12
13
14
15
NOVEMBER 1991

Fig.5la

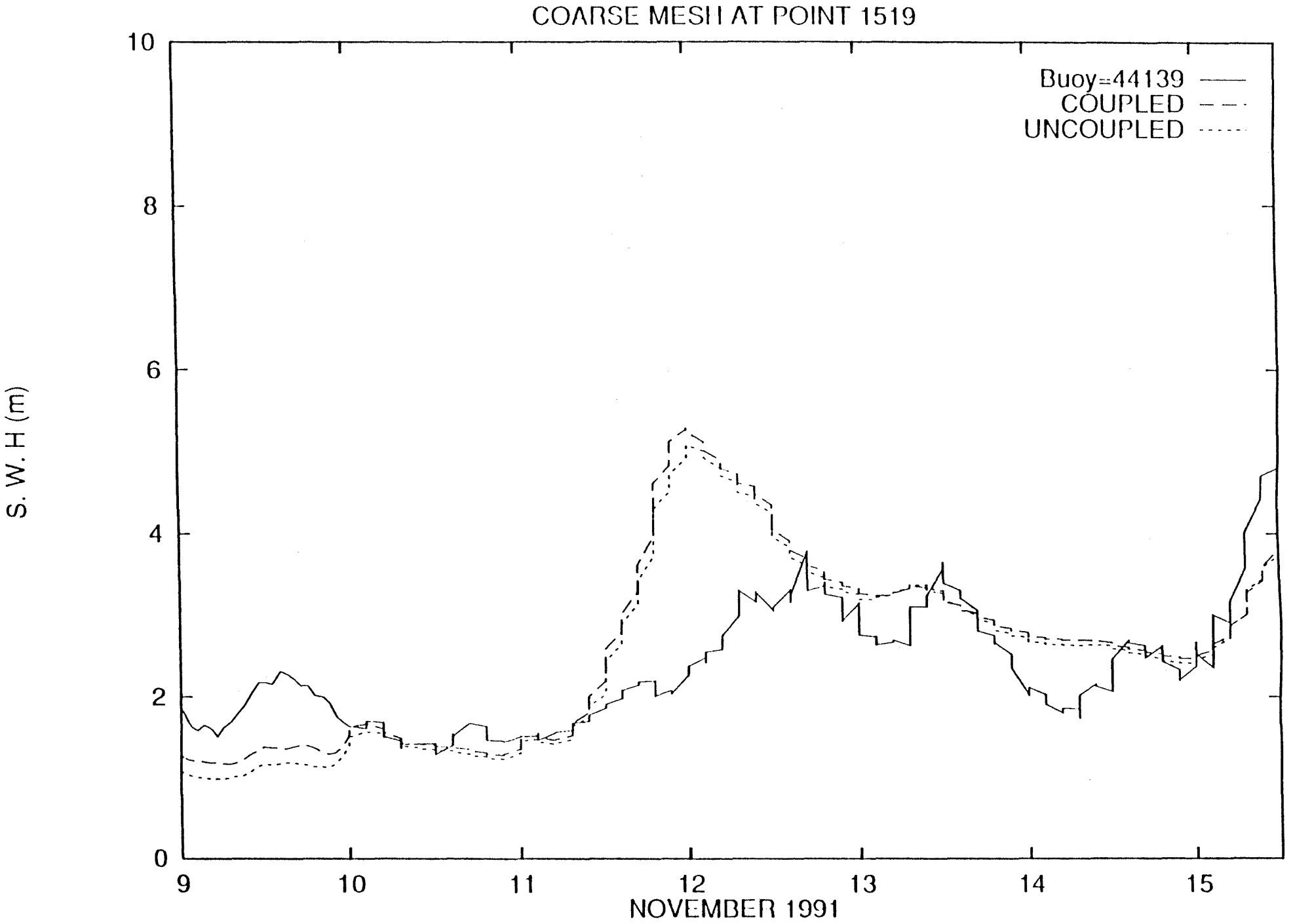
COARSE MESH AT POINT 1519
Buoy=44139
COUPLED
UNCOUPLED
S.W.H (m)
0
2
4
6
8
10
9
10
11
12
13
14
15
NOVEMBER 1991

Fig.51b

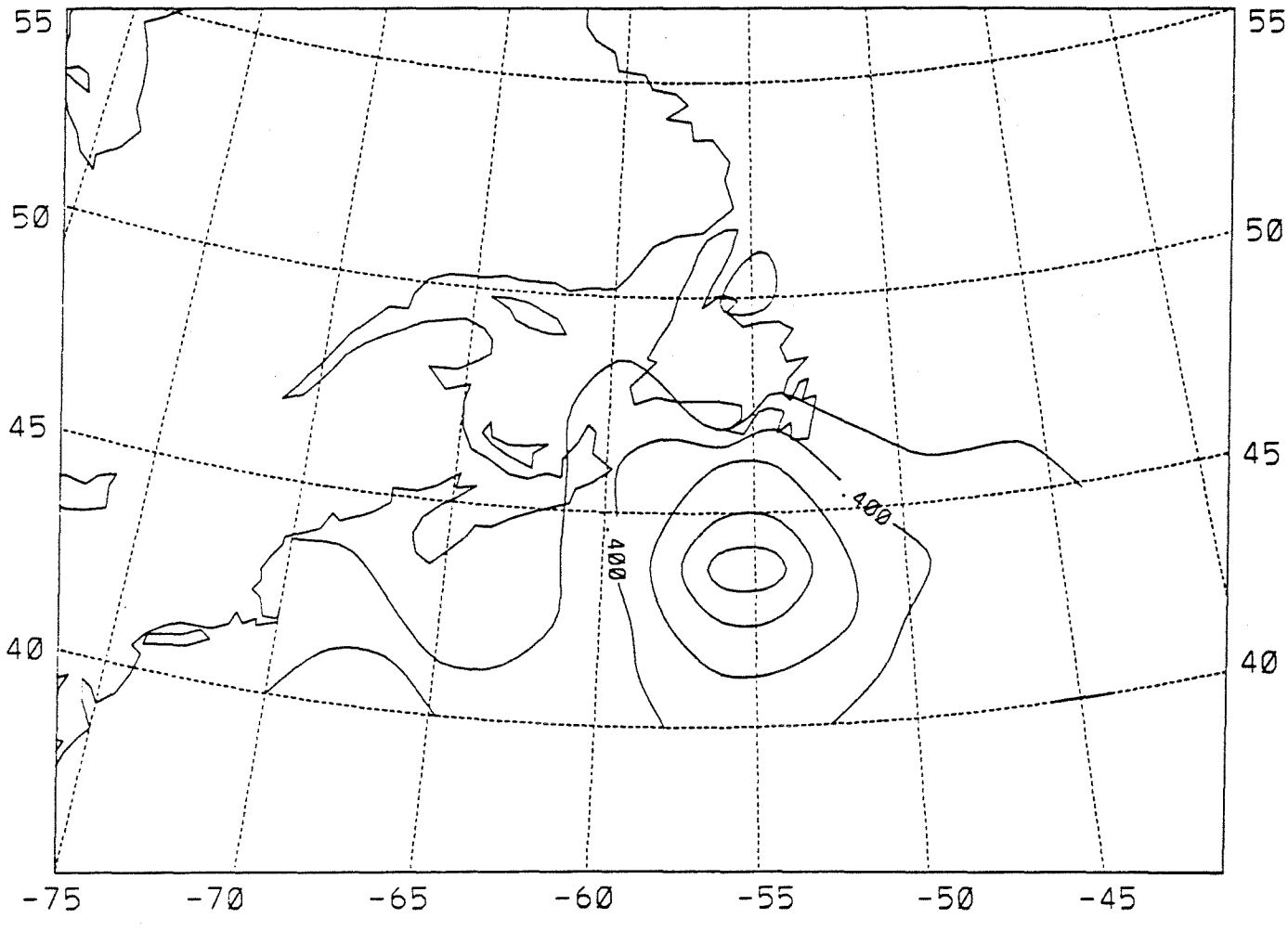

Fig.52a

CONTOUR FROM 0.20000 TO 3.0000 CONTOUR INTERVAL OF 0.20000 PT(3,3)= 0.20000

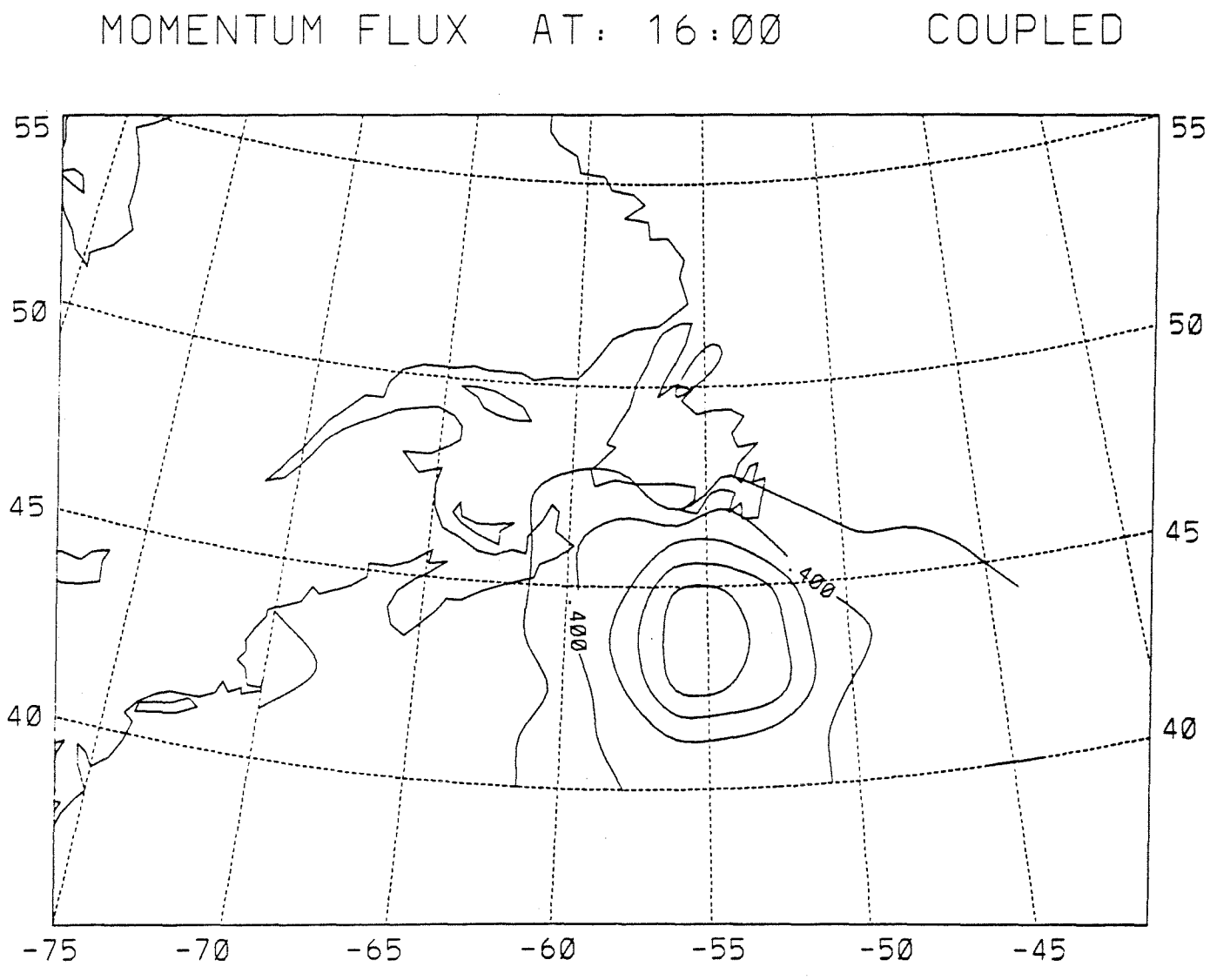

Fig.52b

CONTOUR FROM 0.20000 TO 3.0000 CONTOUR INTERVAL OF 0.20000 PT(3,3)= 0.10000

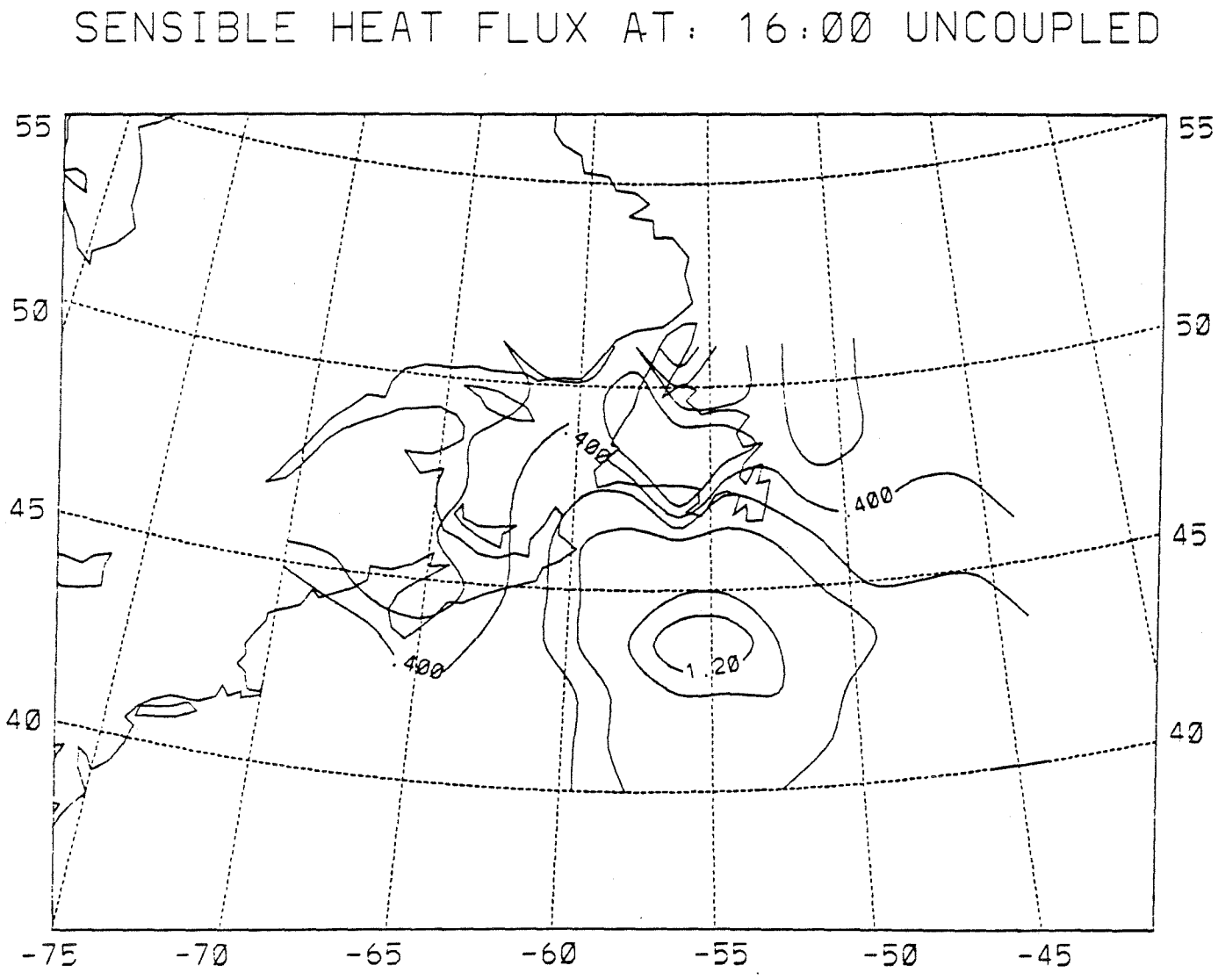

Fig.53a

CONTOUR FROM 0.20000 TO 3.0000 CONTOUR INTERVAL OF 0.20000 PT(3,3)= 0.50000

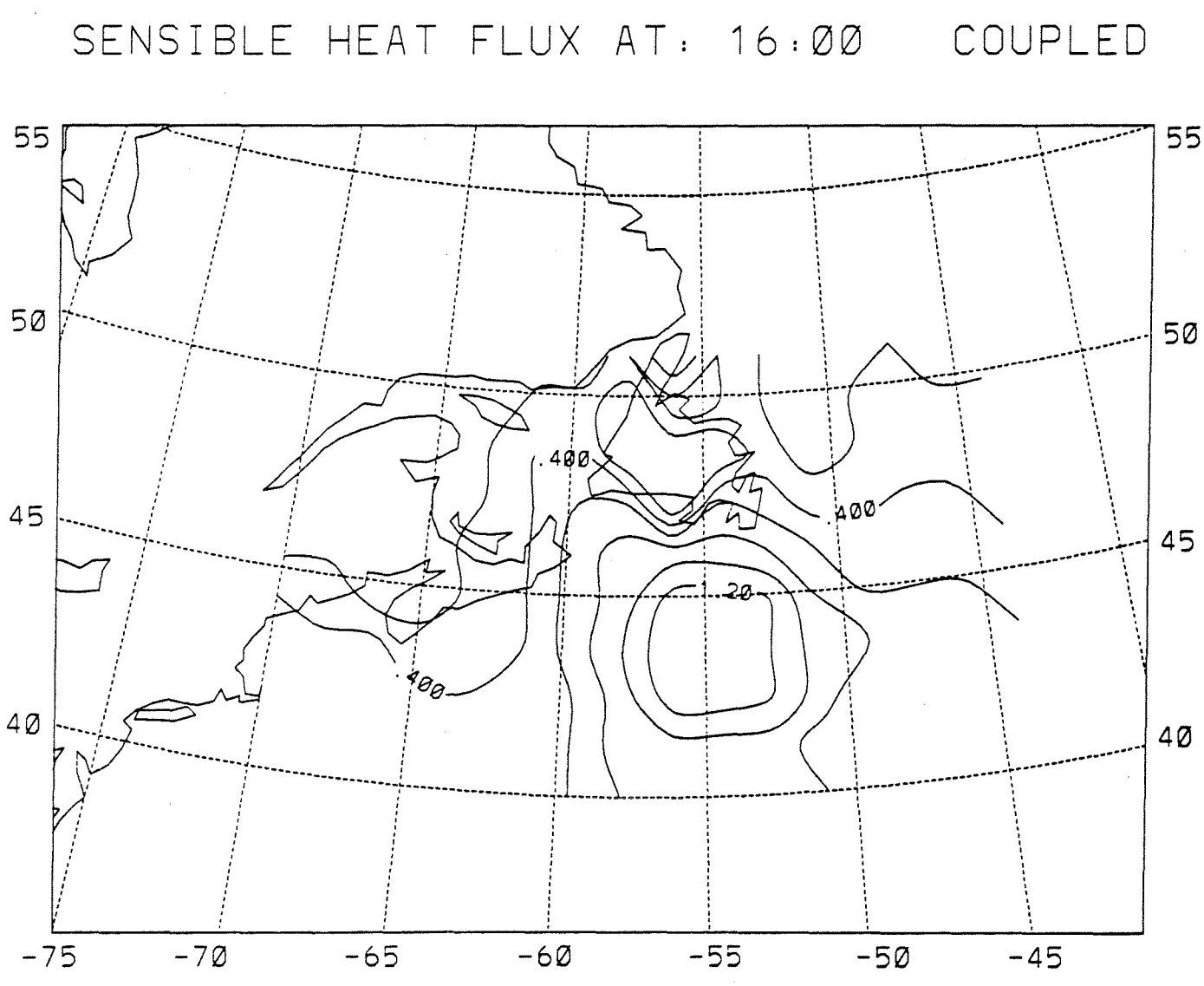

Fig.53b

CONTOUR FROM 0.20000 TO 3.0000 CONTOUR INTERVAL OF 0.20000 PT(3,3)= 0.40000

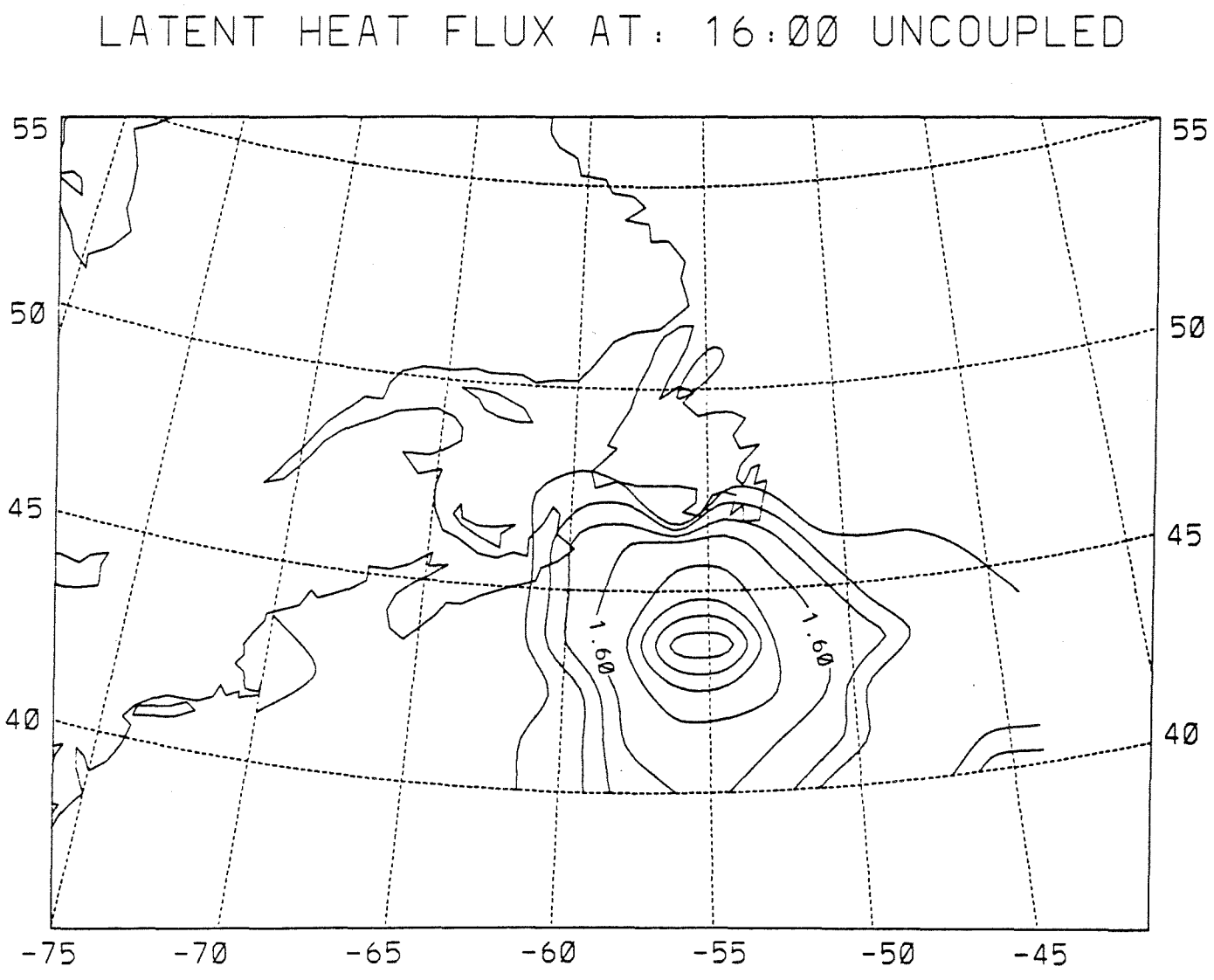

Fig.54a

CONTOUR FROM 1.0000 TO 5.0000 CONTOUR INTERVAL OF 0.20000 PT(3,3)= 0.90000

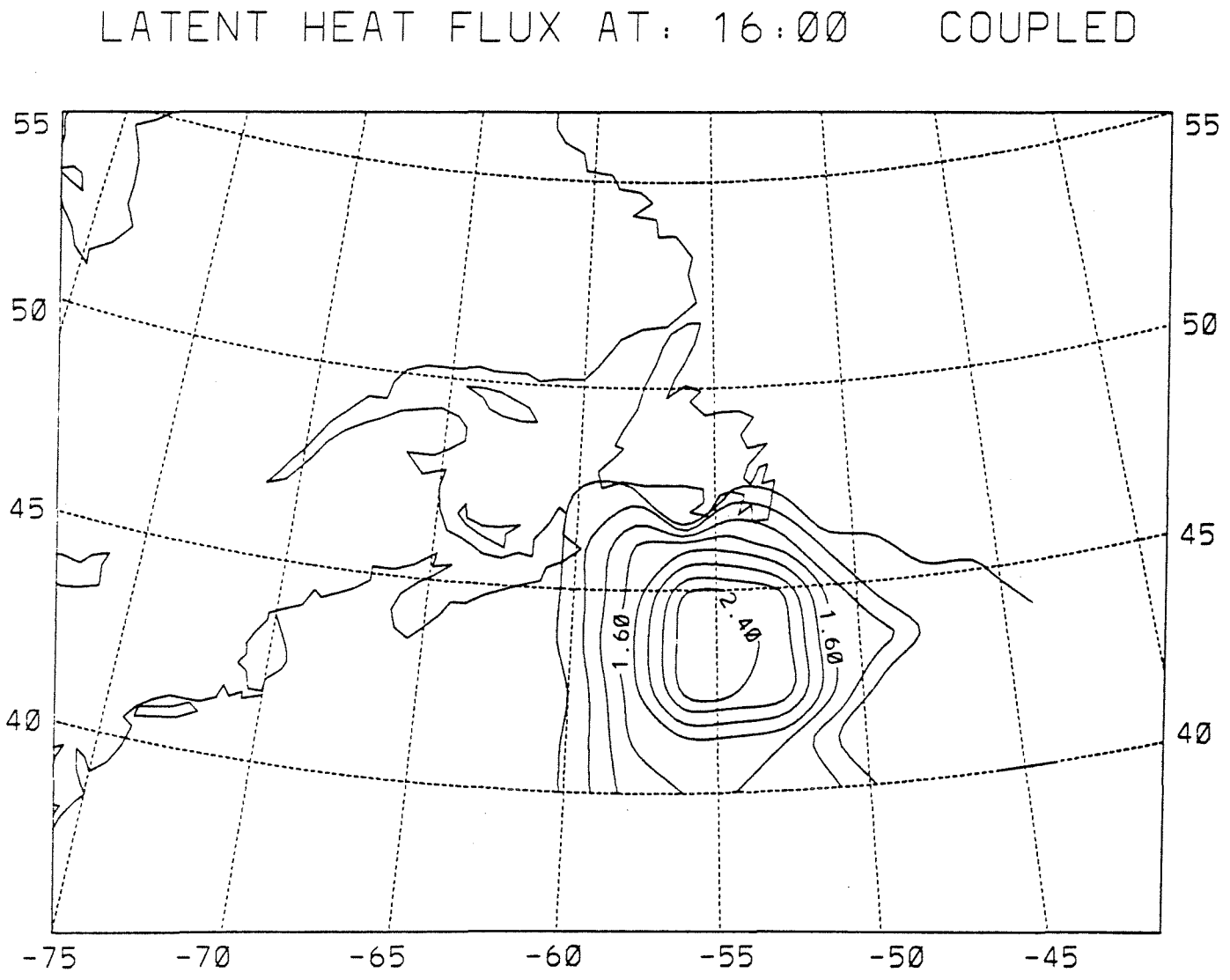

Fig.54b

CONTOUR FROM 1.0000 TO 5.0000 CONTOUR INTERVAL OF 0.20000 PT(3,3)= 0.70000

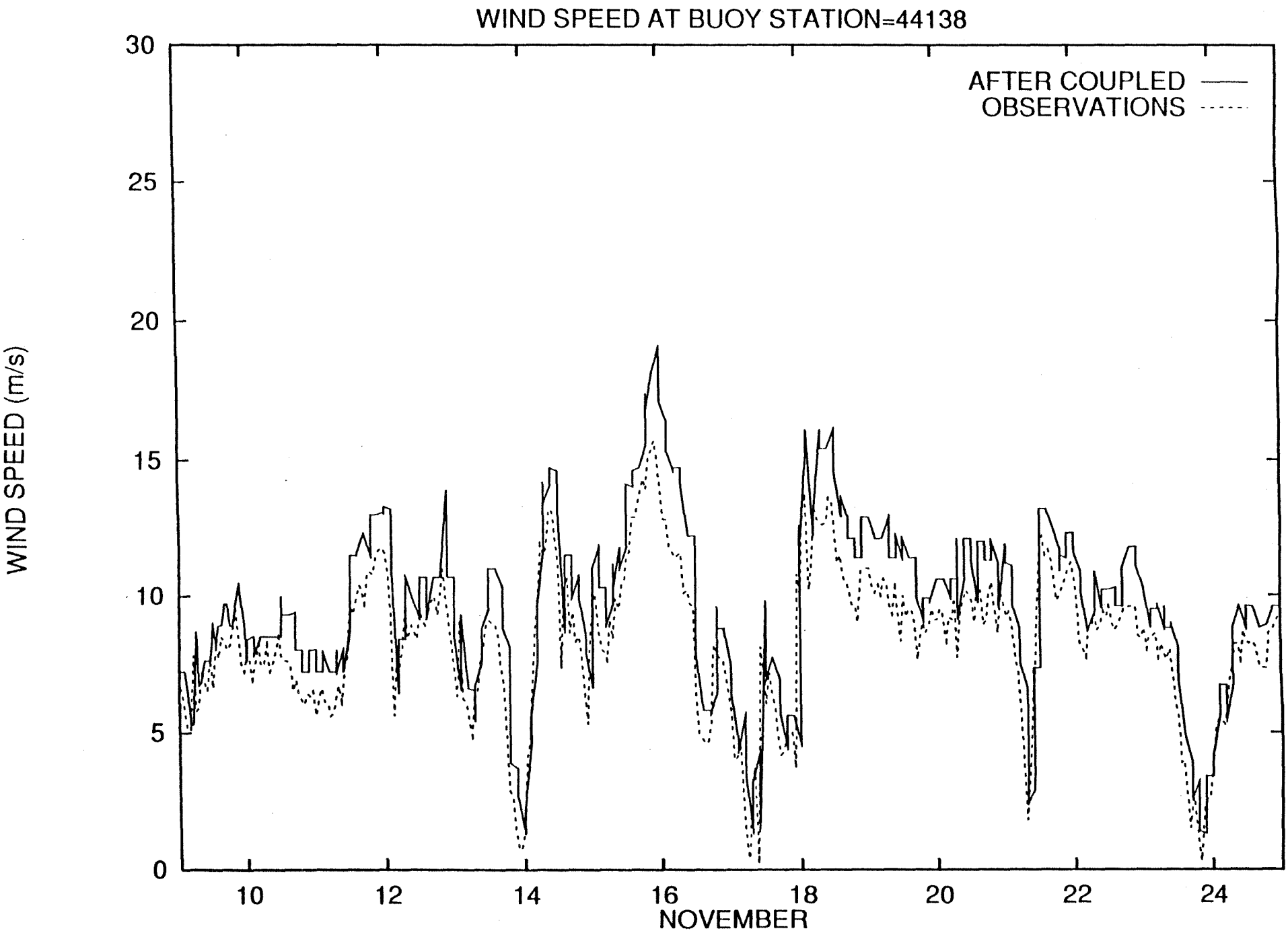
WIND SPEED AT BUOY STATION=44138
AFTER COUPLED
OBSERVATIONS
WIND SPEED (m/s)
30
25
20
15
10
5
0
10
12
14
16
18
20
22
24
NOVEMBER

Fig.55

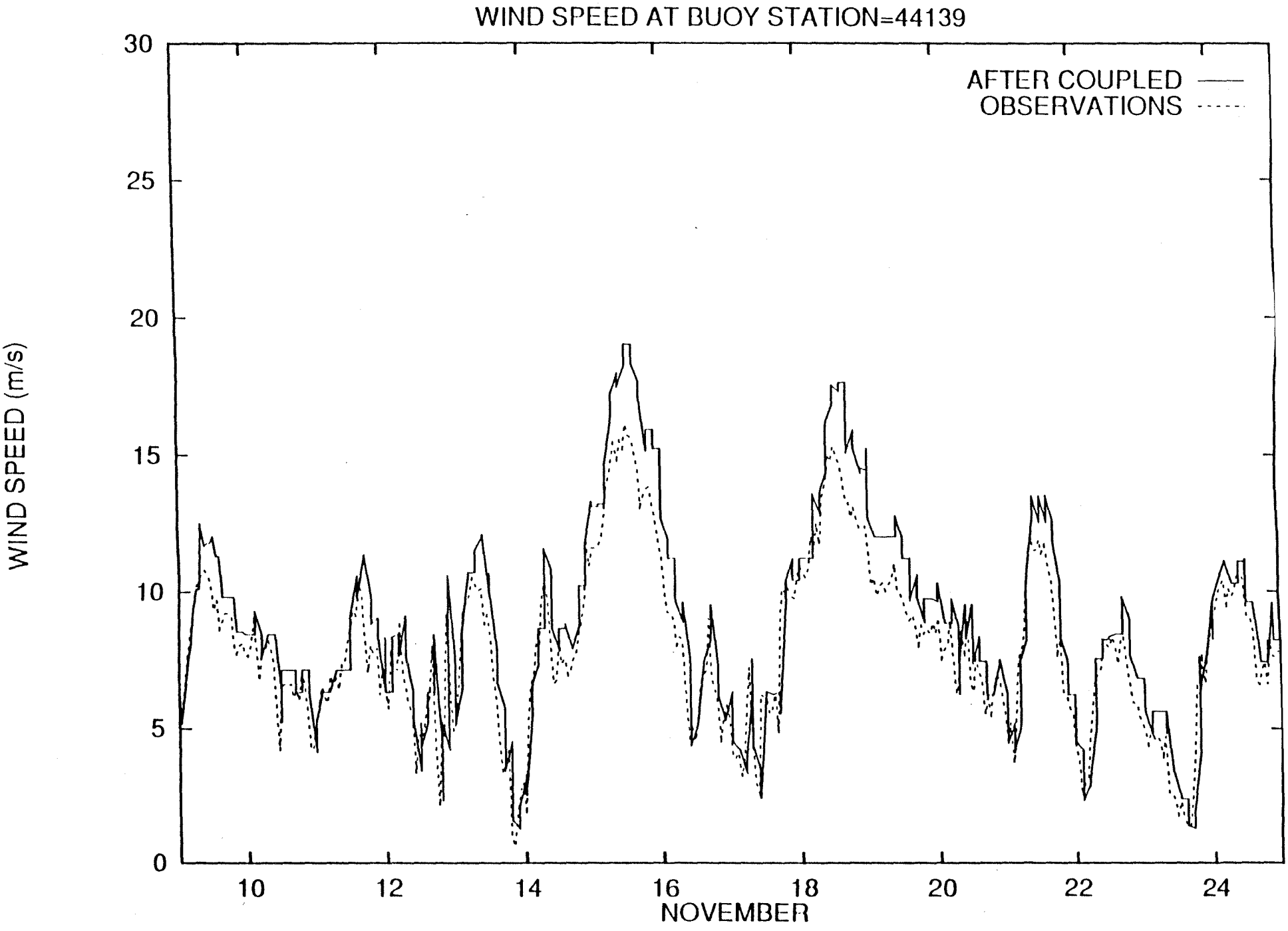
WIND SPEED AT BUOY STATION=44139
AFTER COUPLED
OBSERVATIONS
WIND SPEED (m/s)
30
25
20
15
10
5
0
10
12
14
16
18
20
22
24
NOVEMBER

Fig.56